

Electromagnetic coupling of quantum dots

Citation for published version (APA):

Mokhlespour, S. (2014). *Electromagnetic coupling of quantum dots*. [Phd Thesis 1 (Research TU/e / Graduation TU/e), Applied Physics and Science Education]. Technische Universiteit Eindhoven.
<https://doi.org/10.6100/IR770784>

DOI:

[10.6100/IR770784](https://doi.org/10.6100/IR770784)

Document status and date:

Published: 31/03/2014

Document Version:

Publisher's PDF, also known as Version of Record (includes final page, issue and volume numbers)

Please check the document version of this publication:

- A submitted manuscript is the version of the article upon submission and before peer-review. There can be important differences between the submitted version and the official published version of record. People interested in the research are advised to contact the author for the final version of the publication, or visit the DOI to the publisher's website.
- The final author version and the galley proof are versions of the publication after peer review.
- The final published version features the final layout of the paper including the volume, issue and page numbers.

[Link to publication](#)

General rights

Copyright and moral rights for the publications made accessible in the public portal are retained by the authors and/or other copyright owners and it is a condition of accessing publications that users recognise and abide by the legal requirements associated with these rights.

- Users may download and print one copy of any publication from the public portal for the purpose of private study or research.
- You may not further distribute the material or use it for any profit-making activity or commercial gain
- You may freely distribute the URL identifying the publication in the public portal.

If the publication is distributed under the terms of Article 25fa of the Dutch Copyright Act, indicated by the "Taverne" license above, please follow below link for the End User Agreement:

www.tue.nl/taverne

Take down policy

If you believe that this document breaches copyright please contact us at:

openaccess@tue.nl

providing details and we will investigate your claim.

Electromagnetic Coupling of Quantum Dots

Salman Mokhlespour

Copyright ©2014 by Salman Mokhlespour, Eindhoven, The Netherlands.

All rights are reserved. No part of this publication may be reproduced, stored in a retrieval system, or transmitted, in any form or by any means, electronic, mechanical, photocopying, recording or otherwise, without prior permission of the author.

CIP-DATA LIBRARY TECHNISCHE UNIVERSITEIT EINDHOVEN

Mokhlespour, Salman

Electromagnetic Coupling of Quantum Dots / by Salman Mokhlespour.
Eindhoven: Eindhoven University of Technology, 2014.

A catalogue record is available from the Eindhoven University of Technology Library
ISBN: 978-90-386-3582-8
NUR 924

Subject headings: dipole-dipole interaction, local-field correction, quantum optics, spontaneous emission rate, nano-antenna, quantum dot array, time-resolved differential reflection spectroscopy,

The work described in this thesis was financially supported by the COBRA Inter-University Research Institute and was carried out in the group Photonics and Semiconductor Nanophysics at the department of Applied Physics of the Eindhoven University of Technology, The Netherlands.

The cover is a schematic lattice of quantum dots. The X-STM image of a single quantum dot is taken from Ref. [1].

The cover is designed by Salman Mokhlespour.
Printed by the print service of the Eindhoven University of Technology.

Electromagnetic Coupling of Quantum Dots

PROEFSCHRIFT

ter verkrijging van de graad van doctor aan de Technische Universiteit Eindhoven, op gezag van de rector magnificus, prof.dr.ir. C.J. van Duijn, voor een commissie aangewezen door het College voor Promoties in het openbaar te verdedigen op maandag 31 maart 2014 om 16.00 uur

door

Salman Mokhlespour

geboren te Esfahan, Iran

Dit proefschrift is goedgekeurd door de promotoren:

prof.dr. A. Fiore

en

prof.dr. M.E. Flatté

Copromotor:

dr. J.E.M. Haverkort

To my parents,
to my wife,
and to my sisters

Contents

1	Introduction	1
1.1	Quantum confinement in nano-structured semiconductors	1
1.2	Quantum Dots	2
1.3	The spontaneous emission rate and the photonic density of states	4
1.4	Experimental observations of a modified spontaneous emission rate	6
1.5	Electromagnetic coupling of quantum dots	8
1.5.1	Superradiance and Subradiance	9
1.5.2	Superfluorescence	12
1.5.3	Superluminescence and Radiation Trapping	14
1.5.4	Emission directionality	16
1.6	Scope of this thesis	18
2	Theoretical foundation: Electrodynamics and the Master Equation approach	21
2.1	Maxwell's equations	22
2.2	Field quantization	23
2.2.1	Quantization of cavity field modes	23
2.2.2	Quantization of plane waves	25
2.3	Master equation formalism	27
2.3.1	Interaction of quantum dots positioned in a cavity	27
2.3.2	Interaction of quantum dots in free space	33
2.4	Spontaneous emission	35
3	Collective spontaneous emission from two coupled quantum dots: physical mechanism of quantum nanoantenna	39
3.1	Basic Formalism	42
3.2	Time resolved spontaneous emission	48
3.3	Spontaneous emission pattern	50
3.4	Spontaneous emission spectrum	56
3.5	Population dynamics	59
3.6	Concluding remarks	60
4	Entangled states and collective nonclassical effects in coupled QD-lattices	63
4.1	Model	64

4.2	Radiative Coupling of Quantum Dots Through Cavity Modes	67
4.3	Quantum dot lattices as quantum resonators	70
4.3.1	A single quantum dot lattice	71
4.3.2	Two coupled quantum dot lattices	76
4.4	Summary	80
5	Cooperative spontaneous emission of quantum dots in periodic structures	83
5.1	Model	84
5.1.1	A single planar lattice of quantum dots	84
5.1.2	Two intermixed planar lattices of quantum dots	88
5.2	Planar square lattices of quantum dots	90
5.2.1	A single square lattice of identical quantum dots	91
5.2.2	Two intermixed square lattices of identical quantum dots	92
5.3	Population dynamics in two coupled lattices of quantum dots	95
5.4	Summary	98
6	Modification of the spontaneous emission decay time in self-assembled quantum dots	99
6.1	Theoretical formalism	99
6.1.1	Hamiltonian and the time evolution operator	101
6.1.2	Green's function on the Schwinger-Keldysh contour	104
6.1.3	Single-QD density matrix equation of motion	106
6.1.4	The average local-field in a thin layer of QDs	109
6.1.5	Dyson equation and contour Green's function	109
6.2	The relaxation rates and light-level shifts in a single layer of QDs	111
6.2.1	The spontaneous emission rate and the Lamb shift	114
6.2.2	The collective spontaneous emission rate and collective energy-level shift	117
6.3	Numerical simulation of the spontaneous decay time	118
6.4	Discussion	122
6.5	Summary	125
7	Collective reflection: Time Resolved Differential Reflectivity Experiments	127
7.1	Differential reflection from a planar quantum dot sample	129
7.2	Sample details	135
7.3	Charge carrier dynamics in InAs/GaAs quantum dots	136
7.4	Time Resolved Differential Reflectivity experimental setup	138
7.5	Pump-power dependent measurement	139
7.6	Probe-frequency dependent measurement	144
7.7	Time Resolved Photoluminescence (TRPL) experiments	149
7.8	Summary	151
A	Moments and Cumulants of a probability distribution	153
B	The local field in a thin layer	155

C Derivation of P^{ret} and P^{+-}	159
D Inverse Fourier transformation of the retarded Green's function	161
Bibliography	163
Summary	179
Acknowledgement	181
Curriculum vitae	183

Chapter 1

Introduction

1.1 Quantum confinement in nano-structured semiconductors

Considering the reference of the energy levels in a semiconductor at the edge of the valence band, an electron in the conduction band of a bulk semiconductor material has an energy which includes the energy gap of the semiconductor plus a kinetic energy due to the free motion of the electrons in all directions. A quantum well is a 2D material in which the electrons and holes are confined in one direction and have only two degrees of freedom. Such 2D structures are usually made by sandwiching a thin film of semiconducting material between barriers with a higher band-gap. Assuming a simplified model of a well with infinitely high barriers, the energy for an electron in the conduction band of a quantum well is a sum of three terms. One term is just the energy gap between the highest valence and the lowest conduction band. One term is the kinetic energy for the free motion of the electron in any direction parallel to the well plane and one term represents the quantized confinement energy proportional to $1/L^2$ with L the thickness of the well and corresponds to the confined motion of the electron perpendicular to the well plane. Confining a semiconductor material in one more direction, we have a quantum wire. In such a structure, the electron is confined in two directions and is allowed to move freely only in one direction. In this case, there is an extra term as compared with the electron energy in a quantum well due to the additional degree of confinement in quantum wires. Moreover, the kinetic energy of the electron corresponds to the free motion of the electron in one dimension and along the wire axis. It is now easy to imagine the energy of an electron in a Quantum Dot (QD) in which it is confined in all directions and hence doesn't have any degree of freedom. Therefore, the kinetic term does not appear in QDs and electrons can have only a set of discrete energies. This characteristic of QDs is reminiscent of quantized energy levels in atoms. That is why it is well known in literature that the QDs have atom-like optical behavior.

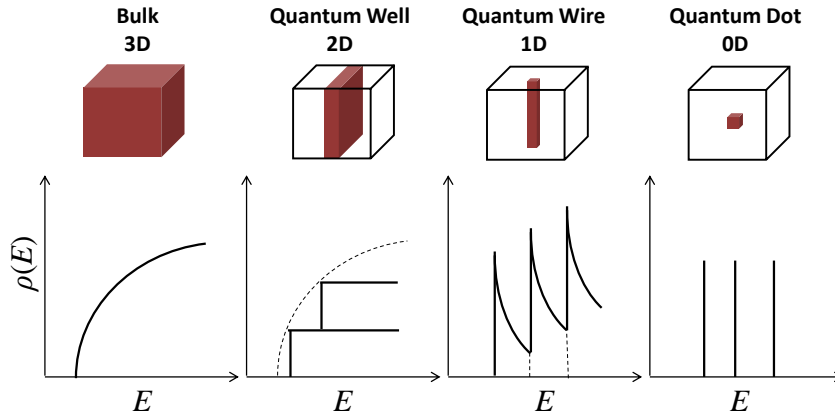


Figure 1.1: Electron density of states in nanostructures for different degrees of freedom.

Some similarities between semiconductor quantum dots and two-level atoms have been shown in references [2–5]. Another important parameter in nano-structured materials that is strongly affected by the degrees of spatial confinement, is the relevant charge carrier Density of States (DOS) and is defined as the number of states per energy per unit volume of real space. In semiconductor materials, this holds for both electrons and holes. In bulk materials, the DOS corresponding to a certain energy E , with respect to the semiconductor bandedge, is proportional to \sqrt{E} , while in quantum wells, it is stepwise and in a quantum wire, it is proportional to $1/\sqrt{E}$ [6]. In the most confined geometry, a QD, the DOS is a sum of delta functions, corresponding to the fully quantized energy levels. The schematic variation of the electron density of states with the energy in different nanostructures is depicted in Fig.(1.1). In QDs, all the electron (hole) states are concentrated at a series of quantized energies rather than distributed over a continuum of energies [6]. The quantization of electronic energy levels as well as the strong modification of the electronic density of states in nanostructures, provides interesting electronic and optical characteristics for such materials and consequently leads to a large variety of outstanding applications in electronic and photonic devices. In the rest of this thesis, our focus is on QDs and the electromagnetic coupling between QDs. that's why in the next section, we briefly introduce these three-dimensionally confined nanostructures with more details.

1.2 Quantum Dots

Quantum Dots (QDs) are small structures containing a tiny droplet of atoms, usually embedded within a shell material. The typical size of a QD varies from a few nanome-

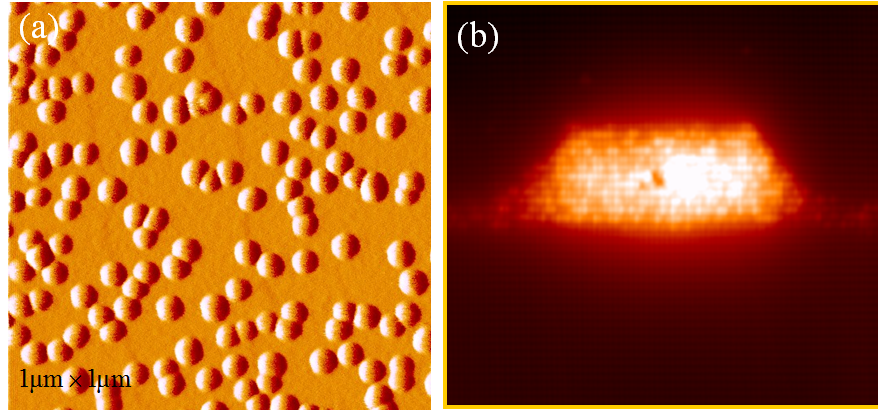


Figure 1.2: (a) Atomic Force Microscopy (AFM) image of uncapped self-assembled InAs/GaAs QDs grown on a GaAs substrate. (b) Cross-sectional scanning tunneling microscopy image of a single QD from a similar sample. Picture from Ref. [1]

ters to a few hundred nanometers. Depending on their size and energy level structure, QDs can accommodate from a single electron up to a collection of several hundred of electrons (or holes). There are many different types of QDs. For example, colloidal semiconductor nanocrystals can be dispersed in a solution and can easily be attached to another object. This type of QDs can contain as few as 100 up to 100000 atoms within the QD volume with a size range of about 2 to 10 nanometers. Another group of QDs can be fabricated by confining a small part of a small bandgap material by another material with a higher bandgap, forming a core-shell structure. Other QDs are spontaneously fabricated as monolayer fluctuations of the quantum well thickness. Self-assembled QDs are a very well known and an intensively studied type of semiconductor QDs. These QDs are formed by a spontaneous nucleation of a semiconductor material on a substrate which is not lattice matched with the QD material. Thanks to continuous advances in epitaxial growth techniques such as Molecular Beam Epitaxy (MBE) [7, 8] and Metal-Organic Vapor Phase Epitaxy (MOVPE), it is possible to fabricate high quality heterostructures. The semiconductor QD sample we have used in the experimental part of our research contains InAs/GaAs self-assembled QDs grown by the so-called Stranski-Krastanow (SK) growth mode [9], grown by the MBE technique [10, 11]. An Atomic Force Microscopy (AFM) image of the uncapped version of our sample is illustrated in Fig.(1.2)(a). The AFM image analysis shows that the QDs have a density of about 10^{10} QDs/cm² and are randomly distributed on the sample. The InAs/GaAs QDs are not identical and all have different sizes, following a Gaussian size distribution. Fig.(1.2)(b) is a cross-sectional Scanning Tunneling Microscopy (X-STM) image of a single InAs/GaAs QD taken from Ref. [1]. It is obvious that this type of QD has a truncated pyramidal shape with a short height as compared with the QD base. That's why these QDs are often described by having a disk-like shape. The size, shape and number density of QDs depend on many growth factors like temperature, deposition rate, annealing time, growth interruption time, etc.

The quantized nature of the energy levels within a QD in addition to the atom-like characteristics of a QD, makes it an ideal structure for opto-electronic devices such as quantum dot lasers and quantum dot optical amplifiers. The application of QDs as sensors in biology [12], in photovoltaic devices, in green emitting InGaN QD light emitting diodes (LEDs) [13], and in quantum dot infrared photodetectors [14,15] are other examples of this. Since in our research, we are mainly interested in the modification of the QD spontaneous decay rate and the collective optical characteristics of an ensemble of QDs, we mention here some examples for the application of the electromagnetic coupling between QDs. For instance, superfluorescence, which is a consequence of the collective spontaneous emission of the QDs, is useful as one of the methods for producing coherent emission without the need for coherent optical excitation. In atomic systems, this is especially important in those regimes, such as x-ray or γ -ray, where there are no effective mirrors which limit the use of ordinary stimulated emission process. With the recent advances of quantum informatics, a decoherence-free subspace (DFS) [16] has been proposed to be one of the candidates to overcome the effects of decoherence in quantum computation and quantum communication. A collective system of many two-level particles is one of the ideal candidates to realize a DFS [16–18]. An ensemble of N two-level atoms with one excitation is also an important system for quantum memories and for quantum networking. Relevant experiments on atomic systems have been carried out by the groups of Lukin [19], Kimble [20] and Vuleti et al. [21]. In this thesis, we treat the optical properties of QDs by considering them as perfect two-level emitters. The spontaneous emission of such a quantum emitter is briefly discussed in the next section.

1.3 The spontaneous emission rate and the photonic density of states

In quantum mechanics, the strength of an optical transition (spontaneous emission) between an initial QD+field state $|i\rangle$ and a final state $|f\rangle$ is governed by Fermis Golden Rule [22],

$$\gamma_{i \rightarrow f}(\omega_0) = \frac{2\pi}{\hbar} \sum_f |\langle f | H_{\text{int}} | i \rangle|^2 \delta(E_f - E_i), \quad (1.3.1)$$

where γ is the emission rate and $H_{\text{int}} = -\hat{\mu} \cdot \hat{\mathbf{E}}$ is the interaction Hamiltonian due to the interaction of the emitter dipole moment, $\hat{\mu}$, with the electric field modes, $\hat{\mathbf{E}}$, available at the position of the quantum emitter. E_i and E_f are the initial and final energies of the QD+field system. We can define the initial and final states of the QD+field system as

$$\begin{aligned} |i\rangle &= |e, \{0\}\rangle = |e\rangle | \{0\} \rangle, \\ |f\rangle &= |g, \{1_{\omega_{k'}}\}\rangle = |g\rangle | \{1_{\omega_{k'}}\} \rangle, \end{aligned} \quad (1.3.2)$$

where $|e\rangle$ and $|g\rangle$ are the excited and ground states of the QD as a two-level emitter and $| \{1_{\omega_{k'}}\} \rangle$ represents a photon state with energy $\hbar\omega_{k'}$. By this definition, the initial and final transition energies become $E_i = \hbar\omega_e$ and $E_f = \hbar\omega_g + \hbar\omega_{k'}$, where $\hbar\omega_e$ is the

energy of QD excited state, $\hbar\omega_g$ is the energy of the QD ground state and $\hbar\omega_{\mathbf{k}'}$ is the energy of a photon in the \mathbf{k}' mode. Then, Eq.(1.3.1) can be written in the form of

$$\gamma_{i \rightarrow f}(\omega_0) = \frac{2\pi}{\hbar^2} \sum_{\mathbf{k}'} |\langle f | \hat{\mu} \cdot \hat{\mathbf{E}} | i \rangle|^2 \delta(\omega_{\mathbf{k}'} - \omega_0), \quad (1.3.3)$$

where $\omega_0 = \omega_e - \omega_g$ is the dipole transition energy and $\hat{\mu}$ is the dipole operator. In quantum mechanics, the operator of the electric field has the general form of [22]

$$\hat{\mathbf{E}}(\mathbf{r}_0) = \sum_{\mathbf{k}} \left[\mathbf{E}_{\mathbf{k}}^+(\mathbf{r}_0) \hat{a}_{\mathbf{k}}(0) e^{-i\omega_{\mathbf{k}}t} + \mathbf{E}_{\mathbf{k}}^-(\mathbf{r}_0) \hat{a}_{\mathbf{k}}^\dagger(0) e^{i\omega_{\mathbf{k}}t} \right], \quad (1.3.4)$$

with $\hat{a}_{\mathbf{k}}^\dagger$ and $\hat{a}_{\mathbf{k}}$ the creation and annihilation operators of the \mathbf{k} mode of the photon state with the corresponding energy of $\hbar\omega_{\mathbf{k}}$. Then the matrix elements in Eq.(1.3.3) become

$$\begin{aligned} \langle f | \hat{H}_{\text{int}} | i \rangle &= \mu \cdot \sum_{\mathbf{k}} \mathbf{E}_{\mathbf{k}}^- e^{i\omega_{\mathbf{k}}t} \langle g, \{1_{\omega_{\mathbf{k}'}}\} | g, \{1_{\omega_{\mathbf{k}}}\} \rangle, \\ \langle i | \hat{H}_{\text{int}} | f \rangle &= \mu \cdot \sum_{\mathbf{k}''} \mathbf{E}_{\mathbf{k}''}^+ e^{-i\omega_{\mathbf{k}''}t} \langle g, \{1_{\omega_{\mathbf{k}''}}\} | g, \{1_{\omega_{\mathbf{k}'}}\} \rangle, \end{aligned} \quad (1.3.5)$$

where we used $\hat{a}_{\mathbf{k}}^\dagger(0) | 0 \rangle = | \{1_{\omega_{\mathbf{k}}}\} \rangle$ and $\hat{a}_{\mathbf{k}}(0) | \{1_{\omega_{\mathbf{k}}}\} \rangle = | 0 \rangle$. Considering the mathematical equation

$$|\langle f | \hat{H}_{\text{int}} | i \rangle|^2 = \langle f | \hat{\mu} \cdot \hat{\mathbf{E}} | i \rangle^* \langle f | \hat{\mu} \cdot \hat{\mathbf{E}} | i \rangle = \langle i | \hat{\mu} \cdot \hat{\mathbf{E}} | f \rangle \langle f | \hat{\mu} \cdot \hat{\mathbf{E}} | i \rangle, \quad (1.3.6)$$

with the assumption $\mu^* = \mu$ and employing Eq.(1.3.6), the transition rate in (1.3.3) can be written as

$$\begin{aligned} \gamma_{i \rightarrow f}(\omega_0) &= \frac{2\pi}{\hbar^2} \sum_{\mathbf{k}} \sum_{\mathbf{k}''} [\mu \cdot (\mathbf{E}_{\mathbf{k}''}^+ \mathbf{E}_{\mathbf{k}}^-) \cdot \mu] e^{i(\omega_{\mathbf{k}''} - \omega_{\mathbf{k}})t} \\ &\times \sum_{\mathbf{k}'} \langle g, \{1_{\omega_{\mathbf{k}'}}\} | g, \{1_{\omega_{\mathbf{k}}}\} \rangle \langle g, \{1_{\omega_{\mathbf{k}''}}\} | g, \{1_{\omega_{\mathbf{k}'}}\} \rangle \delta(\omega_0 - \omega_{\mathbf{k}'}). \end{aligned} \quad (1.3.7)$$

Because of the orthogonality, the nonvanishing modes are those for which $\mathbf{k}' = \mathbf{k}'' = \mathbf{k}$. Then Eq.(1.3.7) can be simplified to

$$\gamma_{i \rightarrow f}(\omega_0) = \frac{2\pi}{\hbar^2} \sum_{\mathbf{k}} [\mu \cdot (\mathbf{E}_{\mathbf{k}}^+ \mathbf{E}_{\mathbf{k}}^-) \cdot \mu] \delta(\omega_0 - \omega_{\mathbf{k}}). \quad (1.3.8)$$

In Eq.(1.3.8), $\mathbf{E}_{\mathbf{k}}^+ \mathbf{E}_{\mathbf{k}}^-$ is a tensorial outer product and is generally a 3×3 matrix. We can transfer Eq.(1.8) to another format to write the spontaneous transition rate in terms of the Local Density of Optical States (LDOS) [22]. We write the field components in terms of normal modes defined as

$$\mathbf{E}_{\mathbf{k}}^+(\mathbf{r}) = \sqrt{\frac{\hbar\omega_{\mathbf{k}}}{2\varepsilon_0}} \mathbf{u}_{\mathbf{k}}(\mathbf{r}), \quad \mathbf{E}_{\mathbf{k}}^-(\mathbf{r}) = \sqrt{\frac{\hbar\omega_{\mathbf{k}}}{2\varepsilon_0}} \mathbf{u}_{\mathbf{k}}^*(\mathbf{r}), \quad (1.3.9)$$

Eq.(1.3.8) becomes

$$\gamma(\mathbf{r}_0, \omega_0) = \frac{\omega_0 \pi \mu^2}{3\hbar\varepsilon_0} \rho_{\text{opt}}(\mathbf{r}_0, \omega_0), \quad (1.3.10)$$

where

$$\rho_{\text{opt}}(\mathbf{r}_0, \omega_0) = 3 \sum_{\mathbf{k}} [\mathbf{e}_{\mu} \cdot (\mathbf{u}_{\mathbf{k}} \mathbf{u}_{\mathbf{k}}^*) \cdot \mathbf{e}_{\mu}] \delta(\omega_0 - \omega_{\mathbf{k}}), \quad (1.3.11)$$

is the local density of optical states. \mathbf{e}_{μ} is the unit vector along the QD dipole moment and μ is the magnitude of the QD dipole moment. As is clear from (1.3.11), that the LDOS includes information about the available field modes at the position of the emitting QD, the transition frequency and the QD dipole orientation. We can write the LDOS also in terms of the Green's function. Starting from solving the differential wave equation for the Green's function and after doing some mathematics, the LDOS in terms of the Green's function becomes

$$\rho_{\text{opt}}(\mathbf{r}_0, \omega_0) = \frac{6\omega_0}{\pi c^2} \left[\mathbf{e}_{\mu} \cdot \text{Im} \left\{ \overset{\leftrightarrow}{\mathbf{G}}(\mathbf{r}_0, \mathbf{r}_0; \omega_0) \right\} \cdot \mathbf{e}_{\mu} \right], \quad (1.3.12)$$

where c is the speed of light. $\overset{\leftrightarrow}{\mathbf{G}}(\mathbf{r}, \mathbf{r}'; \omega)$ is generally a dyadic Green's function that governs the propagation of field modes in the environment. From the mathematical point of view, the spontaneous emission rate modification due to the local density of optical states, LDOS, can be described by a modification of the Green's function, which in turn depends on the local value of the dielectric function $\epsilon(\mathbf{r}, \omega)$ of the medium as well as on the electromagnetic field propagation of the emission from a point-like dipole positioned at the point of consideration. Generally, the emission rate of any emitter strongly depends on the LDOS at the position of the emitter. In mesoscopic structures where the permittivity (dielectric constant) of the medium is inhomogeneous on a spatial scale comparable with the wavelength of light, the fundamental light-matter interaction experiences modifications due to the LDOS. The density of photonic states governs the probability of spontaneous decay of excited atoms, excited QDs and other quantum emitters, and essentially depends on the environmental optical characteristics and geometrical properties of the space around the emitter. We will also call the photonic states around the emitter the reservoir of photonic modes. Every electromagnetic field mode with a wave vector \mathbf{k} can be defined as an oscillator with frequency $\omega_{\mathbf{k}}$. If the propagation of a certain photonic mode is not allowed within the photonic reservoir, it means that the decay of the emitter in that mode becomes prohibited. In the opposite case, when the photonic reservoir offers a concentration of modes in a particular frequency interval, it means that the emission probability of the emitter is enhanced in that particular frequency interval. The engineering of the photonic reservoir in order to achieve a desirable emission rate into a specific mode is nowadays of great interest, since for instance in some applications such as light emitting devices, a faster decay rate is more applicable while in other applications such as quantum information, a slower decay rate to keep coherent state for a longer period of time is more desirable.

1.4 Experimental observations of a modified spontaneous emission rate

In the previous section, we showed that we can achieve any desirable spontaneous emission rate by engineering the local density of optical states (LDOS) in the vicinity of the

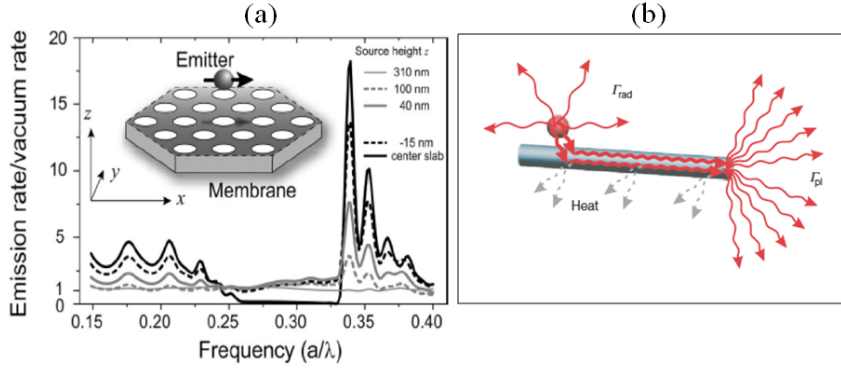


Figure 1.3: (a) Emission rate of a dipole normalized to its vacuum emission rate. The black solid line corresponds to the case where the emitter is in a photonic crystal slab and the other lines correspond to a dipole at different heights outside and close to the surface of the slab. Picture taken from Ref. [34]. (b) A QD coupled to a metallic nanowire can spontaneously emit either into the free space with the rate Γ_{rad} or into the surface plasmon of the nanowire with the rate Γ_{sp} . Picture taken from Ref. [35].

emitter. In this section we discuss some experiments in which the LDOS and hence the spontaneous emission rate is modified. E. M. Purcell proposed a pioneering idea to enhance the spontaneous emission rate by putting the emitter inside a cavity in which the cavity resonance is tuned in resonance to the emitter [23]. The modification of the spontaneous emission rate in the optical wavelength range was reported for the first time by Martini *et al* [24] in an optical microcavity. A five-fold enhancement of the spontaneous emission rate in a semiconductor QDs inside a polymer microsphere has also been reported [25]. Here, the polymer microsphere plays the role of a cavity. Oppositely, a 13-fold suppression of the spontaneous emission from Cs atoms in the infrared region has been reported when the transition frequency of the atoms is detuned from the cavity resonance frequency [26]. The enhancement and inhibition of the spontaneous emission rate in different structures, has presently been experimentally observed by many authors [27, 28]. A few decades after Purcell's prediction, it was understood that the spontaneous emission can be controlled and modified, not only in a cavity, but also in many other mesoscopic systems in which the photonic reservoir can be modified on the scale of the wavelength of light. As an example, by placing an optical emitter near a planar mirror, the spontaneous emission rate of the emitter can be modified, dependent on the distance between the emitter and the mirror [29–31]. In close proximity to a perfect mirror (silver or gold), the spontaneous emission rate is enhanced due to the influence of the surface plasmon polariton on the local density of optical states at the position of the emitter. The inhibition of the spontaneous emission of molecules, ions and QDs within the forbidden frequency gap of a photonic crystal and the spontaneous decay enhancement near the cavity resonances of a photonic crystal have been extensively investigated both theoretically and experimentally (see Fig. 1.3.(a)) [32–34]. Thin films, interfaces of two different dielectrics and stacked layers are other examples

of structures where the density of photonic states can be strongly modified [36,37]. Placing the emitter in the vicinity of a plasmonic nanostructure, like a metallic nanoparticle or a metallic nanowire, is another possibility to modify the LDOS and hence control the spontaneous emission rate of either atoms or QDs [35]. A schematic picture of a QD in the vicinity of a plasmonic nanowire is depicted in Fig.(1.3). 3(b). In the experimental configurations mentioned above, the spontaneous emission rate of an atom or QD is modified by locating it in a cavity-like structure. In this thesis, our focus is on the spontaneous decay rate of QDs when positioned in the vicinity of other identical QDs in various geometrical arrangements, without using an external cavity. Surprisingly, we observe that the spontaneous emission rate of a single QD is strongly modified when it is embedded within an array of identical QDs.

1.5 Electromagnetic coupling of quantum dots

As we explained in previous sections, when a QD is initially excited, the transition of the QD population from the excited to the ground state occurs through a spontaneous decay which is governed by the interaction of the QD with the electromagnetic modes (photonic reservoir) around the emitting QD and is initiated by stochastic vacuum fluctuations of the photonic reservoir. The theory of this phenomenon has been described by Dirac [38] and then by Wigner and Weisskopf [39,40] as one of the first consequences of the development of quantum electrodynamics. In this case, the QD decays single exponentially with decay time τ_0 which is the inverse of the spontaneous decay rate Γ_0 . This situation holds only for an isolated QD or when the density of QDs in the sample is low enough to avoid any interaction between them. The isotropic and single-exponential pattern of the decay is however strongly altered when the QD density in an ensemble becomes high enough that we cannot ignore the electromagnetic coupling between the QDs anymore.

The spontaneous decay rate of a QD in an ensemble strongly depends on how the QD under consideration interacts with the neighboring QDs. We assume that the density of QDs is low enough to avoid the overlap of the wave function of the electron and holes in different QDs, but it is high enough for electromagnetic coupling through the dipole-dipole interaction between different QDs. We categorize the interaction between QDs into either short-range or long-range interactions. The electrostatic dipole-dipole interaction usually referred to as Förster energy transfer [41] is a short range interaction. The Förster rate for the excitation transfer between QDs has been estimated to be in the range of $10^{-2} - 10^{-3} \text{ps}^{-1}$ for InP QDs with an interdot distance of 7 nm [42]. Experimental evidence for this short-range coupling has been reported in [43]. The Förster mechanism, like other types of dipole-dipole interactions, decays with $1/r^6$ where r is the QD-QD separation. Förster energy transfer thus becomes negligible for larger QD-QD separations. In most QD samples, the QDs can be electromagnetically coupled only through long-range interaction channels which vary with the QD-QD separation as $1/r^2$ [44]. In this framework, even QDs at large distances cannot be considered as isolated QDs. In Ref. [44], the electromagnetic coupling between QDs is described in the

language of exciton-polaritons. In bulk semiconductors, due to conservation of crystal momentum, the interaction of free excitons with the electromagnetic field does not give rise to a radiative excitonic decay, but rather to stationary states which are called exciton-polaritons [45]. What is observed as a radiative decay rate is due to thermalization of the exciton followed by escape from the crystal and conversion into photons: therefore the effective radiative lifetime in a bulk semiconductor should be proportional to the crystal size [46]. In QDs, the electron-hole system (exciton) is fully confined. The exciton-polariton state generated as the result of the coupling between the QD-exciton and the radiation field leads to two different effects. One of them is the self energy of a single QD coupled to the electromagnetic field, which gives rise to a finite radiative lifetime and an energy shift of QD levels. This effect has been extensively investigated in literature [47–49]. The other effect is the radiative coupling between different QDs. This effect can be understood as being due to the multiple emission and reabsorption of photons by each of the QDs in a many-QD system. In this situation, the exciton state of a single QD can no longer be described by the excitonic eigenstate of an isolated QD as part of an ensemble. This leads to transfer of excitation from one QD to another. In this thesis, we extensively approach this problem for different configurations of QDs. The electromagnetic coupling of QDs in QD ensembles also gives rise to collective effects which will be briefly introduced in the following section.

1.5.1 Superradiance and Subradiance

The collective spontaneous emission effect has been studied by many physicists since the pioneering work of Dicke in 1954 [50]. In a classical work, Dicke indicated that the collective radiation of a collection of two-level atoms confined inside a volume with dimensions much smaller than the radiation wavelength ($L \ll \lambda$, where L is the sample length and λ is the emission wavelength) can be superradiant (SR). *Superradiance* is a many-body quantum optical phenomenon that occurs when a group of N identical emitters (atoms or QDs) cooperatively emit light as a high intense pulse which is drastically different from the emission of a group of independent emitters. The schematic picture of the superradiance effect is shown in Fig.(1.4). Assume that at the initial time, N identical quantum emitters are in independent coherent states,

$$\psi_j = \frac{1}{\sqrt{2}} \left(|g\rangle_j + |e\rangle_j e^{-i(\omega_0 t + \varphi_j)} \right). \quad (1.5.1)$$

then the system of N distinguishable particles can be written in the factorable form of

$$\Psi = \psi_1 \psi_2 \cdots \psi_j = \prod_{j=1}^N \psi_j. \quad (1.5.2)$$

Such a state can be prepared by resonant excitation of the QDs by a laser pulse. From the classical point of view, the time-averaged power of the emission of an oscillating dipole, which can be obtained from the Maxwell equations, is equal to

$$P = \mu^2 \omega_0^4 / 3\pi \epsilon_0 c^3, \quad (1.5.3)$$

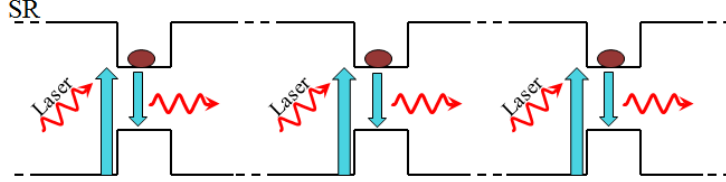


Figure 1.4: Schematic picture of the superradiance (SR) emission in an ensemble of QDs. The QDs are resonantly excited by the pump laser. Then the generated electron-hole pairs in the QDs recombine by emitting coherent photons.

where μ is the dipole moment of the radiating dipole. In a semiclassical approach, in a general case of a many-QD system, μ^2 in Eq(1.3.6) should be replaced by the normally-ordered square $2 \langle \mu^{(-)} \mu^{(+)} \rangle$,

$$\begin{aligned}
 \langle \mu^{(-)} \mu^{(+)} \rangle &= \sum_{i,j} \langle \mu_i^{(-)} \mu_j^{(+)} \rangle \\
 &= \sum_j \langle \psi_j | \mu_j^{(-)} \mu_j^{(+)} | \psi_j \rangle + \sum_{i,j,i \neq j} \langle \psi_i | \mu_i^{(-)} | \psi_i \rangle \langle \psi_j | \mu_j^{(+)} | \psi_j \rangle \\
 &= (\mu^2/2) \left[N + \sum_{i < j} \cos(\varphi_i - \varphi_j) \right] = \mu^2 N(N+1)/4.
 \end{aligned} \tag{1.5.4}$$

Assuming that all QD phases φ_j are equal, the states are mutually coherent. By replacing (1.5.4) in (1.5.3), the coherent emission becomes

$$P_{\text{coh}} = \hbar \omega_0 \gamma_0 N(N+1)/4, \tag{1.5.5}$$

where ω_0 is the transition energy of the QD and $\gamma_0 = \mu^2 \omega_0^3 / 3\pi \epsilon_0 \hbar c^3$ is the spontaneous emission rate of a single QD in free space. If in Eq.(1.5.4), the QD phases are independent random variables distributed uniformly between 0 and 2π , then the sum in the last equality of (1.5.4) tends to zero and hence the system emits incoherently with power

$$P_{\text{incoh}} = \hbar \omega_0 \gamma_0 N/2. \tag{1.5.6}$$

The total energy stored in the sample is $N\hbar\omega_0/2$. Therefore, the corresponding time of the coherent emitted power can be obtained from the ratio of the energy and power, yielding to

$$\tau_{\text{coh}} \simeq 2/(\gamma_0(N+1)). \tag{1.5.7}$$

In the limit of $N \gg 1$, the collective radiative lifetime is $N/2$ times shorter than that of the single QD in free space ($\tau_0 = 1/\gamma_0$).

The concept of Dicke's theory for superradiance was subsequently generalized to spatially extended systems [51, 52]. There have been a lot of theoretical and experimental work performed in this area [53, 54]. The superradiance effect does not occur only for small samples with dimensions $L \ll \lambda$. If the condition of spatial phase matching in an extended system is satisfied, anisotropic superradiance can be emitted from large samples. In this case, the phase of each emitter is determined by $\varphi_j = kz_j$, where \mathbf{k} is the wave vector and z_j is the component of the j th QD coordinate (\mathbf{r}_j) along the wave vector. The direction of \mathbf{k} is the phase matching direction along which the maximum superradiance is emitted. That's why the superradiance from extended systems is not isotropic and is only allowed along a certain direction confined within a corresponding solid angle $\Delta\Omega$. As a consequence, the coherent decay time in (1.5.7) increases by the factor $4\pi/\Delta\Omega$. For stretched samples with the Fresnel number $a^2/L\lambda \sim 1$, the slowing down of the superradiance is in the order of $(a/\lambda)^2 \sim L/\lambda \gg 1$ where a^2 is the sample cross section, and L is the sample length [55]. One of the important features in an extended system is the light propagation. In fact, the emitted field exhibits a strong nonlinear behavior during its propagation along an initially inverted medium. This nonlinear propagation and diffraction gives rise to some well known effects in the context of light pulse propagation. In such a medium, the emitted radiation undergoes strong reshaping, ringing and frequency chirping effects due to the inhomogeneous stimulated emission and reabsorption processes. Such nonlinear effects can be understood only by numerical simulations. These propagation effects can affect the superradiance by reducing the strong inter-QD radiative correlations. Scheibner *et al* [56] have experimentally investigated the superradiance effect in a sample of self-assembled CdSe/ZnSe QDs. They observed that the decay rate from the excited states of QDs by non-resonant (nr) excitation is slower than that of quiresonant (qr) excitation. As is depicted in Fig.(1.5), they showed that the strength of coupling between QDs scales with the number of QDs, N , and the inverse of average QD-QD separation, R , through the relation

$$\frac{\tau_{nr}}{\tau_{qr}} - 1 \propto \frac{N(\lambda)}{R(\lambda)} \propto I(\lambda) \sqrt{I(\lambda)}, \quad (1.5.8)$$

where τ_{nr} is the radiative decay time of the uncoupled QDs and τ_{qr} is the radiative decay time of the coupled QDs. $I(\lambda)$ is the time-integrated PL intensity at wavelength λ . It has been assumed in a first order approximation that $N(\lambda) \propto I(\lambda)$ and $1/R(\lambda) \propto \sqrt{I(\lambda)}$. Scheibner *et al* [56] showed that the QDs that are closer to the peak of PL spectrum (size distribution) and hence are denser, decay faster in the case of resonant excitation. This is an evidence for superradiance of QDs. Different collective states are possible in an extended ensemble of quantum emitters. Many of these states are emission-free states in which collective effects suppress the dipole spontaneous emission. This phenomenon is opposite to superradiance and is called *subradiance*. In contrary to superradiance, subradiance is a destructive interference effect leading to the partial trapping of light in the system. In this effect, the emission intensity is reduced and the decay time of the emission is larger than that of a single quantum emitter in free space. Subradiance is a fragile phenomenon and is difficult to observe experimentally.

Subradiance for a system of two ions has been already observed [57] and in N -atom systems, reduced decay rate into a single radiation mode has been reported [58]. It has been shown in Ref. [59] that a dilute cloud of atoms is an ideal system to look for

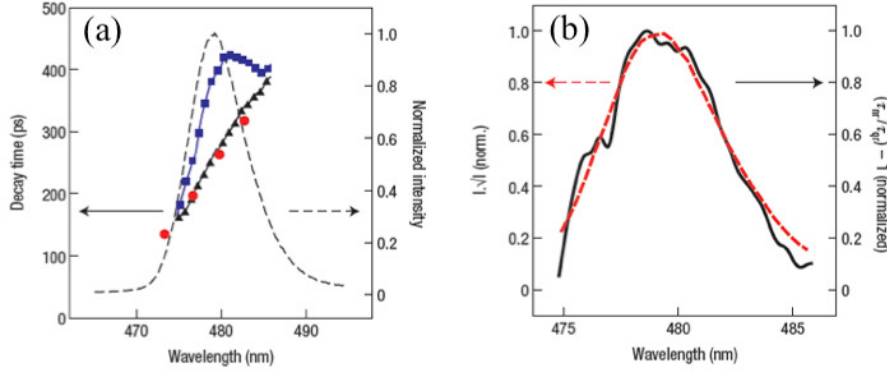


Figure 1.5: (a) PL decay time from self-assembled CdSe/ZnSe QDs in the case of quasi-resonant excitation (triangles) and nonresonant excitation (squares). (b) The corresponding curve (dashed line) of $I(\lambda)\sqrt{I(\lambda)}$ where $I(\lambda)$ is the integrated PL shown as dashed lines in (a) and the corresponding curve (solid line) of $\frac{\tau_{nr}}{\tau_{qr}} - 1$ obtained from time resolved PL measurements. Figure from Ref. [56]

subradiance in free space in the case of single-photon excitation. They have proposed to use the atomic cloud optical thickness, the cloud temperature, or the driving laser intensity as possible experimental control parameters for observing subradiance.

1.5.2 Superfluorescence

The *superfluorescence* (SF) phenomenon is the consequence of the cooperative emission from a system of initially uncorrelated excited two level atoms [60] and always starts with a first spontaneous emission event that initiates the strong correlations which emerge in the system at a later time [61]. The main difference between superfluorescence and superradiance is in the initial excitation of the medium. In superfluorescence, there is no initial macroscopic dipole in the system. In this section, we briefly explain the basic concepts of superfluorescence effect in a quantum mechanical framework. Assuming that the atoms or QDs are indistinguishable and arranged in a sample with dimensions smaller than the wavelength ($L \ll \lambda$), a system of NQDs has $N + 1$ equidistant energy levels depending on the excitation of the system. The lowest energy is the ground state of the system and the highest one belongs to a fully excited system. All the other intermediate levels are degenerate and can be subsequently obtained by acting the dipole lowering operator on the highest level. We can represent any arbitrary state of such a system by a spin-like state $|N/2, M\rangle$, where N is the total number of quantum emitters (atoms or QDs) and $M + N/2$ is the number of excited QDs. Assuming that all QDs are initially excited, the radiative decay of this ensemble is a cascade of subsequent transitions between adjacent states with the same value of the total angular momentum

but a difference of unity in the number of excited QDs,

$$\left| \frac{N}{2}, \frac{N}{2} \right\rangle \rightarrow \left| \frac{N}{2}, \frac{N}{2} - 1 \right\rangle \rightarrow \dots \rightarrow \left| \frac{N}{2}, -\frac{N}{2} \right\rangle. \quad (1.5.9)$$

The transition matrix element for the transition

$$|N/2, M\rangle \rightarrow |N/2, M-1\rangle$$

is given by [62, 63] $\mu_{M, M-1} = \mu_0 \sqrt{(N/2 + M)(N/2 - M + 1)}$ and hence the corresponding spontaneous decay rate becomes

$$\gamma_{M, M-1} = \gamma_0 (N/2 + M)(N/2 - M + 1), \quad (1.5.10)$$

where γ_0 is as mentioned earlier, the spontaneous emission rate of a single QD in free space. In deriving Eq.(1.5.10), we have made use of the relation

$$\gamma_{M, M-1} = \mu_{M, M-1}^2 \omega_0^3 / (3\pi\epsilon_0 \hbar c^3),$$

with ω_0 the QD transition frequency. It is obvious from (1.5.10) that the maximum decay rate takes place at $M = 0$ for an even number of QDs and at $M = 1/2$ for an odd number of QDs. In the first case, exactly half of the QDs are excited and in the second case, almost half of the QDs are excited. In both cases, the decay rate is proportional to N^2 . The mean radiation intensity (the averaged number of photons emitted per unit time) can be derived in the limit of $N \gg 1$ as

$$I(t) = \frac{1}{4} \gamma_0 N^2 \text{Sech}^2 \left[\frac{N}{2} \gamma_0 (t - t_D) \right], \quad (1.5.11)$$

where $t_D = (\gamma_0 N)^{-1} \ln N$ is a delay time [63]. This emission intensity has a hyperbolic secant pulse shape. Although this equation is not an exact solution, it still reveals the most important features of a superfluorescent pulse:

- i. The intensity of the pulse is initially equal to $I(0) = \gamma_0 N$ which corresponds to the emission from N uncorrelated emitters.
- ii. The pulse duration, which is the pulse width at half maximum, is of the order $(\gamma_0 N)^{-1}$, which is N times shorter than the radiative decay time of a single emitter.
- iii. The peak of the intensity appears after a delay time t_D and is proportional to the square of the total number of atoms, $I_{\max} \propto N^2$ similar to superradiance.

The schematic mechanism of superfluorescence is depicted in Fig.(1.6). In this effect, the emitters are not initially correlated. But after the delay time t_D , the emitters reach the maximum correlation and a coherent macroscopic polarization is created. This correlation is due to the dipole-dipole coupling of different quantum emitters in the ensemble. It is shown in Ref. [63] that the expectation value of a pair-correlation function of the dipole moments from different emitters in the ensemble, is equal to $(N^2/4 - M^2)/N(N-1)$, which is maximum when the ensemble is half excited ($M = 0$) and tends to zero for

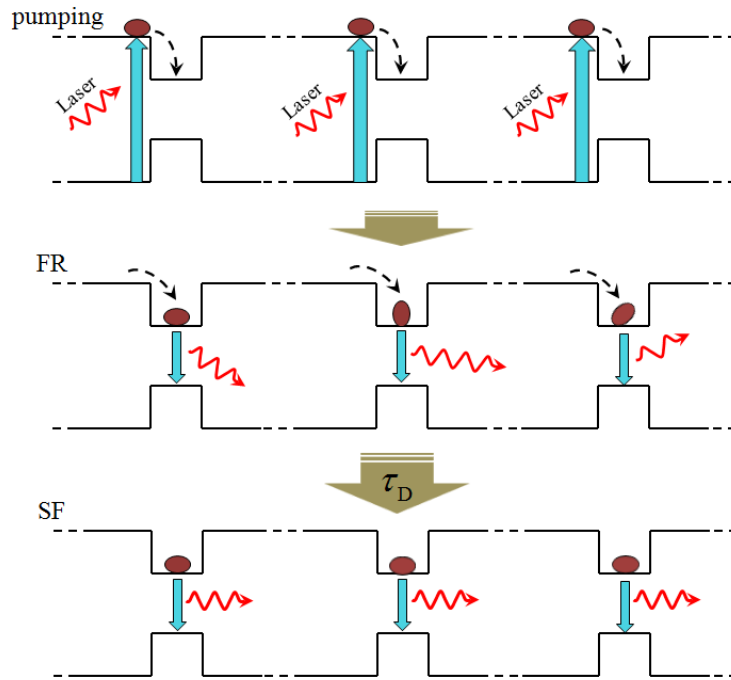


Figure 1.6: Schematic picture of superfluorescence emission from an ensemble of QDs. First charge carriers are generated by a pump laser with energy above the barrier. Then the QDs will be incoherently populated by the carrier diffusion and carrier capture into the QDs. First, an incoherent fluorescence (FR) emission starts. After a correlation delay time, τ_D , a coherent emission develops and all QDs emit coherently.

$M \rightarrow -N/2$ or $N/2$. So Superluminescence effect has two main stages. At the first stage, near $t = 0$, when the emission starts by stochastic quantum noise, the quantum fluctuations of the vacuum modes of the electromagnetic field act on independent quantum emitters that eventually gives rise to dipole-dipole correlations. That's why this stage is a quantum stage. The second stage is a classical stage at which the subsequent emission is due to the radiation from an ordered array of dipoles analogous to classical antennas radiating in-phase through the medium.

1.5.3 Superluminescence and Radiation Trapping

We all know that the effective field which acts on an atom or a QD in a dense medium is different from the macroscopic Maxwell field in such a medium, due to local-field cor-

rection. Local-field corrections were first introduced by Lorentz and Lorenz [64, 65] and are proportional to the polarization of the medium [66, 67]. Such a local-field correction will modify the linear index of refraction according to the Clausius-Mossotti relation [66] and the nonlinear susceptibility [68]. It also modifies the spectral resonances and causes energy level shifts [69–72].

In the framework of quantum mechanics, the Hamiltonian governs the dynamics of the corresponding atomic or QD quantum states. In quantum electrodynamics, the Hamiltonian consists of the interaction of the QD dipole moment and the local field acting on the QD. Therefore, a more precise correction of the local-field would be very helpful to give a better understanding of the quantum effects and physical observables caused by the interaction of atom or QD dipole moment by the field modes at the position of the QD. The intrinsic optical bistability [73–76] and the piezophotonic switching [77] effects are the other results of these local-field corrections. The local-field corrections originate in fact from the superposition of the radiative QD-QD interactions of all other QDs in the medium with the QD under study. Considering these interactions in the framework of quantum mechanics, the quantum nature of the radiative QD-QD interaction gives rise to cooperative emission in the extreme case of an anisotropic and high density sample, which was already introduced as superradiance and superfluorescence. Its opposite corresponds to subradiance [51, 62, 78]. However, if the conditions of the cooperative effects are not fulfilled, the presence of the spontaneous photons in the system might yield noncooperative phenomenon such as *superluminescence* and *radiation trapping* [79]. Although these two phenomenon are not cooperative effects, they are still a consequence of the electromagnetic interaction between the QDs.

Superluminescence (SL), which is also known as Amplified Spontaneous Emission (ASE) is a kind of incoherent spontaneous emission that is optically amplified through stimulated emission processes in a gain medium. ASE can play either a useful or destructive role in laser gain media. The feedback of ASE by the lasers optical cavity can initiate and produce laser operation if the laser threshold is reached. But if it occurs below threshold, then the gain medium may be depleted by the incoherent ASE rather than by the coherent laser emission. This means that ASE is a serious problem for high-gain lasers [80]. Therefore, in contrast to superfluorescence and superradiance, the superluminescence is a collective incoherent emission rather than a cooperative coherent process.

The opposite case of superluminescence is called *radiation trapping*. In an ensemble of quantum emitters, the photon emitted by an excited emitter (atom or QD) might be absorbed and reemitted by another emitter in the system which is in its ground state. This process may continue repeatedly until the photon escapes from the system. This phenomenon is known as *radiation trapping* [81, 82]. This effect strongly depends on the absorption coefficient of the quantum emitters. Under the condition of strong coupling of the QD ensemble by means of an intense laser pulse, the ratio of the ground-state and excited-state QDs can be equal to the statistical weights of the levels. In this case, the stimulated emission becomes equal to the effective absorption and radiation trapping effect vanishes [83]. This phenomenon happens especially for samples with dimensions larger than the emission wavelength. From the experimental point of view, when we excite a part of the atomic or QD ensemble with a short and strong laser pulse, the QDs

become populated and hence the absorption decreases. At an increasing delay time, more and more quantum emitters start to decay and the absorption coefficient increases. However some of the spontaneously emitted photons in the system will be reabsorbed which suppress the increase of absorption coefficient and hence the effective decay time of the ensemble becomes larger than the natural lifetime of a single isolated QD. This phenomenon is a strong nonlinear effect and has attracted more attention after development of strong pulsed lasers. We will present experimental evidence for this effect in chapter (7) of this thesis. From the experimental point of view, the multi-QD optical effects such as superradiance, superfluorescence, and superluminescence have similar impacts on the experiments. The experimental observation of spectral line narrowing, an exponentially growing luminescence intensity as a function of pump power, a drastically shortened lifetime and anisotropic light emission, are some examples. That's why it is usually difficult to attribute one of these cooperative or collective effects to a specific experimental measurement [84]. Superradiance and superfluorescence have already been measured and reported in gaseous systems [53, 85]. There are some hints that might be helpful to realize which of these effects is dominant in an experiment: (i) the initial excitation mechanism is very important. As has been shown in Fig.(1.7), the superradiance effect is most probable if the QDs are resonantly excited by a pump laser. If the excitation is not coherent, we should exclude superradiance from our analysis. (ii) In a pump-power dependent experiment, if the emission intensity exponentially grows with an explicit exponent of 2.0 (in the case of single-photon excitation) or 4.0 (in the case of two-photon excitation), then it can be potentially superradiance or superfluorescence. In superluminescence emission, the exponent can be any number. (iii) In the time domain, if we observe some quantum effects such as quantum beats which is basically a characteristic of the emission from coherent states, then we can conclude that our measurement is in the superradiance or superfluorescence regime rather than superluminescence. (iv) observation of first an increase in the time evolution of the emission followed by a decay, is a sign of superfluorescence in which the coherent emission starts after a delay time τ_D with respect to the initial uncorrelated emission. (v) Checking all dephasing processes in the system, if the total dephasing time T_2^* is shorter than the time required for building up the coherence (τ_D), we cannot expect any coherent effect like superradiance or superfluorescence. In atomic gasses, the largest contribution to the dephasing time originates from an inhomogeneous broadening due to the Doppler effect. But in self-assembled QD samples, the inhomogeneous broadening is due to the QD size distribution and is often much larger than the correlation rate ($T_2^* \ll \tau_D$). Consequently, coherent effects such as superradiance and superfluorescence are very improbable in a QD sample. However, incoherent collective effects such as superluminescence and radiation trapping are very well possible in a QD sample [60, 84].

1.5.4 Emission directionality

As we mentioned earlier, Dicks theory says that a radiating atomic gas can radiate spontaneously and coherently in a particular direction. Directionality of emission in multi-atomic systems or ensemble of QDs is a consequence of the radiative coupling between the individual quantum emitters. Directional emission from an ensemble of

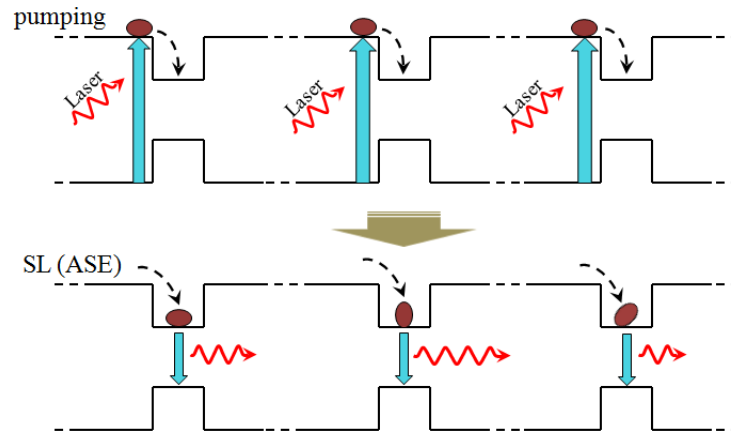


Figure 1.7: Schematic picture of superluminescence (SL) emission from an ensemble of QDs. First charge carriers are generated by a pump laser with energy above the barrier. Then the QDs are incoherently populated by the diffusion of charge carriers into the QDs. Finally, the electron-hole pairs inside the QDs recombine and emit an incoherent emission which is amplified through a stimulated process.

coherently excited atoms has been studied in Ref. [52]. The physical concept of this phenomenon has been employed in experiments such as photon echo [86], self-induced transparency [87], optical solitons [88, 89], lasing without inversion [90], ultraslow light [91] and production of entangled light from phase coherent atoms [92]. In Dicke superradiance, all quantum emitters are initially excited. Now imagine that in an ensemble of N QDs, only one QD is excited but we don't know which one. You might think that such a system should decay with a rate equal to the rate of a single isolated QD, γ_0 . However this system decays with a rate $N\gamma_0$ which is N times faster [93]. This kind of single-photon systems has recently attracted a lot of attention because of its highly potential application for storing quantum information and investigating the physics of virtual processes [53, 94–102]. Another advantage of single-photon states is that it can show enhanced emission even in large samples. As we mentioned earlier, in samples large compared with the emission wavelength, the Dicke superradiance is suppressed and there is even subradiance or radiation trapping in the system. However, even in large ensembles, it is possible to get an enhanced radiation out by preparing the ensemble in the single-photon state. In such a system, the cooperative emission is due to N entangled quantum emitters (not N coherent emitters as in the case of superradiance).

It has been shown in Ref. [95] that if we prepare a single-photon entangled Dicke-like state by means of a laser pulse with wave vector \mathbf{k}_0 , then the following spontaneous emission from such a state will be in the same direction as \mathbf{k}_0 and if we excite such an

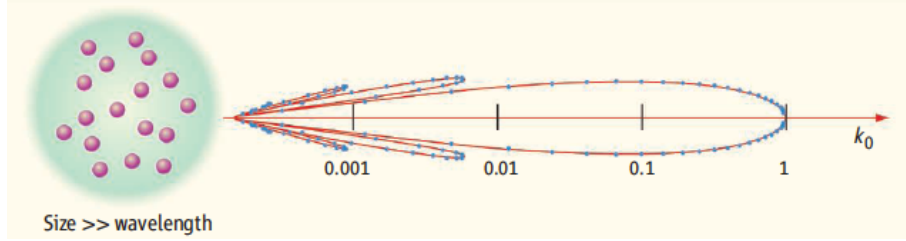


Figure 1.8: For a large atomic sample, the single-photon state results in a radiation pattern that is strongly peaked in the k_0 direction. To a good approximation, the timed excitation yields emission speedup, which is proportional to the number of atoms and the solid diffraction angle given by the squared ratio of the wavelength to the sample size. Evolution of the single-photon timed state in the large sample has much in common with evolution of the symmetric state for a small atomic cloud. Figure and caption from Ref. [93].

ensemble with two photons there will be a phase match between wave vectors of two emitted photons and that of the incident radiation. The schematic picture of this directionality phenomenon is shown in Fig.(1.8). The interesting and fundamental physics behind this strong directionality relies on the excitation timing of quantum emitters positioned at different positions within the ensemble. The QDs or atoms closer to the front of the sample will be excited earlier and QDs at the back will be excited later. This retarded excitation manifests itself as a spatial phase factor, will eventually lead to the directionality of the emitted light. Without such an excitation timing, the radiation will be trapped in the system and the decay rate decreases [101]. This single-photon superradiance phenomenon has been named as the *super of superradiance* [93] and is extensively investigated for atomic clouds.

1.6 Scope of this thesis

In chapter (2), we present the theory of electromagnetism and quantum electrodynamics. We derive the general form of the Master equation formalisms, which is the basis for the calculations and simulations in the remainder of this thesis. In this chapter, after a short introduction of the Maxwells equations, we approach the quantization of electromagnetic fields and, we present the general form of the QD spontaneous emission rates in an arbitrary environment as well as the coherent and incoherent energy transfer rate between QDs due to their mutual dipole-dipole coupling.

In chapter (3), we treat the simplest problem of QD-QD optical coupling where only two QDs are present. We show how the electromagnetic coupling between two QDs can strongly modify the lifetime of the excited system. We show that the main result of coupling is the appearance of two extra emission modes called the superradiant and the subradiant mode. In the first case, the total emission rate from the sample is faster than

the spontaneous emission rate of a single QD, while in the latter, the inverse situation applies. Most importantly, we explain that such a simple double-QD system can act as a quantum antenna in which the nano-scale quantum correlations between the QDs have a remarkable effect on the radiation pattern of the system in the far field. At the end of this chapter, we investigate the influence of the optical coupling between the two QDs on the spectrum of the spontaneous emission. We verify our results for different initial conditions where only one or both QDs can be initially excited. We will see that all of these implications of optical coupling strongly depend on the distance between the two QDs, their initial excitation and the mutual orientation of their dipole moments. The main message of this chapter is that a two-QD system shows a strong directionality of the emission. A two-QD system thus acts as a nanoantenna.

In chapter (4), we approach a more complicated QD structure. We study an infinite number of interacting QDs with parallel dipole moments, arranged in a regular periodic lattice. In this chapter, we assume that the QD states are entangled. The periodicity of the QD lattice is a great help to simplify the open-ended set of differential equations of motion. Instead, of solving this open-ended set of equations, we only have to solve the interaction of a single QD with the optical field modes of a virtual cavity. In this case, all other identical QDs in the QD-lattice constitute the virtual cavity. The spontaneous decay rate of the excited QD is determined by the density of optical field modes of the virtual cavity at the position of the radiating QD. We then extend the concept of the virtual cavity to the case of two intermixed QD lattices. We observe that, in addition to the electromagnetic coupling between the QDs in each separate lattice, there is also optical coupling between the two different QD lattices which leads to a superradiant or subradiant modification of the single lattice spontaneous emission rate. We study the influence of an optical induced phase shift on the spontaneous emission rate as well.

In chapter (5), we again look to the case of a QD lattice, but this time in the weak excitation regime. In this regime, only one QD among an infinitely large number of QDs in the lattice is excited and subsequently, only one photon will be emitted. We assume that the presence of QDs on the lattice points does not disturb the photonic reservoir. In the weak coupling regime, we would be able to separate out the correlated terms between population and coherence. The weak coupling limit allows to obtain simplified equations of motion from which the relevant physical observables can be obtained. We again see that the spontaneous emission rate of a single lattice strongly depends on the lattice periodicity. We finally show that the optical coupling between the two different lattices varies as a function of the translational shift between the two lattices.

In chapter (6), we deal with an even more complicated system, in which the QDs are not uniformly but randomly distributed in a plane. In contrary to chapters 4 and 5, we are not able anymore to bypass the set of an infinite number of differential equations. In this chapter, we try to make some approximations but still keep the main physical concepts of the problem. We treat the problem of the modification of the spontaneous emission rate as a consequence of the quantum correction of the local electromagnetic field acting upon each QD in the ensemble. We show that in samples with dimensions much larger than the emission wavelength, the local-field correction gives rise to the reduction of the spontaneous emission rate known as radiation trapping.

In chapter (7), we provide experimental evidence for the electromagnetic interaction between self-assembled InAs/GaAs QDs which are randomly distributed in a plane and feature a broadened size distribution. We employ the Time Resolved Differential Reflectivity (TRDR) technique to probe the population dynamics of these QDs. In our experimental setup, we are able to look at any desired small part of the QD ensemble by tuning the frequency of the probe beam in resonance with a small fraction of the QD ensemble. This fraction is determined by the probe laser linewidth. We also present excitation power dependent measurements. We compare our experimental data and analysis with our theoretical approach in chapter (6).

Chapter 2

Theoretical foundation: Electrodynamics and the Master Equation approach

In this chapter, we introduce the physical basis required to explain the electromagnetic coupling between different QDs. In the field of light-matter coupling, interaction of light and QDs can be treated in a semiclassical or quantum mechanical framework. In the semiclassical approach, the QD is considered as a two-level dipole with corresponding raising, lowering and population difference operators, but the field is still considered as a classical quantity with its electric and magnetic components. In classical electrodynamics, in order to have any electromagnetic radiation, there should be an oscillating dipole moment in the system which can emit light. But in the absence of any external field, such a dipole cannot be created and we have to manually assume an appropriate value for the initial QD polarization. Moreover, the radiative damping rates do not follow from theory, but rather have to be manually entered into the equation of motions. On the other hand, in quantum electrodynamics, we don't have to make any approximation or manually include additional terms, but all relevant terms will be generated naturally in an accurate way. In the quantum formalism, the spontaneous emission from a sample of QDs as well as the influence of optical coupling between different QDs on the decay time, the directionality and the spectrum of the total spontaneous emission can be treated in detail.

We start with the introduction of classical fields and Maxwell's equations. Then we switch to the quantized field. In general, the electromagnetic field can propagate in a free or homogeneous (isotropic) space or in an anisotropic medium in which only one mode or a group of field modes are available. Such an anisotropic environment is normally called a cavity. In free space, the QD can interact with all the plane-wave field modes that are allowed in the medium, but in a cavity, the QD can only interact with

the cavity modes. This means that if the QD transition energy is in resonance with one of the cavity modes, the excited QD can emit more efficiently and hence its spontaneous emission is enhanced. In the nonresonant situation, the case is vice versa and the emission is suppressed. Then by introducing and making use of the master equation formalism, we indicate how two or more QDs can interact with each other mediated by electromagnetic field modes. If these QDs are located in free space, their interaction is through plane-wave field modes and if they are positioned in a cavity, they can be coupled through the cavity modes. We start with the general form of master equation and then we go deeper into the case where the coupling is mediated by free space plane-wave field modes. At the end, we demonstrate how the spontaneous emission of QDs can be fully described in the quantum electrodynamics approach.

2.1 Maxwell's equations

The fundamental equations that form the foundation of electromagnetic theory are Maxwell's equations. These equations in the differential form are [103]

$$\begin{aligned}\nabla \times \mathbf{E} &= -\frac{\partial \mathbf{B}}{\partial t}, \\ \nabla \times \mathbf{H} &= \mathbf{J} + \frac{\partial \mathbf{D}}{\partial t}, \\ \nabla \cdot \mathbf{D} &= \rho, \\ \nabla \cdot \mathbf{B} &= 0,\end{aligned}\tag{2.1.1}$$

where \mathbf{E} is the electric field intensity, \mathbf{D} is the electric flux density, \mathbf{H} is the magnetic field intensity and \mathbf{B} is the magnetic flux density. The electric current density \mathbf{J} and electric charge density ρ are the sources of electromagnetic fields and are related to each other through the equation of continuity as

$$\nabla \cdot \mathbf{J} = -\frac{\partial \rho}{\partial t},\tag{2.1.2}$$

which originates from the conservation of charge.

In linear, nondispersive and isotropic media, we have also the constitutive relations

$$\begin{aligned}\mathbf{D} &= \epsilon_r \epsilon_0 \mathbf{E}, \\ \mathbf{B} &= \mu_r \mu_0 \mathbf{H},\end{aligned}\tag{2.1.3}$$

where ϵ_0 , μ_0 , ϵ_r and μ_r are the free space permittivity, free space permeability, relative permittivity (dielectric constant) and relative permeability of the medium respectively. In the following of this chapter, we assume $\epsilon_r = \mu_r = 1$.

The remaining fundamental equation is Lorentz's force equation which determines the total electromagnetic force on a charge q to be

$$\mathbf{F} = q (\mathbf{E} + \mathbf{v} \times \mathbf{B})\tag{2.1.4}$$

where \mathbf{v} is the velocity of the moving charge. Although the Maxwell's equations are not independent and the last two terms can be derived from the first two terms by using (2.1.2), the four Maxwell's equations in (2.1.1), together with the equation of continuity (2.1.2), the constitutive relations (2.1.3) and the Lorentz's force equation (2.1.4), provide the necessary framework to predict all macroscopic electromagnetic interactions. The electromagnetic flux density can be represented by the Poynting vector as the electromagnetic energy passing through a unit area within a unit of time. This is mathematically demonstrated by

$$\mathbf{S}(\mathbf{r}, t) = \mathbf{E}(\mathbf{r}, t) \times \mathbf{H}(\mathbf{r}, t). \quad (2.1.5)$$

We will make use of the Poynting vector in next chapters to calculate the spontaneous and reflected emission from specific structures of QDs.

2.2 Field quantization

In order to quantize the electromagnetic field, we should first write the Hamiltonian in terms of coordinates q_i and conjugate momentum p_i so that the dynamics of these quantities are given by

$$\dot{q}_i = \frac{\partial H}{\partial p_i}, \quad \dot{p}_i = -\frac{\partial H}{\partial q_i}, \quad (2.2.1)$$

which yield the equations of motion for the system [104]. Then we should switch from the classical to the quantum mechanical formalism by considering the variables q_i, p_i as operators that satisfy the commutation relation

$$[q_i, p_j] = i\hbar\delta_{ij}. \quad (2.2.2)$$

The noncommutativity of a coordinate and its conjugate momentum is a fundamental postulate of quantum mechanics and brings the Planck's constant into the equations. Finally the solution to Schrödinger's equation must be obtained. In Schrödinger's picture, when the Hamiltonian is not an explicit function of time, the solutions are given by

$$|\psi_n\rangle = \exp\left(-i\frac{E_n}{\hbar}t\right)|n\rangle, \quad (2.2.3)$$

where $|n\rangle$ and E_n are respectively the eigenvectors and eigenvalues of the Hamiltonian operator H that satisfy the time-independent eigenvalue equation

$$H|n\rangle = E_n|n\rangle. \quad (2.2.4)$$

2.2.1 Quantization of cavity field modes

In this section, we quantize the electromagnetic field modes of a cavity. We assume that our cavity resonator contains no free charge or current with walls that are perfectly

conducting. On one hand, the electromagnetic energy stored in such a cavity is

$$\mathbb{E} = \frac{1}{2} \int (\epsilon_0 \mathbf{E} \cdot \mathbf{E}^* + \mu_0 \mathbf{H} \cdot \mathbf{H}^*) dV, \quad (2.2.5)$$

where \mathbf{E} and \mathbf{H} are the electric and magnetic fields respectively. On the other hand, by identifying $q_i(t)$ and $p_i(t)$ as the coordinates and conjugate momentum, respectively, the Hamiltonian of the system becomes

$$H = \frac{1}{2} \sum_{\mathbf{k}} (p_{\mathbf{k}}^2 + \omega_{\mathbf{k}}^2 q_{\mathbf{k}}^2). \quad (2.2.6)$$

If we equal the Hamiltonian of the system (2.2.6) to the energy stored in the resonator(2.2.5), we see that the field distribution within the cavity can be expressed as a sum of normal mode solutions like

$$\mathbf{E}(\mathbf{r}, t) = -\frac{1}{\sqrt{\epsilon_0}} \sum_{\mathbf{k}} p_{\mathbf{k}}(t) \mathbf{E}_{\mathbf{k}}(\mathbf{r}), \quad \mathbf{H}(\mathbf{r}, t) = \frac{1}{\sqrt{\mu_0}} \sum_{\mathbf{k}} \omega_{\mathbf{k}} q_{\mathbf{k}}(t) \mathbf{H}_{\mathbf{k}}(\mathbf{r}), \quad (2.2.7)$$

where $\mathbf{E}_{\mathbf{k}}(\mathbf{r})$ and $\mathbf{H}_{\mathbf{k}}(\mathbf{r})$ are the orthonormal field modes and satisfy the Maxwell equations. From the equations of motion (2.2.1), we can check that all Maxwell equations are satisfied, which indicates that the field distributions in (2.2.7) are appropriate choices.

The Hamiltonian for the electromagnetic field (2.2.6), is identical to the Hamiltonian for a summation of unit mass harmonic oscillators. Therefore the problem of field quantization reduces to the problem of the quantization of a harmonic oscillator.

For solving the eigenvalue equation (2.2.4), we follow the so called second quantization approach in which we should construct a set of eigenvectors and determine their corresponding eigenvalues by a technique based on the manipulation of the abstract bra and ket formalism [105]. We begin by defining very useful following operators:

$$\begin{aligned} a_{\mathbf{k}} &= \frac{1}{\sqrt{2\hbar\omega_{\mathbf{k}}}} (\omega_{\mathbf{k}} q_{\mathbf{k}} + ip_{\mathbf{k}}), \\ a_{\mathbf{k}}^{\dagger} &= \frac{1}{\sqrt{2\hbar\omega_{\mathbf{k}}}} (\omega_{\mathbf{k}} q_{\mathbf{k}} - ip_{\mathbf{k}}). \end{aligned} \quad (2.2.8)$$

where $a_{\mathbf{k}}$ and $a_{\mathbf{k}}^{\dagger}$ are the annihilation and creation operators of photons. Since p and q are observable and hence Hermitian and they satisfy the commutation relation $[q, p] = i\hbar$, therefore, $a_{\mathbf{k}}^{\dagger}$ is the adjoint of $a_{\mathbf{k}}$ and satisfies the commutation relation

$$[a_{\mathbf{k}}, a_{\mathbf{k}}^{\dagger}] = 1. \quad (2.2.9)$$

The operators p and q can be written in terms of $a_{\mathbf{k}}$ and $a_{\mathbf{k}}^{\dagger}$ as

$$q_{\mathbf{k}} = \sqrt{\frac{\hbar}{2\omega_{\mathbf{k}}}} (a_{\mathbf{k}}^{\dagger} + a_{\mathbf{k}}), \quad p_{\mathbf{k}} = i\sqrt{\frac{\hbar\omega_{\mathbf{k}}}{2}} (a_{\mathbf{k}}^{\dagger} - a_{\mathbf{k}}). \quad (2.2.10)$$

Substitution of (2.2.10) into (2.2.6) by applying the commutation relation (2.2.9) yields the Hamiltonian

$$H = \hbar \sum_{\mathbf{k}} \omega_{\mathbf{k}} \left(a_{\mathbf{k}}^{\dagger} a_{\mathbf{k}} + \frac{1}{2} \right), \quad (2.2.11)$$

and substitution of (2.2.10) into (2.2.7) yields expressions for the electric and magnetic fields in terms of the $a_{\mathbf{k}}$ and $a_{\mathbf{k}}^\dagger$ operators,

$$\begin{aligned}\mathbf{E} &= -i \sum_{\mathbf{k}} \sqrt{\frac{\hbar\omega_{\mathbf{k}}}{2\varepsilon_0}} \mathbf{E}_{\mathbf{k}}(\mathbf{r}) (a_{\mathbf{k}}^\dagger - a_{\mathbf{k}}), \\ \mathbf{H} &= \sum_{\mathbf{k}} \sqrt{\frac{\hbar\omega_{\mathbf{k}}}{2\mu_0}} \mathbf{H}_{\mathbf{k}}(\mathbf{r}) (a_{\mathbf{k}}^\dagger + a_{\mathbf{k}}).\end{aligned}\quad (2.2.12)$$

By choosing the cavity modes as $\mathbf{u}_{\mathbf{k}}(\mathbf{r}) = i\mathbf{E}_{\mathbf{k}}(\mathbf{r})$, Eq. (2.2.12) can be written in the form

$$\begin{aligned}\mathbf{E} &= \sum_{\mathbf{k}} \sqrt{\frac{\hbar\omega_{\mathbf{k}}}{2\varepsilon_0}} (\mathbf{u}_{\mathbf{k}}(\mathbf{r}) a_{\mathbf{k}} + \mathbf{u}_{\mathbf{k}}^*(\mathbf{r}) a_{\mathbf{k}}^\dagger), \\ \mathbf{H} &= \sum_{\mathbf{k}} \sqrt{\frac{\hbar\omega_{\mathbf{k}}}{2\mu_0}} \hat{\mathbf{e}}_{\mathbf{k}} \times (\mathbf{u}_{\mathbf{k}}(\mathbf{r}) a_{\mathbf{k}} + \mathbf{u}_{\mathbf{k}}^*(\mathbf{r}) a_{\mathbf{k}}^\dagger).\end{aligned}\quad (2.2.13)$$

This form, in which the fields are expressed in terms of the cavity modes will be used in next chapters to serve as the electromagnetic field in a cavity made up by periodic lattices of quantum dots.

2.2.2 Quantization of plane waves

In this section, we expand the field in terms of propagating plane wave basis functions instead of the orthonormal modes in a cavity. The electromagnetic field propagates as plane waves in free space or within large enough isotropic and homogeneous media. The wave equation for the electric field \mathbf{E} in a source-free region is

$$\nabla \times (\nabla \times \mathbf{E}) + \frac{n^2}{c^2} \frac{\partial^2 \mathbf{E}}{\partial t^2} = 0, \quad (2.2.14)$$

where $c = 1/\sqrt{\mu_0\varepsilon_0}$ and $n = \sqrt{\mu_h\varepsilon_h/\mu_0\varepsilon_0}$ is the index of refraction. A similar equation can be derived for \mathbf{H} . The solutions of the wave equation (4.2.6) can be written in terms of plane wave exponentials of the form $\hat{\mathbf{e}}_s e^{\pm i(\omega_{\mathbf{k}}t - \mathbf{k}\cdot\mathbf{r})}$, where $\hat{\mathbf{e}}_s$ is a unit vector in the polarization direction and \mathbf{k} is the propagation vector. There are two independent polarization direction, $s = 1, 2$, corresponding to each \mathbf{k} which due to the transversality condition are orthogonal to each other and to \mathbf{k} as well. By applying the identity $\nabla \times (\hat{\mathbf{e}}_s e^{\pm i\mathbf{k}\cdot\mathbf{r}}) = \mp i (\hat{\mathbf{e}}_s \times \mathbf{k}) e^{\pm i\mathbf{k}\cdot\mathbf{r}}$, we find that \mathbf{k} and $\omega_{\mathbf{k}}$ are related by $k^2 = \omega_{\mathbf{k}}^2 n^2 / c^2$ where $k^2 \equiv \mathbf{k} \cdot \mathbf{k}$.

In order to express the fields in terms of discrete and orthogonal modes, we can assume the fields in a cube with spatial dimensions L and volume $V = L^3$ in which the electric and magnetic fields satisfy periodic boundary conditions on opposite faces of the cube. The periodic boundary conditions fulfill the requirement that translation by a distance L parallel to the edges of the cube should not change the value of the exponential solutions. The requirement is satisfied provided that

$$k_x = \frac{2\pi n_x}{L}, \quad k_y = \frac{2\pi n_y}{L}, \quad k_z = \frac{2\pi n_z}{L}, \quad (2.2.15)$$

where n_x , n_y , and n_z are integers from $-\infty$ to ∞ . In this framework, the propagation constants are thus restricted to a discrete set of values.

If we choose exponential solutions in the form of

$$\mathbf{U}_{\mathbf{k}s}(\mathbf{r}) = \frac{1}{\sqrt{V}} \hat{\mathbf{e}}_s e^{-i\mathbf{k}\cdot\mathbf{r}}, \quad (2.2.16)$$

then the $\mathbf{U}_{\mathbf{k}s}(\mathbf{r})$ functions satisfy the orthonormality condition

$$\int_V \mathbf{U}_{\mathbf{k}s}^*(\mathbf{r}) \cdot \mathbf{U}_{\mathbf{k}'s'}(\mathbf{r}) dV = \delta_{\mathbf{k}\mathbf{k}'} \delta_{ss'} \quad (2.2.17)$$

where the integral is over the volume of the cube, V . By substituting Eq.(2.2.16) in Eq.(2.2.13), the electric and magnetic fields can be written as the summation of quantized plane-wave modes

$$\begin{aligned} \mathbf{E} &= i \sum_{\mathbf{k},s} \sqrt{\frac{\hbar\omega_{\mathbf{k}}}{2\varepsilon_0 V}} \hat{\mathbf{e}}_s \left[a_{\mathbf{k}s} e^{i\mathbf{k}\cdot\mathbf{r}} - a_{\mathbf{k}s}^\dagger e^{-i\mathbf{k}\cdot\mathbf{r}} \right], \\ \mathbf{H} &= i \sum_{\mathbf{k},s} \sqrt{\frac{\hbar\omega_{\mathbf{k}}}{2\mu_0 V}} (\hat{\mathbf{e}}_{\mathbf{k}} \times \hat{\mathbf{e}}_s) \left[a_{\mathbf{k}s} e^{i\mathbf{k}\cdot\mathbf{r}} - a_{\mathbf{k}s}^\dagger e^{-i\mathbf{k}\cdot\mathbf{r}} \right]. \end{aligned} \quad (2.2.18)$$

It is obvious that the electric and magnetic fields are orthogonal and they are both perpendicular to the wave propagation direction \mathbf{k} .

If the Hamiltonian is chosen to be the electromagnetic energy within the normalization volume V as in Eq.(2.2.5), then we arrive at

$$H = \hbar \sum_{\mathbf{k},s} \omega_{\mathbf{k}} \left(a_{\mathbf{k}s}^\dagger a_{\mathbf{k}s} + \frac{1}{2} \right), \quad (2.2.19)$$

for the Hamiltonian. With the same procedure explained in the last section for resonators, we can conclude that $a_{\mathbf{k}s}$ and $a_{\mathbf{k}s}^\dagger$ are the annihilation and creation operators of photons respectively.

If the volume becomes very large, so that $L \rightarrow \infty$, the summations in the expressions of this section are replaced by integrals

$$\frac{1}{\sqrt{V}} \sum_{\mathbf{k}} \rightarrow \frac{1}{(2\pi)^{3/2}} \int d\mathbf{k}, \quad (2.2.20)$$

and the orthogonality relationship (2.2.17) becomes

$$\frac{1}{(2\pi)^{3/2}} \int_V \mathbf{U}_{\mathbf{k}s}^*(\mathbf{r}) \cdot \mathbf{U}_{\mathbf{k}'s'}(\mathbf{r}) dV = \delta(\mathbf{k}' - \mathbf{k}) \delta_{ss'}, \quad (2.2.21)$$

where $\delta(\mathbf{k}' - \mathbf{k})$ is the Dirac delta function. We will make use of the quantized plane-wave modes to describe the electromagnetic coupling of QDs in a two-QD system and in a planar sample of QDs considered as a thin film in which all QDs are randomly and uniformly distributed.

2.3 Master equation formalism

The standard formalism for the calculations of the time evolution and correlation properties of a collective system of QDs (dipoles) is the master equation method. In this approach, the dynamics are studied in terms of the reduced density operator $\hat{\rho}_{\text{QD}}$ of the atomic system interacting with the quantized electromagnetic (EM) field regarded as a reservoir [106–109]. There are many possible realizations of reservoirs. The typical reservoir to which QD systems are coupled is the quantized three-dimensional multi-mode field (plane-wave modes) which we will use to explain the radiative coupling between two QDs located in free space or a dielectric host medium. This kind of reservoir can be modeled as a vacuum field whose modes are in ordinary vacuum states, or in thermal states, or even in squeezed vacuum states. In another realization of the electromagnetic reservoir, we will deal with the quantized electromagnetic modes confined in a cavity built up with the neighboring QDs in order to interpret the optical properties of QDs in a QD lattice. The major advantage of the master equation is that it allows us to consider the evolution of the QDs and the electromagnetic field entirely in terms of average values of QD operators. We can derive equations of motion for expectation values of an arbitrary combination of the QD operators, and solve these equations for time-dependent averages or the steady-state. In this section, we will give an outline of the derivation of the master equation of a system of N nonidentical nonoverlapping QDs coupled to a quantized EM field. In general forms, The QDs are modeled as two-level systems, with excited state $|e_i\rangle$, ground state $|g_i\rangle$, transition frequency ω_i , and transition dipole moments μ_i . We assume that the QDs are located at different points $\mathbf{r}_1, \dots, \mathbf{r}_N$, having different transition frequencies $\omega_1 \neq \omega_2 \neq \dots \neq \omega_N$, and different transition dipole moments $\mu_1 \neq \mu_2 \neq \dots \neq \mu_N$.

2.3.1 Interaction of quantum dots positioned in a cavity

In the electric dipole approximation, the total Hamiltonian of a system of quantum dots combined with the electromagnetic field is given by $\hat{H} = \hat{H}_0 + \hat{H}_I + \hat{H}_{\text{Ex}}$, where \hat{H}_0 is the Hamiltonian of the noninteracting QDs and the EM field, \hat{H}_I is the interaction Hamiltonian between the QDs and the EM field modes and \hat{H}_{Ex} is the interaction Hamiltonian of the QDs with an external field like a classical coherent laser field [110],

$$\begin{aligned}\hat{H}_0 &= \sum_{i=1}^N \hbar\omega_i S_i^z + \sum_{\mathbf{k}} \hbar\omega_{\mathbf{k}} \left(\hat{a}_{\mathbf{k}}^\dagger \hat{a}_{\mathbf{k}} + \frac{1}{2} \right), \\ \hat{H}_I &= - \sum_i \mu_i \cdot \mathbf{E}(\mathbf{r}_i, t) = - \sum_i \sum_{\mathbf{k}} \sqrt{\frac{\hbar\omega_{\mathbf{k}}}{2\epsilon_0}} (\mu_{0i} S_i^+ + \mu_{0i}^* S_i^-) (\mathbf{u}_{\mathbf{k}}(\mathbf{r}_i) \mathbf{a}_{\mathbf{k}}(t) + \text{H.c.}), \\ \hat{H}_{\text{Ex}} &= - \sum_i \mu_i \cdot \mathbf{E}_L(\mathbf{r}_i, t) = - \frac{1}{2} \sum_i (\mu_{0i} S_i^+ + \mu_{0i}^* S_i^-) \cdot \mathbf{E}_L(t) \left(e^{-i(\omega_L t - \mathbf{k}_L \cdot \mathbf{r}_i)} + \text{H.c.} \right),\end{aligned}\tag{2.3.1}$$

where $S_i^+ = |e_i\rangle \langle g_i|$ and $S_i^- = |g_i\rangle \langle e_i|$ are the dipole raising and lowering operators and $S_i^z = (|e_i\rangle \langle e_i| - |g_i\rangle \langle g_i|)/2$ is the population operator of the i th QD. In the Eq.(2.3.1), we

have made use of the definition for the electric field modes as

$$\begin{aligned}\mathbf{E}(\mathbf{r}, t) &= \mathbf{E}^{(+)}(\mathbf{r}, t) + \mathbf{E}^{(-)}(\mathbf{r}, t), \\ \mathbf{E}^{(+)}(\mathbf{r}, t) &= \sum_{\mathbf{k}} \sqrt{\frac{\hbar\omega_{\mathbf{k}}}{2\varepsilon_0}} \mathbf{u}_{\mathbf{k}}(\mathbf{r}) \mathbf{a}_{\mathbf{k}}(t)\end{aligned}\quad (2.3.2)$$

where $\mathbf{E}^{(-)} = (\mathbf{E}^{(+)})^*$ are the positive and negative frequency parts of the complex electric field [22] and the external electric field is assumed to be a monochromatic plane wave

$$\mathbf{E}_L(\mathbf{r}, t) = \frac{1}{2} \mathbf{E}_L(t) \left(e^{-i(\omega_L t - \mathbf{k}_L \cdot \mathbf{r})} + e^{i(\omega_L t - \mathbf{k}_L \cdot \mathbf{r})} \right), \quad (2.3.3)$$

where $\mathbf{E}_L(t)$ is the time-dependent amplitude and ω_L and \mathbf{k}_L are the frequency and the wave vector of the external electric field respectively. The dipole moment of each QD is also defined as

$$\mu_i = \mu_{0i} S_i^+ + \mu_{0i}^* S_i^-, \quad (2.3.4)$$

where μ_0 is the transition dipole matrix element [111]. The transition of the electric dipole moment is allowed for $\Delta m = 0, \pm 1$, where m is the secondary total angular momentum quantum number and parameterizes the z -projection of the total angular momentum. If the transition from state $|e\rangle$ to state $|g\rangle$ corresponds to a $\Delta m = 0$ transition of a real quantum dot, we may take μ_0 to be a real vector. On the other hand, if the transition corresponds to a $\Delta m = \pm 1$ transition which might be induced for instance by a circularly polarized light, μ_0 should be considered to be a complex vector. In most of the cases, we can treat μ_0 as a real vector which simplifies (2.3.4) to

$$\mu_i = \mu_{0i} (S_i^+ + S_i^-). \quad (2.3.5)$$

For simplicity we ignore the contribution of the external field and proceed in the interaction picture in which the total Hamiltonian evolves in time according to the interaction with the vacuum field. At the end, we will add the effect of the external field. Therefore the total Hamiltonian (2.3.1) is transferred to

$$\hat{H}(t) = e^{i\hat{H}_0 t/\hbar} (\hat{H} - \hat{H}_0) e^{-i\hat{H}_0 t/\hbar} = \hat{V}(t), \quad (2.3.6)$$

where

$$\hat{V}(t) = - \sum_{\mathbf{k}} \sum_{i=1}^N \sqrt{\frac{\hbar\omega_{\mathbf{k}}}{2\varepsilon_0}} \left\{ \left(\mu_i S_i^+ e^{-i(\omega_{\mathbf{k}} - \omega_i)t} + S_i^- e^{-i(\omega_{\mathbf{k}} + \omega_i)t} \right) \cdot \mathbf{u}_{\mathbf{k}}(\mathbf{r}_i) \mathbf{a}(t) + \text{H.c.} \right\}. \quad (2.3.7)$$

We will follow the Master Equation approach in which the time evolution of the collection of QDs interacting with the electromagnetic field is considered in terms of the density operator $\hat{\rho}_{\text{QD-F}}$ characterizing the statistical state of the combined system of the QDs and the field. The transformation of the density operator into the interaction picture reads

$$\tilde{\rho}_{\text{QD-F}} = e^{i\hat{H}_0 t/\hbar} \hat{\rho}_{\text{QD-F}} e^{-i\hat{H}_0 t/\hbar}. \quad (2.3.8)$$

The time evolution of the transformed density operator of the combined system in the interaction picture obeys the equation

$$\frac{\partial}{\partial t} \tilde{\rho}_{\text{QD-F}}(t) = \frac{1}{i\hbar} [\hat{V}(t), \tilde{\rho}_{\text{QD-F}}(t)]. \quad (2.3.9)$$

The differential equation in (2.3.9) can be simply solved. Taking

$$\tilde{\rho}_{\text{QD-F}}(0)$$

as the initial value of the reduced density matrix, we can write from Eq.(2.3.9),

$$\tilde{\rho}_{\text{QD-F}}(t) = \tilde{\rho}_{\text{QD-F}}(0) + \frac{1}{i\hbar} \int_0^t dt' [\hat{V}(t'), \tilde{\rho}_{\text{QD-F}}(t')]. \quad (2.3.10)$$

Substituting (2.3.10) in (2.3.9), we can write Eq.(2.3.9) to the second order in $\hat{V}(t)$,

$$\frac{\partial}{\partial t} \tilde{\rho}_{\text{QD-F}}(t) = \frac{1}{i\hbar} [\hat{V}(t), \tilde{\rho}_{\text{QD-F}}(0)] - \frac{1}{\hbar^2} \int_0^t dt' \{[\hat{V}(t), [\hat{V}(t'), \tilde{\rho}_{\text{QD-F}}(t')]]\}. \quad (2.3.11)$$

We assume that initially there is no correlation between the quantum dots and the field so that it is allowed to factorize the initial density operator of the combined system as

$$\tilde{\rho}_{\text{QD-F}}(0) = \tilde{\rho}_{\text{QD}}(0) \tilde{\rho}_{\text{F}}(0), \quad (2.3.12)$$

where $\hat{\rho}_{\text{QD}}$ and $\hat{\rho}_{\text{F}}$ are the density operators of the QD system and the vacuum field respectively. We now employ the Born approximation [112], in which the interaction between the QD system and the field is supposed to be weak, and there is no back reaction effect of the QDs on the field. So the state of the EM field does not change in time, and we can write the density operator $\tilde{\rho}_{\text{QD-F}}(t')$, appearing in (2.3.12), as

$$\tilde{\rho}_{\text{QD-F}}(t') = \tilde{\rho}_{\text{QD}}(t') \tilde{\rho}_{\text{F}}(0). \quad (2.3.13)$$

Under this approximation and the initial condition introduced above, we find that to the second order in $\hat{V}(t)$, after changing the time variable to $t' \rightarrow t - \tau$, Eq.(2.3.9) leads to the reduced density operator for the QDs, $\tilde{\rho}_{\text{QD}}(t) = \text{Tr}_{\text{F}} \tilde{\rho}_{\text{QD-F}}(t)$, satisfying the integro-differential equation

$$\begin{aligned} \frac{\partial}{\partial t} \tilde{\rho}(t) &= \frac{1}{i\hbar} \text{Tr}_{\text{F}} [\hat{V}(t), \tilde{\rho}(0) \tilde{\rho}_{\text{F}}(0)] \\ &\quad - \frac{1}{\hbar^2} \int_0^t d\tau \text{Tr}_{\text{F}} \{[\hat{V}(t), [\hat{V}(t-\tau), \tilde{\rho}(t-\tau) \tilde{\rho}_{\text{F}}(0)]]\}, \end{aligned} \quad (2.3.14)$$

where we have used a shorter notation $\tilde{\rho} = \tilde{\rho}_{\text{QD}}$. After substituting the explicit form of $\hat{V}(t)$ into Eq.(2.3.14), we find that the evolution of the density operator depends on the first- and second-order correlation functions of the vacuum field operators. In the absence of any squeezing in the vacuum field, the correlation functions are given by [113]

$$\begin{aligned} \text{Tr}_{\text{F}} [\tilde{\rho}_{\text{F}}(0) \hat{a}_{\mathbf{k}s}] &= \text{Tr}_{\text{F}} [\tilde{\rho}_{\text{F}}(0) \hat{a}_{\mathbf{k}s}^\dagger] = 0, \\ \text{Tr}_{\text{F}} [\tilde{\rho}_{\text{F}}(0) \hat{a}_{\mathbf{k}s} \hat{a}_{\mathbf{k}'s'}^\dagger] &= \delta^3(\mathbf{k} - \mathbf{k}'), \\ \text{Tr}_{\text{F}} [\tilde{\rho}_{\text{F}}(0) \hat{a}_{\mathbf{k}s}^\dagger \hat{a}_{\mathbf{k}'s'}] &= \text{Tr}_{\text{F}} [\tilde{\rho}_{\text{F}}(0) \hat{a}_{\mathbf{k}s} \hat{a}_{\mathbf{k}'s'}] = \text{Tr}_{\text{F}} [\tilde{\rho}_{\text{F}}(0) \hat{a}_{\mathbf{k}s}^\dagger \hat{a}_{\mathbf{k}'s'}^\dagger] = 0. \end{aligned} \quad (2.3.15)$$

In the next step, using the correlation functions in (2.3.15), the general master equation (2.3.14) can be written as

$$\begin{aligned} \frac{\partial \tilde{\rho}}{\partial t} = & \sum_{i,j=1}^N \left\{ S_i^+ [S_j^-, \hat{X}_{ij}^1] + S_i^- [S_j^+, \hat{X}_{ij}^2] + [\hat{X}_{ij}^3, S_i^+] S_j^- + [\hat{X}_{ij}^4, S_i^-] S_j^+ \right\} \\ & + \left\{ S_i^+ [S_j^+, \hat{X}_{ij}^5] + S_i^- [S_j^-, \hat{X}_{ij}^6] + [\hat{X}_{ij}^7, S_i^+] S_j^+ + [\hat{X}_{ij}^8, S_i^-] S_j^- \right\}, \end{aligned} \quad (2.3.16)$$

where the two-time evolution operators are

$$\begin{aligned} \hat{X}_{ij}^1(t) &= -\frac{e^{i(\omega_i - \omega_j)t}}{\hbar^2} \sum_{\mathbf{k}} \frac{\hbar \omega_{\mathbf{k}}}{2\varepsilon_0} [\boldsymbol{\mu}_i \cdot \mathbf{u}_{\mathbf{k}}(\mathbf{r}_i)] [\boldsymbol{\mu}_j^* \cdot \mathbf{u}_{\mathbf{k}}^*(\mathbf{r}_j)] \int_0^t d\tau \tilde{\rho}(t - \tau) e^{-i(\omega_{\mathbf{k}} - \omega_j)\tau}, \\ \hat{X}_{ij}^2(t) &= -\frac{e^{-i(\omega_i - \omega_j)t}}{\hbar^2} \sum_{\mathbf{k}} \frac{\hbar \omega_{\mathbf{k}}}{2\varepsilon_0} [\boldsymbol{\mu}_i \cdot \mathbf{u}_{\mathbf{k}}(\mathbf{r}_i)] [\boldsymbol{\mu}_j^* \cdot \mathbf{u}_{\mathbf{k}}^*(\mathbf{r}_j)] \int_0^t d\tau \tilde{\rho}(t - \tau) e^{-i(\omega_{\mathbf{k}} + \omega_j)\tau}, \\ \hat{X}_{ij}^3(t) &= -\frac{e^{i(\omega_i - \omega_j)t}}{\hbar^2} \sum_{\mathbf{k}} \frac{\hbar \omega_{\mathbf{k}}}{2\varepsilon_0} [\boldsymbol{\mu}_i \cdot \mathbf{u}_{\mathbf{k}}(\mathbf{r}_i)] [\boldsymbol{\mu}_j^* \cdot \mathbf{u}_{\mathbf{k}}^*(\mathbf{r}_j)] \int_0^t d\tau \tilde{\rho}(t - \tau) e^{i(\omega_{\mathbf{k}} - \omega_i)\tau}, \\ \hat{X}_{ij}^4(t) &= -\frac{e^{-i(\omega_i - \omega_j)t}}{\hbar^2} \sum_{\mathbf{k}} \frac{\hbar \omega_{\mathbf{k}}}{2\varepsilon_0} [\boldsymbol{\mu}_i \cdot \mathbf{u}_{\mathbf{k}}(\mathbf{r}_i)] [\boldsymbol{\mu}_j^* \cdot \mathbf{u}_{\mathbf{k}}^*(\mathbf{r}_j)] \int_0^t d\tau \tilde{\rho}(t - \tau) e^{i(\omega_{\mathbf{k}} + \omega_i)\tau}, \\ \hat{X}_{ij}^5(t) &= -\frac{e^{i(\omega_i + \omega_j)t}}{\hbar^2} \sum_{\mathbf{k}} \frac{\hbar \omega_{\mathbf{k}}}{2\varepsilon_0} [\boldsymbol{\mu}_i \cdot \mathbf{u}_{\mathbf{k}}(\mathbf{r}_i)] [\boldsymbol{\mu}_j^* \cdot \mathbf{u}_{\mathbf{k}}^*(\mathbf{r}_j)] \int_0^t d\tau \tilde{\rho}(t - \tau) e^{-i(\omega_{\mathbf{k}} + \omega_j)\tau}, \\ \hat{X}_{ij}^6(t) &= -\frac{e^{-i(\omega_i + \omega_j)t}}{\hbar^2} \sum_{\mathbf{k}} \frac{\hbar \omega_{\mathbf{k}}}{2\varepsilon_0} [\boldsymbol{\mu}_i \cdot \mathbf{u}_{\mathbf{k}}(\mathbf{r}_i)] [\boldsymbol{\mu}_j^* \cdot \mathbf{u}_{\mathbf{k}}^*(\mathbf{r}_j)] \int_0^t d\tau \tilde{\rho}(t - \tau) e^{-i(\omega_{\mathbf{k}} - \omega_j)\tau}, \\ \hat{X}_{ij}^7(t) &= -\frac{e^{i(\omega_i + \omega_j)t}}{\hbar^2} \sum_{\mathbf{k}} \frac{\hbar \omega_{\mathbf{k}}}{2\varepsilon_0} [\boldsymbol{\mu}_i \cdot \mathbf{u}_{\mathbf{k}}(\mathbf{r}_i)] [\boldsymbol{\mu}_j^* \cdot \mathbf{u}_{\mathbf{k}}^*(\mathbf{r}_j)] \int_0^t d\tau \tilde{\rho}(t - \tau) e^{i(\omega_{\mathbf{k}} - \omega_i)\tau}, \\ \hat{X}_{ij}^8(t) &= -\frac{e^{-i(\omega_i + \omega_j)t}}{\hbar^2} \sum_{\mathbf{k}} \frac{\hbar \omega_{\mathbf{k}}}{2\varepsilon_0} [\boldsymbol{\mu}_i \cdot \mathbf{u}_{\mathbf{k}}(\mathbf{r}_i)] [\boldsymbol{\mu}_j^* \cdot \mathbf{u}_{\mathbf{k}}^*(\mathbf{r}_j)] \int_0^t d\tau \tilde{\rho}(t - \tau) e^{i(\omega_{\mathbf{k}} + \omega_i)\tau}. \end{aligned} \quad (2.3.17)$$

In general, as you can see in (2.3.17), the state of the QD system depends on its past history, because its earlier states induce some changes in the vacuum field reservoir which in turn affects the present state of the QD system. If, however the photon reservoir is a large system maintained in thermal equilibrium, we don't expect the reservoir to preserve the minor changes brought by its interaction with the QD system for a long time and therefore it cannot significantly affect the future state of the QDs. This is the Markov approximation in which the dynamics of the QD system has a slow time scale while the photonic reservoir correlation functions decay much faster (13). In another words, the Markov approximation holds when there is no memory in the system. In this case, the density operator $\tilde{\rho}(t - \tau)$ can be replaced by $\tilde{\rho}(t)$ and the integral in (2.3.17) is extended

to infinity. We can perform the integration over τ and obtain [114]

$$\lim_{t \rightarrow \infty} \int_0^t d\tau \tilde{\rho}(t - \tau) e^{i(\omega_0 \pm \omega_k)\tau} \approx \tilde{\rho}(t) \left[\pi \delta(\omega_0 \pm \omega_k) + i \frac{P}{(\omega_0 \pm \omega_k)} \right], \quad (2.3.18)$$

where P represents the principal value of the integral. To further simplify this expression, we will now introduce the coupling parameters γ_{ij} and Ω_{ij} , which read

$$\gamma_{ij} = \frac{\pi}{\hbar^2} \sum_{\mathbf{k}} \frac{\hbar \omega_{\mathbf{k}}}{2\epsilon_0} (\boldsymbol{\mu}_i \cdot \mathbf{u}_{\mathbf{k}}) (\boldsymbol{\mu}_j^* \cdot \mathbf{u}_{\mathbf{k}}^*) \delta(\omega_{\mathbf{k}} - \omega_0) \quad (2.3.19)$$

and

$$\Omega_{ij}^{(\pm)} = \frac{1}{\hbar^2} \sum_{\mathbf{k}} \frac{\hbar \omega_{\mathbf{k}}}{2\epsilon_0} (\boldsymbol{\mu}_i \cdot \mathbf{u}_{\mathbf{k}}) (\boldsymbol{\mu}_j^* \cdot \mathbf{u}_{\mathbf{k}}^*) \frac{P}{\omega_{\mathbf{k}} \pm \omega_0}, \quad (2.3.20)$$

where the parameter γ_{ij} is the spontaneous energy transfer rate between i th and j th quantum dots and the parameters $\Omega_{ij}^{(\pm)}$ describe the energy shift of the QD levels due to the dipole-dipole coupling. The combination of (2.3.16)-(2.3.20) leads to

$$\begin{aligned} \frac{\partial \tilde{\rho}}{\partial t} = & -i \sum_{i=1}^N \delta_i [S_i^z, \tilde{\rho}] - i \sum_{i \neq j}^N \Omega_{ij} e^{i(\omega_i - \omega_j)t} [S_i^+ S_j^-, \tilde{\rho}] \\ & - \sum_{i,j=1}^N \gamma_{ij} e^{i(\omega_i - \omega_j)t} \left(\tilde{\rho} S_i^+ S_j^- + S_i^+ S_j^- \tilde{\rho} - 2S_j^- \tilde{\rho} S_i^+ \right) \\ & - \left(\gamma_{ij} - i\Omega_{ij}^{(-)} \right) e^{-i(\omega_i + \omega_j)t} \left(S_i^- S_j^- \tilde{\rho} - S_i^- \tilde{\rho} S_j^- \right) \\ & - \left(\gamma_{ij} + i\Omega_{ij}^{(-)} \right) e^{i(\omega_i + \omega_j)t} \left(\tilde{\rho} S_i^+ S_j^+ - S_i^+ \tilde{\rho} S_j^+ \right) \\ & - i\Omega_{ij}^{(+)} e^{-i(\omega_i + \omega_j)t} \left(\tilde{\rho} S_i^- S_j^- - S_i^- \tilde{\rho} S_j^- \right) \\ & + i\Omega_{ij}^{(+)} e^{i(\omega_i + \omega_j)t} \left(S_i^+ S_j^+ \tilde{\rho} - S_i^+ \tilde{\rho} S_j^+ \right). \end{aligned} \quad (2.3.21)$$

where

$$\delta_i = \Omega_{ii}^{(+)} - \Omega_{ii}^{(-)}, \quad (2.3.22)$$

is a part of the Lamb shift of the QD levels and is usually included into the QD frequencies ω_i and is not often explicitly included in the master equations, while

$$\Omega_{ij} = - \left(\Omega_{ij}^{(+)} + \Omega_{ij}^{(-)} \right) (i \neq j), \quad (2.3.23)$$

arises from the interaction between the QDs through the vacuum field. It is clear from Eq.(2.3.23) that the parameter Ω_{ij} contributes to the coherent (dipole-dipole) coupling between the quantum dots through the vacuum field. Thus, the collective interactions between the QDs give rise not only to the modified dissipative spontaneous emission but also lead to a coherent coupling between the QDs. The collective coupling parameters γ_{ij} and Ω_{ij} determine the collective properties of the ensemble of coupled QDs. The incoherent coupling parameter γ_{ij} introduces an incoherent coupling between QDs mediated by the photon field. This means that the spontaneous emission from one of

the QDs influences the spontaneous emission from other QDs in the ensemble. The coherent interaction parameter Ω_{ij} represents a coherent dipole-dipole interaction between the QDs in which the population is coherently transferred back and forth from one QD to the other.

In the interaction Hamiltonian, in the Rotating-Wave-Approximation (RWA) [114] in which we ignore all fast oscillating terms at higher frequencies, $2\omega_i$, $\omega_i + \omega_j$, the general master equation (2.3.11) can be simplified to

$$\begin{aligned} \frac{\partial \tilde{\rho}}{\partial t} = & -i \sum_{i=1}^N \delta_i [S_i^z, \tilde{\rho}] - i \sum_{i \neq j}^N e^{i(\omega_i - \omega_j)t} \Omega_{ij} [S_i^+ S_j^-, \tilde{\rho}] \\ & - \sum_{i,j=1}^N e^{i(\omega_i - \omega_j)t} \gamma_{ij} \left(\tilde{\rho} S_i^+ S_j^- + S_i^+ S_j^- \tilde{\rho} - 2S_i^+ \tilde{\rho} S_j^- \right). \end{aligned} \quad (2.3.24)$$

In a more general case by considering the contribution of the external field, after transferring back to the Schrödinger picture and ignoring the terms oscillating with the frequencies $\pm(\omega_i + \omega_L)$, the master equation of motion in (2.3.24) becomes

$$\begin{aligned} \frac{\partial \hat{\rho}}{\partial t} = & -i \sum_{i=1}^N (\omega_i + \delta_i) [S_i^z, \hat{\rho}] - i \sum_{i \neq j}^N \Omega_{ij} [S_i^+ S_j^-, \hat{\rho}] \\ & - \sum_{i,j=1}^N \gamma_{ij} \left(\hat{\rho} S_i^+ S_j^- + S_i^+ S_j^- \hat{\rho} - 2S_i^+ \hat{\rho} S_j^- \right) \\ & + \frac{i}{2} \sum_{i=1}^N \left[\left(\Omega(\mathbf{r}_i) S_i^+ e^{-i(\omega_L t + \phi_L)} + \text{H.c.} \right), \hat{\rho} \right], \end{aligned} \quad (2.3.25)$$

where $\Omega(\mathbf{r}_i)$ is called the Rabi frequency of the driving field which is evaluated at the positions of the QDs and are defined as [114]

$$\Omega(\mathbf{r}_i) \equiv \Omega_i = \frac{\boldsymbol{\mu}_i \cdot \mathbf{E}_L(t)}{\hbar} e^{i\mathbf{k}_L \cdot \mathbf{r}_i}. \quad (2.3.26)$$

The Rabi frequencies in general, depend on the positions of the QDs and can be different for the QDs located at different points. Since the electromagnetic modes of the field strongly depend on the geometry and structural properties of the system, the electromagnetic field and thus also the Rabi frequency should be calculated for any specific case.

In the Master Equation approach, the mean value of any QD-based operator Q can be obtained by $\langle Q \rangle = \text{Tr}\{\rho Q\}$ in which, ρ is the QD density matrix [110]. Therefore, in the

rotating wave approximation (RWA), from Eq.(2.3.25) we find that

$$\begin{aligned} \frac{\partial \langle Q \rangle}{\partial t} = & i \sum_{i=1}^N (\omega_i + \delta_i) \langle [S_i^z, Q] \rangle + i \sum_{i \neq j}^N \Omega_{ij} \langle [S_i^+ S_j^-, Q] \rangle \\ & - \frac{1}{2} \sum_{i,j=1}^N \Gamma_{ij} \left\{ \langle [Q, S_i^+] S_j^- \rangle + \langle S_i^+ [S_j^-, Q] \rangle \right\} \\ & - \frac{i}{2} \sum_{i=1}^N \langle [(\Omega(\mathbf{r}_i) S_i^+ e^{-i\omega_L t} + \text{H.c.}), Q] \rangle. \end{aligned} \quad (2.3.27)$$

For deriving the equation above, we have made use of the mathematical identity for matrix calculus [45] that $\text{Tr}\{ABCD\} = \text{Tr}\{BCDA\} = \text{Tr}\{CDAB\} = \text{Tr}\{DABC\}$. Eq.(2.3.27) is the most important achievement of this chapter and will be used afterwards to calculate the dynamics of 2 coupled QDs in chapter (3) and of QD lattices and coupled QD lattices in chapter (4).

2.3.2 Interaction of quantum dots in free space

In this section, we define a special structure in which there are only two QDs located in a dielectric host medium at an arbitrary distance r_{ij} from each other with any arbitrary dipole orientation. In this structure, we should consider the three-dimensional quantized form of the electromagnetic plane-wave modes (vacuum field) in free space or a dielectric host material. Using the Expressions (2.2.18) for the electric field

$$\mathbf{E} = i \sum_{\mathbf{k}, s} \sqrt{\frac{\hbar \omega_{\mathbf{k}}}{2\epsilon_0 V}} \hat{\mathbf{e}}_{\mathbf{k}s} \left[a_{\mathbf{k}} e^{i\mathbf{k} \cdot \mathbf{r}} - a_{\mathbf{k}}^\dagger e^{-i\mathbf{k} \cdot \mathbf{r}} \right], \quad (2.3.28)$$

and applying to (2.3.1), the Hamiltonian of such a system in Rotating Wave Approximation (RWA) can be written as

$$\begin{aligned} \hat{H}_0 &= \sum_{i=1}^N \hbar \omega_i S_i^z + \sum_{\mathbf{k}s} \hbar \omega_{\mathbf{k}} \left(\hat{a}_{\mathbf{k}}^\dagger \hat{a}_{\mathbf{k}} + \frac{1}{2} \right), \\ \hat{H}_I &= -i\hbar \sum_{\mathbf{k}s} \sum_{i=1}^N [\boldsymbol{\mu}_i \cdot \mathbf{g}_{\mathbf{k}s}(\mathbf{r}_i) S_i^+ \hat{a}_{\mathbf{k}} - \text{H.c.}], \\ \hat{H}_{\text{Ex}} &= -\frac{1}{2} \sum_i [\boldsymbol{\mu}_i \cdot \mathbf{E}_L(t)] \left(S_i^+ e^{-i(\omega_L t - \mathbf{k}_L \cdot \mathbf{r}_i)} + S_i^- e^{i(\omega_L t - \mathbf{k}_L \cdot \mathbf{r}_i)} \right), \end{aligned} \quad (2.3.29)$$

where $\hat{a}_{\mathbf{k}s}$ and $\hat{a}_{\mathbf{k}s}^\dagger$ are the annihilation and creation operators of the field mode $\mathbf{k}s$, which has the wave vector \mathbf{k} , frequency $\omega_{\mathbf{k}}$ and the index of polarization s . The coupling constant

$$\mathbf{g}_{\mathbf{k}s}(\mathbf{r}_i) = \left(\frac{\omega_{\mathbf{k}}}{2\epsilon_0 \hbar V} \right)^{1/2} \hat{\mathbf{e}}_{\mathbf{k}s} e^{i\mathbf{k} \cdot \mathbf{r}_i}, \quad (2.3.30)$$

is the mode function of the three-dimensional vacuum field, evaluated at the position \mathbf{r}_i of the i th QD, V is the normalization volume, and $\hat{\mathbf{e}}_{\mathbf{k}s}$ is the unit polarization vector of the \mathbf{k} -th mode of the field. Comparing Eq.(2.3.28) with (2.3.2) implies that we can replace the cavity modes in the last section with the plane-wave modes,

$$\mathbf{u}_{\mathbf{k}}(\mathbf{r}) \rightarrow \frac{i}{\sqrt{V}} \sum_s \hat{\mathbf{e}}_{\mathbf{k}s} e^{i\mathbf{k}\cdot\mathbf{r}} = i \sqrt{\frac{2\varepsilon_0 \hbar}{\omega_{\mathbf{k}}}} \sum_s \mathbf{g}_{\mathbf{k}s}(\mathbf{r}). \quad (2.3.31)$$

In order to have all terms in the equation of motion of the density operator and hence the expectation value of physical variables clearly, we should calculate the collective parameters γ_{ij} and Ω_{ij} introduced in previous section. Combination of (2.3.31) and (2.3.19) leads to

$$\gamma_{ij} = \frac{\pi}{2\varepsilon_0 \hbar V} \sum_{\mathbf{k},s} \omega_{\mathbf{k}} (\boldsymbol{\mu}_i \cdot \mathbf{e}_{\mathbf{k}s}) (\boldsymbol{\mu}_j^* \cdot \mathbf{e}_{\mathbf{k}s}) e^{i\mathbf{k}\cdot(\mathbf{r}_i - \mathbf{r}_j)} \delta(\omega_{\mathbf{k}} - \omega_i), \quad (2.3.32)$$

$$\Omega_{ij} = \frac{-\pi}{2\varepsilon_0 \hbar V} \sum_{\mathbf{k},s} \omega_{\mathbf{k}} (\boldsymbol{\mu}_i \cdot \mathbf{e}_{\mathbf{k}s}) (\boldsymbol{\mu}_j^* \cdot \mathbf{e}_{\mathbf{k}s}) e^{i\mathbf{k}\cdot(\mathbf{r}_i - \mathbf{r}_j)} \left(\frac{P}{\omega_{\mathbf{k}} + \omega_0} + \frac{P}{\omega_{\mathbf{k}} - \omega_0} \right), \quad (i \neq j) \quad (2.3.33)$$

We start with changing the sum over $\mathbf{k}s$ into an integral

$$\sum_{\mathbf{k},s} \rightarrow \frac{V}{(2\pi c)^3} \sum_{s=1}^2 \int_0^\infty d\omega_{\mathbf{k}} \omega_{\mathbf{k}}^2 \int d\Omega_{\mathbf{k}}. \quad (2.3.34)$$

In order to sum over the polarizations s and integrate over the wave vector solid angle $d\Omega_{\mathbf{k}}$ in Eq.(2.3.34), we use the spherical coordinates for the propagation vector \mathbf{k} . The integral over $d\Omega_{\mathbf{k}}$ contains integrals over the spherical angular coordinates $\theta_{\mathbf{k}}$ and $\phi_{\mathbf{k}}$ in which the angle $\theta_{\mathbf{k}}$ is formed by \mathbf{r}_{ij} and \mathbf{k} directions, so we can have

$$\mathbf{k} = k [\sin \theta_{\mathbf{k}} \cos \phi_{\mathbf{k}}, \sin \theta_{\mathbf{k}} \sin \phi_{\mathbf{k}}, \cos \theta_{\mathbf{k}}]. \quad (2.3.35)$$

In this representation, the unit polarization vectors $\mathbf{e}_{\mathbf{k}1}$ and $\mathbf{e}_{\mathbf{k}2}$ can be chosen as [108]

$$\begin{aligned} \mathbf{e}_{\mathbf{k}1} &= [-\cos \theta_{\mathbf{k}} \cos \phi_{\mathbf{k}}, -\cos \theta_{\mathbf{k}} \sin \phi_{\mathbf{k}}, \sin \theta_{\mathbf{k}}], \\ \mathbf{e}_{\mathbf{k}2} &= [\sin \phi_{\mathbf{k}}, -\cos \phi_{\mathbf{k}}, 0]. \end{aligned} \quad (2.3.36)$$

In Eq.(2.3.32), we take the term with $i = j$ out of the summation. Then we can write the incoherent interaction as a sum of the self reaction interaction γ_{ii} which is the interaction of the QD with its own field and the interaction between two different QDs, γ_{ij} ($i \neq j$). With this choice of the polarization vectors in (2.3.36) and with the help of (2.3.34), the spontaneous emission rate of a single QD, from Eq.(2.3.32) reads

$$\Gamma_i = \frac{\omega_i^3 \mu_i^2}{3\varepsilon_0 \pi \hbar c^3}, \quad (2.3.37)$$

where $\Gamma_i = 2\gamma_{ii}$. From Eq.(2.3.32), the incoherent spontaneous energy transfer rate between two different QDs, mediated through the modes of the electromagnetic field in

a dielectric host material is [106, 107, 109, 115–117]

$$\begin{aligned} \Gamma_{ij} = \Gamma_{ji} = \frac{3}{2} \sqrt{\Gamma_i \Gamma_j} \left\{ [(\mathbf{e}_{\mu_i} \cdot \mathbf{e}_{\mu_j}) - (\mathbf{e}_{\mu_i} \cdot \mathbf{e}_{r_{ij}}) (\mathbf{e}_{\mu_j} \cdot \mathbf{e}_{r_{ij}})] \frac{\sin(k_0 r_{ij})}{k_0 r_{ij}} \right. \\ \left. + [(\mathbf{e}_{\mu_i} \cdot \mathbf{e}_{\mu_j}) - 3 (\mathbf{e}_{\mu_i} \cdot \mathbf{e}_{r_{ij}}) (\mathbf{e}_{\mu_j} \cdot \mathbf{e}_{r_{ij}})] \left[\frac{\cos(k_0 r_{ij})}{(k_0 r_{ij})^2} - \frac{\sin(k_0 r_{ij})}{(k_0 r_{ij})^3} \right] \right\}, \end{aligned} \quad (2.3.38)$$

In expression(2.3.38), $\Gamma_{ij} = 2\gamma_{ij}$, \mathbf{e}_{μ_i} , \mathbf{e}_{μ_j} and $\mathbf{e}_{r_{ij}}$ are unit vectors along the QD transition dipole moments and the vector $\mathbf{r}_{ij} = \mathbf{r}_j - \mathbf{r}_i$ respectively. Moreover, $k_0 = \omega_0/c$, where $\omega_0 = (\omega_i + \omega_j)/2$, and we have assumed that $(\omega_i - \omega_j) \ll \omega_0$. When $kr_{ij} \neq 0$, we obtain the coherent coupling potential in Eq.(2.3.33) by contour methods and obtain [106, 107, 109, 115, 118, 119]

$$\begin{aligned} \Omega_{ij} = \Omega_{ji} = \frac{3}{4} \sqrt{\Gamma_i \Gamma_j} \left\{ - [(\mathbf{e}_{\mu_i} \cdot \mathbf{e}_{\mu_j}) - (\mathbf{e}_{\mu_i} \cdot \mathbf{e}_{r_{ij}}) (\mathbf{e}_{\mu_j} \cdot \mathbf{e}_{r_{ij}})] \frac{\cos(k_0 r_{ij})}{k_0 r_{ij}} \right. \\ \left. + [(\mathbf{e}_{\mu_i} \cdot \mathbf{e}_{\mu_j}) - 3 (\mathbf{e}_{\mu_i} \cdot \mathbf{e}_{r_{ij}}) (\mathbf{e}_{\mu_j} \cdot \mathbf{e}_{r_{ij}})] \left[\frac{\sin(k_0 r_{ij})}{(k_0 r_{ij})^2} + \frac{\cos(k_0 r_{ij})}{(k_0 r_{ij})^3} \right] \right\}. \end{aligned} \quad (2.3.39)$$

When $kr_{ij} = 0$ which happens for example for two dipole moments in the same QD, Ω_{ij} reduces to a form similar to the Lamb shift. The coupling parameters Γ_{ij} and Ω_{ij} strongly depend on the inter-QD separation. Generally speaking, the coupling parameter Γ_{ij} is in fact the imaginary part and Ω_{ij} is the real component of the electromagnetic Green's function in the medium. Γ_{ij} governs the resonant QD-field coupling strength which manifests itself in the spontaneous energy transfer rate between two QDs. In this context, a real photon is emitted from an excited QD and is subsequently absorbed by another QD which is in ground state. However, Ω_{ij} represents the resonant dipole-dipole coupling and hence the coherent exchange of energy (virtual photon) between the QDs. Since the real and imaginary components of the Green's function are related to each other, it is obvious that the resonant QD-field coupling and the resonant dipole-dipole coupling between QDs cannot be chosen independently from each other [120].

2.4 Spontaneous emission

In this section we would like to introduce the basis for the spontaneous emission of a QD positioned in an anisotropic medium characterized by the cavity field modes $\mathbf{u}_{\mathbf{k}}(\mathbf{r})$. Similar to the procedure we followed in the previous section, if the emitting QD is located in free space, then everything we obtain here for the case of a cavity holds true, if we replace the cavity modes by the plane-wave modes.

Based on Eq.(2.3.2), in order to obtain the spontaneous emission dynamics and directionality, $\mathbf{E}(\mathbf{r}, t)$, we need to know the time profile of the EM field creator and annihilator operators, $a_{\mathbf{k}}(\mathbf{r})$ and the spatial characteristics of the field amplitudes, $\mathbf{u}_{\mathbf{k}}(\mathbf{r})$. The spatial dependence of the emission strongly depends on the structure of the environment in which the QD emitter is located. Such a structure can be engineered by designing a large variety of cavities like microcavities and photonic crystals or by placing the other

nanoparticles in the vicinity of the QD emitter. These nanoparticles can be the other neighboring QDs as well. In this chapter, we keep the general form of the field amplitude without introducing any specific spatial dependence. Specific structures will be considered in the next chapters extensively. At this point we try to obtain a general form of the wave equation for the emission from a QD emitter as a basis.

By implementing the Hamiltonian $\hat{H} = \hat{H}_0 + \hat{H}_I + \hat{H}_{Ex}$ in the Heisenberg equation of motion,

$$\frac{d}{dt} \hat{a}_{\mathbf{k}}(t) = \frac{i}{\hbar} [\hat{H}, \hat{a}_{\mathbf{k}}(t)], \quad (2.4.1)$$

the following coupled equations can be obtained,

$$\dot{\hat{a}}_{\mathbf{k}} = -i\omega_{\mathbf{k}} \hat{a}_{\mathbf{k}} + \frac{i}{\hbar} \sum_{i=1}^N \sqrt{\frac{\hbar\omega_{\mathbf{k}}}{2\varepsilon_0}} (\hat{S}_i^+ + \hat{S}_i^-) \mu_i \cdot \mathbf{u}_{\mathbf{k}}^*(\mathbf{r}_i), \quad (2.4.2)$$

$$(\dot{\hat{S}}_i^+ + \dot{\hat{S}}_i^-) = i\omega_i (\hat{S}_i^+ - \hat{S}_i^-). \quad (2.4.3)$$

In obtaining Eq.(2.4.3), we have assumed that the time-dependent amplitude of the external electric field has a real value. By taking the time-derivative of both sides of Eq. and combining with Eq.(2.4.3), we arrive at

$$\ddot{\hat{a}}_{\mathbf{k}}(t) + \omega_{\mathbf{k}}^2 \hat{a}_{\mathbf{k}}(t) = \sum_{i=1}^N \sqrt{\frac{\omega_{\mathbf{k}}}{2\varepsilon_0 \hbar}} \mu_i \cdot \mathbf{u}_{\mathbf{k}}^*(\mathbf{r}_i) \{(\omega_{\mathbf{k}} - \omega_i) \hat{S}_i^+(t) + (\omega_{\mathbf{k}} + \omega_i) \hat{S}_i^-(t)\}. \quad (2.4.4)$$

Multiplying both parts of the Eq.(2.4.4) by $\sqrt{\hbar\omega_{\mathbf{k}}/2\varepsilon_0\varepsilon_h} \mathbf{u}_{\mathbf{k}}(\mathbf{r}_i)$ and applying the correspondence $\mathbf{k} \leftrightarrow -i\nabla$ and then summing over \mathbf{k} , Eq.(2.4.4) can be transferred to

$$\begin{aligned} \nabla^2 \mathbf{E}^{(+)}(\mathbf{r}, t) - \frac{1}{c^2} \frac{\partial^2}{\partial t^2} \mathbf{E}^{(+)}(\mathbf{r}, t) = \\ \frac{1}{2\varepsilon_0 c^2} \sum_i \sum_{\mathbf{k}} \omega_{\mathbf{k}} [\mu_i \cdot \mathbf{u}_{\mathbf{k}}^*(\mathbf{r}_i)] \mathbf{u}_{\mathbf{k}}(\mathbf{r}_i) \{(\omega_i - \omega_{\mathbf{k}}) \hat{S}_i^+ - (\omega_i + \omega_{\mathbf{k}}) \hat{S}_i^-\}. \end{aligned} \quad (2.4.5)$$

Eq.(2.4.5) corresponds to the wave equation of the positive part of the electric field

$$\nabla^2 \mathbf{E}^{(+)}(\mathbf{r}, t) - \frac{1}{c^2} \frac{\partial^2}{\partial t^2} \mathbf{E}^{(+)}(\mathbf{r}, t) = \frac{1}{\varepsilon_0 c^2} \frac{\partial \mathbf{J}^{(+)}(\mathbf{r}, t)}{\partial t}, \quad (2.4.6)$$

where

$$\frac{\partial \mathbf{J}^{(+)}(\mathbf{r}, t)}{\partial t} = \frac{1}{2} \sum_i \sum_{\mathbf{k}} \omega_{\mathbf{k}} [\mu_i \cdot \mathbf{u}_{\mathbf{k}}^*(\mathbf{r}_i)] \mathbf{u}_{\mathbf{k}}(\mathbf{r}_i) \{(\omega_i - \omega_{\mathbf{k}}) \hat{S}_i^+ - (\omega_i + \omega_{\mathbf{k}}) \hat{S}_i^-\}. \quad (2.4.7)$$

The solution of such a wave equation is of the form

$$\begin{aligned} \mathbf{E}^{(+)}(\mathbf{r}, t) = & -\frac{1}{4\pi\varepsilon_0} \int \frac{d\mathbf{r}'}{|\mathbf{r} - \mathbf{r}'|} \frac{\partial \mathbf{J}(\mathbf{r}', t - |\mathbf{r} - \mathbf{r}'|/c)}{\partial t} \\ = & \frac{-1}{8\pi\varepsilon_0} \int \sum_i \sum_{\mathbf{k}} \frac{d\mathbf{r}'}{|\mathbf{r} - \mathbf{r}'|} \{ \omega_{\mathbf{k}} [\mu_i \cdot \mathbf{u}_{\mathbf{k}}^*(\mathbf{r}_i)] \mathbf{u}_{\mathbf{k}}(\mathbf{r}') \\ & \times [(\omega_{\mathbf{k}} - \omega_i) \hat{S}_i^+(t - |\mathbf{r} - \mathbf{r}'|/c) + (\omega_{\mathbf{k}} + \omega_i) \hat{S}_i^-(t - |\mathbf{r} - \mathbf{r}'|/c)] \}. \end{aligned} \quad (2.4.8)$$

The spatially dependent part of the electric field greatly depends on its environment. The magnetic field can also be obtained in a similar way. In the following of this thesis, the electromagnetic wave equations of the kind presented in Eq.(2.4.8) will be solved for different systems of QDs.

Chapter 3

Collective spontaneous emission from two coupled quantum dots: physical mechanism of quantum nanoantenna

Spontaneous radiation of excited systems is a fundamental physical effect which has been in the focus of the research for a long time. The properties of the spontaneous radiation are strongly influenced by many factors, such as energy spectrum of the emitter and the emitter-electromagnetic field coupling constant. The simplest model is an isolated two-level emitter in the vacuum weakly interacting with the field (the Wigner-Weisskopf theory of spontaneous emission [40]). In this model, the decay is exponential and the decay rate is proportional to the partial density of photonic states (PDOS) of the emitter and to the coupling factor [22, 121, 122]. A possibility to control the decay rate arises when a two-level oscillator is placed in a transparent dielectric medium [123] or into an electrodynamic system such as microcavity [124], photonic crystal [125] or nanoantenna [22]. In all mentioned cases, the modification of the PDOS takes place resulting in the decay rate change. This effect is commonly referred to as the Purcell effect [23]. In the strong coupling regime the Wigner-Weisskopf approach becomes invalid: the exponential decay law becomes violated [121] and an oscillating behavior appears due to the multiple emission and reabsorption of photons by the emitter (the so-called vacuum Rabi oscillations). The Rabi frequency is proportional to the coupling factor.

The spontaneous emission is strongly affected by the interaction between the emitters in an ensemble. If the separation between the emitters, exemplified e.g. by quantum dots (QDs), is small, there is a probability that the excitation can be transferred via charge tunneling [28, 126–129] or long-range radiative interaction [44]. If the inter-emitter dis-

tance is a little bit longer, they are coupled by a near-field quasi electrostatic dipole-dipole ($d-d$) interaction mostly referred to as the Förster energy transfer [41,43,130]. It should be noted that in actual experimental conditions, one of the mechanisms prevails over the others allowing to study them separately.

The interaction of multiple emitters in an ensemble changes the energy spectrum of the system, introducing additional energy levels which correspond to correlated multi-particle states of the system, i.e. entangled states [121]. As a consequence, the temporal dynamics of the spontaneous emission is strongly modified even in the weak-coupling regime. The superradiance effect [50] illustrates this statement. It should be noted that the Dicke's model [50] is restricted to systems with linear extension much less than the wavelength. The increase of the system size makes the phase relations between emitters important. This enables not only the control of the temporal behavior but also the control of the spatial structure of the spontaneous emission. The latter appears in e.g. directed spontaneous emission from an extended ensemble [95], correlated emission of single photon [99, 131], quantum interference in cooperative Dicke emission [98], collective Lamb shift in single photon superradiance [102] and finite time disentanglement via spontaneous emission [132].

In the strong coupling regime the cooperative effects manifest themselves in essentially nonmonotonous oscillating behavior of the spontaneous emission [99, 133]. Obviously, theoretical modeling of such systems gets significantly more complex: a solution of the quantum many-body problem is required. That is why e.g. collective effects in the strong coupling regime are commonly modeled by a reduced two-particle system placed in a free space [110, 115, 134], in a waveguide [135], in a microcavity [133], in the vicinity of a plasmon nanowire [136]. The main attention is paid to the evaluation of the total irradiated power and its spectral characteristics. The latter is of importance for the interpretation of the photoluminescence measurements. Temporal correlations of the spontaneous emission are also studied [137] while the role of the spontaneous emission spatial structure seems to be underestimated. Meanwhile, by analogy with classical optical nanoantennas [138–141], the spatial inhomogeneity of spontaneous emission leads to the concept of a quantum nanoantenna – a device converting quantized near field of a source into the radiation far field [139, 142]. A quantum antenna proposed in Ref. [139] is based on the spontaneous emission of an isolated emitter weakly coupled to a metal-dielectric structure of a special type. In Ref. [142], the excitation source is a terahertz tunneling current induced by an optical Rabi wave propagating along the chain of tunneling-coupled QDs. In the present paper we propose a quantum antenna utilizing collective spontaneous emission of strongly coupled oscillators. A system of two $d-d$ coupled QDs is the simplest realization of such a system.

In order to experimentally observe the modified decay dynamics due to strong coupling in semiconductor quantum dots, one should realize a set of requirements: (i) the excitonic dipole moments in all QDs should be mutually aligned, (ii) the QDs should spectrally overlap and (iii) one needs full QD position control in order to reproducibly change the distance between the QDs. In addition, it would be highly recommended when (iv) the QDs could be embedded in a low refractive index material which will substantially enhance the coupling and (v) that the QD-QD detuning should, when pos-

sible, be variable in a reproducible manner.

It should first be stated that in almost all photoluminescence experiments on e.g. Stranski-Krastanov InAs/GaAs QDs, one employs non-resonant excitation into the barrier material, followed by incoherent relaxation of the electron-hole pairs into the semiconductor quantum dot. Since in such samples, the bases of QDs are usually elongated in a certain direction, we might be able to observe the effect of coupling even by employing non-resonant excitation into the barrier. But for the QDs which are circularly shaped in the plane perpendicular to the growth direction, then the in-plane excitonic dipole moment averages out to zero and a modified decay dynamics can only be observed in the case of resonant excitation [56] in which a laser beam is exactly resonant with the QDs, resulting in a net alignment of the excitonic dipoles.

As compared to the frequently studied Stranski-Krastanov InAs/GaAs QDs, the nanowire quantum dots, which are e.g. thin InAs segments inside narrow GaAs nanowires, look much more promising to study the effects of strong coupling and thus the modified decay dynamics. Indeed, nanowire QDs feature an accurate and full position control using either nano-imprint [143] or electron beam lithography [144] for positioning the Au nanoparticles which catalyzes the nanowire growth. The effects of strong coupling are probably most easily observed in zinc-blende/wurtzite crystal phase QDs [145] which feature perfectly atomically flat interfaces, thus providing a good opportunity to spectrally overlap different QDs, either in the same nanowire, or in different nanowires. Moreover, nanowire quantum dots can be embedded into a low refractive index material like PDMS [146], SiO₂ or Si₃N₄ for increasing the coupling and getting rid of the substrate-based photoluminescence. Finally, it has already been shown that a nanowire can be individually contacted [147], thus in principle allowing to tune the mutual QD-QD detuning by using the quantum confined Stark effect. In view of this recent progress in the preparation of nanowire quantum dots, we feel that a study towards the effects of strong coupling between two QDs is presently particularly timely as we expect that the (i)-(v) criteria mentioned above can soon be realized in nanowire quantum dots.

In this chapter, we have extensively simulated the spontaneous emission decay dynamics, spectrum and spatial structure of an InAs double-QD system embedded in GaAs material in the strong coupling regime with a great emphasis on the photoluminescence emission pattern from such a sample. In section (3.1), we state the model and specify the corresponding master equation formalism. A general solution of the master equation and observable antenna characteristics are also presented in this section. Based on this theory, in sections (3.2), (3.3) and (3.4) we investigate respectively the dynamics, spatial structure and spectrum of the two-QD spontaneous emission for different initial excitations and we check the influence of QD-QD distance. A short discussion on the population dynamics is presented in section(3.5) and finally the summary and concluding remarks are contained in section (3.6).

3.1 Basic Formalism

Consider a system of two identical nonoverlapping QDs embedded into a dielectric medium with relative permittivity ϵ_h . We assume the host medium to be homogeneous, nondispersive and nonabsorptive. The QDs are modeled as atom-like emitters [2–5] – two-level systems, with excited state $|e\rangle$, ground state $|g\rangle$, transition frequency ω , and transition dipole moments $\boldsymbol{\mu}$. Since the size of the QD is much smaller than the wavelength of the emitted radiation, a QD can be approximated by a transition dipole moment which only has in-plane components. We assume that the QDs are located at positions \mathbf{r}_1 and \mathbf{r}_2 . The QD structure interacts with quantum electromagnetic (EM) field regarded as a reservoir [106–109]. As introduced in chapter 2, the field is described by the operator

$$\hat{\mathbf{E}} = \hat{\mathbf{E}}^{(+)} + \text{H.c.}, \quad (3.1.1)$$

where

$$\hat{\mathbf{E}}^{(+)}(\mathbf{r}, t) = i \sum_{\mathbf{k}, s} \sqrt{\frac{\hbar\omega_{\mathbf{k}}}{2\epsilon_0\epsilon_h V}} \mathbf{e}_{\mathbf{k}s} \hat{a}_{\mathbf{k}s} e^{i\mathbf{k}\cdot\mathbf{r}}. \quad (3.1.2)$$

The abbreviation H.c. denotes Hermitian conjugation. A single mode is characterized by the wave vector \mathbf{k} , frequency $\omega_{\mathbf{k}}$ and the unit polarization vector $\mathbf{e}_{\mathbf{k}s}$ with orthogonal polarization directions ($s = 1, 2$). V is the normalization volume. Operators $\hat{a}_{\mathbf{k}s}$ and $\hat{a}_{\mathbf{k}s}^\dagger$ are the annihilation and creation operators of this field mode which satisfy Bosonic commutation relations. In the electric dipole approximation, the Hamiltonian of the system “double-QD + EM field” can be written as a sum of two terms,

$$\hat{H}_0 = \sum_{i=1}^2 \hbar\omega_0 \hat{S}_i^z + \sum_{\mathbf{k}s} \hbar\omega_{\mathbf{k}} \left(\hat{a}_{\mathbf{k}s}^\dagger \hat{a}_{\mathbf{k}s} + \frac{1}{2} \right), \quad (3.1.3)$$

$$\hat{H}_I = -i\hbar \sum_{\mathbf{k}s} \sum_{i=1}^2 \left[\boldsymbol{\mu} \cdot \mathbf{g}_{\mathbf{k}s}(\mathbf{r}_i) (\hat{S}_i^+ + \hat{S}_i^-) \hat{a}_{\mathbf{k}s} - \text{H.c.} \right], \quad (3.1.4)$$

where \hat{H}_0 corresponds to the bare systems and \hat{H}_I is the interaction Hamiltonian. Hereafter one should distinguish the index i from the imaginary unit. The quantities $\hat{S}_i^+ = |e_i\rangle\langle g_i|$ and $\hat{S}_i^- = |g_i\rangle\langle e_i|$ are the dipole raising and lowering operators and $\hat{S}_i^z = (|e_i\rangle\langle e_i| - |g_i\rangle\langle g_i|)/2$ is the population operator of the i th QD. The coupling constant

$$\mathbf{g}_{\mathbf{k}s}(\mathbf{r}_i) = \left(\frac{\omega_{\mathbf{k}}}{2\epsilon_0\epsilon_h\hbar V} \right)^{1/2} \mathbf{e}_{\mathbf{k}s} e^{i\mathbf{k}\cdot\mathbf{r}_i} \quad (3.1.5)$$

is the mode function of the three-dimensional vacuum field, evaluated at the position \mathbf{r}_i of the i th QD. Our model will be valid for both Stranski-Krastanov pyramidal InAs/GaAs QDs and disk-like nanowire QDs in which the QD-height is much smaller than its diameter. In the further analysis we will follow the master equation approach in which the time evolution of the collection of QDs interacting with the electromagnetic field is considered in terms of the density operator $\hat{\rho}_{\text{QF}}$ characterizing the statistical state of the combined system of the QDs and the field. In the Born approximation [112], the interaction between the QDs and the field is supposed to be weak, and there is no back

response of the QDs on the field. So the state of the EM field does not change in time, and we can write the density operator $\hat{\rho}_{\text{QF}}(t)$ as $\hat{\rho}_{\text{Q}}(t)\hat{\rho}_{\text{F}}(0)$, where $\hat{\rho}_{\text{Q}}$ and $\hat{\rho}_{\text{F}}$ are the density operators of the QDs and the electromagnetic field, respectively. In the master equation approach, the mean value of any QD-based operator \hat{Y} can be obtained by $\langle \hat{Y} \rangle = \text{Tr}\{\hat{\rho}\hat{Y}\}$ where $\hat{\rho} = \hat{\rho}_{\text{Q}}$ and, in the rotating wave approximation, the density matrix obeys the equation of motion,

$$\begin{aligned} \frac{\partial \hat{\rho}}{\partial t} = & -i \sum_{i=1}^2 \omega_0 [\hat{S}_i^z, \hat{\rho}] - i \sum_{i \neq j}^2 \Omega_{ij} [\hat{S}_i^+ \hat{S}_j^-, \hat{\rho}] \\ & - \frac{1}{2} \sum_{i,j=1}^2 \Gamma_{ij} (\hat{\rho} \hat{S}_i^+ \hat{S}_j^- + \hat{S}_i^+ \hat{S}_j^- \hat{\rho} - 2 \hat{S}_j^- \hat{\rho} \hat{S}_i^+), \end{aligned} \quad (3.1.6)$$

where

$$\Gamma_{ii} \equiv \Gamma = \frac{\varepsilon_{\text{h}}^{1/2} \omega_0^3 \mu^2}{3\pi \varepsilon_0 \hbar c^3} \quad (3.1.7)$$

is the spontaneous emission rate of a single QD and μ is the QD dipole moment.

The parameters Ω_{12} and Γ_{12} are respectively the diagonal and off-diagonal matrix elements of the interaction energy operator \hat{V}

$$\hat{V} = \hbar \begin{pmatrix} \Omega_{12} & i\Gamma_{12} \\ i\Gamma_{12} & \Omega_{12} \end{pmatrix}. \quad (3.1.8)$$

Making use of expressions (2.3.38) and (2.3.39), the quantity Γ_{12} is shown to be [106–109, 115–117]

$$\Gamma_{12} = \frac{3}{2} \Gamma \left\{ \alpha_{12} \frac{\sin(k_0 r_{12})}{k_0 r_{12}} + \beta_{12} \left(\frac{\cos(k_0 r_{12})}{(k_0 r_{12})^2} - \frac{\sin(k_0 r_{12})}{(k_0 r_{12})^3} \right) \right\}, \quad (3.1.9)$$

where $\alpha_{12} = (\mathbf{e}_{\mu 1} \cdot \mathbf{e}_{\mu 2}) - (\mathbf{e}_{\mu 1} \cdot \mathbf{e}_{12})(\mathbf{e}_{\mu 2} \cdot \mathbf{e}_{12})$ and $\beta_{12} = (\mathbf{e}_{\mu 1} \cdot \mathbf{e}_{\mu 2}) - 3(\mathbf{e}_{\mu 1} \cdot \mathbf{e}_{12})(\mathbf{e}_{\mu 2} \cdot \mathbf{e}_{12})$. Here $\mathbf{e}_{\mu 1}, \mathbf{e}_{\mu 2}$ are unit vectors along the QD transition dipole moments and $\mathbf{e}_{12} = (\mathbf{r}_2 - \mathbf{r}_1)/r_{12}$, $k_0 = \sqrt{\varepsilon_{\text{h}}} \omega_0/c$.

The parameter $\hbar \Omega_{12}$ in Eq. (3.1.6) is the dipole-dipole interaction energy between quantum dots coupled through the vacuum field. When $kr_{12} \neq 0$, this coherent coupling potential is [106–109, 115, 118, 119]

$$\Omega_{12} = \frac{3}{4} \Gamma \left\{ -\alpha_{12} \frac{\cos(k_0 r_{12})}{k_0 r_{12}} + \beta_{12} \left(\frac{\sin(k_0 r_{12})}{(k_0 r_{12})^2} + \frac{\cos(k_0 r_{12})}{(k_0 r_{12})^3} \right) \right\}, \quad (3.1.10)$$

and can be understood as the exchange of a virtual photon between an empty and an excited QD mediated by the quantized electromagnetic field. The coupling parameters Γ_{12} and Ω_{12} determine the correlation properties of the multi-QD system and as indicated in Fig.3.1, strongly depend on the inter-QD separation.

Calculation of the Lamb shift is possible based on Eq. (3.1.10) in the limit $r_{12} \rightarrow 0$. The divergence appeared in this case requires a special renormalization [148] of the frequency shift. We will not consider this technique here, but assume that the renormalized shift is included into the transition frequency ω_0 in Eq. (3.1.6) [110].

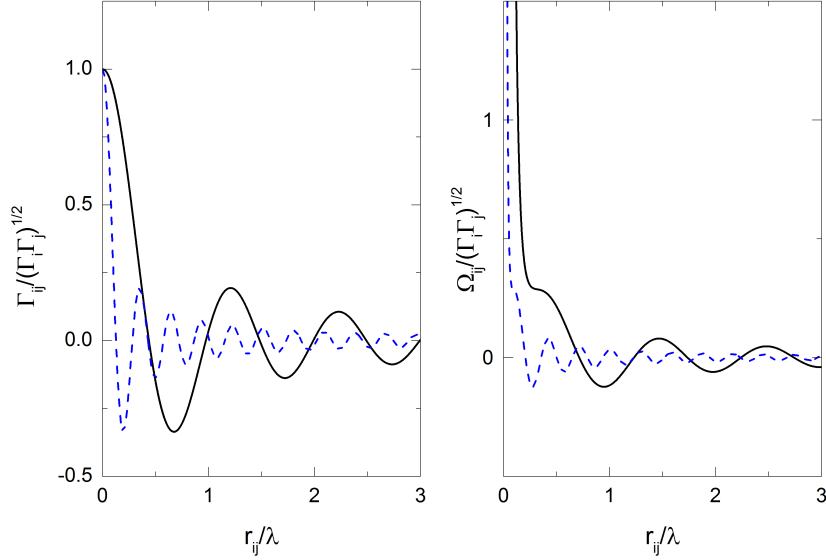


Figure 3.1: (a) Collective damping $\Gamma_{12}/\sqrt{\Gamma_1\Gamma_2}$ and (b) the dipole-dipole interaction $\Omega_{12}/\sqrt{\Gamma_1\Gamma_2}$ as a function of r_{12}/λ_0 for $\hat{\mu}_1 \parallel \hat{\mu}_2$, $\hat{\mu}_1 \perp \hat{\mu}_2$ (solid line) and $\hat{\mu}_1 \parallel \hat{\mu}_2$, $\hat{\mu}_1 \parallel \hat{\mathbf{r}}_{12}$ (dashed line).

For obtaining Eqs. (3.1.6) to (3.1.10), we have used the Markov approximation in which the dynamics of the QD system is slow as compared to the much faster decay of correlation functions of the photonic reservoir [149]. In other words, the Markov approximation holds when there is no memory in the system. It is clear from Eq. (3.1.9) and (3.1.10) that when the QD dipole moments are perpendicular to each other, the collective parameters will vanish and there will be no coupling between the QDs. By contrast, if the QD dipole moments are parallel or anti parallel, the collective parameters attain their maximal values, with opposite signs.

To obtain a better understanding of the nature of a double-QD system at different initial excitation conditions, we should calculate the eigenstates of the combined system "QDs + photonic reservoir", which correspond to the eigenstates of Eq. (3.1.6). This system behaves as a single four-level system with eigenstates $|g\rangle = |g_1\rangle|g_2\rangle$ and $|e\rangle = |e_1\rangle|e_2\rangle$ with energies $E_g = -\hbar\omega_0$ and $E_e = \hbar\omega_0$ respectively as well as the entangled states $|s\rangle = \frac{1}{\sqrt{2}}(|e_1\rangle|g_2\rangle + |g_1\rangle|e_2\rangle)$ and $|a\rangle = \frac{1}{\sqrt{2}}(|e_1\rangle|g_2\rangle - |g_1\rangle|e_2\rangle)$ with energies $E_s = \hbar\Omega_{12}$ and $E_a = -\hbar\Omega_{12}$. The ground state $|g\rangle$ and the fully excited state $|e\rangle$ are not influenced by the dipole-dipole interaction, but the energy of the symmetric $|s\rangle$ and the antisymmetric $|a\rangle$ states are shifted from their unperturbed energies by $\hbar\Omega_{12}$. The symmetric and antisymmetric transitions are uncorrelated and decay with the rates Γ_s and Γ_a respectively, $\Gamma_{s,a} = \Gamma \pm \Gamma_{12}$. These entangled states are schematically indicated in Fig.3.2.

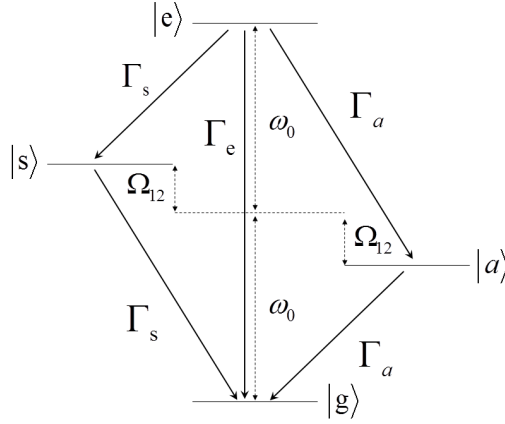


Figure 3.2: Schematic of the energy levels in a double-QD system. When two QDs are strongly coupled, two systems of two-level QDs change to a single system of four levels. The energy levels from top to bottom are the excited state $|e\rangle = |e_1\rangle |e_2\rangle$, the symmetric state $|s\rangle = \frac{1}{\sqrt{2}} (|e_1\rangle |g_2\rangle + |g_1\rangle |e_2\rangle)$, the antisymmetric state $|a\rangle = \frac{1}{\sqrt{2}} (|e_1\rangle |g_2\rangle - |g_1\rangle |e_2\rangle)$ and the ground state $|g\rangle = |g_1\rangle |g_2\rangle$.

The origin of the Dicke-type [50] cooperative spontaneous emission comes from the entanglement of the QD system with the electromagnetic field modes. This means that the interference of the radiation patterns from each of the individually oscillating dipoles should be taken into account. The constructive interference leads to faster decay of the system (superradiance) while the destructive interference leads to the slower decay (subradiance). We are mostly interested in the time profile of the spontaneous emission intensity $I(t)$ as well as in spatial profile in meridional and azimuthal planes. The time variation of the population can be directly probed in time resolved transmission or differential reflectivity [150] measurements. The dynamics of the emission intensity can be recorded in a time resolved photoluminescence measurement.

To analyze the spontaneous decay dynamics it is convenient to use the complete set of single-time correlators as follows $x_1 = \langle \hat{S}_1^+ \hat{S}_1^- \rangle$, $x_2 = \langle \hat{S}_2^+ \hat{S}_2^- \rangle$, $x_3 = \langle \hat{S}_1^+ \hat{S}_2^- \rangle$, $x_4 = \langle \hat{S}_2^+ \hat{S}_1^- \rangle$, $x_5 = \langle \hat{S}_1^+ \hat{S}_1^- \hat{S}_2^+ \hat{S}_2^- \rangle$. Then, for the 4-vector $\mathbf{x}^T = (x_1, x_2, x_3, x_4)$ (the superscript T denotes transposed matrix) we obtain from Eq. (3.1.6) the system of differential equations

$$\frac{d\mathbf{x}}{dt} = \underline{A}\mathbf{x} + \mathbf{f}, \quad (3.1.11)$$

where \underline{A} is the following matrix

$$\underline{A} = \begin{pmatrix} -\Gamma & 0 & \xi & \xi^* \\ 0 & -\Gamma & \xi^* & \xi \\ \xi & \xi^* & -\Gamma & 0 \\ \xi^* & \xi & 0 & -\Gamma \end{pmatrix},$$

and $\mathbf{f}(t) = 2\Gamma_{12}x_5(0)\mathbf{f}_0 \exp(-2\Gamma t)$, $\mathbf{f}_0^T = (0, 0, 1, 1)$, $\xi = -i\Omega_{12} - \Gamma_{12}/2$. Due to the

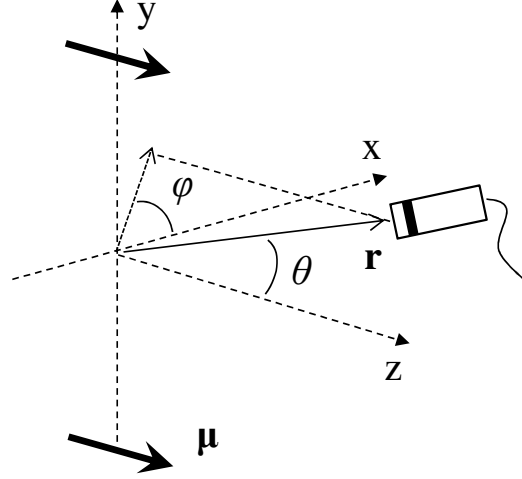


Figure 3.3: Schematic indication of the position of the observation point with respect to the QD positions and dipole orientations in circular coordinates. In this picture, the QD dipoles are perpendicular to the QD-QD axis. the z-axis is along the QD dipole directions. y-axis is along the line connecting the QDs and the x-axis is perpendicular to y and z.

special symmetry properties of the matrix the general exact solution of Eq. (3.1.11) can be written in the simple analytical form. It reads

$$\mathbf{x}(t) = e^{-\Gamma t} \underline{Q}(t) \left[\frac{1}{4} \underline{U} \mathbf{x}(0) - \frac{\gamma}{2} \mathbf{b} \right] - \gamma \mathbf{a} e^{-2\Gamma t}, \quad (3.1.12)$$

where $\gamma = 2\Gamma_{12}^2 \kappa_5(0) / \Gamma_s \Gamma_a$ and symbols $\underline{Q}(t)$ and \underline{U} respectively denote the matrices

$$\underline{Q}(t) = \begin{pmatrix} e^{\Gamma_{12}t} & e^{-\Gamma_{12}t} & e^{2i\Omega_{12}t} & e^{-2i\Omega_{12}t} \\ e^{\Gamma_{12}t} & e^{-\Gamma_{12}t} & -e^{2i\Omega_{12}t} & -e^{-2i\Omega_{12}t} \\ -e^{\Gamma_{12}t} & e^{-\Gamma_{12}t} & -e^{2i\Omega_{12}t} & e^{-2i\Omega_{12}t} \\ -e^{\Gamma_{12}t} & e^{-\Gamma_{12}t} & e^{2i\Omega_{12}t} & -e^{-2i\Omega_{12}t} \end{pmatrix},$$

$$\underline{U} = \begin{pmatrix} 1 & 1 & -1 & -1 \\ 1 & 1 & 1 & 1 \\ 1 & -1 & -1 & 1 \\ 1 & -1 & 1 & -1 \end{pmatrix}, \quad (3.1.13)$$

while $\mathbf{a}^T = (1, 1, \Gamma/\Gamma_{12}, \Gamma/\Gamma_{12})$ and $\mathbf{b}^T = (\Gamma_a/\Gamma_{12}, -\Gamma_s/\Gamma_{12}, 0, 0)$. Expression (3.1.12) is the basis for the subsequent analysis.

Following the same method as introduced in Ref. [109], the far-field spontaneous emission intensity at a distance r from origin of the double-QD system (see Fig. 3.3) is actually the radial component of the Poynting vector at that point. The positive-frequency

part of outgoing electric field operator for the system of two identical QDs can be written similar to Ref. [121] as

$$\hat{\mathbf{E}}^{(+)}(\mathbf{r}, \mathbf{t}) = \frac{k_0^2 \mu \mathbf{e}_\theta}{r} \sin \theta [\hat{\mathcal{S}}_1^-(t - \sqrt{\epsilon_h} r_1/c) + \hat{\mathcal{S}}_2^-(t - \sqrt{\epsilon_h} r_2/c)], \quad (3.1.14)$$

where $r_{1,2} = d \mp (d/2) \sin \theta \sin \phi$, and r, θ, ϕ are the spherical coordinates with zero at the center of the QD connecting axis. The observed value of intensity is defined as $I(\mathbf{r}, \mathbf{t}) = \langle \hat{\mathbf{E}}^{(-)}(\mathbf{r}, \mathbf{t}) \hat{\mathbf{E}}^{(+)}(\mathbf{r}, \mathbf{t}) \rangle$. For the intensity calculations we need the correlators $\langle \hat{\mathcal{S}}_i^-(\mathbf{r}, \mathbf{t}) \hat{\mathcal{S}}_j^+(\mathbf{r}, \mathbf{t} + \tau) \rangle$, which is reduced to $\langle \hat{\mathcal{S}}_i^-(\mathbf{r}, \mathbf{t}) \hat{\mathcal{S}}_j^+(\mathbf{r}, \mathbf{t}) \rangle$ in the quasi-stationary approximation.

For the sake of a better analysis and comparison, we write the final result of the emission intensity in a form similar to the macroscopic antenna theory [151] as

$$I(\mathbf{r}, \mathbf{t}) = \frac{k_0^4 \mu^2}{r^2} g(\theta) f(\theta, \varphi, \mathbf{t} - \mathbf{t}_r), \quad (3.1.15)$$

where $\mathbf{t}_r = \sqrt{\epsilon_h} \mathbf{r}/c$ is the propagation time, $g(\theta) = \sin^2 \theta$ is the energy radiation pattern of the single emitter which in our case is the single QD and

$$f(\theta, \varphi, \mathbf{t}) = \sum_{i,j=1}^2 \exp\{ik_0(\mathbf{r} \cdot \mathbf{e}_{12})\} \langle \hat{\mathcal{S}}_i^+(\mathbf{t}) \hat{\mathcal{S}}_j^-(\mathbf{t}) \rangle \Theta(\mathbf{t})$$

is the emission pattern originating from the interaction between the two QDs; $\Theta(\mathbf{t})$ is the Heaviside step function equal to zero at $\mathbf{t} \leq 0$ and equal to unity at $\mathbf{t} \geq 0$. As is depicted in the schematic picture of Fig. (3.3), in deriving Eq. (3.1.15), we have assumed that the QD dipole moments are parallel and we are in the far-field regime ($r \gg r_{12}$). In the antenna theory, the quantity $f(\theta, \varphi, \mathbf{t})$ is conventionally referred to as array factor [151]. Generally, the array factor characterizes antenna arrays with arbitrary number of elements but can also be applied to arrays with two elements as we deal with in our case. Hereafter we shall follow this fixed terminology.

The total emitted luminescence power can be represented by

$$I_\Sigma(\mathbf{t}) = -dP(\mathbf{t})/d\mathbf{t}, \quad (3.1.16)$$

where $P(\mathbf{t}) = \hbar \omega_0(x_1 + x_2) + \hbar \Omega_{12}(x_3 + x_4)$ is the total energy of the QD system. Using the general solution (3.1.12), we can consider the temporal behavior of $I_\Sigma(\mathbf{t})$ for different initial states. Note that the quantity $I_\Sigma(\mathbf{t})$ is an integral characteristic and thus does not comprise spatial variables. The relation

$$I_\Sigma(\mathbf{t}) = \lim_{r \rightarrow \infty} \left(r^2 \int I(\mathbf{r}, \mathbf{t}) d\mathcal{O} \right) \quad (3.1.17)$$

couples this characteristic with the far-field spontaneous emission intensity $I(\mathbf{r}, \mathbf{t})$ at a space point \mathbf{r} ($d\mathcal{O} = \sin \theta d\theta d\varphi$ is the solid angle).

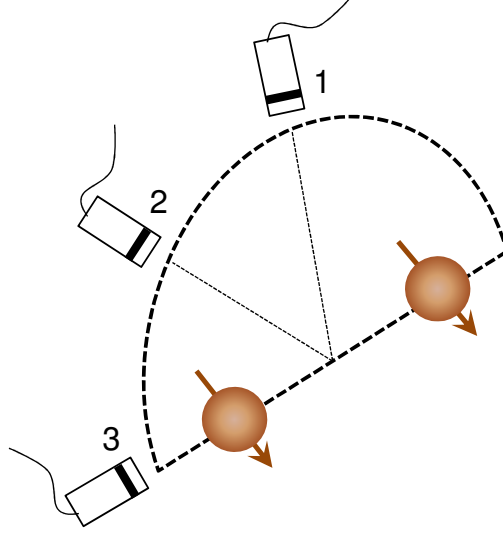


Figure 3.4: Schematic of the observation points. Point 1 is denoted for $(\theta = \pi/2, \varphi = 0)$, 2 for $(\theta = \pi/2, \varphi = \pi/4)$ and 3 for $(\theta = \pi/2, \varphi = \pi/2)$.

3.2 Time resolved spontaneous emission

As it has been demonstrated in the previous section, in the absence of any external laser field the master equation (3.1.6) is reduced to a close set of coupled equations, Eq. (3.1.11), which fully describes the population dynamics and time decay rate of the spontaneous emission. By replacing the correlated terms $\langle \hat{S}_i^+ \hat{S}_j^- \rangle$ presented by Eq. (3.1.12) into Eq. (3.1.15), we arrive at

$$f_{ee}(\theta, \varphi, t) = \frac{2}{\Gamma_a} (\Gamma_s e^{-\Gamma_s t} - 2\Gamma_{12} e^{-2\Gamma t}) \cos^2 \frac{\Psi}{2} + \frac{2}{\Gamma_s} (\Gamma_a e^{-\Gamma_a t} + 2\Gamma_{12} e^{-2\Gamma t}) \sin^2 \frac{\Psi}{2}, \quad (3.2.1)$$

for the array factor f_{ee} of the initially double-excited state $|\psi_{ee}\rangle = |e_1\rangle |e_2\rangle$. Analogously, for the array factor f_{ent} of the initially entangled state $|\psi_{ent}\rangle = \cos \Phi |e_1\rangle |g_2\rangle + \sin \Phi |g_1\rangle |e_2\rangle$ with the excitation phase shift Φ , we obtain

$$f_{ent}(\theta, \varphi, t) = -\sin \Psi \cos 2\Phi \sin(2\Omega_{12}t) e^{-\Gamma t} + (1 + \sin 2\Phi) \cos^2 \frac{\Psi}{2} e^{-\Gamma_s t} + (1 - \sin 2\Phi) \sin^2 \frac{\Psi}{2} e^{-\Gamma_a t} \quad (3.2.2)$$

Here $\Psi = k_0 r_{12} \sin \theta \sin \varphi$. In the particular case of $\Phi = 0$, the entangled state $|\psi_{ent}\rangle$ is transformed into the initially single-QD excited state $|\psi_{eg}\rangle = |e_1\rangle |g_2\rangle$. In that case Eq.

(3.2.2) reduces to an expression for the array factor f_{eg} :

$$f_{\text{eg}}(\theta, \varphi, t) = \sin \Psi \sin(2\Omega_{12}t) e^{-\Gamma t} + \cos^2 \frac{\Psi}{2} e^{-\Gamma_s t} + \sin^2 \frac{\Psi}{2} e^{-\Gamma_a t}. \quad (3.2.3)$$

In the case of $|\psi_{\text{ee}}\rangle$, where both QDs are initially excited, there is a channel decaying with the emission rate 2Γ . This channel is attributed to the Two-Photon Emission (TPE) phenomena and is a consequence of exciton-exciton coupling. For the case of the biexciton which is actually a system of two coupled excitons in a single QD, the TPE process has been experimentally observed [152]. In our case, the difference is that the coupled excitons belong to two separate QDs.

Let us compare the array factors for the system of two QDs with the array factors for two classical dipoles. Following Ref. [151], the latter quantity can be presented as

$$f_{\text{cla}}(\Psi) = B \sin \Psi + B_+ \cos^2 \frac{\Psi}{2} + B_- \sin^2 \frac{\Psi}{2}, \quad (3.2.4)$$

where $B = -2J_1 J_2 \sin \delta\varphi$, $B_{\pm} = J_1^2 + J_2^2 \pm 2J_1 J_2 \cos \delta\varphi$, $J_{1,2}$ are the dipole currents and $\delta\varphi$ is the mutual phase shift. It should be noted that the dipole currents are induced by independent sources. That is why they both the dipole currents and phases are a priori independent quantities. The factor (3.2.4) completely determines the directional emission pattern of a two-dipole antenna. For in-phase and opposite-phase dipoles $B_+ \geq B_-$ and $B_+ \leq B_-$, respectively.

The factors analogous to all three terms in (3.2.4) are also presented in Eqs. (3.2.1)–(3.2.3). The essential difference is that these factors decay in time for the system of QDs. This means that the directional emission pattern of two coupled QDs becomes time-dependent since different decay channels are dominant for different emission directions. Indeed, for the entangled state the correlation $(1 \pm \sin(2\Phi)) \exp\{-\Gamma_{s,a}t\} \rightarrow B_{\pm}$ is obvious. Consequently, the second term in (3.2.4) corresponds to symmetrical (superradiant) mode while the third one corresponds to asymmetrical (subradiant) mode. Thus, the time dependence of the directional emission pattern is a consequence of the $d-d$ interaction, i.e. of the process which has no analogs in classical antennas. If one of the dipoles in the classical antenna is unloaded, for example $J_2 = 0$, we arrive at $f_{\text{cla}}(\Psi) = J_1^2$. This means that the second dipole does not manifest itself and the antenna radiates as a single dipole. In a system of QDs such a situation corresponds to the state $|\psi_{\text{eg}}\rangle$, see Eq. (3.2.3). The difference is that the aforementioned nonstationarity provides the array factor dependence on Ψ . As a result, the radiation directivity converges with the decay. The value $\Phi = \pi/4$ in (3.2.2) corresponds to the excitation of $|s\rangle$ mode in the QD system. In this case $f_{\text{ent}}(\Psi) \sim \cos^2(\Psi/2)$, which corresponds to the in-phase excitation of classical dipoles by identical currents: $B_- = B = 0$ if we assume in (3.2.4) $J_1 = J_2$ and $\delta\varphi = 0$. Analogously, one can find that $\Phi = 3\pi/4$ corresponds to the excitation of the $|\alpha\rangle$ mode and thus corresponds to the antiphase excitation of classical dipoles: letting $J_1 = J_2$ and $\delta\varphi = \pi$ in (3.2.4) we arrive at $B = 0$.

For the double-excited state $|\psi_{\text{ee}}\rangle$, from (3.2.1), the relations $2(\Gamma_a e^{-\Gamma_a t} + 2\Gamma_{12} e^{-2\Gamma t})/\Gamma_s \rightarrow B_+$ and $2(\Gamma_s e^{-\Gamma_s t} - 2\Gamma_{12} e^{-2\Gamma t})/\Gamma_a \rightarrow B_-$ are followed. It can easily be found that $B_+ \simeq$

B_- at small t and thus $f_{ee}(\Psi) = \text{const}$, i.e. in that case the system radiates as a single dipole, situation is changed at large t when contributions of symmetrical mode and two-photon channel becomes negligible. As a result, the radiation gains directionality (at large t , $B_+ \gg B_-$ providing $f_{ee}(\Psi) \sim \cos^2(\Psi/2)$).

It should be emphasized that the discussed nonstationarity of the array factors, which is inherent to quantum emitters is not the only difference to classical dipoles. The second important factor is the oscillations in the first term in (3.2.3) and (3.2.2) originated from quantum correlations between states in different QDs. This term is odd with respect to Ψ and corresponds to coupling of dipoles in classical antennas. Moreover, this term describes oscillations of the array factor with the frequency Ω_{12} . A strong d-d coupling between the QDs induces this process (the terms $\sim O(\Omega_{12})$ can not be treated as small perturbations).

Thus, in the strong coupling regime the dipole-dipole interaction qualitatively changes the emission pattern as compared with macroscopic antennas. As has been shown above, in two-QD antennas the emission pattern becomes nonstationary. Moreover, from Eqs. (3.2.1)-(3.2.2) it follows that, in general case, the spatial and temporal behavior of the spontaneous emission are not factored. This is because every eigenstate of the system (symmetric, antisymmetric and two-photon state) is characterized by its own emission rate (Γ_s , Γ_a and 2Γ , respectively) and its own emission pattern.

From now on, we focus on the observation points located at $(\theta = \pi/2, \varphi = 0)$, $(\theta = \pi/2, \varphi = \pi/4)$ and $\theta = \pi/2, \varphi = \pi/2$ which are respectively denoted by 1, 2 and 3 in Fig. (3.4).

The time profile of the spontaneous emission from a two-QD system into different angular directions has been indicated in Fig. (3.5). It is observed that at $\varphi = 0$, both $|\psi_{eg}\rangle$ and $|\psi_{ent}\rangle$ decay with the same emission rate, but in other directions, each channel decays with its own rate. The oscillations due to the first term of Eqs. (3.2.2) and (3.2.3) with the frequency Ω_{12} are also observable.

The influence of the QD-QD separation on the decay time of the emission is demonstrated in Fig. (3.6). In each graph, you can compare the emission decay in the coupled case with the uncoupled case. Depending on the QD-QD separation, it is shown that the emission can be either faster or slower than the emission of the uncoupled system. The role of the coherent part of the dipole-dipole coupling, Ω_{12} , becomes evident for very closely spaced QDs. This role is to introduce oscillations with frequency Ω_{12} on the decay dynamics of the emission from the $|\psi_{eg}\rangle$ and $|\psi_{ent}\rangle$ states.

3.3 Spontaneous emission pattern

The spontaneous emission pattern from a double-QD system can be measured by positioning detectors at different angular positions (θ, φ) with respect to the centre of the

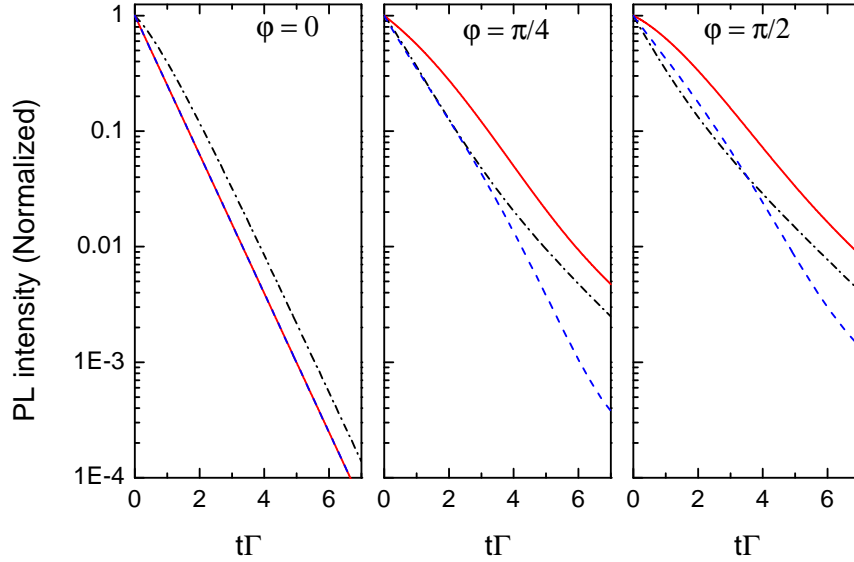


Figure 3.5: Time Resolved PL from a two-QD system into different angular directions of $\varphi = 0$ (left), $\varphi = \pi/4$ (middle) and $\varphi = \pi/2$ (right) when both QDs are initially excited (dash-dotted line), one QD is excited (solid line) and the system is prepared in an entangled state with $\Phi = \pi/6$. In this graph, $r_{12} = 100\text{nm}$ and $\theta = \pi/2$ (dashed line). The emission is normalized with the emission at $t = 0$.

QD-QD axis and keeping the radial distance fixed. The detected signal is actually the time-integral of the intensity introduced in Eq. (3.1.15) and reads

$$f^{\text{int}}(r, \theta, \varphi) = \int_{t_r}^{\infty} f(\theta, \varphi, t - t_r) dt. \quad (3.3.1)$$

By substituting the array factors given by Eqs. (3.2.1)-(3.2.2) into this equation, we obtain for the different initial states

$$f_{\text{ee}}^{\text{int}}(\theta, \varphi) = \frac{2}{\Gamma}, \quad (3.3.2)$$

$$f_{\text{ent}}^{\text{int}}(\theta, \varphi) = \sin \Psi \cos 2\Phi \frac{2\Omega_{12}}{4\Omega_{12}^2 + \Gamma^2} + \frac{1 + \sin 2\Phi}{\Gamma_s} \cos^2 \frac{\Psi}{2} + \frac{1 - \sin 2\Phi}{\Gamma_a} \sin^2 \frac{\Psi}{2}, \quad (3.3.3)$$

$$f_{\text{eg}}^{\text{int}}(\theta, \varphi) = \frac{1}{\Gamma_a} \sin^2 \frac{\Psi}{2} + \frac{1}{\Gamma_s} \cos^2 \frac{\Psi}{2} + \frac{2\Omega_{12} \sin \Psi}{4\Omega_{12}^2 + \Gamma^2}, \quad (3.3.4)$$

It is evident from Eq. (3.3.2) that if both QDs are initially excited, the intensities measured at different angular positions are equal to the emission intensity in the uncoupled

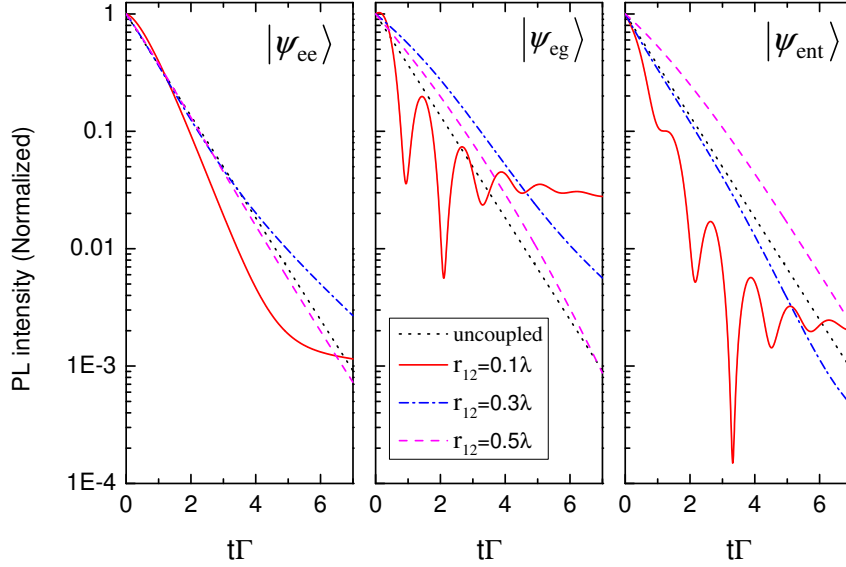


Figure 3.6: Time Resolved PL from a two-QD system into the direction $\varphi = \pi/4$ for the emission from $|\psi_{ee}\rangle$ (left), $|\psi_{eg}\rangle$ (middle) and $|\psi_{ent}\rangle$ with $\Phi = \pi/6$ (right). The QD-QD separation is $r_{12} = 0.1\lambda$ (solid line), $r_{12} = 0.3\lambda$ (dash-dotted line), $r_{12} = 0.5\lambda$ (dashed line) and the uncoupled case (dotted line). In this graph, $r_{12} = 100\text{nm}$ and $\theta = \pi/2$. The graph is on a logarithmic scale and the emission is normalized with the emission at $t = 0$.

case. So for the remainder, we only consider the spontaneous emission pattern in which only one QD is initially excited or the double-QD system is initially prepared in an entangled state. The angular emission pattern from a double-QD system is depicted in Fig. (3.7) It is clear that the emission is maximum at $\theta = \pi/2$ for all initial conditions. It is clear that if initially only one QD is excited or the system is prepared in an entangled state, the emission pattern is not symmetric between $0 < \varphi < \pi$ and $\pi < \varphi < 2\pi$.

As follows from (3.1.15), the correlated spontaneous emission is a superposition of three wave packets propagating in the radial direction under different angles. The radial dependence of the intensity $I(\mathbf{r}, t)$ is essentially different from the corresponding dependence of the spherical wave, $O(1/r^2)$, and has an additional coefficient which is a superposition of three exponents. Note that for entangled states, this dependence contains also oscillations with period $2\Omega_{12}\sqrt{\epsilon_h}/c$, which are due to the asymmetry of the array factor mentioned above.

As it is seen from Eqs. (3.2.2) and (3.2.3), these oscillations can be presented as a superposition of two counter-propagating spherical modes. These modes have complex-conjugated wave numbers that correspond to the interaction of two modes with op-

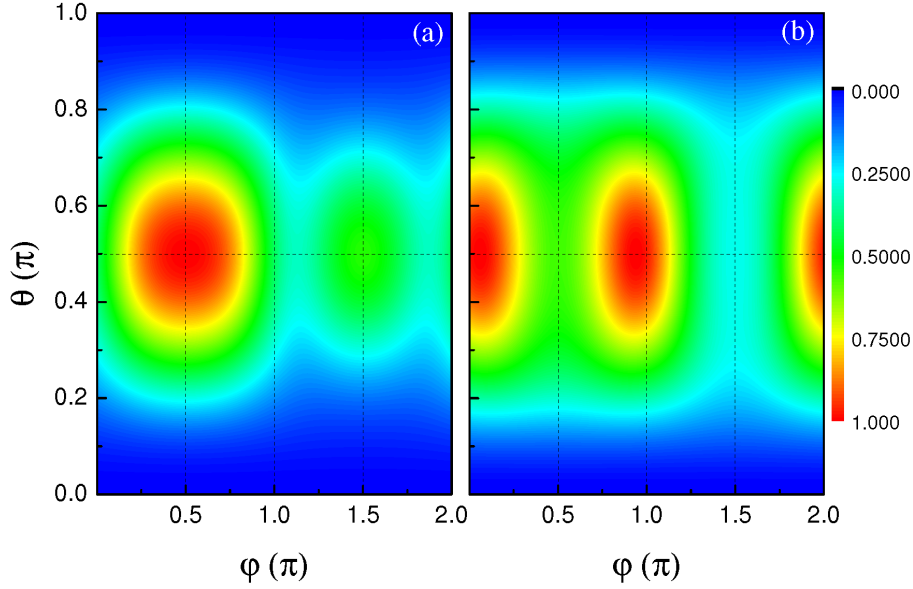


Figure 3.7: Emission pattern, $PL(\theta, \varphi)/\Gamma$, of a double-QD system when (a) one QD is initially excited and (b) the system is initially prepared in an entangled state with $\Phi = \pi/6$. In all cases $r_{12} = 100$ nm.

positively directed energy fluxes. Such waves, in microwave electrodynamics conventionally referred to as complex waves, have been detected in plane waveguides with anisotropic walls and in some other waveguiding structures, see Ref. [153] for a brief overview. These waves are pairwise excited and do not transfer energy. In our case, instead of guided waves, we deal with spherical complex waves which also do not transfer energy.

The existence of such waves is mediated by the photonic reservoir and is governed by the spatial-temporal field correlations, being induced due to the dipole-dipole interaction between the QDs. Thus, the contribution of the additional modes into the integrated intensity vanishes as a result of the integration in (3.1.17) which is in agreement with Ref. [110]. As a result, the existence of complex spherical waves does not contradict the radiation conditions, which have more general form for complex waves than the classical Sommerfeld radiation conditions [153].

In order to investigate the effect of radiative coupling between QDs on the emission pattern of the system, we need to normalize the graphs in Fig. 3.7 with the emission pattern of the non-interacting systems with identical initial excitation when $\Gamma_{12} = \Omega_{12} = 0$. For a QD-QD separation of 100 nm, this is demonstrated in Fig. (3.8). For the case where only one QD is initially excited (a), there is a large asymmetry. The emission intensity is stronger for $0 < \varphi < \pi$, and weaker for $\pi < \varphi < 2\pi$, as compared to

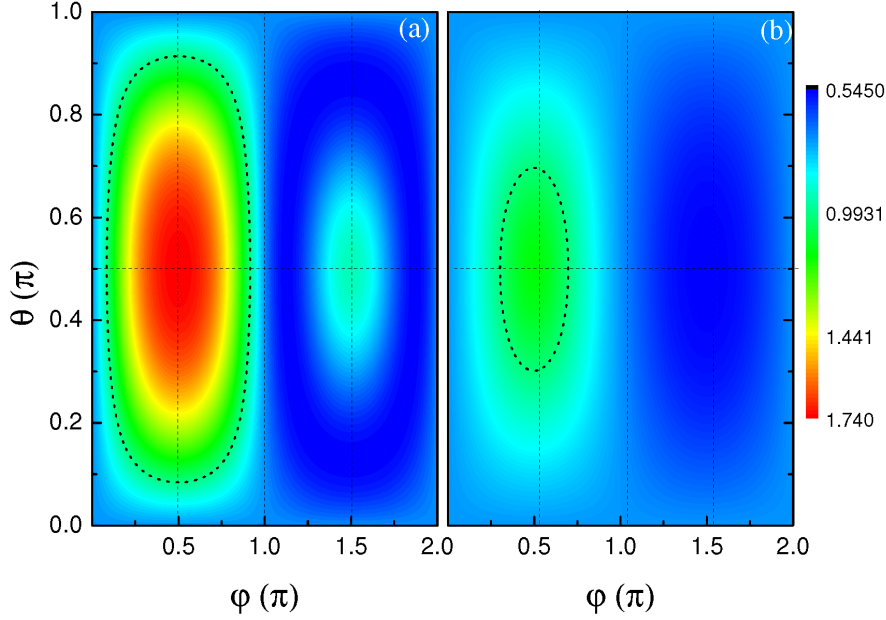


Figure 3.8: Angular emission pattern normalized with the emission pattern of two non-interacting QDs, $PL(\theta, \varphi)/PL_{\text{uncoupled}}(\theta, \varphi)$, when (a) only one QD is initially excited and (b) the system is initially prepared in an entangled state with $\Phi = \pi/6$. In all cases $r_{12} = 100\text{nm}$. Inside the dotted circles, the total emission is stronger and outside the circles, the emission is weaker than the emission of uncoupled QDs.

the uncoupled case. If the system is initially prepared in an entangled state (b), the angular pattern greatly depends on the phase shift Φ and in general, the pattern is not symmetric.

The angular emission pattern of the entangled state is depicted in Fig. (3.9) for different initial entanglement. We observe that the emission pattern is only symmetric for a particular initial entanglement, but in general it is not symmetric. By changing the initial entanglement, we alter the spatial distribution of the incoming and outgoing components, leading to a large variety of emission patterns. In Fig. (3.8), inside the dotted circles, the emission intensity is stronger and outside the circles, it is weaker than for the uncoupled double-QD system with the same initial conditions.

The QD-QD distance is another important item in a double-QD system which governs the strength of radiative coupling between the QDs and also influences the emission pattern. The influence of this quantity is evident in coupling parameters Γ_{12} , Ω_{12} as well as in the detection point dependent parameter Ψ . It is clear in Fig. (3.10) that the PL intensity at some particular angular positions is enhanced by the QD-QD coupling, while it is reduced for other angles, as compared to the uncoupled case. The asymmetry between the regions $0 < \varphi < \pi$ and $\pi < \varphi < 2\pi$ is also observed for almost all QD-QD

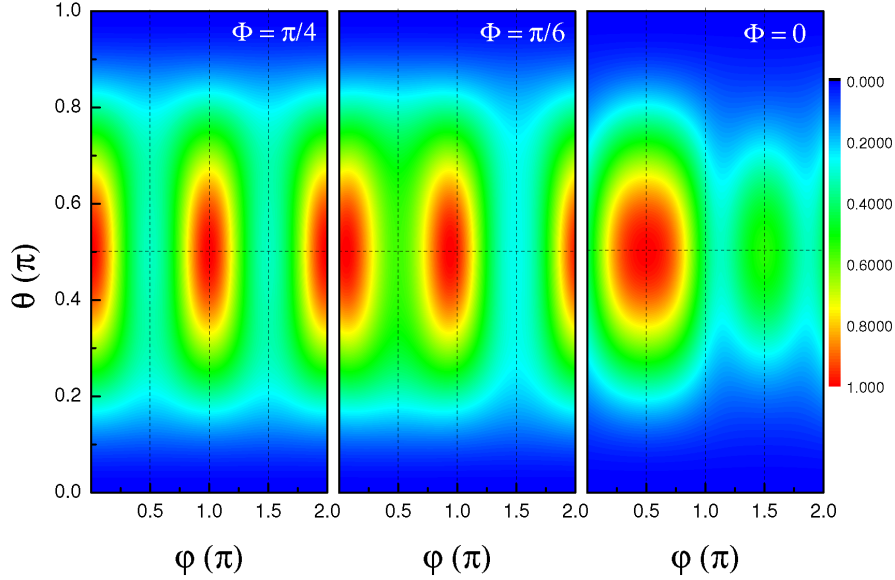


Figure 3.9: Angular emission pattern of a double-QD system, $PL(\theta, \varphi)/\Gamma$, when it is initially prepared at an entangled state for (left panel) $\Phi = \pi/4$, (middle panel) $\Phi = \pi/6$ and (right panel) $\Phi/2$. In all cases $r_{12} = 100\text{nm}$.

separations. For larger QD-QD separations, r_{12} , oscillations between the superradiant and subradiant regimes are more frequent as a function of the azimuthal angle φ .

The corresponding PL intensities at the observation points indicated in Fig. (3.4) are shown in Fig. (3.11) as a function of the QD-QD separation. In this figure, it is clear that if the detector is located exactly perpendicular to the sample substrate, no difference between the emission intensity from $|\psi_{eg}\rangle$ and $|\psi_{ent}\rangle$ is observable. At this position, the collective PL is weaker than the PL of uncoupled QDs for the case of very closely spaced QDs. Subsequently by increasing the QD-QD separation, the PL intensity oscillates between the superradiant and subradiant regimes. By locating the detector at positions 2 and 3 of Fig. (3.4), the emission from $|\psi_{eg}\rangle$ and $|\psi_{ent}\rangle$ will be more distinguishable from each other. At these positions, the PL-emission from the system of very closely spaced QDs might be either stronger or weaker than the emission of uncoupled QDs.

In this section we have considered the spatial distribution of far-field intensity for the spontaneous emission of two QDs. The problem is of interest because the correlations governed by $d - d$ interaction are able to essentially transform the spatial distribution. The ability to tune the directivity of the spontaneous emission, in fact, was noted previously [95]: if the initial state of an infinitely large and homogeneous medium of two-level atoms is prepared by the absorption of a photon, the emitted photon is directed

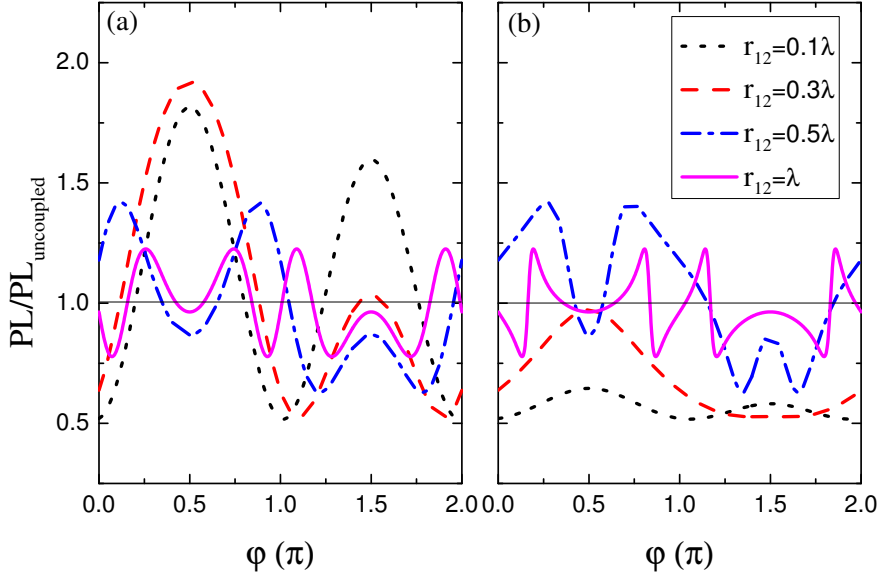


Figure 3.10: Relative PL intensity normalized to the emission of uncoupled QDs for $|\psi_{eg}\rangle$ (a) and $|\psi_{ent}\rangle$ with $\Phi = \pi/6$ (b), as a function of φ for different QD-QD distances of $r_{12} = 0.1\lambda$ (dotted line), $r_{12} = 0.3\lambda$ (dashed line), $r_{12} = 0.5\lambda$ (dash-dotted line) and $r_{12} = \lambda$ (solid line). In this graph $\theta = \pi/2$.

along the absorbed one. As we have shown in our analysis, new possibilities for the control of the spontaneous emission direction arise for the emitters with sizes which are in a particular direction comparable with the wavelength. One can conclude that such emitters can play the role of quantum-optical antennas, whereby we can generate an effective correlated spontaneous emission. Different nano-sized objects can be utilized for the practical realization of such antennas, which can be referred to as quantum nanoantennas. As an example of such a two-element antenna we have considered the system of two identical QDs.

3.4 Spontaneous emission spectrum

Here we consider another interesting property of the correlated spontaneous emission which takes place for quantum states without geometrical center of inversion (such as $|\psi_{ent}\rangle$ and $|\psi_{eg}\rangle$). The spontaneous emission spectrum for such states is a triplet, a central line at the frequency $\omega = \omega_0$ and two additional lines appearing at the frequencies $\omega = \omega_0 + \Omega_{12}$ and $\omega = \omega_0 - \Omega_{12}$. The contribution of these emission lines to the field intensity is described by the first terms in Eqs. (3.3.4)-(3.3.3). The equations (3.2.1)-(3.2.2)

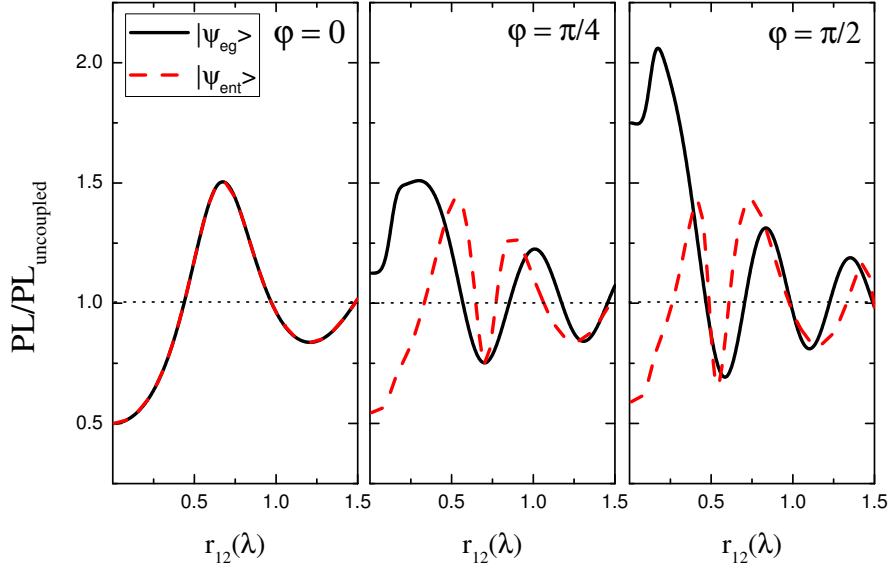


Figure 3.11: Relative PL intensity normalized to the uncoupled QD system for $|\psi_{eg}\rangle$ (solid line) and $|\psi_{ent}\rangle$ with $\Phi = \pi/6$ (dashed line) at the observation points 1,2,3 indicated in Fig. (3.4). Left: $\theta = \pi/2, \varphi = 0$, Middle: $\theta = \pi/2, \varphi = \pi/4$, Right: $\theta = \pi/2, \varphi = \pi/2$

are time-averages over the oscillation period. But, in order to obtain the PL emission spectrum $S(\theta, \varphi, \omega)$, we need to take a Fourier transform of the two-time correlation function $f(\theta, \varphi, t_1, t_2)$, which is given by

$$S(\theta, \varphi, \omega) = \frac{1}{\pi} \text{Re} \int_0^{\infty} \int_{-t}^{\infty} f(\theta, \varphi, t, t+\tau) e^{i\omega\tau} d\tau dt, \quad (3.4.1)$$

where

$$\begin{aligned} f(\theta, \varphi, t_1, t_2) = & \langle \hat{S}_1^+(t_1) \hat{S}_1^-(t_2) \rangle + \langle \hat{S}_2^+(t_1) \hat{S}_2^-(t_2) \rangle \\ & + \cos \Psi [\langle \hat{S}_1^+(t_1) \hat{S}_2^-(t_2) \rangle + \langle \hat{S}_1^-(t_1) \hat{S}_2^+(t_2) \rangle] \\ & + i \sin \Psi [\langle \hat{S}_1^+(t_1) \hat{S}_2^-(t_2) \rangle - \langle \hat{S}_1^-(t_1) \hat{S}_2^+(t_2) \rangle]. \end{aligned} \quad (3.4.2)$$

To evaluate the two-time correlation functions $f(\theta, \varphi, t_1, t_2)$, we utilize a standard technique based on the Onsager theorem [121]. As a result, the two-time correlation functions are expressed in terms of the corresponding single-time correlators which are spec-

ified from the initial conditions. After some algebra we arrive at ($\tau > 0$)

$$\langle \hat{S}_1^+(t)\hat{S}_1^-(t+\tau) + \hat{S}_2^+(t)\hat{S}_2^-(t+\tau) \rangle = [\mathbf{B}_{es}(\tau) + \mathbf{B}_{ea}(\tau)]\rho_{ee}(t) + C_{sg}(\tau)\rho_{ss}(t) + C_{ag}(\tau)\rho_{aa}(t), \quad (3.4.3)$$

$$\langle \hat{S}_1^+(t)\hat{S}_2^-(t+\tau) + \hat{S}_2^+(t)\hat{S}_1^-(t+\tau) \rangle = [\mathbf{B}_{es}(\tau) - \mathbf{B}_{ea}(\tau)]\rho_{ee}(t) + C_{sg}(\tau)\rho_{ss}(t) - C_{ag}(\tau)\rho_{aa}(t), \quad (3.4.4)$$

$$\langle \hat{S}_1^+(t)\hat{S}_2^-(t+\tau) - \hat{S}_2^+(t)\hat{S}_1^-(t+\tau) \rangle = C_{sg}(\tau)\rho_{sa}(t) - C_{ag}(\tau)\rho_{as}(t). \quad (3.4.5)$$

Here,

$$C_{sg}(\tau) = \exp\{-i\omega_+\tau - \Gamma_s\tau/2\} \quad (3.4.6)$$

$$\mathbf{B}_{es}(\tau) = (1 + \xi_s) \exp\{-i\omega_-\tau - \gamma_s\tau\} - \xi_s C_{sg}(\tau) \quad (3.4.7)$$

$\xi_s = \Gamma_s/(-2i\Omega_{12} + \Gamma)$, $\xi_a = \Gamma_a/(-2i\Omega_{12} - \Gamma)$, $\gamma_{s,a} = \Gamma + \Gamma_{s,a}/2$ and $\omega_{\pm} = \omega_0 \pm \Omega_{12}$. The equations for C_{ag} and \mathbf{B}_{ea} are obtained from (3.4.6) and (3.4.7) by the substitutions $\omega_{\pm} \rightarrow \omega_{\mp}$, $\Gamma_s \rightarrow \Gamma_a$ and $\gamma_s \rightarrow \gamma_a$.

The calculation of the frequency spectrum by Eq. (3.4.2) using (3.4.3)–(3.4.7) leads to very awkward final expressions. That is why we restrict ourselves to some partial cases of the initial conditions which are of most physical interest. In particular, the initial conditions $\rho_{ee}^0 = 0$, $\rho_{ss,aa}^0 = (1 \pm \sin 2\Phi)/2$, $\rho_{sa}^0 = \rho_{as}^0 = \cos 2\Phi/2$ in (3.4.3)–(3.4.5) correspond to the entangled state. In that case, using (3.4.2) we obtain the following spectrum

$$S_{\text{ent}}(\omega) = \frac{1}{\pi}(S(\omega) + S(-\omega)), \quad (3.4.8)$$

where

$$S(\omega) = \frac{\rho_{aa}^0(1 - \cos \Phi)}{(\omega - \omega_-)^2 + (\frac{\Gamma_a}{2})^2} + \frac{\rho_{ss}^0(1 + \cos \Phi)}{(\omega - \omega_+)^2 + (\frac{\Gamma_s}{2})^2} - \frac{\rho_{as}^0 \sin \Psi [\Gamma_s(\omega_- - \omega) - \Gamma_a(\omega_+ - \omega)]}{\left[(\omega - \omega_-)^2 + (\frac{\Gamma_s}{2})^2 \right] \left[(\omega - \omega_+)^2 + (\frac{\Gamma_a}{2})^2 \right]}. \quad (3.4.9)$$

Analyzing (3.4.8), (3.4.9) one can conclude that the entangled state spectrum comprises two resonant lines with frequencies ω_+ and ω_- (as is dictated by Eq. (3.4.9)) and a non-resonant component induced by the second term in (3.4.8). It should be emphasized that resonant lines are non-Lorentzian. Their antisymmetrical component is proportional to $\sin \Psi$, i.e. is determined by the azimuthal asymmetry of the directional emission pattern. In the absence of the $d-d$ interaction, these resonant lines merge to form a single symmetric line. Note that these peculiarities are the characteristics of the density of the energy flux into a particular angle. In the total radiation intensity the antisymmetric components are averaged out due to integration over the space angle.

An even more important example is a mixed $|a\rangle$ and $|s\rangle$ initial state, which is described by the diagonal density matrix ($\rho_{as}^0 = \rho_{sa}^0 = 0$) satisfying the normalization condition $\rho_{ss}^0 + \rho_{aa}^0 = 1$ with arbitrary ρ_{aa}^0 . The spectrum for such an initial state can be obtained from (3.4.9) letting $\rho_{as}^0 = 0$. One can see that the spectrum is a superposition of two Lorentzian lines with different frequencies, directional emission patterns and damping constants. Both directional diagrams are symmetrical with respect to the angle Ψ .

In a similar manner one can obtain the spectrum of the initially double-excited state $|\Psi_{ee}\rangle$. This spectrum can be represented as

$$S_{ee}(\omega) = (1 + \cos \Psi)[S_s(\omega) + S_s(-\omega)] + (1 - \cos \Psi)[S_a(\omega) + S_a(-\omega)], \quad (3.4.10)$$

where

$$S_{s,a}(\omega) = \frac{1}{\pi}(\Gamma_{s,a}D(\omega) + G_{s,a}(\omega)), \quad (3.4.11)$$

and

$$D(\omega) = \frac{\Gamma}{\Gamma^2 + 4\Omega_{12}^2}(G_s(\omega) - G_a(\omega)) - \frac{2\Omega_{12}}{\Gamma^2 + 4\Omega_{12}^2}(K_s(\omega) + K_a(\omega)), \quad (3.4.12)$$

with

$$G_s(\omega) = \frac{\Gamma_a \gamma_s / 2 + (\omega_- - \omega)^2}{[(\omega_- - \omega)^2 + (\frac{\Gamma_a}{2})^2][(\omega_- - \omega)^2 + \gamma_s^2]}, \quad (3.4.13)$$

$$K_s(\omega) = \frac{\Gamma_s(\omega_- - \omega)}{[(\omega_- - \omega)^2 + (\frac{\Gamma_a}{2})^2][(\omega_- - \omega)^2 + \gamma_s^2]}.$$

In Eq.(3.4.12), the parameters G_a and K_a can be obtained from G_s and K_s by exchanging $\Gamma_a \leftrightarrow \Gamma_s$, $\gamma_s \rightarrow \gamma_a$ and $\omega_- \rightarrow \omega_+$. The spectrum (3.4.10) is a superposition of two cascade processes $|e\rangle \rightarrow |s\rangle \rightarrow |g\rangle$ and $|e\rangle \rightarrow |a\rangle \rightarrow |g\rangle$ described by the terms $S_s(\omega)$ and $S_a(\omega)$, respectively. The corresponding non-resonant background is given by the terms $S_{s,a}(-\omega)$. The spontaneous emission spectra of a double-QD system for emission into different angular directions is indicated in Fig. (3.12). In the case where both QDs are initially excited, the spectrum consists of three Lorentzian terms, each with amplitudes which are a function of the angular direction. That's why the emission spectra are different for the different emission directions.

3.5 Population dynamics

The total population probability of the double-QD system is equal to $\mathcal{P}(t) = \langle \hat{S}_1^+ \hat{S}_1^- \rangle + \langle \hat{S}_2^+ \hat{S}_2^- \rangle$ which is initially 0 if both QDs are empty, 1 if one of them is excited and 2 if both QDs are excited, and $\mathcal{P}(t)$ varies between 0 and 2 for arbitrary populations. The total population dynamics can be directly probed in pump-probe reflectivity techniques by measuring the time profile of the reflected probe. It should be emphasized that the outgoing energy of the mode belonging to the first terms in Eqs. (3.2.2) –(3.2.3) for a given direction (θ, φ) is exactly compensated by the incoming energy of this mode in the opposite direction $(\theta, \pi + \varphi)$. Thus the contribution of these modes to the total emission intensity $I_\Sigma(t)$ vanishes as a result of summation over all propagation angles.

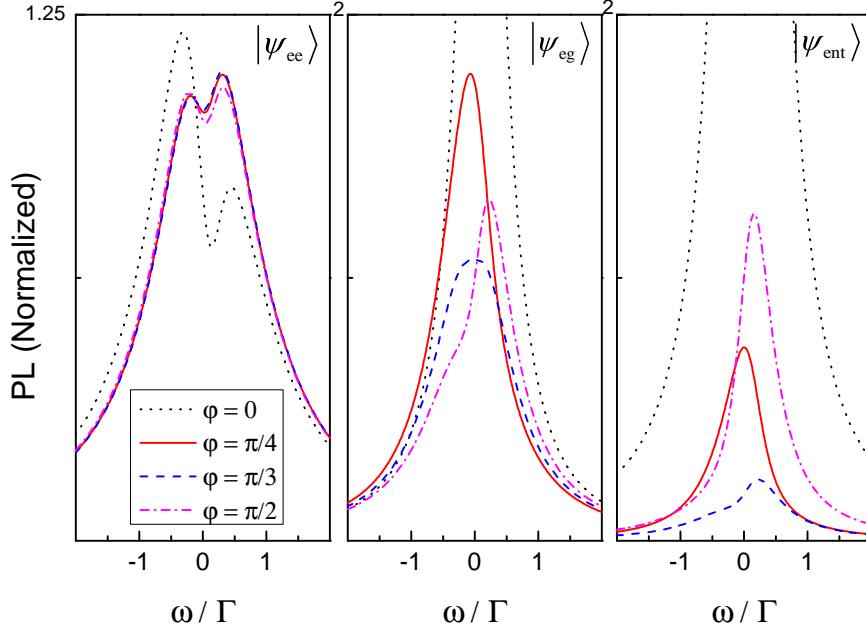


Figure 3.12: Spontaneous emission spectra from $|\psi_{ee}\rangle$ (left), $|\psi_{eg}\rangle$ (middle) and $|\psi_{ent}\rangle$ with $\Phi = \pi/3$ (right). The emission is calculated into the directions $\varphi = 0$ (dotted), $\varphi = \pi/4$ (solid), $\varphi = \pi/3$ (dashed) and $\varphi = \pi/2$ (dashed-dotted). The PL intensity in each graph is normalized to the emission of the two-QD system at $\omega = 0$ with $\varphi = \pi/2$ and the same initial condition. In this graph $r_{12} = 50$ nm and $\theta = \pi/2$.

3.6 Concluding remarks

In this paper, we have investigated the collective spontaneous emission in a system of two QDs strongly coupled via the dipole-dipole interaction. Resonant frequencies and dipole moments of QDs are assumed to be identical and oriented orthogonal to the QD–QD axis. The d – d interaction was described by the exchange of virtual photon through the photonic reservoir. The analysis was based on the master equation approach. The main conclusions of the paper are

1. There are three channels of the spontaneous decay in the two-QD system: superradiance, subradiance and two-photon emission. Each of these decay channels is characterized by not only a differing radiative decay factor but also by its own directional emission pattern. The relative contribution of each of these channels into the total radiation pattern is determined by the initial state of the system. Thus, the antenna characteristics of the two-QD system depends on its initial state.

2. The difference in the decay factors of each of these channels leads to a time-dependent total radiative emission pattern. Such an effect has no analogs in classical macroscopic antennas. For the entangled initial state, the total directional emission pattern shows oscillations with a frequency corresponding to the dipole-dipole interaction. The oscillating component is antisymmetric with respect to azimuthal angle. It should be emphasized that this oscillation effect is inherent to particular directional emission diagram and vanishes for the total radiation intensity as a result of the integration of the radiation pattern over solid angle. The oscillations are due to the strong coupling and cannot be described by a perturbation to the dipole-dipole interaction energy.
3. The frequency spectrum of the spontaneous emission of the two-QD system is formed by a superposition of two resonant lines with frequencies $\omega_{\pm} = \omega_0 \pm \Omega_{12}$ imposed on the non-resonant background, where $\hbar\Omega_{12}$ is the d – d interaction energy. It should be noted that the amplitudes of resonant lines depend on the meridial and azimuthal observation angles. Generally, the resonant lines are non-Lorentzian – each of them is a superposition of two Lorentzian lines with the same frequency but with different amplitudes and widths. This property must be taken into account for the calculation of the spectral lineshape.

The analysis carried out allows us to propose that the collective spontaneous emission of a QD ensemble provides an opportunity for the design of quantum nanoantennas whose radiative properties are dictated by the initial state of the system. Just by changing the QD-QD distance, we are able to increase (superradiance) or decrease (subradiance) the PL intensity as well as the spontaneous emission rate in a particular emission direction compared to those of the uncoupled system. A change of the QD-QD separation, r_{12} , will also modify the amplitude and width of the emission spectrum. From the experimental point of view, the spontaneous emission spectrum (PL), and the emission dynamics can be easily measured by locating the detectors at different angular positions around the system.

The two-QD system considered in this paper is the simplest of this kind. As a next step, more complex systems can be considered, such as 1D- and 2D arrays of quantum dots, quantum dot rings and also different combinations of emitting QDs with passive scattering elements (antennas of the Udo-Yagi type [151]).

Chapter 4

Entangled states and collective nonclassical effects in coupled QD-lattices

The experimental realization of quantum entanglement for quantum computation [154, 155] or quantum metrology [156–160] is currently a subject of intense study by many groups. It is already known for several decades that spontaneous emission from cooperative systems of many two-level quantum emitters is able to provide quantum entanglement between the individual two-level emitters [161–163]. It is however still a major challenge to fully understand and control the transfer of the excitation energy from one emitter to another nearby emitter within a cooperative system of quantum emitters such as e.g. a periodic lattice. For such a study, quantum dots (QDs) are particularly well suited since QDs have atom-like behavior and can be approximated as two-level systems with appropriate dipole moments [2–5, 28]. The energy transfer between 2 QDs can be mediated by nonradiative Förster coupling in closely-packed arrangement of QDs, i.e., when the inter-QD distance is on the order of the QD size or smaller. Examples of these structures are quantum dot molecules [164], chains [165], rings [166], two-dimensional [167] and three-dimensional [168], arrays as well as dendrites [169] based on QDs. In this chapter, we will however focus on a more general treatment of radiative coupling including the long range radiative [44] coupling between different QDs. In particular, we will study an infinitely large periodic QD-lattice, as well as two coupled QD-lattices. Such a study has not yet been reported.

The simplest structure for investigating the time evolution of an entangled state is a system of two 2-level emitters. Such a system has already been extensively studied for atoms [57, 98, 110, 132, 163] and QDs in free space [170, 171], in optical nanocavities [172], in photonic-crystal microcavities [173] and in micropillar cavities [174]. In the previous chapter, we investigated the simple system of two QDs positioned in free space or a

homogeneous medium. We indicated that how optical coupling of QDs can give rise to a correlated emission in the far-field. For structures composed of more than a few emitters, we encounter a complex many body problem, which presently, can neither be treated analytically nor numerically.

In this chapter, we will simplify the situation by focusing on an infinite and periodic 2D lattice of identical QDs. Inspired by solid state physics in which the electronic states of an infinite lattice of atoms is described in terms of the Bloch wave functions [175] to describe electronic coupling, we will apply similar periodic functions to describe the radiative coupling in an infinite 2-dimensional periodic array of QDs. The natural choice for the relevant "Bloch functions" in the case of radiative coupling, are the eigenmodes of the EM field in the 2D array as obtained by Floquet's theorem. It will be shown in Sec.(4.1) that the radiative coupling in a periodic and infinitely large lattice of QDs is formally equivalent to the coupling of a QD with a cavity. In Sec.(4.2), we present a general treatment of the radiative coupling of a single QD or two coupled QDs with arbitrary cavity modes, using the Master Equation approach. In Sec.(4.3.1), we will focus on radiative coupling in a single QD-lattice. It will become clear how a reservoir of EM resonator eigenmodes couples to the QD-dipoles and thus modifies the QD spontaneous emission. The entanglement between the cavity modes and the QD system gives rise to spontaneous radiation transfer between the QDs which is due to the exchange of virtual photons. In Sec.(4.3.2), we demonstrate the entanglement in a more complicated structure of two intermixed 2D lattices of QDs. We indicate how the spacing between two adjacent QD-lattices influences the collective spontaneous emission rates.

4.1 Model

Consider a two-dimensional structure in which identical QDs are distributed over rectangular lattice points with the periodicity a in both the x and y directions, see Fig.(4.1). We assume that an excitation pulse in the $y - z$ plane is incident on the surface of the QDs with an incidence angle of θ_{inc} with respect to the y -axis. Each QD is considered as a two-level system with the transition frequency ω_0 and transition dipole moments μ . Location of QDs in the lattice is determined by the radius-vector $\mathbf{r} = \mathbf{r}_i = a(q_x \mathbf{n}_x + q_y \mathbf{n}_y)$ where $\mathbf{n}_{x,y}$ are the unite vectors in the lattice plane and $q_x, q_y = 0, \pm 1, \pm 2, \dots$. The dual index $i = \{q_x, q_y\}$ completely determines the QD location. The general shape of the wave equation for the scalar Green's function is [176]

$$\nabla^2 G_0(\mathbf{r}, \mathbf{r}') + k_0^2 G_0(\mathbf{r}, \mathbf{r}') = \delta(\mathbf{r}, \mathbf{r}'). \quad (4.1.1)$$

In order to solve Eq.(4.1.1) for any arbitrary observation and source point, we should know the boundary conditions. In our case, the boundary condition is periodic in the $x - y$ plane. Assuming that the periodic surface is infinitely large, there are an infinite number of lattice points on which the boundary conditions should be fulfilled. Treating the problem in this way is very time consuming and analytically impossible. We can make a trick by employing the Bloch-Floquet formalism. In this formalism, instead of considering the observation and source points in free space by an infinite number of

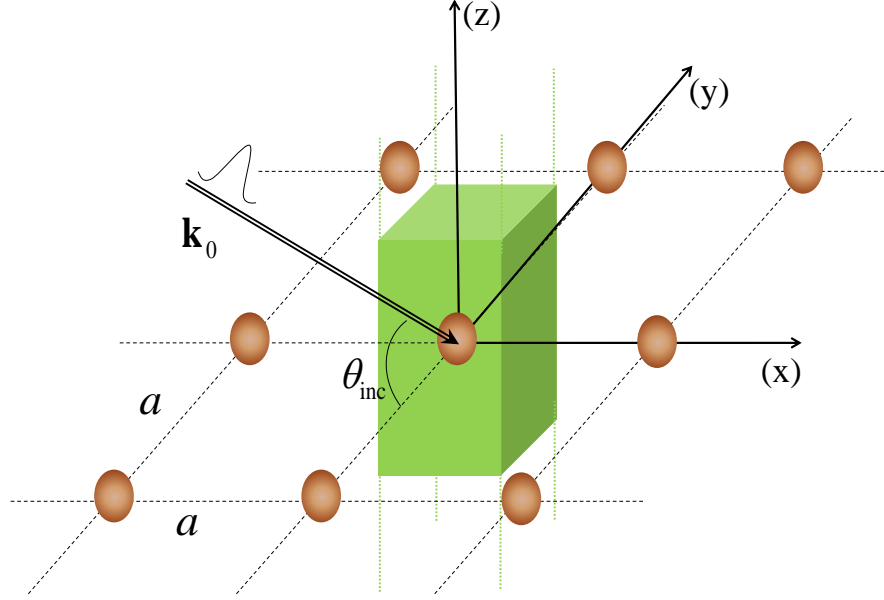


Figure 4.1: Schematic illustration of a 2D rectangular lattice of QDs in the $x - y$ plane and the equivalent cavity shown as the green box.

boundaries, we assume the observation and source points in a unit cell with perfectly conducting walls which embeds one of the lattice points and repeats periodically in the plane. Of course the length of each unit cell in the z -direction is infinitely large. This is equivalent to choosing a periodicity of infinity in this direction. The condition of perfectly conducting walls ensures the periodicity. Then the Green's function in such a rectangular box should satisfy the differential equation

$$\nabla^2 G_p(\mathbf{r}, \mathbf{r}') + k_0 G_p(\mathbf{r}, \mathbf{r}') = \lim_{l \rightarrow \infty} \sum_{q_x, q_y, q_z = -\infty}^{\infty} \delta(x - x' - q_x a) \delta(y - y' - q_y a) \delta(z - z' - q_z l), \quad (4.1.2)$$

in which we have employed the expansion and form of the Dirac delta function in the rectangular cavity. This equation has been solved in many text books and papers for rectangular lattices with periodic boundaries [103, 176–182] and gives

$$G_p(\mathbf{r}, \mathbf{r}') = \frac{1}{4\pi} \lim_{l \rightarrow \infty} \sum_{q_x, q_y, q_z = -\infty}^{\infty} \frac{e^{ik_0 R_{q_x q_y q_z}}}{R_{q_x q_y q_z}} e^{ik_0 \cos \theta_{inc} q_y a}, \quad (4.1.3)$$

$$R_{q_x q_y q_z} = \sqrt{(x - x' - q_x a)^2 + (y - y' - q_y a)^2 + (z - z' - q_z l)^2}.$$

We should emphasize again that the periodic Green's function G_p is the Green's function in a unit cell.

This shape of the Green's function is in the spatial domain and can be written as the Fourier transform of the spectral Green's function

$$G_p(\mathbf{r}, \mathbf{r}') = \frac{1}{(2\pi)^3} \lim_{l \rightarrow \infty} \int_{-\infty}^{\infty} \int_{-\infty}^{\infty} \int_{-\infty}^{\infty} dk_x dk_y dk_z \times \sum_{q_x, q_y, q_z = -\infty}^{\infty} \frac{e^{i[k_x(x-x'-q_x a) + k_y(y-y'-q_y a) + k_z(z-z'-q_z l)]}}{k_x^2 + k_y^2 + k_z^2 - k_0^2} e^{ik_0 \cos \theta_{\text{inc}} q_y a}. \quad (4.1.4)$$

By making use of the Poisson's summation formula,

$$\sum_{q=-\infty}^{\infty} e^{iqx} = 2\pi \sum_{m=-\infty}^{\infty} \delta(x + 2\pi m), \quad (4.1.5)$$

we obtain

$$G_p(\mathbf{r}, \mathbf{r}') = \lim_{l \rightarrow \infty} \frac{1}{a^2 l} \sum_{m, n, p = -\infty}^{\infty} \frac{e^{\frac{2\pi i m}{a}(x-x')} e^{i(\frac{2\pi n}{a} + k_0 \cos \theta_{\text{inc}})(y-y')} e^{\frac{2\pi i p}{l}(z-z')}}{(\frac{2\pi m}{a})^2 + (\frac{2\pi n}{a} + k_0 \cos \theta_{\text{inc}})^2 + (\frac{2\pi p}{l})^2 - k_0^2}, \quad (4.1.6)$$

where l represents the periodicity in the z direction which is infinitely large and p is the z -index of the lattice points in the reciprocal lattice. In Eq.(4.1.6), the components of $2\pi(m/a, n/a, p/l)$ belong to the reciprocal-lattice vector. These Floquet functions are in fact the optical modes of a box-shaped cavity (indicated in Fig.(4.1)) with perfect electric (E-field normal to the boundary) and magnetic walls (B-field normal to the boundary) [103, 105]. We now go one step further to simplify Eq.(4.1.6). As is indicated in all the equations of the Green's function so far, since our system is a periodic 2-dimensional surface in the $x - y$ plane, l tends to infinity and we can convert the summation over p in Eq.(4.1.6) to an integral. Using the mathematical rule

$$\lim_{l \rightarrow \infty} \frac{2\pi}{l} \sum_{p=-\infty}^{\infty} f\left(\frac{2\pi p}{l}\right) \rightarrow \int_{-\infty}^{\infty} f(\xi) d\xi, \quad (4.1.7)$$

Eq.(4.1.6) would be converted to

$$G_p(\mathbf{r}, \mathbf{r}'; \omega_0) = \frac{1}{2\pi a^2} \sum_{m, n = -\infty}^{\infty} V_{mn} \left(\int_{-\infty}^{\infty} \frac{e^{i\xi(z-z')}}{\xi^2 - k_{mn}^2} d\xi \right), \quad (4.1.8)$$

with

$$k_{mn}^2 = k_0^2 - \left(\frac{2\pi m}{a}\right)^2 - \left(\frac{2\pi n}{a} + k_0 \cos \theta_{\text{inc}}\right)^2, \quad (4.1.9)$$

$$V_{mn} = e^{\frac{2\pi i m}{a}(x-x')} e^{i(\frac{2\pi n}{a} + k_0 \cos \theta_{\text{inc}})(y-y')}.$$

By applying contour integration, the integration in Eq.(4.1.8) can be solved as

$$\int_{-\infty}^{\infty} \frac{e^{i\xi(z-z')}}{\xi^2 - k_{mn}^2} d\xi = \frac{i\pi}{k_{mn}} e^{ik_{mn}|z-z'|}, \quad (4.1.10)$$

which guarantees that the outgoing waves along the z axis are upward propagating for $z > z'$ and downward propagating for $z < z'$. This solution in turn leads to the simplified expression for the Green's function as

$$G_p(\mathbf{r}, \mathbf{r}'; \omega_0) = \frac{i}{2a^2} \sum_{m,n=-\infty}^{\infty} V_{mn} \frac{e^{ik_{mn}|z-z'|}}{k_{mn}}. \quad (4.1.11)$$

Up to this point, we derived the scalar Green's function which can be used to calculate the scalar and vector potentials. In the case of electric and magnetic fields, we need a Green's function that relates all components of the source with all components of the fields, or, in other words, the Green's function must be a tensor. The dyadic Green's function satisfies the equation,

$$\nabla \times \nabla \times \overleftrightarrow{\mathbf{G}}(\mathbf{r}, \mathbf{r}') - \mathbf{k}^2 \overleftrightarrow{\mathbf{G}}(\mathbf{r}, \mathbf{r}') = \overleftrightarrow{\mathbf{I}} \delta(\mathbf{r}, \mathbf{r}'). \quad (4.1.12)$$

the dyadic Green's function is thus related to the scalar Green's function through the relation

$$\overleftrightarrow{\mathbf{G}}(\mathbf{r}, \mathbf{r}') = [\overleftrightarrow{\mathbf{I}} + \frac{1}{\mathbf{k}^2} \nabla \nabla] G_p(\mathbf{r}, \mathbf{r}'). \quad (4.1.13)$$

For example, the tensor element $G_{\alpha\beta}$ of the Green's function relates the α -component of the field at the observation point \mathbf{r} to the β -component of the dipole moment at the source position \mathbf{r}' . In this section, we introduced the Bloch-Floquet formalism which says that a periodic lattice of QDs is formally equivalent to a single QD embedded within a cavity. In the following of this chapter, we will see that this argument also holds for two coupled QD-lattices that is formally equivalent to a cavity (unit cell) containing 2 QDs.

4.2 Radiative Coupling of Quantum Dots Through Cavity Modes

In this Section, we will first study the electromagnetic coupling between a single QD embedded within a cavity by arbitrary quantized cavity modes. We will subsequently treat two QDs coupled with the cavity modes and will indicate that these QDs can be mutually coupled through the cavity modes. We follow the Master Equation approach [109] in which the time evolution of the QDs interacting with the electromagnetic field is considered in terms of the QD-field (QF) density operator $\hat{\rho}_{QF}$ where the index Q stands for the QD and F for the field. This operator characterizes the statistical state (averaged state) of the combined system of the QDs and the reservoir of quantized cavity EM field modes.

As introduced in chapter 2, in the electric dipole approximation, the total Hamiltonian of a QD in a cavity is given by $\hat{H} = \hat{H}_0 + \hat{H}_I$, where \hat{H}_0 is the Hamiltonian of both the noninteracting QDs and the EM field, and \hat{H}_I is the interaction Hamiltonian between

the QDs and the EM field [109] and can be written as

$$\begin{aligned}\hat{H}_0 &= \sum_{i=1}^N \hbar\omega_i S_i^z + \sum_{\mathbf{k}} \hbar\omega_{\mathbf{k}} (\hat{a}_{\mathbf{k}}^\dagger \hat{a}_{\mathbf{k}} + \frac{1}{2}) \\ \hat{H}_I &= - \sum_{\mathbf{k}} \sum_{i=1}^N \sqrt{\frac{\hbar\omega_{\mathbf{k}}}{2\varepsilon_0}} [\boldsymbol{\mu}_i \cdot \mathbf{u}_{\mathbf{k}}(\mathbf{r}_i) (S_i^+ + S_i^-) \hat{a}_{\mathbf{k}s} + \text{H.c.}],\end{aligned}\quad (4.2.1)$$

where ω_i is the transition energy. If the QDs are modeled as two-level systems with excited state $|e_i\rangle$, ground state $|g_i\rangle$, then $S_i^z = (|e_i\rangle\langle e_i| - |g_i\rangle\langle g_i|)/2$ is the population difference operator, $S_i^+ = |e_i\rangle\langle g_i|$ and $S_i^- = |g_i\rangle\langle e_i|$ are the dipole raising and lowering operators respectively and $\hat{\boldsymbol{\mu}}_i = \boldsymbol{\mu}_i (S_i^+ + S_i^-)$ is the dipole moment of the i th QD. $\hat{a}_{\mathbf{k}}$ and $\hat{a}_{\mathbf{k}}^\dagger$ are the annihilation and creation operators of the field mode \mathbf{k} respectively, with wave vector \mathbf{k} and frequency $\omega_{\mathbf{k}}$. Moreover, $\mathbf{u}_{\mathbf{k}}(\mathbf{r}_i)$ are the orthonormal EM field modes in the cavity which can be engineered by the shape and structure of the cavity.

When we transform to the interaction picture, the time evolution of the transformed density operator, $\tilde{\rho}_{\text{QF}}(t)$, of the combined system obeys the equation

$$\frac{\partial}{\partial t} \tilde{\rho}_{\text{QF}}(t) = \frac{1}{i\hbar} [\tilde{H}(t), \tilde{\rho}_{\text{QF}}(t)]. \quad (4.2.2)$$

We assume that there is initially no correlation between the quantum dots and the field, thus allowing to factorize the initial density operator of the combined system as $\tilde{\rho}_{\text{QF}}(0) = \tilde{\rho}_{\text{Q}}(0)\tilde{\rho}_{\text{F}}(0)$, where $\tilde{\rho}_{\text{Q}}$ and $\tilde{\rho}_{\text{F}}$ are the density operators of the QD system and the vacuum field respectively. In the next step we employ the Born approximation [112], in which the interaction between the QD system and the field is supposed to be weak, and there is no back response of the QDs on the field. So the EM field state does not change in time, and we can write the density operator as $\tilde{\rho}_{\text{QF}}(t) = \tilde{\rho}_{\text{Q}}(t)\tilde{\rho}_{\text{F}}(0)$. Under this approximation and the initial condition introduced above, Eq.(4.2.2) leads to the reduced density operator of the QDs, $\tilde{\rho}_{\text{Q}}(t) = \text{Tr}_{\text{F}}\{\tilde{\rho}_{\text{QF}}(t)\}$, satisfying the differential equation

$$\begin{aligned}\frac{\partial \hat{\rho}}{\partial t} &= -i \sum_{i=1}^N \omega_i [S_i^z, \hat{\rho}] - i \sum_{i \neq j}^N \Omega_{ij} [S_i^+ S_j^-, \hat{\rho}] \\ &\quad - \frac{1}{2} \sum_{i,j=1}^N \Gamma_{ij} (\hat{\rho} S_i^+ S_j^- + S_i^+ S_j^- \hat{\rho} - 2S_j^- \hat{\rho} S_i^+),\end{aligned}\quad (4.2.3)$$

where we have used a shorter notation $\hat{\rho} = \tilde{\rho}_{\text{Q}}$. In deriving Eq.(4.2.3), we applied the Rotating Wave Approximation (RWA) where, we neglect the cases in which the QD is raised to the excited state and simultaneously one photon is emitted or vice versa. Γ_{ij} is the imaginary part of the interaction energy which is known as the spontaneous energy transfer rate from i th QD to j th QD through the cavity field modes, and is equal to

$$\Gamma_{ij} = \frac{\pi\omega_0}{\varepsilon_0\hbar} \sum_{\mathbf{k}} [\boldsymbol{\mu}_i \cdot \mathbf{u}_{\mathbf{k}}(\mathbf{r}_i)] [\mathbf{u}_{\mathbf{k}}^*(\mathbf{r}_j) \cdot \boldsymbol{\mu}_j^*] \delta(\omega_0 - \omega_{\mathbf{k}}), \quad (4.2.4)$$

where $\omega_0 = (\omega_i + \omega_j)/2$. The coherent component of the dipole-dipole coupling is defined as

$$\Omega_{ij} = \frac{-\omega_0}{2\varepsilon_0\hbar} \sum_{\mathbf{k}} [\boldsymbol{\mu}_i \cdot \mathbf{u}_{\mathbf{k}}(\mathbf{r}_i)][\mathbf{u}_{\mathbf{k}}^*(\mathbf{r}_j) \cdot \boldsymbol{\mu}_j^*] \left(\frac{P}{\omega_{\mathbf{k}} + \omega_0} + \frac{P}{\omega_{\mathbf{k}} - \omega_0} \right), \quad (4.2.5)$$

where P indicates the principal value of the integral $\lim_{t \rightarrow \infty} \int_0^t d\tau \rho(t - \tau) e^{i(\omega_0 \pm \omega_{\mathbf{k}})\tau}$ [110]. We obtained these general forms of the coupling parameters in chapter 2. In this chapter we only focus on the incoherent part of the dipole-dipole coupling which leads to the modification of spontaneous emission rates. The spontaneous energy transfer from i th QD to j th QD is not a surprise in an entangled system of QDs and cavity modes. This entanglement also results in the interference of the radiation patterns from the individual oscillating dipoles in the cavity. In deriving Eq.(4.2.3), we used the Markov approximation in which the QD-dynamics has a slow time scale as compared to the photonic reservoir correlation functions which decay much faster [149]. In other words, the Markov approximation holds when there is no memory in the system.

At this point, we try to make a relationship between the EM field normal modes and the dyadic Green's function $\overset{\leftrightarrow}{\mathbf{G}}$ in the cavity. Subsequently, this relationship will be used to express the spontaneous energy transfer rate Γ_{ij} between the QDs embedded in the cavity. Following the same notation used in Ref. [22] and chapter 2, we start from this fact that the normal modes $\mathbf{u}_{\mathbf{k}}(\mathbf{r}, \omega_{\mathbf{k}})$ should satisfy the wave equation

$$\nabla \times \nabla \times \mathbf{u}_{\mathbf{k}}(\mathbf{r}, \omega_{\mathbf{k}}) - \frac{\varepsilon_r(\mathbf{r})\omega_{\mathbf{k}}^2}{c^2} \mathbf{u}_{\mathbf{k}}(\mathbf{r}, \omega_{\mathbf{k}}) = 0, \quad (4.2.6)$$

and they fulfill a mutual orthogonality relation. It is clear that the relative dielectric constant of the medium $\varepsilon_r(\mathbf{r})$ is also a periodic function with the same periodicity of the cavity mode which is actually the lattice constant. By expanding the Green's function $\overset{\leftrightarrow}{\mathbf{G}}$ in terms of the normal modes as

$$\overset{\leftrightarrow}{\mathbf{G}}(\mathbf{r}, \mathbf{r}'; \omega) = \sum_{\mathbf{k}} \mathbf{A}_{\mathbf{k}}(\mathbf{r}', \omega) \mathbf{u}_{\mathbf{k}}(\mathbf{r}, \omega_{\mathbf{k}}), \quad (4.2.7)$$

we arrive at the appropriate expansion of the Green's function in terms of the cavity modes

$$\overset{\leftrightarrow}{\mathbf{G}}(\mathbf{r}, \mathbf{r}'; \omega) = \sum_{\mathbf{k}} \frac{c^2}{\varepsilon_r(\mathbf{r}')} \frac{\mathbf{u}_{\mathbf{k}}^*(\mathbf{r}', \omega_{\mathbf{k}}) \otimes \mathbf{u}_{\mathbf{k}}(\mathbf{r}, \omega_{\mathbf{k}})}{\omega_{\mathbf{k}}^2 - \omega^2}, \quad (4.2.8)$$

where \otimes is the tensorial product. We can still manipulate Eq.(4.2.8) and convert it to a different form which is more useful for making a bridge between the energy transfer rate and the Green's function. We first introduce the following mathematical identity, which can be easily proven by complex contour integration [22]

$$\lim_{\eta \rightarrow 0} \text{Im} \left\{ \frac{1}{\omega_{\mathbf{k}}^2 - (\omega + i\eta)^2} \right\} = \frac{\pi}{2\omega_{\mathbf{k}}} [\delta(\omega - \omega_{\mathbf{k}}) - \delta(\omega + \omega_{\mathbf{k}})]. \quad (4.2.9)$$

By multiplying both sides with $\mathbf{u}_{\mathbf{k}}^*(\mathbf{r}, \omega_{\mathbf{k}}) \otimes \mathbf{u}_{\mathbf{k}}(\mathbf{r}, \omega_{\mathbf{k}})$ and summing over all \mathbf{k} , we obtain

$$\text{Im} \left\{ \lim_{\eta \rightarrow 0} \sum_{\mathbf{k}} \frac{\mathbf{u}_{\mathbf{k}}^*(\mathbf{r}, \omega_{\mathbf{k}}) \otimes \mathbf{u}_{\mathbf{k}}(\mathbf{r}, \omega_{\mathbf{k}})}{\omega_{\mathbf{k}}^2 - (\omega + i\eta)^2} \right\} = \frac{\pi}{2} \sum_{\mathbf{k}} \frac{1}{\omega_{\mathbf{k}}} \mathbf{u}_{\mathbf{k}}^*(\mathbf{r}, \omega_{\mathbf{k}}) \otimes \mathbf{u}_{\mathbf{k}}(\mathbf{r}, \omega_{\mathbf{k}}) \delta(\omega - \omega_{\mathbf{k}}) \quad (4.2.10)$$

Since we are only concerned with positive frequencies, we drop the term $\delta(\omega + \omega_{\mathbf{k}})$. By comparison with Eq.(4.2.8), Eq.(4.2.10) can be written as

$$\text{Im}\{\overset{\leftrightarrow}{\mathbf{G}}(\mathbf{r}, \mathbf{r}; \omega)\} = \frac{\pi c^2}{2\omega} \sum_{\mathbf{k}} \mathbf{u}_{\mathbf{k}}^*(\mathbf{r}, \omega_{\mathbf{k}}) \otimes \mathbf{u}_{\mathbf{k}}(\mathbf{r}, \omega_{\mathbf{k}}) \delta(\omega - \omega_{\mathbf{k}}), \quad (4.2.11)$$

where the left hand side is the imaginary part of the Green's function evaluated at its origin $\mathbf{r} = \mathbf{r}'$ and the frequency disappears from the summation due to the delta function on the right hand side. Employing Eq.(4.2.11) in Eq.(4.2.4), in terms of the Green's function in the environment around the i th and j th QDs, the energy transfer rate between two QDs can be rewritten as

$$\Gamma_{ij} = \frac{2\omega_0^2}{\varepsilon_0 \hbar c^2} [\boldsymbol{\mu}_i \cdot \text{Im}\{\overset{\leftrightarrow}{\mathbf{G}}(\mathbf{r}_i, \mathbf{r}_j; \omega_0)\} \cdot \boldsymbol{\mu}_j^*]. \quad (4.2.12)$$

Based on Eq.(4.2.12), the spontaneous emission rate of a single QD becomes

$$\Gamma_i = \frac{\pi \omega_0 \mu_i^2}{3 \hbar \varepsilon_0 \varepsilon_h} \rho_i(\mathbf{r}_i, \omega_0), \quad (4.2.13)$$

where $\boldsymbol{\mu}_i = \mu_i \mathbf{n}_i$. We have introduced the partial local density of optical states $\rho_i(\mathbf{r}_i, \omega_0)$, which corresponds to the number of modes per unit volume and frequency at the origin \mathbf{r}_i of the point-like QD. This density of states represents the probability for spontaneous emission of a photon with energy $\hbar \omega_0$ [22],

$$\rho_i(\mathbf{r}_i, \omega_0) = \frac{6\omega_0}{\pi c^2} [\mathbf{n}_i \cdot \text{Im}\{\overset{\leftrightarrow}{\mathbf{G}}(\mathbf{r}_i, \mathbf{r}_i; \omega_0)\} \cdot \mathbf{n}_i]. \quad (4.2.14)$$

As an example, if there is one QD located in an isotropic and homogeneous medium, then the dielectric constant is not position-dependent anymore. In this case, Eq.(4.2.13) and (4.2.14) give rise to the well known [22] spontaneous emission rate

$$\Gamma_0 = \frac{\omega_0^3 \mu^2}{3\pi \varepsilon_0 \hbar c^3}, \quad (4.2.15)$$

where we have assumed $\mu_i = \mu$. In the case where a radiating QD (dipole) is located in an inhomogeneous medium like a periodic structure of QDs, we need to know the Green's function of the EM field everywhere in the system which strongly depends on the cavity geometry and needs to be calculated.

4.3 Quantum dot lattices as quantum resonators

Here we present two different geometries of the unit cell. In the first case, we have a simple rectangular lattice of QDs with the unit cell containing only one QD and in the second case, two rectangular lattices of different QDs are intermixed and hence the unit cell contains two different QDs with an arbitrary distance between them. In both structures, we should be able to indicate the resonator modes with corresponding resonant

frequencies. Any intracavity radiation field can be expanded [183] in terms of these resonator modes. In sec.(4.1), an approach similar to the Bloch wave functions in solid state physics was followed to describe the photonic states in a periodic structure [176]. It is our objective to show how these resonator modes modify the QD spontaneous emission rate and also mediate the energy transfer between two different QDs within a unit cell.

4.3.1 A single quantum dot lattice

In sec.(4.1), we derived the periodic Green's function in an infinitely large rectangular lattice of QDs which is in the $x - y$ plane. In order to obtain the spontaneous emission rates, as is shown in (4.2.14), we need to calculate various components of $[\mathbf{n}_i \cdot \vec{\mathbf{G}}(\mathbf{r}_i, \mathbf{r}_i; \omega_0) \cdot \mathbf{n}_i]$. In this chapter, we assume that the dipole moment of QDs does not have a fixed direction and can be oriented in all directions with equal probabilities. In this situation, we should average over various orientations of the Green's tensor leading to

$$G(\mathbf{r}_i, \mathbf{r}_i; \omega_0) = \langle \mathbf{n}_i \cdot \vec{\mathbf{G}}(\mathbf{r}_i, \mathbf{r}_i; \omega_0) \cdot \mathbf{n}_i \rangle = \frac{1}{3} \text{Tr}[\vec{\mathbf{G}}(\mathbf{r}_i, \mathbf{r}_i; \omega_0)]. \quad (4.3.1)$$

By inserting (4.1.11) in Eq.(4.1.13) and then averaging over the orientations by employing Eq.(4.3.1), we will have

$$G(\mathbf{r}_i, \mathbf{r}_i; \omega_0) = \frac{i}{3a^2} \sum_{m,n=-\infty}^{\infty} \frac{1}{k_{mn}}, \quad (4.3.2)$$

$$k_{mn} = \sqrt{k_0^2 - \left(\frac{2\pi m}{a}\right)^2 - \left(\frac{2\pi n}{a} + k_0 \cos\theta_{\text{inc}}\right)^2}.$$

The combination of Eq.(4.2.14), (4.3.1) and (4.3.2) finally leads to the local density of optical states in a QD-lattice, at the lattice positions of the QDs,

$$\rho(\mathbf{r}_i, \omega_0) = \frac{2\omega_0}{\pi c^2 a^2} \sum_{m,n \in \{\dots\}} \frac{1}{k_{mn}}, \quad (4.3.3)$$

where $\{\dots\}$ stands for the range where $m, n = 0, \pm 1, \pm 2, \dots$ provided that $m^2 + n^2 \leq (ka/2\pi)^2$. For deriving the equations above, we have assumed that QDs are identical. Based on Eq.(4.2.13), the spontaneous emission rate of a single two dimensional QD-lattice will be

$$\Gamma_{\text{Single}} = \frac{2\omega_0^2 \mu^2}{3\hbar \epsilon_0 c^2 a^2} \sum_{m,n \in \{\dots\}} \frac{1}{k_{mn}}. \quad (4.3.4)$$

Depending on the ratio a/λ , the graph of the spontaneous emission rate consists of different segments shown in left graph of Fig.4.2. For clarity, the first two segments are magnified in the inset. The corresponding decay time is indicated in the right graph which is in fact, the inverse of the emission rate.

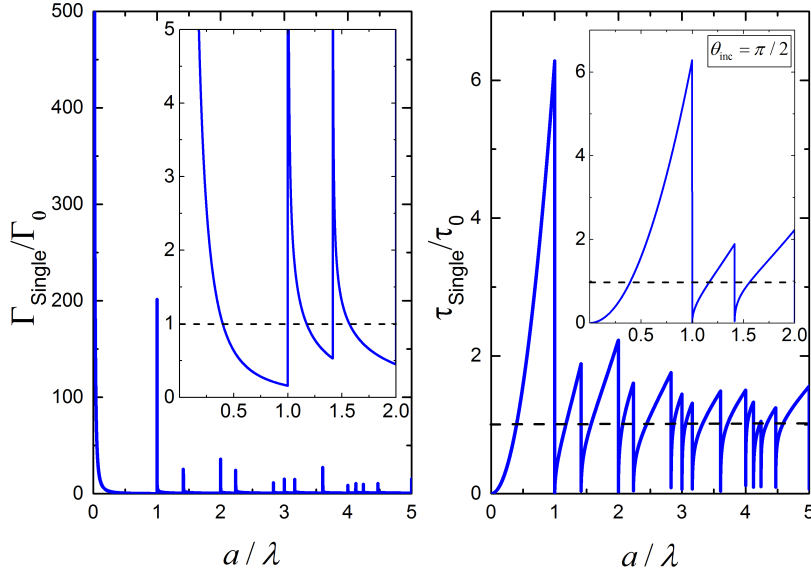


Figure 4.2: On the left, modified spontaneous emission rate of a QD within a periodic QD-lattice, Γ_{Single} , normalized to the uncoupled spontaneous emission rate Γ_0 . On the right, the corresponding life time which is in fact the inverse of left graph. QDs have all parallel dipole moments.

As we already mentioned, the effect of dipole-dipole (d-d) interactions between QDs on the collective spontaneous emission is equal to the action of a structured photonic reservoir. The regime $a/\lambda \ll 1$ in Fig.(4.2) corresponds to the continuum limit of a dense medium discussed in details in Ref. [121]. In this limit, the influence of the d-d interactions looks like the action of a uniform refracting medium. In this case, the spontaneous emission rate is proportional to the medium density which leads to the superradiance effect ($\Gamma_{\text{Single}}/\Gamma_0 \gg 1$). By increasing of a/λ , the band structure of the spectrum which is dictated by the periodicity becomes more and more significant. In this situation, there is a finite probability for the spontaneous emission into all diffraction rays characterized by the set of m, n . The contributions of these emission channels are different for different a/λ and consequently give rise to various peaks with different magnitudes in Fig.(4.2).

The equivalence of the d-d interactions between the QDs by the action of a structured photonic reservoir can be better understood in a semiclassical framework by using the method of electrical images. In this approach, the presence of the real boundaries is equal to the interference of partial fields radiated by the real emitter and some other additional sources. In this view, the collective spontaneous emission may be considered as an interference of virtual photons governed by the d-d interaction of QDs. The emission rates faster than the emission rate of a single isolated QD corresponds to the constructive interference of such partial fields while the slower rate corresponds to the

destructive interference.

At this point we refer back to chapter(3) where we extensively studied the spontaneous emission from a two-QD system. We said that, the two-particle collective excited eigenstates are given by the symmetric, $|s\rangle = \frac{1}{\sqrt{2}} (|e_1\rangle |g_2\rangle + |g_1\rangle |e_2\rangle)$, and the antisymmetric, $|a\rangle = \frac{1}{\sqrt{2}} (|e_1\rangle |g_2\rangle - |g_1\rangle |e_2\rangle)$, states. Radiative decay rates for these states are $\Gamma_s = \Gamma_0 + \Gamma_{12}$ and $\Gamma_a = \Gamma_0 - \Gamma_{12}$ respectively. The quantity Γ_{12} is expressed by Eq.(4.2.4) with $r_{ij} = a$. The decay rates $\Gamma_{s,a}$ can easily be reduced to the form of Eq.(4.3.4). In a cavity view, the state $|s\rangle$ corresponds to the entangled state of a QD and a perfect electric wall located at the distance $a/2$. The perfect electric wall is a virtual boundary on which the tangential component of the electric field is zero. Such a perfect electric wall increases the Photonic Density of States (PDOS) and consequently, $\Gamma_s > \Gamma_0$ that corresponds to the superradiance effect. For the state $|a\rangle$ the opposite situation occurs: the perfect magnetic wall (the wall on which the tangential magnetic field is zero) positioned at the distance $a/2$ from the QD, decreases the PDOS thus yielding the inequality $\Gamma_a < \Gamma_0$, dictating the subradiance effect.

For the 2D-periodic structure under consideration, Eq.(4.3.2) represents the Green's function of a hollow rectangular waveguide. On the walls at $x = \pm a/2$ and $y = \pm a/2$, the conditions of the perfect conductivity and Floquet-Bloch quasi-periodicity are fulfilled respectively, while at the $z \rightarrow \pm\infty$ the radiation condition is fulfilled. This means that Eq.(4.3.3) is the photonic density of states (PDOS) coupled with the dipole at the point r_i . Consequently, (4.3.4) is identical to the radiative decay rate of an isolated QD placed into a structured photonic reservoir (cavity), having the form of an infinite rectangular waveguide. In another words, the expression (4.3.4) is analogous to the Purcell effect [23] although physically, situations are quite different. In the periodic structure of QDs, we deal with the decay of a multi-particle state while in the Purcell effect only the single-particle states spontaneously decay. In our case, the following reasoning allows introducing the effective PDOS. In the Purcell effect, the excited emitter is located inside an actual cavity and modification of the PDOS with respect to the free space is due to reflection and scattering of radiation on the interfaces. In our case actual boundaries are absent, but interference of virtual photons governed by the d-d interacting QDs organized in a regular array leads to the same result as a sequence of reflections from real boundaries. The narrow peaks on Fig.(4.2) correspond to the Van-Hove singularities of PDOS at the boundaries of forbidden and allowed zones.

The normalized spontaneous emission rate of a single lattice of QDs has been shown in Fig.(4.3) as a function of the lattice periodicity for two different cases of excitation angle. The red dash-dotted line corresponds to an excitation pulse which is parallel to the lattice surface and thus imposes the maximum phase shift and the blue solid line corresponds to the normal excitation which does not impose any phase shift. The comparison of these two situations indicates that for a fixed lattice periodicity, just by changing the phase shift $k_0 \cos \theta_{inc}$, we can manipulate the spontaneous emission rate of the lattice, Γ_{Single} . This novel way of dynamical manipulation would be very helpful especially for those periodicities for which Γ_{Single} is very small, by imposing an appropriate phase shift, the emission rate can be enhanced significantly. The rate of the spontaneous emission from a single lattice as a function of the excitation phase shift is shown in Fig.(4.4) for three different periodicities which are equal or larger than the emission wavelength.

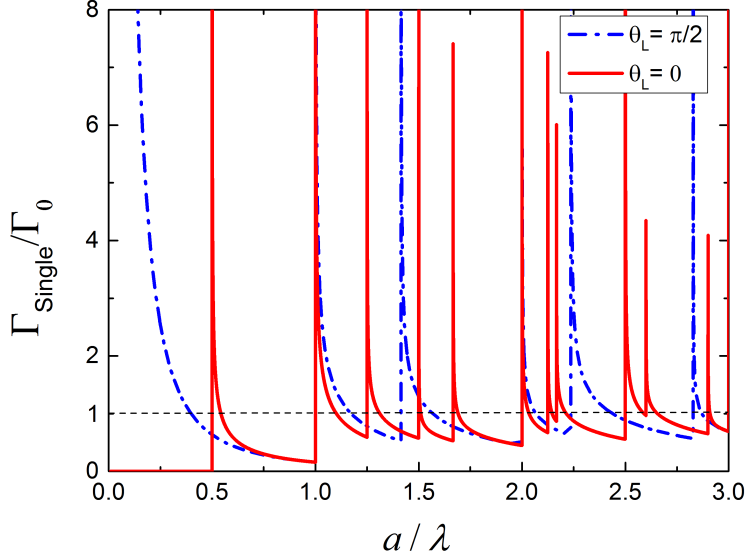


Figure 4.3: The spontaneous emission rate of a single lattice of QDs normalized with the emission rate of a single QD in the homogeneous medium as a function of the lattice periodicity for the excitation pulse parallel to the lattice surface, $\theta_{\text{inc}} = 0$, (solid line) and normal to the lattice surface, $\theta_{\text{inc}} = \pi/2$, (dash-dotted line).

It is clear that for large phase shifts (small excitation angles), the emission rate is greatly enhanced and by decreasing the phase shift, the emission also decreases. For periodicities equal or smaller than the wavelength, the emission rate becomes slower than the emission rate of an isolated QDs at excitation angles larger than about 10° . However for periodicities larger than the wavelength, although the emission rate is mostly slower than that of the isolated QD, the emission rate sharply enhances at some certain phase shifts. The position of these peaks on the axis of the phase shift, strongly depends on the value of the lattice periodicity. The main message of figures (4.3) and (4.4) is that, for achieving enhanced emission rates, we should engineer the lattice constant to be smaller than the wavelength and try to keep the excitation beam as parallel as possible to the sample surface (less than 10°). But for obtaining reduced emission rates as compared with the emission rate of an isolated QD, we have much more options. Regardless of the value of the lattice constant, we should try to reduce the phase shift by adjusting the excitation beam as perpendicular to the surface as possible.

Here we show that if the QD-QD lattice constant is much larger than the emission wavelength, the QDs lose their mutual coupling and the spontaneous emission rate of the lattice in Eq.(4.3.4), will approach the spontaneous emission rate of a single isolated QD. For a large lattice constant a , using the mathematical formalism of Eq.(4.1.7), the

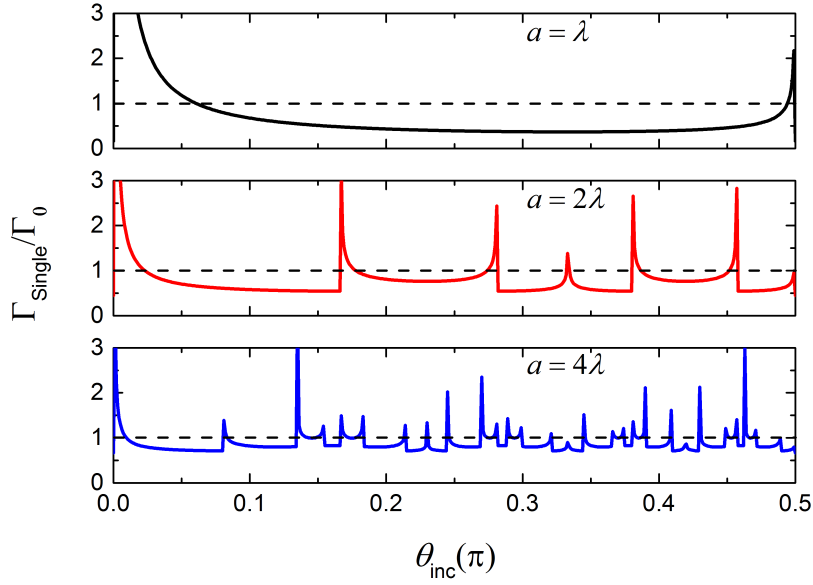


Figure 4.4: The emission rate of a single lattice as a function of the pumping phase shift normalized with the emission rate of a single and isolated QD for $a = \lambda$ (upper), $a = 2\lambda$ (middle) and $a = 4\lambda$ (lower). In this graph $D = a/2$

summations can be converted to an integral,

$$\begin{aligned} \Gamma_{\text{Single}} &= \lim_{a \rightarrow \infty} \frac{2\omega_0^2 \mu^2}{3\hbar \epsilon_0 c^2 a^2} \sum_{m, n \in \{\dots\}} \frac{1}{\sqrt{k_0^2 - \left(\frac{2\pi m}{a}\right)^2 - \left(\frac{2\pi n}{a} + k_0 \cos \theta_{\text{inc}}\right)^2}} \\ &= \frac{2\omega_0^2 \mu^2}{3\hbar \epsilon_0 c^2} \left(\frac{a}{2\pi}\right)^2 \int_{-k_0}^{k_0} d\xi \int_{-\sqrt{k_0^2 - \xi^2}}^{\sqrt{k_0^2 - \xi^2}} \frac{d\xi'}{\sqrt{k_0^2 - \xi^2 - \xi'^2}}, \end{aligned} \quad (4.3.5)$$

where $\{\dots\}$ denotes for the condition $(m^2 + n^2) < (ak_0/2\pi)^2$. The solution of the integrals in the equation above, leads to the spontaneous emission rate of a single QD in an isotropic dielectric medium as

$$\Gamma_0 = \frac{\omega_0^3 \mu^2}{3\pi \epsilon_0 \hbar c^3}. \quad (4.3.6)$$

This is of course the result that we expect to see, because, when the lattice constant is infinitely large and hence the QDs are apart from each other, there is no longer any effective dipole-dipole coupling between them and thus the QDs decay individually.

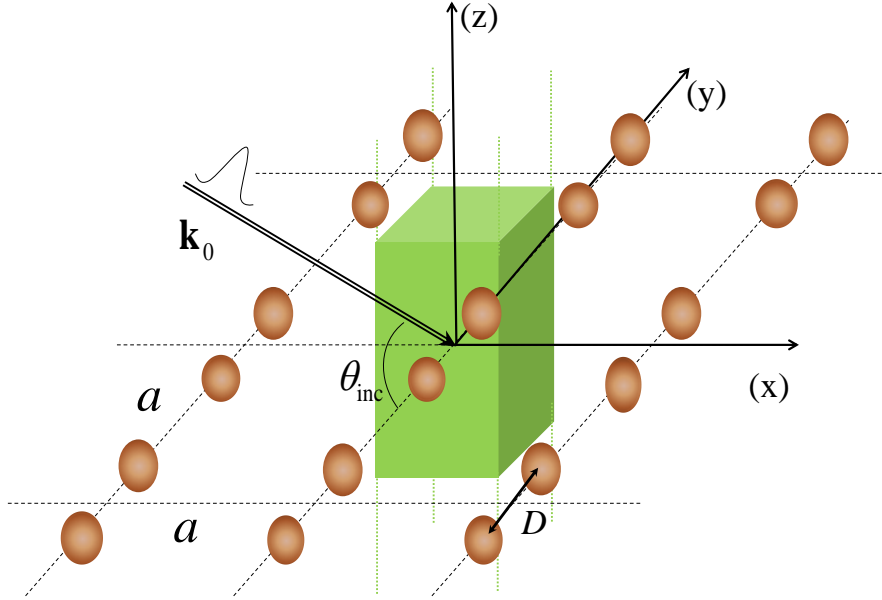


Figure 4.5: Two coupled planar QD-lattices in the $(x - y)$ plane with the same lattice constant, which are shifted over a distance D along the y -axis. The equivalent virtual cavity is indicated in green, and is centered in the middle of the QD-pair. All QD dipole moments are parallel to the x -axis.

4.3.2 Two coupled quantum dot lattices

In this section we show that the system of two intermixed layer of QDs can be reduced to the problem of two QDs embedded in a cavity characterized by the periodic structure of QDs. Then we will obtain the appropriate emission rates. Instead of a single lattice of identical QDs, we now consider two mutually translated QD-lattices with the same lattice constant, as schematically shown in Fig.(4.5). We assume that both QD-lattices are in the $(x - y)$ plane and mutually shifted over a distance D along the y direction. In this situation, each unit cell (virtual cavity) of the new structure contains two QDs which are generally not identical. The main difference between this cavity and the previous one is that, in the new cavity, the spontaneous emission rate of each QD is influenced by energy transfer between QDs belonging to the two different QD-lattices, in addition to the emission rate modifications due to cavity mode fluctuations. In analogy to the case of a diatomic lattice in solid state physics, we again need the analogue of the Bloch function, which in our case are the cavity modes of the 2 coupled QD-lattices. In this case, the periodic Green's function is similar to the case of the single lattice except that QDs of different lattices in each unit cell are now symmetrically positioned at a distance $D/2$ along the y direction from the lattice point as indicated in Fig.(4.5).

It has already been indicated [110] that two entangled QDs form a four-level system with a ground state, an excited state and two entangled intermediate states which one of them is symmetric and the other one antisymmetric. If Γ_{Single} is the individual spontaneous emission rate of each QD lattice or equivalently the emission rate of each QD in the virtual rectangular cavity in a double-lattice system and Γ_{12} is the spontaneous energy transfer rate between them, then the charge carrier decays from the symmetric state with the emission rate $\Gamma_s = \Gamma_{\text{Single}} + \Gamma_{12}$ and from the antisymmetric state with the emission rate $\Gamma_a = \Gamma_{\text{Single}} - \Gamma_{12}$. In chapter 3, we obtained these collective emission rates for the case of two QDs located in free space or homogeneous medium. But, when QDs are embedded in an inhomogeneous medium like a cavity, although the four-level system still holds true, the symmetric and antisymmetric emission rates will be modified significantly.

At this point, we should calculate the spontaneous energy transfer rate between the two lattices. We know from Eq.(4.2.12) that we should first average over all possible dipole orientations in $\mathbf{n}_i \cdot \text{Im}\{\overleftrightarrow{\mathbf{G}}(\mathbf{r}_i, \mathbf{r}_j; \omega_0)\} \cdot \mathbf{n}_j$. Since the QD dipole moments can be aligned in all directions with the same probability, like the procedure we followed for the single-lattice case, we can write

$$G(\mathbf{r}_i, \mathbf{r}_j; \omega_0) = \langle \mathbf{n}_i \cdot \text{Im}\{\overleftrightarrow{\mathbf{G}}(\mathbf{r}_i, \mathbf{r}_j; \omega_0)\} \cdot \mathbf{n}_j \rangle = \frac{1}{9} \sum_{\alpha, \beta=x, y, z} \overleftrightarrow{\mathbf{G}}_{\alpha, \beta}(\mathbf{r}_i, \mathbf{r}_j; \omega_0). \quad (4.3.7)$$

The combination of (4.1.11), (4.1.13) and (4.3.7) gives rise to a general expression for the corresponding Green's function of a 2D periodic lattice,

$$G(\mathbf{r}_i, \mathbf{r}_j; \omega_0) = \frac{i}{9a^2} \sum_{m, n \in \{\dots\}} \frac{1}{k_{mn}} e^{i \frac{2\pi m}{a} (x_i - x_j)} e^{i (\frac{2\pi n}{a} + k_0 \cos \theta_{\text{inc}}) (y_i - y_j)} e^{i k_{mn} |z_i - z_j|} \\ \times \left\{ 1 - \frac{1}{k_0^2} \left[\left(\frac{2\pi m}{a} \right) \left(\frac{2\pi n}{a} + k_0 \cos \theta_{\text{inc}} \right) + \left(\frac{2\pi m}{a} + \frac{2\pi n}{a} + k_0 \cos \theta_{\text{inc}} \right) k_{mn} \frac{(z_i - z_j)}{|z_i - z_j|} \right] \right\}. \quad (4.3.8)$$

When both lattices are in the $x - y$ plane and are apart from each other only along the y -axis, then we have $x_i - x_j = 0$, $y_i - y_j = D$ and $z_i - z_j = 0$. Then Eq.(4.3.8) will be simplified to

$$G(\mathbf{r}_i, \mathbf{r}_j; \omega_0) = \frac{i}{9a^2} \sum_{m, n \in \{\dots\}} \frac{e^{i (\frac{2\pi n}{a} + k_0 \cos \theta_{\text{inc}}) D}}{k_{mn}} \\ \times \left\{ 1 - \frac{1}{k_0^2} \left[\left(\frac{2\pi m}{a} \right) \left(\frac{2\pi n}{a} + k_0 \cos \theta_{\text{inc}} \right) + \left(\frac{2\pi m}{a} + \frac{2\pi n}{a} + k_0 \cos \theta_{\text{inc}} \right) k_{mn} \right] \right\}. \quad (4.3.9)$$

It has been shown in Fig.4.6 that this coupling parameter strongly depends on the distance between the QDs in each unit cell, D , and has an oscillatory behavior. The periodicity of these oscillations inversely depends on the periodicity of the QD lattice structure. For a bigger periodicity, the lattice-lattice interaction has more oscillations as a function of the lattice-lattice separation in the available range of this displacement ($0 < D < a/2$). This means that, for bigger periodicities, a larger variety of possible

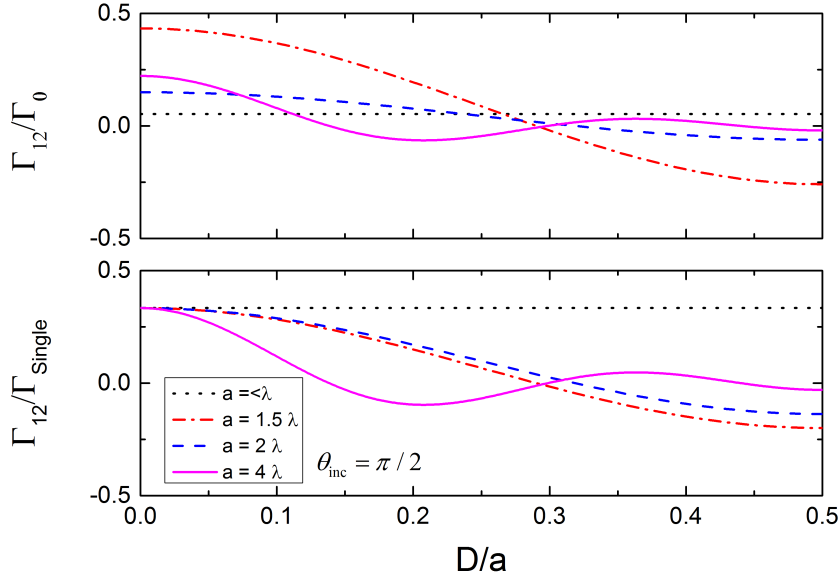


Figure 4.6: The spontaneous energy transfer rate, Γ_{12} , normalized with the emission rate of a single isolated QD (upper) and emission rate of a single lattice (lower) in double-lattice system, as a function of the distance between QDs of different lattices within each unit cell. In this graph, the phase shift is zero.

lattice-lattice coupling is accessible just by tuning the lattice-lattice displacement. These oscillations have already been indicated for the case of two QDs in free space [110, 118]. The difference in our work is that the energy transfer rate is mediated by the cavity field modes characterized by the periodic structure of QD lattices.

The engineering of the spontaneous energy transfer between QDs in two inter-mixed lattices, will consequently lead to the modification of the symmetric and antisymmetric emission rates. It is clearly shown in Fig.4.7 that by choosing an appropriate lattice periodicity and a relevant distance between QDs of the two different lattices, we are able to obtain the collective rates which are either faster or slower than the emission rate of a single lattice. In the left graph of Fig.4.7 for the symmetric emission, Γ_s , in the regions enclosed by the solid lines, the emission is slower and outside these regions, the emission is faster than the single-lattice emission rate. But, for the antisymmetric emission rate on the right graph, Γ_a , it is inverse. It is clear that for any arbitrary value of a and D , if the symmetric emission rate is faster than Γ_{Single} , the antisymmetric emission rate is slower and vice versa. Up to this point, we considered the effect of the QD-QD distance on the collective spontaneous emission rates. We indicated that by changing D , we can modify the emission rates to obtain a desired rate which can be faster or slower than the individual emission rate. However, the excitation phase shift, θ_{inc} , can also influence the spontaneous coupling of two intermixed lattices. The influences of these

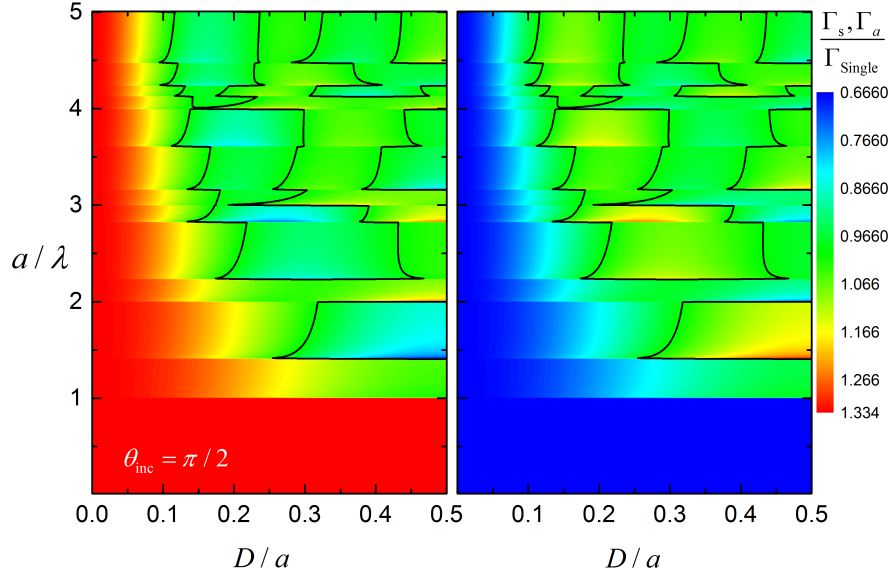


Figure 4.7: The symmetric (on the left) and the antisymmetric spontaneous emission rate normalized with the single-lattice emission rate in the double-lattice system as a function of the lattice periodicity, a , and the distance between the two QDs in each unit cell, D . The solid lines determine the points where the collective and the single-lattice emission rates are equal. In this graph, the phase shift between the two lattices is zero.

two parameters on the collective emission rates are simultaneously presented in Fig.4.8 for $a = \lambda/2$. For a fixed value of the lattice periodicity ($a = \lambda/2$), the left panel shows the symmetric emission rate and the right panel shows the antisymmetric emission rate.

It can be seen that, the symmetric emission rate is always faster and the antisymmetric emission rate is slower than the emission rate of the single lattice. We should emphasize that this graph is drawn for $a = \lambda/2$. For the other lattice constants, a different pattern is observable. It is clear that by engineering an appropriate QD-QD separation, D , or imposing a relevant phase shift between the lattices, the collective emission rates can be enhanced or reduced. This phenomena known as superradiance, has already been shown for the case of two dipole moments in a homogeneous medium [50] and in the previous chapter.

The approach of this chapter is based on this assumption that the electromagnetic field modes in the system obey the Floquet's theorem in which the field modes have a spatial periodicity equal to the periodicity of the periodic structure. This condition is fulfilled only when all QDs in the sample are identical and the surface area of the sample is large enough to make the approximation of an infinitely large surface valid. Thus from experimental point of view, it is important to grow high quality site-controlled QDs on

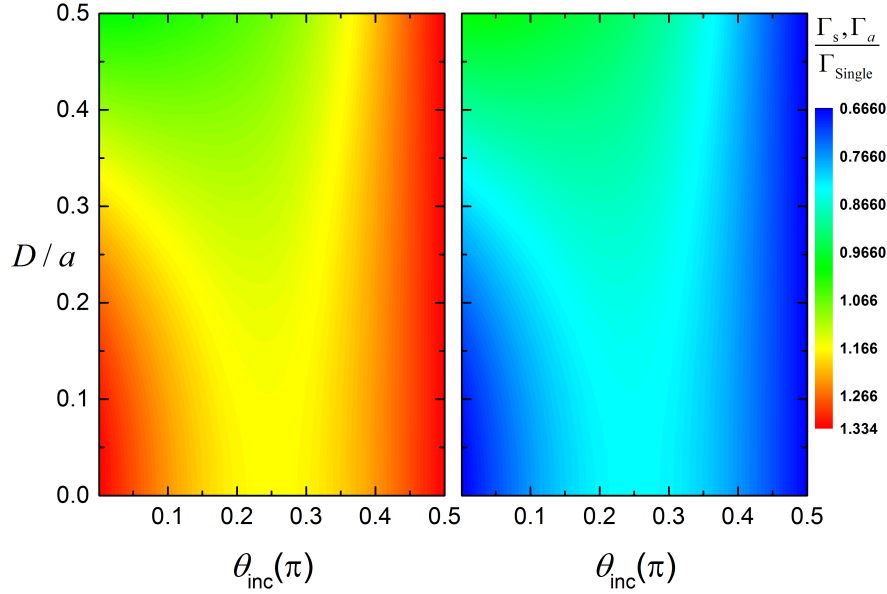


Figure 4.8: The symmetric (on the left) and antisymmetric (on the right) spontaneous emission rates normalized with the emission rate of a single-lattice emission rate in a double-lattice system as a function of the QD-QD separation, D , and the pumping phase shift between QDs of the two different lattices, θ_{inc} . In this graph $a = \lambda/2$.

a periodic pattern. The QDs should be all in resonance which means $\Delta\omega \ll \Gamma_0$, where $\Delta\omega$ is the mutual energy mismatch of QDs and Γ_0 is the homogeneous emission rate of a single QD.

4.4 Summary

Any periodic structure of QDs can act as a cavity in which, any single QD interacts with the photonic reservoir within the cavity, which is characterized by the periodicity of the QD lattice. Depending on the lattice constant, the spontaneous emission rate of any QD embedded in such a cavity can be either enhanced or inhibited.

When two single lattices with the same periodicity are intermixed, there are two QDs within each unit cell. The two entangled lattices of QDs as a whole again will now play the role of a cavity. In this case, the cavity contains two spatially separated QDs (the two QDs within the unit cell). These two QDs within the cavity of the QD-lattice form entangled symmetric and anti symmetric states. The time evolution of the total spontaneous emission of this system now becomes a triple-exponential function. Two of these emission rates are actually the collective emission rates corresponding to the entangled

states. The collective emission rates are a function of the individual QD emission rates within the cavity, and the energy transfer rate between the QDs which is strongly dependent on the QD-QD separation.

We found that the phase shift imposed between the QDs of the two entangled lattices is another parameter for changing the collective emission rates. By engineering appropriate values for the lattice periodicity, the QD-QD separation and the phase shift, we can achieve almost any desired value for the individual and collective QD emission rates.

Chapter 5

Cooperative spontaneous emission of quantum dots in periodic structures

The process of cooperative spontaneous emission is a consequence of the collective interaction between N two level emitters through the modes of an electromagnetic field. Such a problem can only be described by a many-body quantum approach. In the previous chapter, we studied the entanglement that originates from the electromagnetic interaction between QDs in a lattice in which the optical coupling between the QDs is mediated by the modes of a virtual cavity electromagnetic field. In that approach we took the correlation terms between QD population and polarization into account. In this chapter, we treat the same QD lattice structures in a full quantum mechanical approach where we assume that the system of QDs is weakly excited and only one QD out of system of N QDs is excited with one photon. In this chapter, we assume that we can separate out the correlated terms between population and coherence. This approximation allows obtaining simplified equations of motion from which the relevant physical observables can be obtained. The problem of the electromagnetic interaction between QDs in the weak excitation level is interesting, because one may think that the radiative emission rate should be equal to the spontaneous emission rate of a single QD. In this chapter, we will see that this is not correct and the QD lattice as a whole is a quantum state which decays cooperatively with a spontaneous emission rate that strongly depends on the lattice periodicity. The dynamics of an excited atom in the presence of $N - 1$ other atoms in the free space has been studied and a suppression of the radiative decay rate was predicted [184]. Some important properties of the cooperative emission in atomic systems have been recently investigated, like the directionality of the emission from an extended ensemble of atoms [95], the dynamical evolution of correlated spontaneous emission of a single photon from a uniformly excited cloud of atoms [99, 131] and the collective lamb shift in superradiant emission [102].

In literature, the two-level objects which have been investigated, are usually atoms, but here in this chapter, we extend this concept to the case of quantum dots (QDs) which have atom-like behavior in the dipole approximation. In sec.(5.1) we propose the general form of our model. In sec.(5.2) we employ our model to specific structures of a single and a double lattice of QDs. We study the spontaneous emission rate of a single QD lattice as well as the coupling between two lattices of QDs as a function of the lattice periodicity and the translational shift between both lattices. In sec.(5.3) we investigate the time evolution of the excitations of such a QD lattice and finally, we end up with a brief overview of the whole chapter.

5.1 Model

We assume that an infinitely large number of identical QDs are located in a two dimensional square lattice with periodicity a along both the x and y directions. The position of each QD in the lattice is represented by \mathbf{r}_j . The QDs are considered as atom-like two level systems with excited and ground state energies E_e and E_g respectively. So, the transition energy of all QDs is $E_e - E_g = \hbar\omega_0$. The QDs are optically coupled due to the electromagnetic field modes of the system. We assume that the interaction between the QDs and the EM modes is in weak coupling regime, which means that the QDs cannot alter the photonic reservoir and we can quantize the EM field by an expansion of plane-wave modes in free space. We consider two different QD structures, a simple system of a single square lattice of QDs and a system of two intermixed lattices of QDs. In the latter structure, the QDs within the two lattices are not necessarily identical. Of course it is possible to define many other complicated structures, but at this stage, we believe that these two structures are comprehensive enough to indicate the most important characteristics of the electromagnetic coupling between the QDs in the weak coupling regime.

5.1.1 A single planar lattice of quantum dots

First we assume that the QDs are arranged in a single lattice. In the dipole approximation and in the interaction picture, the interaction Hamiltonian of the combined QD lattice and the EM Field system can be written as the product of two sums,

$$\hat{H}_I = \sum_{\mathbf{k}} \sum_{j=1}^N g_{\mathbf{k}} \left(\hat{S}_j e^{-i\omega_0 t} + \hat{S}_j^\dagger e^{i\omega_0 t} \right) \left(\hat{a}_{\mathbf{k}}^\dagger e^{i\omega_{\mathbf{k}} t - i\mathbf{k} \cdot \mathbf{r}_j} + \hat{a}_{\mathbf{k}} e^{-i\omega_{\mathbf{k}} t + i\mathbf{k} \cdot \mathbf{r}_j} \right), \quad (5.1.1)$$

where \hat{S}_j and \hat{S}_j^\dagger are respectively the lowering and rising operators of the j th QD with the electric-dipole transition matrix element μ . $\hat{a}_{\mathbf{k}}$ is the annihilation operator of the photon in mode \mathbf{k} with frequency $\omega_{\mathbf{k}}$ and $g_{\mathbf{k}}$ is the coupling constant between the QD

and the electromagnetic field [111],

$$g_k = \omega_0 \mu \sqrt{\frac{1}{\epsilon_0 \hbar \omega_k V_{\text{ph}}}}, \quad (5.1.2)$$

where V_{ph} is the volume of photonic reservoir. For simplicity, we have not taken into account the effect of the polarization of the EM field in the Hamiltonian of Eq.(5.1.1). Similar to the procedure followed in Ref. [99], we write the solution of the Schrödinger equation for the QDs and the EM field as a superposition of Fock states

$$\begin{aligned} \Psi = & \sum_{j=1}^N \beta_j(t) |g_1 g_2 \cdots e_j \cdots g_N\rangle |0\rangle + \sum_{\mathbf{k}} \gamma_{\mathbf{k}}(t) |g_1 g_2 \cdots g_N\rangle |\mathbb{1}_{\mathbf{k}}\rangle \\ & + \sum_{u < v} \sum_{\mathbf{k}} \alpha_{uv,\mathbf{k}}(t) |g_1 g_2 \cdots e_u, \cdots e_v, \cdots g_N\rangle |\mathbb{1}_{\mathbf{k}}\rangle, \end{aligned} \quad (5.1.3)$$

where $\alpha_{uv,\mathbf{k}} = \alpha_{vu,\mathbf{k}}$. The first summation corresponds to the state in which the j th QD is excited and there is no photon in the system. In the second summation, all QDs are in ground state and there is one photon in the system. The third term corresponds to the presence of two excited QDs inside the sample and one virtual photon with negative energy [99]. The concept of virtual photon arises in the perturbation theory of quantum field theory. Virtual photon is a transient field fluctuation that exhibits many of the characteristics of a real photon but exists for a limited time. Due to the Heisenberg uncertainty principle, virtual particles will appear from the energy of a vacuum and always appear in pairs. These particles borrow energy from the vacuum and immediately collide and annihilate themselves, repaying the energy back into the vacuum so as not to violate the laws of thermodynamics. In the pair, one virtual particle has a positive and another one a negative energy. In our case, our virtual pair includes a virtual exciton (excited QD) with positive energy and a virtual photon with negative energy. From mathematical point of view, the counter-rotating terms in the Hamiltonian (5.1.1) are responsible for the virtual photon. Therefore, the virtual photon disappears when the Rotating-Wave Approximation (RWA) is made.

By inserting Eq.(5.1.3) into the Schrödinger equation, we obtain a set of three coupled differential equations for the single QD population amplitudes (β), the single photon occupation amplitude (γ) and the 2-QD correlation probability amplitude (α) as

$$\begin{aligned} \dot{\beta}_j(t) = & -\frac{i}{\hbar} \sum_{\mathbf{k}} g_{\mathbf{k}} \gamma_{\mathbf{k}}(t) \exp[-i(\omega_{\mathbf{k}} - \omega_0)t + i\mathbf{k} \cdot \mathbf{r}_j] \\ & -\frac{i}{\hbar} \sum_{\mathbf{k}} g_{\mathbf{k}} \sum_{j' \neq j} \alpha_{jj',\mathbf{k}}(t) e^{i\mathbf{k} \cdot \mathbf{r}_{j'}} e^{-i(\omega_{\mathbf{k}} + \omega_0)t}, \end{aligned} \quad (5.1.4)$$

$$\dot{\gamma}_j(t) = -\frac{ig_{\mathbf{k}}}{\hbar} \sum_j \beta_j(t) \exp[i(\omega_{\mathbf{k}} - \omega_0)t - i\mathbf{k} \cdot \mathbf{r}_j], \quad (5.1.5)$$

$$\dot{\alpha}_{uv,\mathbf{k}}(t) = -\frac{ig_{\mathbf{k}}}{\hbar} \beta_v \exp[i(\omega_{\mathbf{k}} + \omega_0)t - i\mathbf{k} \cdot \mathbf{r}_u] + (u \leftrightarrow v), \quad (5.1.6)$$

where the last term, ($u \leftrightarrow v$), is the repeat of the first term in Eq.(5.1.6) by exchanging u by v . Since we assume that initially only one single QD is excited and there is still no photon in the system, the initial conditions $\gamma_{\mathbf{k}}(0) = \alpha_{uv,\mathbf{k}}(0) = 0$ is obtained. By integrating Eqs.(5.1.5) and (5.1.6) over time and substituting for $\gamma_{\mathbf{k}}(t)$ and $\alpha_{uv,\mathbf{k}}(t)$ in Eq.(5.1.4), an equation for the amplitude $\beta(t)$ can be obtained,

$$\begin{aligned} \dot{\beta}_j(t) = & - \sum_{\mathbf{k}} \sum_{j'=1}^N \frac{g_{\mathbf{k}}^2}{\hbar^2} \int_0^t dt' \beta_{j'}(t') e^{i(\omega_{\mathbf{k}} - \omega_0)(t'-t) + i\mathbf{k} \cdot (\mathbf{r}_j - \mathbf{r}_{j'})} \\ & - (N-1) \sum_{\mathbf{k}} \frac{g_{\mathbf{k}}^2}{\hbar^2} \int_0^t dt' \beta_{j'}(t') e^{i(\omega_{\mathbf{k}} + \omega_0)(t'-t)} \\ & - \sum_{\mathbf{k}} \sum_{j'=1, j' \neq j}^N \frac{g_{\mathbf{k}}^2}{\hbar^2} \int_0^t dt' \beta_{j'}(t') e^{i(\omega_{\mathbf{k}} + \omega_0)(t'-t) - i\mathbf{k} \cdot (\mathbf{r}_j - \mathbf{r}_{j'})}, \end{aligned} \quad (5.1.7)$$

Since the radiative decay time of a typical QD, for instance an InAs QD, is in the order of a few nanoseconds, we can apply the Markov approximation which is valid when the QD decay time is larger than the time of flight of the photon through the QD sample. Now we assume that the system is initially prepared in the first eigenstate of Eq.(5.1.3). In the Markov approximation, $\beta_j(t')$ can be replaced by $\beta_j(t)$ and can be taken outside the integral. Taking the time integrations and replacing the summation over \mathbf{k} by an integration, we obtain an expression for $\dot{\beta}_j(t')$ from Eq.(5.1.7) as

$$\begin{aligned} \dot{\beta}_j(t) = & \frac{iV_{\text{ph}}}{\hbar^2(2\pi)^3} \beta_j(t) \int d^3\mathbf{k} g_{\mathbf{k}}^2 \left(\frac{1 - e^{-i(\omega_{\mathbf{k}} - \omega_0)t}}{\omega_{\mathbf{k}} - \omega_0} \right) \\ & + (N-1) \frac{iV_{\text{ph}}}{\hbar^2(2\pi)^3} \beta_j(t) \int d^3\mathbf{k} g_{\mathbf{k}}^2 \left(\frac{1 - e^{-i(\omega_{\mathbf{k}} + \omega_0)t}}{\omega_{\mathbf{k}} + \omega_0} \right) \\ & + \frac{iV_{\text{ph}}}{\hbar^2(2\pi)^3} \int d^3\mathbf{k} \sum_{j'=1, j' \neq j}^N g_{\mathbf{k}}^2 \left[\left(\frac{1 - e^{-i(\omega_{\mathbf{k}} - \omega_0)t}}{\omega_{\mathbf{k}} - \omega_0} \right) e^{i\mathbf{k} \cdot (\mathbf{r}_j - \mathbf{r}_{j'})} \right. \\ & \quad \left. + \left(\frac{1 - e^{-i(\omega_{\mathbf{k}} + \omega_0)t}}{\omega_{\mathbf{k}} + \omega_0} \right) e^{-i\mathbf{k} \cdot (\mathbf{r}_j - \mathbf{r}_{j'})} \right] \beta_{j'}(t). \end{aligned} \quad (5.1.8)$$

All the exponential factors containing t can be removed since they oscillate fast as a function of \mathbf{k} within the integral [99]. We subsequently perform the integration over \mathbf{k} in spherical coordinates,

$$\begin{aligned} \dot{\beta}_j(t) = & \frac{i\Gamma_0}{2\pi k_0} \beta_j(t) \int_0^\infty \frac{dkk}{k - k_0} + (N-1) \frac{i\Gamma_0}{2\pi k_0} \beta_j(t) \int_0^\infty \frac{dkk}{k + k_0} \\ & + \frac{i\Gamma_0}{4\pi k_0} \sum_{j' \neq j}^N \int_0^\infty dkk \int_0^\pi d\theta_{\mathbf{k}} \sin \theta_{\mathbf{k}} \left[\frac{e^{i\mathbf{k} \cdot (\mathbf{r}_j - \mathbf{r}_{j'}) \cos \theta_{\mathbf{k}}}}{k - k_0} + \frac{e^{-i\mathbf{k} \cdot (\mathbf{r}_j - \mathbf{r}_{j'}) \cos \theta_{\mathbf{k}}}}{k + k_0} \right] \beta_{j'}(t), \end{aligned} \quad (5.1.9)$$

where $\omega_k = kc$, $\omega_0 = k_0c$ and $\Gamma_0 = k_0^3\mu^2/\pi\epsilon_0\hbar$. In all terms, we replace k_0 by $k_0 + i0$. Then the first two terms of Eq.(5.1.9) can be simplified to

$$\begin{aligned} \frac{i\Gamma_0}{2\pi k_0} \beta_j(t) \int_0^\infty dk k \left(\frac{1}{k-k_0} + \frac{(N-1)}{k+k_0} \right) \\ = \frac{i\Gamma_0}{2\pi k_0} \beta_j(t) \int_0^\infty dk k \left(\frac{1}{k-k_0-i0} + \frac{(N-1)}{k+k_0+i0} \right). \end{aligned} \quad (5.1.10)$$

As also introduced in chapter (2), if we use the mathematical identity,

$$\frac{1}{x \mp i0} = P \frac{1}{x} \pm i\pi\delta(x) \quad (5.1.11)$$

where P is the Cauchy principle value of the integral. We then apply Eq.(5.1.11) to Eq.(5.1.10) and we obtain

$$\begin{aligned} \frac{i\Gamma_0}{2\pi k_0} \beta_j(t) \int_0^\infty dk k \left(\frac{1}{k-k_0} + \frac{(N-1)}{k+k_0} \right) \\ = \frac{i\Gamma_0}{2\pi k_0} \beta_j(t) \int_0^\infty dk k \left(P \frac{1}{k-k_0} + P \frac{(N-1)}{k+k_0} \right) - \frac{\Gamma_0}{2} \beta_j(t). \end{aligned} \quad (5.1.12)$$

Since the first term on the right hand side of Eq.(5.1.12) is imaginary, it corresponds to a frequency shift for all amplitudes $\beta_j(t)$. In this work, we assume that this shift is a minor modification to the central transition energy of the QDs and is hidden in ω_0 .

Now we go back to the second term in Eq.(5.1.9). After performing the angular integration over θ_k , we obtain

$$\begin{aligned} \frac{i\Gamma_0}{4\pi k_0} \sum_{j' \neq j}^N \int_0^\infty dk k \int_0^\pi d\theta_k \sin \theta_k \left[\frac{e^{ik|\mathbf{r}_j - \mathbf{r}_{j'}| \cos \theta_k}}{k-k_0-i0} + \frac{e^{-ik|\mathbf{r}_j - \mathbf{r}_{j'}| \cos \theta_k}}{k+k_0+i0} \right] \beta_{j'}(t) \\ = \frac{i\Gamma_0}{2\pi k_0} \sum_{j' \neq j}^N \beta_{j'}(t) \int_0^\infty dk \left[\frac{1}{k-k_0-i0} + \frac{1}{k+k_0+i0} \right] \frac{\sin(k|\mathbf{r}_j - \mathbf{r}_{j'}|)}{|\mathbf{r}_j - \mathbf{r}_{j'}|} \\ = \frac{i\Gamma_0}{2\pi k_0} \sum_{j' \neq j}^N \frac{\beta_{j'}(t)}{|\mathbf{r}_j - \mathbf{r}_{j'}|} \int_0^\infty dk \left(\frac{\sin(k|\mathbf{r}_j - \mathbf{r}_{j'}|)}{k-k_0-i0} \right) \\ = \frac{\Gamma_0}{4\pi k_0} \sum_{j' \neq j}^N \frac{\beta_{j'}(t)}{|\mathbf{r}_j - \mathbf{r}_{j'}|} \int_{-\infty}^\infty dk \left(\frac{\exp(ik|\mathbf{r}_j - \mathbf{r}_{j'}|)}{k-k_0-i0} - \frac{\exp(-ik|\mathbf{r}_j - \mathbf{r}_{j'}|)}{k-k_0-i0} \right). \end{aligned} \quad (5.1.13)$$

We perform the integration over k in Eq.(5.1.13) by the contour method. For the first term, we close the integration in the upper half-plane and for the second term in the lower half-plane of complex k ,

$$\frac{\Gamma_0}{4\pi k_0} \sum_{j' \neq j}^N \frac{\beta_{j'}(t)}{|\mathbf{r}_j - \mathbf{r}_{j'}|} \int_{-\infty}^\infty dk \frac{\exp(ik|\mathbf{r}_j - \mathbf{r}_{j'}|)}{k-k_0-i0} = \frac{i\Gamma_0}{2k_0} \sum_{j' \neq j}^N \frac{\exp(ik_0|\mathbf{r}_j - \mathbf{r}_{j'}|)}{|\mathbf{r}_j - \mathbf{r}_{j'}|} \beta_{j'}(t). \quad (5.1.14)$$

The second term vanishes due to the integration. As a result, the substitution of (5.1.12) and (5.1.14) in Eq.(5.1.9) gives

$$\dot{\beta}_j(t) = -\frac{\Gamma_0}{2}\beta_j(t) + \frac{i\Gamma_0}{2k_0} \sum_{j' \neq j}^N \frac{\exp(i\mathbf{k}_0 \cdot |\mathbf{r}_j - \mathbf{r}_{j'}|)}{|\mathbf{r}_j - \mathbf{r}_{j'}|} \beta_{j'}(t). \quad (5.1.15)$$

Eq.(5.1.15) has been derived beyond the Rotating Wave Approximation (RWA) and counter-rotating terms in the interaction Hamiltonian have also been taken into account. It has already been shown for the case of atomic systems [99] that the RWA leads to an extra imaginary term in the emission rate which is improper and is not physically meaningful. Eq.(5.1.15) is a general expression and should be calculated for $\beta_j(t)$ in a specific lattice of QDs. In section (5.2.1), we solve the QD population probability $\beta_j(t)$ for a single rectangular lattice.

5.1.2 Two intermixed planar lattices of quantum dots

In previous section, we obtained the equation of motion for the population probability of a single lattice of QDs. Now we go one step further and we will treat two intermixed QD lattices, in which the QDs can be different in both lattices. The Hamiltonian of such a system can be written in the form

$$\begin{aligned} \hat{H}_I = & \sum_{\mathbf{k}} \sum_{j_1=1}^N g_{1\mathbf{k}} \left(\hat{S}_{j_1} e^{-i\omega_1 t} + \hat{S}_{j_1}^\dagger e^{i\omega_1 t} \right) \left(\hat{a}_{\mathbf{k}}^\dagger e^{i\omega_{\mathbf{k}} t - i\mathbf{k} \cdot \mathbf{r}_{j_1}} + \hat{a}_{\mathbf{k}} e^{-i\omega_{\mathbf{k}} t + i\mathbf{k} \cdot \mathbf{r}_{j_1}} \right) \\ & + \sum_{\mathbf{k}} \sum_{j_2=1}^N g_{2\mathbf{k}} \left(\hat{S}_{j_2} e^{-i\omega_2 t} + \hat{S}_{j_2}^\dagger e^{i\omega_2 t} \right) \left(\hat{a}_{\mathbf{k}}^\dagger e^{i\omega_{\mathbf{k}} t - i\mathbf{k} \cdot \mathbf{r}_{j_2}} + \hat{a}_{\mathbf{k}} e^{-i\omega_{\mathbf{k}} t + i\mathbf{k} \cdot \mathbf{r}_{j_2}} \right), \end{aligned} \quad (5.1.16)$$

where indexes 1, 2 represent the operators and QD positions belonging to the first and second lattice respectively. Here, ω_1 and ω_2 are the transition energies of QDs in the first and second lattice respectively and $g_{1,2\mathbf{k}} = \omega_{1,2} \mu_{1,2} / \sqrt{\varepsilon_0 \hbar \omega_{\mathbf{k}} V_{\text{ph}}}$ are the coupling constants between a single QD-lattice and the EM field modes. We also need to introduce a new Fock state for our new system,

$$\begin{aligned} \Psi = & \sum_{j_1=1}^N \beta_{j_1}(t) |g_1 \cdots e_{j_1} \cdots\rangle_1 |g_1 \cdots\rangle_2 |0\rangle + \sum_{j_2=1}^N \beta_{j_2}(t) |g_1 \cdots\rangle_1 |g_1 \cdots e_{j_2} \cdots\rangle_2 |0\rangle \\ & + \sum_{\mathbf{k}} \gamma_{\mathbf{k}}(t) |g_1 \cdots\rangle_1 |g_1 \cdots\rangle_2 |1_{\mathbf{k}}\rangle \\ & + \sum_{u_1, v_2} \sum_{\mathbf{k}} \alpha_{u_1 v_2}(t) |g_1 \cdots e_{u_1} \cdots\rangle_1 |g_1 \cdots e_{v_2} \cdots\rangle_2 |1_{\mathbf{k}}\rangle \\ & + \sum_{u_1 < v_1} \sum_{\mathbf{k}} \alpha_{u_1 v_1}(t) |g_1 \cdots e_{u_1} \cdots e_{v_1} \cdots\rangle_1 |g_1 \cdots\rangle_2 |1_{\mathbf{k}}\rangle \\ & + \sum_{u_2 < v_2} \sum_{\mathbf{k}} \alpha_{u_2 v_2}(t) |g_1 \cdots\rangle_1 |g_1 \cdots e_{u_2} \cdots e_{v_2} \cdots\rangle_2 |1_{\mathbf{k}}\rangle, \end{aligned} \quad (5.1.17)$$

By applying the Fock state introduced in Eq.(5.1.17) and the Hamiltonian of Eq.(5.1.16) into the Schrödinger equation and employing the same method as used in the case of single lattice, we arrive at the following equation of motion for $\beta_{j_1}(t)$ in the Markov approximation,

$$\begin{aligned} \dot{\beta}_{j_1}(t) = & -i\beta_{j_1}(t) \sum_{\mathbf{k}} \frac{g_{1\mathbf{k}}^2}{\omega_1 - \omega_{\mathbf{k}}} \\ & + i(N_1 - 1)\beta_{j_1}(t) \sum_{\mathbf{k}} \frac{g_{1\mathbf{k}}^2}{\omega_1 + \omega_{\mathbf{k}}} + iN_2\beta_{j_1}(t) \sum_{\mathbf{k}} \frac{g_{2\mathbf{k}}^2}{\omega_2 + \omega_{\mathbf{k}}} \\ & + i \sum_{\mathbf{k}} \sum_{j'_1 \neq j_1} g_{1\mathbf{k}}^2 \beta_{j'_1}(t) \left\{ \frac{e^{i\mathbf{k} \cdot (\mathbf{r}_{j_1} - \mathbf{r}_{j'_1})}}{\omega_{\mathbf{k}} - \omega_1} + \frac{e^{-i\mathbf{k} \cdot (\mathbf{r}_{j_1} - \mathbf{r}_{j'_1})}}{\omega_{\mathbf{k}} + \omega_1} \right\} \\ & + ie^{i(\omega_1 - \omega_2)t} \sum_{\mathbf{k}} \sum_{j'_2} g_{1\mathbf{k}} g_{2\mathbf{k}} \beta_{j'_2}(t) \left\{ \frac{e^{i\mathbf{k} \cdot (\mathbf{r}_{j_1} - \mathbf{r}_{j'_2})}}{\omega_{\mathbf{k}} - \omega_2} + \frac{e^{-i\mathbf{k} \cdot (\mathbf{r}_{j_1} - \mathbf{r}_{j'_2})}}{\omega_{\mathbf{k}} + \omega_1} \right\}. \end{aligned} \quad (5.1.18)$$

In Eq.(5.1.18), we have again ignored the exponential terms with exponents of the kind $i\omega_{\mathbf{k}}t$, since these terms oscillate fast under the integration over \mathbf{k} . The first four terms on the right hand side of Eq.(5.1.18) correspond to the time evolution of the QDs in lattice 1 when they are not coupled with the QDs of lattice 2. Following exactly the same procedure as we did for the case of single lattice, we can write the first four terms as

$$-\frac{\Gamma_0^1}{2}\beta_{j_1}(t) + \frac{i\Gamma_0^1}{2k_1} \sum_{j'_1 \neq j_1}^N \frac{\exp(i\mathbf{k}_1 \cdot |\mathbf{r}_{j_1} - \mathbf{r}_{j'_1}|)}{|\mathbf{r}_{j_1} - \mathbf{r}_{j'_1}|} \beta_{j'_1}(t), \quad (5.1.19)$$

where $\Gamma_1 = k_1^3 \mu_1^2 / \pi \epsilon_0 \hbar$ is the spontaneous emission rate of isolated QDs in lattice 1 and $k_1 = \omega_1/c$. Regarding the last term in Eq.(5.1.18), by changing the sum over \mathbf{k} to the integration in circular coordinates, we can write

$$\begin{aligned} & ie^{i(\omega_1 - \omega_2)t} \sum_{\mathbf{k}} \sum_{j'_2} g_{1\mathbf{k}} g_{2\mathbf{k}} \beta_{j'_2}(t) \left\{ \frac{e^{i\mathbf{k} \cdot (\mathbf{r}_{j_1} - \mathbf{r}_{j'_2})}}{\omega_{\mathbf{k}} - \omega_2} + \frac{e^{-i\mathbf{k} \cdot (\mathbf{r}_{j_1} - \mathbf{r}_{j'_2})}}{\omega_{\mathbf{k}} + \omega_1} \right\} \\ & = \frac{2ik_1 k_2 \mu_1 \mu_2}{\hbar \pi} e^{i(\omega_1 - \omega_2)t} \sum_{j'_2} \beta_{j'_2}(t) \int_0^\infty dk \left(\frac{1}{k - k_2} + \frac{1}{k + k_1} \right) \frac{\sin(k |\mathbf{r}_{j_1} - \mathbf{r}_{j'_2}|)}{|\mathbf{r}_{j_1} - \mathbf{r}_{j'_2}|}. \end{aligned} \quad (5.1.20)$$

In Eq.(5.1.20), we replace k_1 and k_2 by $k_{\text{ave}} = (k_1 + k_2)/2$. This is a good approximation if $k_1 - k_2 \ll k_{\text{ave}}$ which is normally the case. Then by changing k_{ave} by $k_{\text{ave}} + i0$ and similar to the single lattice case, Eq.(5.1.20) can be simplified to

$$\begin{aligned} & \frac{k_{\text{ave}}^2 \mu_1 \mu_2}{\hbar \pi} e^{i(\omega_1 - \omega_2)t} \sum_{j'_2} \frac{\beta_{j'_2}(t)}{|\mathbf{r}_{j_1} - \mathbf{r}_{j'_2}|} \\ & \times \int_{-\infty}^{\infty} dk \left(\frac{\exp(i\mathbf{k} \cdot |\mathbf{r}_{j_1} - \mathbf{r}_{j'_2}|)}{k - k_{\text{ave}} - i0} - \frac{\exp(-i\mathbf{k} \cdot |\mathbf{r}_{j_1} - \mathbf{r}_{j'_2}|)}{k - k_{\text{ave}} - i0} \right). \end{aligned} \quad (5.1.21)$$

Again, after doing the contour integration and assuming that the QDs from the two different lattices have equal dipole moments, $\mu_1 = \mu_2 = \mu$, Eq.(5.1.21) becomes

$$\frac{i\Gamma_{\text{ave}}}{2k_{\text{ave}}} e^{i(\omega_1 - \omega_2)t} \sum_{j'_2} \frac{\exp\left(ik_0 |\mathbf{r}_{j_1} - \mathbf{r}_{j'_2}|\right)}{|\mathbf{r}_{j_1} - \mathbf{r}_{j'_2}|} \beta_{j'_2}(t), \quad (5.1.22)$$

where $\Gamma_{\text{ave}} = k_{\text{ave}}^3 \mu^2 / \pi \epsilon_0 \hbar$. Substituting (5.1.19) and (5.1.22) in Eq.(5.1.18), the equation of motion for the population probability of lattice 1 is obtained to be

$$\begin{aligned} \dot{\beta}_{j_1}(t) = & -\frac{\Gamma_0^1}{2} \beta_{j_1}(t) + \frac{i\Gamma_0^1}{2k_1} \sum_{j'_1 \neq j_1} \frac{\exp\left(ik_1 |\mathbf{r}_{j_1} - \mathbf{r}_{j'_1}|\right)}{|\mathbf{r}_{j_1} - \mathbf{r}_{j'_1}|} \beta_{j'_1}(t) \\ & + \frac{i\Gamma_{\text{ave}}}{2k_{\text{ave}}} e^{i(\omega_1 - \omega_2)t} \sum_{j'_2} \frac{\exp\left(ik_0 |\mathbf{r}_{j_1} - \mathbf{r}_{j'_2}|\right)}{|\mathbf{r}_{j_1} - \mathbf{r}_{j'_2}|} \beta_{j'_2}(t). \end{aligned} \quad (5.1.23)$$

Similarly, the equation of motion for the population probability of lattice 2 can be derived as

$$\begin{aligned} \dot{\beta}_{j_2}(t) = & -\frac{\Gamma_0^2}{2} \beta_{j_2}(t) + \frac{i\Gamma_0^2}{2k_2} \sum_{j'_2 \neq j_2} \frac{\exp\left(ik_2 |\mathbf{r}_{j_2} - \mathbf{r}_{j'_2}|\right)}{|\mathbf{r}_{j_2} - \mathbf{r}_{j'_2}|} \beta_{j'_2}(t) \\ & + \frac{i\Gamma_{\text{ave}}}{2k_{\text{ave}}} e^{-i(\omega_1 - \omega_2)t} \sum_{j'_1} \frac{\exp\left(ik_0 |\mathbf{r}_{j_2} - \mathbf{r}_{j'_1}|\right)}{|\mathbf{r}_{j_2} - \mathbf{r}_{j'_1}|} \beta_{j'_1}(t). \end{aligned} \quad (5.1.24)$$

We should emphasize that all the series are convergent yielding finite values. It is obvious from (5.1.23) and (5.1.24) that the population probabilities of the two intermixed QD lattices are coupled. Eqs.(5.1.23) and (5.1.24) constitute a closed set of differential equations for any two intermixed lattices with arbitrary QD properties, lattice unit cell, lattice periodicity and mutual lattice displacement. In next section, we treat the case of two intermixed rectangular lattices in more detail.

5.2 Planar square lattices of quantum dots

In this section we try to quantitatively and qualitatively interpret the equations we derived in previous section for the case of planar square lattices. The quantum dots are identical within each lattice, but different QD lattices are constituted by different QDs. The main goal is to see how the collective radiative decay rates of the QD lattices are modified by changing e.g. the lattice periodicity. In addition, we like to show how the coupling between both QD lattices is modified by changing the translational shift D between both QD-lattices. We will also study the influence of the initial excitation conditions on the population dynamics of the QD lattice. As is schematically illustrated in Fig.(5.1), in the structure of interest, the QDs are positioned on the lattice points of an infinitely large and planar square lattice with periodicity a .

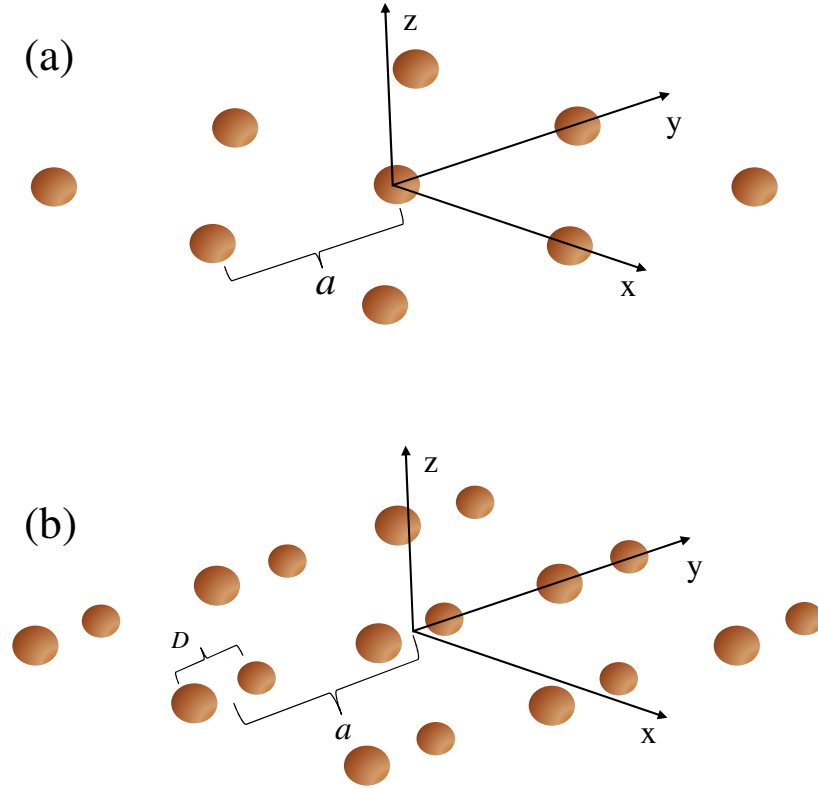


Figure 5.1: Schematic picture of (a) a single square QD lattice and (b) a system of two intermixed QD lattices. The periodicity of both lattices is a and the translational shift between the QDs of the two different lattices is D .

5.2.1 A single square lattice of identical quantum dots

We first assume that QDs are located at the lattice points of a single square lattice with periodicity a along both x and y directions. The schematic picture of this structure is demonstrated in Fig.(5.1).a. Since we assume that our periodic structure is infinitely large, all probability amplitudes $\beta_j(t)$ are equal but for the sake of more flexibility in the problem, we can also assume that the probability amplitudes can be phase shifted along the y direction with an amount of κ_y . This phase shift can be induced during the optical excitation process. So by employing the equality

$$\beta_{j'}(t) = \beta_j(t) \exp [i\kappa_y (y_j - y_{j'})] \quad (5.2.1)$$

into Eq.(5.1.15) and indexing the position of the QDs by

$$(x_j, y_j) \rightarrow a(p, q),$$

$$(x_{j'}, y_{j'}) \rightarrow a(p', q'), \quad (5.2.2)$$

the equation of motion for the population probability of a single rectangular lattice becomes

$$\begin{aligned} \dot{\beta}_j(t) = & -\frac{\Gamma_0}{2}\beta_j(t) \\ & + \frac{i\Gamma_0}{2k_0a}\beta_{j'}(t) \sum_{p' \neq p} \sum_{q' \neq q} \frac{\exp\left(ik_0a\sqrt{(p-p')^2 + (q-q')^2}\right)}{\sqrt{(p-p')^2 + (q-q')^2}} e^{i(q-q')a\kappa} \end{aligned} \quad (5.2.3)$$

Rearranging the indexes by $p-p' \rightarrow m$ and $q-q' \rightarrow n$, we can write (5.2.3) in a simpler form,

$$\dot{\beta}_j(t) = -\frac{\Gamma_{SL}}{2}\beta_j(t), \quad (5.2.4)$$

where

$$\Gamma_{SL} = \frac{\Gamma_0}{2} - \frac{i\Gamma_0}{k_0a} \sum_{m=1}^{\infty} \sum_{n=1}^{\infty} \frac{\exp\left(ik_0a\sqrt{m^2 + n^2}\right)}{\sqrt{m^2 + n^2}} \cos(na\kappa). \quad (5.2.5)$$

The first message of Eq.(5.2.5) is that the population of an infinitely large single QD lattice decays single-exponentially with the a spontaneous emission rate which is equal to the real part of Γ_{SL} . Assuming that there is no phase shift in the lattice, the single QD lattice emission rate has been displayed in Fig.(5.2) as a function of the lattice periodicity. The real part of the emission contributes to the cooperative decay rate while the imaginary part yields the frequency shift. Since our focus in this work is mainly on the cooperative decay rate, we will examine the real part more in detail. It is evident from Fig.(5.2) that depending on the value of the periodicity, the cooperative population decay rate is sometimes faster and sometimes slower than the emission rate of a single QD. For some periodicities, the constructive interferences between the available optical modes are stronger than the destructive interferences. In this case, the local density of optical states is enhanced, giving rise to a faster decay rate of the QD lattice. Focusing on the range of periodicities smaller than the emission wavelength, $a < \lambda$, we see that for very small lattice constants ($a \ll 0.2\lambda$), the emission rate of the QD- lattice is drastically increased with respect to the decay rate of a single QD. But for $0.2\lambda < a$, the QD lattice emission rate becomes slower than the single QD emission rate, reaching a minimum at around 0.3λ and again increasing for larger QD-QD spacing. It is easy to calculate that for very large periodicities, the optical coupling between QDs is negligible and the QD lattice emission rate tends to the emission rate of a single QD.

5.2.2 Two intermixed square lattices of identical quantum dots

At this point, we would like to see how two intermixed lattices can be optically coupled. We assume that the structure of lattice 2 is identical to the structure of lattice 1, but the two lattices are spatially translated by a distance D in the y direction. We can also imagine this system as a square unit cell consisting of two different QDs within each

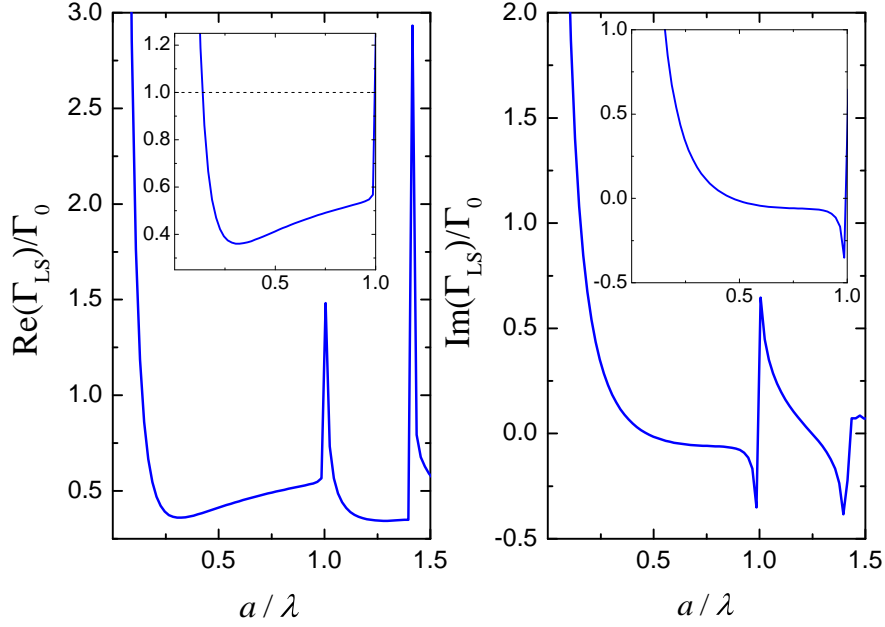


Figure 5.2: The real (Left) and the imaginary (Right) parts of the spontaneous emission rate of a single lattice of QDs. The inset is the zoom of the original graph for periodicities smaller than the wavelength.

unit cell. Choosing the origin of the coordinate system on the center of the QD-QD axis within one unit cell, the positions of the QDs in such a double-lattice structure can be determined via

$$\begin{aligned} (x_{j_1}, y_{j_1}) &\rightarrow (ap, aq + D/2), \\ (x_{j_2}, y_{j_2}) &\rightarrow (ap, aq - D/2). \end{aligned} \quad (5.2.6)$$

To keep the generality of the problem, we assume that there is a phase shift κ along the y direction, similar to the case of single lattice. So the population amplitudes of the QDs in the two different lattices are of the form

$$\begin{aligned} \beta_{j_1'}(t) &= \beta_{j_1}(t) e^{i(q_1 - q_1')\kappa a}, \\ \beta_{j_2'}(t) &= \beta_{j_2}(t) e^{i(q_2 - q_2')\kappa a}. \end{aligned} \quad (5.2.7)$$

Substituting (5.2.6) and (5.2.7) in Eq.(5.2.3), the two equation of motion for the populations of the two lattices become

$$\dot{\beta}_{j_1}(t) = -\frac{\Gamma_{SL}^1}{2}\beta_{j_1}(t) + \frac{\Gamma_{12}}{2}\beta_{j_2}(t), \quad (5.2.8)$$

$$\dot{\beta}_{j_2}(t) = -\frac{\Gamma_{SL}^2}{2}\beta_{j_2}(t) + \frac{\Gamma_{21}}{2}\beta_{j_1}(t). \quad (5.2.9)$$

where $\Gamma_{\text{SL}}^1, \Gamma_{\text{SL}}^2$ can be obtained from Eq.(5.2.5) and the coupling parameter is

$$\frac{\Gamma_{12}}{2} = \frac{i\Gamma_{\text{ave}}e^{i(\omega_1-\omega_2)t}}{2k_{\text{ave}}a} \sum_{m=-\infty}^{\infty} \sum_{n=-\infty}^{\infty} \frac{\exp\left(ik_{\text{ave}}a\sqrt{m^2+(n+D/a)^2}\right)}{\sqrt{m^2+(n+D/a)^2}} e^{ina\kappa}. \quad (5.2.10)$$

Γ_{21} can be obtained from Γ_{12} by exchanging the indexes $1 \leftrightarrow 2$ and $D \rightarrow -D$. But since the summation index, n , has both positive and negative values, the total series remains unchanged by $D \rightarrow -D$ and we can write

$$\frac{\Gamma_{21}}{2} = \frac{i\Gamma_{\text{ave}}e^{-i(\omega_1-\omega_2)t}}{2k_{\text{ave}}a} \sum_{m=-\infty}^{\infty} \sum_{n=-\infty}^{\infty} \frac{\exp\left(ik_{\text{ave}}a\sqrt{m^2+(n+D/a)^2}\right)}{\sqrt{m^2+(n+D/a)^2}} e^{ina\kappa}, \quad (5.2.11)$$

where $k_{\text{ave}} = (k_1 + k_2) / 2$. The lattice-lattice coupling parameters, Γ_{12} and Γ_{21} , represent the spontaneous energy transfer rates between two lattices. Now we assume that QDs of two lattices are identical and there is no phase shift applied to the system. Then Γ_{12} and Γ_{21} become identical and can be simplified to

$$\frac{\Gamma_{12}}{2} = \frac{\Gamma_{21}}{2} = \frac{i\Gamma_0}{2k_0a} \sum_{m=-\infty}^{\infty} \sum_{n=-\infty}^{\infty} \frac{\exp\left(ik_0a\sqrt{m^2+(n+D/a)^2}\right)}{\sqrt{m^2+(n+D/a)^2}}. \quad (5.2.12)$$

In Fig.(5.3), we see how the lattice-lattice coupling parameters are modified by changing the lattice periodicity for a fixed lattice-lattice separation D . The real part of the interaction, which modifies the emission rate, has a negative value for periodicities smaller than the wavelength, $a < \lambda$, but is independent from the lattice-lattice separation, D . But the imaginary part is much more sensitive to the lattice-lattice separation D . In Fig.(5.4), the lattice-lattice coupling parameter has been drawn as a function of the lattice-lattice separation for different lattice periodicities. It is obvious that the distance between a QD in lattice 2 and a QD in lattice 1, D , in the same unit cell cannot be larger than half of the lattice periodicity. We can see that the real part of Γ_{12} oscillates as a function of the lattice-lattice separation. Of course these oscillations are not visible if the periodicity is very small, since in this case the range of possible lattice-lattice separations is not large enough to observe the oscillations.

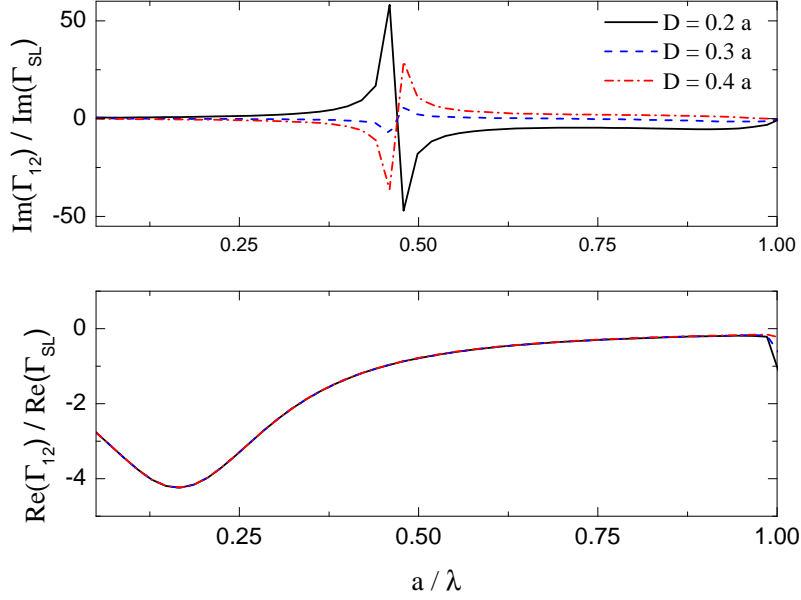


Figure 5.3: The real and imaginary parts of the QD lattice-QD lattice coupling parameter, Γ_{12} , as a function of the lattice periodicity a for different lattice-lattice separations D .

5.3 Population dynamics in two coupled lattices of quantum dots

After the excitation with one single photon, the probability as a function of time, that one single QD within lattice 1 or lattice 2 is populated is given by

$$P_1(t) = \frac{\sum_{j_1=1}^N |\beta_{j_1}(t)|^2}{\sum_{j_1=1}^N |\beta_{j_1}(0)|^2 + \sum_{j_2=1}^N |\beta_{j_2}(0)|^2}, \quad P_2(t) = \frac{\sum_{j_2=1}^N |\beta_{j_2}(t)|^2}{\sum_{j_1=1}^N |\beta_{j_1}(0)|^2 + \sum_{j_2=1}^N |\beta_{j_2}(0)|^2}. \quad (5.3.1)$$

For the case of a single lattice, the population probability simply decays single-exponentially with decay rate Γ_{SL} , which is

$$P_{SL} = e^{-\Gamma_{SL}t}. \quad (5.3.2)$$

In the case of two intermixed lattices, the time variation of the lattice populations is more complicated and strongly depends on the initial excitation condition of both lattices and the coupling between them, which in turn is a function of the lattice-lattice separation. For simplicity and without losing the most important consequences of the problem, we again assume that there is no phase shift in the system ($\kappa = 0$) and the QDs

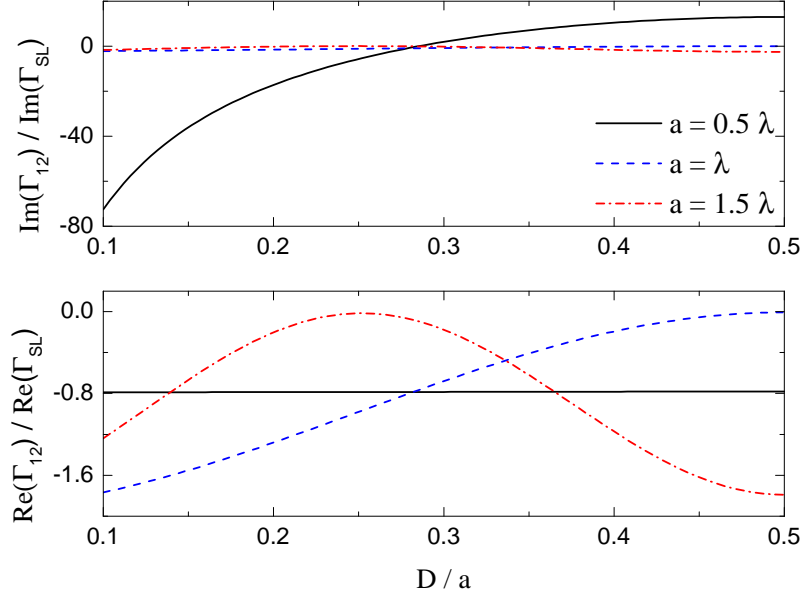


Figure 5.4: The real and imaginary parts of the lattice-lattice coupling parameter, Γ_{12} , as a function of the lattice-lattice separation, D for different lattice periodicities.

of two lattices are identical, implying $\Gamma_{SL}^1 = \Gamma_{SL}^2 = \Gamma_{SL}$. Under this condition, the coupled differential equations in (5.1.23) and (5.1.24) can be simplified to

$$\begin{aligned}\dot{\beta}_{j_1}(t) &= -\frac{\Gamma_{SL}}{2}\beta_{j_1}(t) + \frac{\Gamma_{12}}{2}\beta_{j_2}(t), \\ \dot{\beta}_{j_2}(t) &= -\frac{\Gamma_{SL}}{2}\beta_{j_2}(t) + \frac{\Gamma_{12}}{2}\beta_{j_1}(t).\end{aligned}\quad (5.3.3)$$

The solution of the equations of motion in (5.3.3), gives rise to

$$\begin{aligned}\beta_{j_1}(t) &= \frac{1}{2}(\beta_{j_1}(0) + \beta_{j_2}(0))e^{-\frac{(\Gamma_{SL}-\Gamma_{12})}{2}t} + \frac{1}{2}(\beta_{j_1}(0) - \beta_{j_2}(0))e^{-\frac{(\Gamma_{SL}+\Gamma_{12})}{2}t}, \\ \beta_{j_2}(t) &= \frac{1}{2}(\beta_{j_1}(0) + \beta_{j_2}(0))e^{-\frac{(\Gamma_{SL}-\Gamma_{12})}{2}t} - \frac{1}{2}(\beta_{j_1}(0) - \beta_{j_2}(0))e^{-\frac{(\Gamma_{SL}+\Gamma_{12})}{2}t}.\end{aligned}\quad (5.3.4)$$

We assume that all QDs have equal chance to become excited. So we drop the indexes j_1, j_2 and represent the corresponding amplitudes of lattice 1 by β_1 and those of lattice 2 by β_2 . Then Eq.(5.3.1) will be simplified to

$$P_1(t) = \frac{|\beta_1(t)|^2}{|\beta_1(0)|^2 + |\beta_2(0)|^2}, \quad P_2(t) = \frac{|\beta_2(t)|^2}{|\beta_1(0)|^2 + |\beta_2(0)|^2}.\quad (5.3.5)$$

By inserting Eq.(5.3.4) into Eq.(5.3.5), the population dynamics for lattice 1 and 2 are obtained

$$\begin{aligned}P_1(t) &= Ae^{-\Gamma_{SL}t} \cos(\Omega t) + A^a e^{-\Gamma_a t} + A^s e^{-\Gamma_s t}, \\ P_2(t) &= -Ae^{-\Gamma_{SL}t} \cos(\Omega t) + A^a e^{-\Gamma_a t} + A^s e^{-\Gamma_s t},\end{aligned}\quad (5.3.6)$$

where

$$A = \frac{1}{2} \frac{(\beta_1^2(0) - \beta_2^2(0))}{(\beta_1^2(0) + \beta_2^2(0))}, \quad A^\alpha = \frac{1}{4} \frac{(\beta_1(0) + \beta_2(0))^2}{(\beta_1^2(0) - \beta_2^2(0))}, \quad A^s = \frac{1}{4} \frac{(\beta_1(0) - \beta_2(0))^2}{(\beta_1^2(0) - \beta_2^2(0))}, \quad (5.3.7)$$

and

$$\begin{aligned} \Gamma_s &= \Gamma_{SL} + \text{Re}(\Gamma_{12}), \\ \Gamma_\alpha &= \Gamma_{SL} - \text{Re}(\Gamma_{12}), \\ \Omega &= \text{Im}(\Gamma_{12}). \end{aligned} \quad (5.3.8)$$

The collective emission rates Γ_s and Γ_α correspond respectively to the symmetric and asymmetric emission rates that have already been introduced in chapter 2 for the system of two QDs. The difference is that in this chapter, instead of two coupled QDs, we have two coupled lattices of QDs. As demonstrated in Fig. 5. 2 and Fig. 5. 4, depending on whether Γ_s or Γ_α are enhanced or reduced as compared with the spontaneous emission rate of a single lattice, they can represent either the superradiant emission which decays faster than a single lattice or subradiant emission which corresponds to a slower decay. We found that by engineering the lattice parameters, we are able to obtain almost arbitrary values for the lattice-lattice coupling parameter and hence almost arbitrary values for the superradiant and subradiant spontaneous emission rates.

As is shown in Eqs.(5.3.6), the population of lattices decay by three different decay channels. The first decay channel corresponds to the emission rate of a single isolated QD lattice and is modulated by (population) oscillations (between the two lattices) with a frequency equal to the imaginary part of the lattice-lattice coupling. The second and the third decay channels correspond to the asymmetric and symmetric emission rates, respectively.

Now we study the influence of different initial excitation conditions. First we assume that lattice 1 is initially excited and lattice 2 is initially in the ground state, $\beta_1(0) = 1, \beta_2(0) = 0$. For this case, the population decay probabilities are of the form

$$\begin{aligned} P_1(t) &= \frac{1}{2} e^{-\Gamma_{SL}t} \cos(\Omega t) + \frac{1}{4} e^{-\Gamma_\alpha t} + \frac{1}{4} e^{-\Gamma_s t}, \\ P_2(t) &= -\frac{1}{2} e^{-\Gamma_{SL}t} \cos(\Omega t) + \frac{1}{4} e^{-\Gamma_\alpha t} + \frac{1}{4} e^{-\Gamma_s t}. \end{aligned} \quad (5.3.9)$$

The most important message of the population dynamics in (5.3.9) is that although lattice 2 is not initially excited, a part of the population of lattice 1 is transferred to lattice 2 and eventually decays to the ground state.

A second initial excitation condition is when both lattices are initially excited with the same probability, $\beta_1(0) = 1/2, \beta_2(0) = 1/2$. In this case, the population dynamics is given by

$$P_1(t) = P_2(t) = \frac{1}{2} e^{-\Gamma_\alpha t}. \quad (5.3.10)$$

It is clear from Eq.(5.3.10) that when both lattices are initially equally excited, the populations decay becomes single exponential with an asymmetric emission rate which can be either superradiant or subradiant, depending on the lattice structure. We can imagine many other initial conditions. For any specific arrangement of the initial excitation of the two lattices, there are generally three exponential decay channels with amplitudes given by Eq.(5.3.7).

5.4 Summary

In this chapter, we investigated the electromagnetic coupling between periodic arrays of QDs in the weak excitation regime when the QD many-body system is excited with only one photon. We found that a large enough single rectangular lattice of QDs has a single exponential population decay which strongly depends on the lattice periodicity. For some periodicities, the lattice emission rate is faster than the spontaneous emission rates of a single and isolated QD and for some other periodicities, it is slower. For the lattice constants smaller than the emission wavelength, the lattice emission rate is mostly slower than the emission of the single QD implying subradiant emission.

We also demonstrated that if two lattices with equal periodicities are intermixed together in addition to the optical coupling of the QDs in their own lattice, there is also optical coupling between the two different lattices. We calculated this coupling as a function of the lattice-lattice separation which shows an oscillatory behavior. We found that for periodicities smaller than the wavelength, the lattice-lattice coupling is not so sensitive to the lattice-lattice separation. The imaginary part of the lattice-lattice coupling gives rise to oscillations in the population decay of each of the lattices. The population decay of the lattices is described by 3 different decay channels in which the first channel describes a population oscillation between the two different lattices, with an oscillation frequency equal to the imaginary part of the lattice-lattice coupling and an overall decay with the emission rate of a single isolated lattice. The second channel decays with the asymmetric and the third channel decays with the symmetric emission rate. The symmetric emission rate is the sum of the single lattice emission rate and the lattice-lattice coupling while the asymmetric emission rate corresponds to the difference of these two. Depending on the lattice parameters (the periodicity and the lattice-lattice separation), the symmetric and the asymmetric emission rates can either be faster or slower than the emission rate of a single lattice.

Chapter 6

Modification of the spontaneous emission decay time in self-assembled quantum dots

6.1 Theoretical formalism

The decay time of the QD population in a self-assembled sample has been measured by employing the Time Resolved Differential Reflectivity (TRDR) spectroscopy and presented in Ref. [150]. In the next chapter, we will extensively introduce this technique, but at this point we show you the main observation of this work that drew our attention. The differential reflectivity from the plane of QDs as a function of the pump-probe delay time is shown in Fig.(6.1). This graph corresponds to the dynamics of the QD population. It is obvious in Fig.(6.1) that the population decay time for the QDs near the center of the QD size distribution (PL spectrum) is larger. We know that the density of resonant QDs around this point is higher and the electromagnetic coupling between QDs is stronger. It is obvious that the effect of this radiative coupling is to slow down the decay and hence having a larger decay time. In this chapter, we try to explain this novel and interesting effect of radiative coupling between QDs by following a quantum mechanical theoretical approach. The population dynamics of atoms or QDs in dilute ensembles can be usually described in the dipole approximation through the well-known semi-classical Maxwell-Bloch equations. But for the case of dense media, this formalism fails to describe the dynamic properties of the QDs since the electromagnetic interaction between the QDs or the atoms play an important role in modifying the energy levels and the damping rates of the atoms or QDs. From the classical point of view, the electromagnetic coupling between atoms is known from the time of Lorentz and Lorenz [64, 65]. They showed that in a dense medium, the electric field that couples to an atom (oscillator) is different from the macroscopic field by a term which is proportional to the

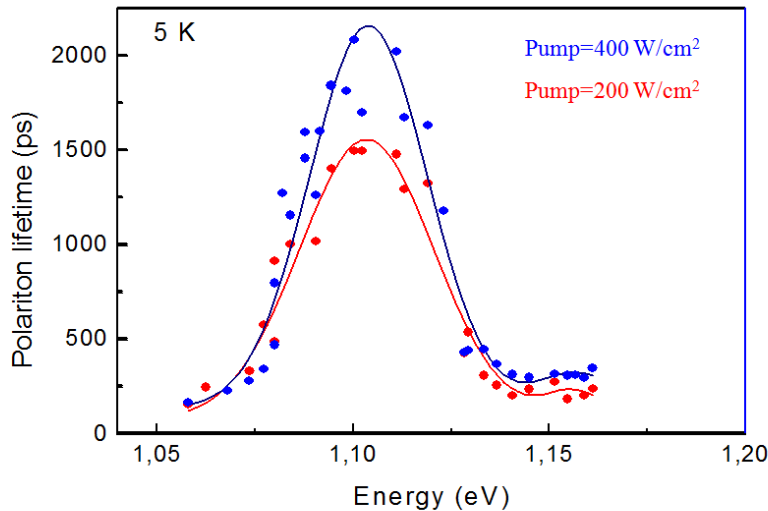


Figure 6.1: polariton lifetime (decay time of the QD population) as a function of the QD transition energy (figure from Ref. [150]).

polarization of the medium. In fact, this term is caused by the dipole-dipole coupling between the atom under consideration and all the other atoms in the medium. It has been shown that if the medium has a small absorption and is strongly scattering, this term becomes more important [66–68]. This local-field correction leads to many interesting phenomena. One of the most important effects of the Lorentz-Lorenz (LL) correction is the modification of the linear index of refraction according to the Clausius-Mossotti relation [66].

When the atomic (QD) density is large, the quantum nature of the electromagnetic field which mediates the dipole-dipole coupling becomes more important. As explained in the introductory chapter of this thesis, superfluorescence [79, 185, 186] is one consequence of the atom-atom coupling in a very dense and small medium of atoms, which was introduced by Dicke [51]. Dicke found that if the size of the medium containing the atoms is less than the wavelength of light, the atoms emit photons in a cooperative way. Since this effect happens for identical atoms or QDs, when there is inhomogeneous broadening, for example in self-assembled QDs due to the QD size distribution, the superradiance effect is absent and we cannot observe any cooperative emission. But this doesn't mean that we do not see any influence of electromagnetic QD-QD coupling on the dynamical properties of the QDs and their corresponding light emission. In such samples, the presence of confined spontaneous (incoherent) photons can alter for instance the long-lived ground-state coherences. The spontaneous photons can lead to effects like the amplified spontaneous emission (superluminescence) if the QDs are in the excited state and to the radiation trapping if they are initially in the ground-state [79].

In this chapter, we follow an approach similar to the formalism introduced in Ref. [187, 188] in which the equation of motion for the many-atom system is described by a Lindblad-type equation of a density matrix originating from a quantized interaction Hamiltonian. In this approach, the interaction between quantum dots mediated by the quantized field such as multiple scattering and reabsorption of spontaneously emitted photons as well as the local-field corrections are taken into account. The theoretical approach of this chapter is based on the analysis of the Fourier transform of the appropriate Green's functions obtained from the derivation of the Dyson's equation. In sec.(6.1), we introduce our theoretical formalism. Then in sec.(6.2), we derive the relaxation rates and the energy level shifts. In sec.(6.3), we solve the nonlinear equations numerically and perform some numerical simulations. Finally in sec.(6.4), we try to explain our numerical simulations analytically by making some approximations.

6.1.1 Hamiltonian and the time evolution operator

The interaction between a probe QD and the field in a many-QD sample can be consistently described by single-QD Bloch-type equations only if QD-QD correlations are neglected. This means that the single-QD equations of motion work only in the non-cooperative limit. This approximation is justified in highly symmetric geometries or if the inverse of the so-called superradiance time of a transition in a thin film of QDs represented by [63, 189]

$$T_{\text{SR}} = \frac{2\varepsilon_0\hbar c}{N_v L \omega_0 \mu_0^2} = \frac{2\varepsilon_0\hbar c}{N \omega_0 \mu_0^2}, \quad (6.1.1)$$

is smaller than the respective inhomogeneous line-width in the system. Here, N_v is the volume density of QDs and N is the QD surface density and L is the thickness of the thin layer that in our case is infinitely small, since we have a planar distribution of QDs. In Eq.(6.1.1), we have made use of the equation $N = N_v L$. ω_0 is the QD transition energy and μ_0 is the magnitude of the QD dipole moment. In QD samples, the inhomogeneous broadening is due to the size distribution of the QDs and can be represented by a Gaussian function

$$g(\omega, \omega_0) = \frac{1}{\sqrt{2\pi}\sigma} e^{-\frac{1}{2}\left(\frac{\omega - \omega_0}{\sigma}\right)^2}, \quad (6.1.2)$$

where σ is the inhomogeneous line-width and ω_0 is the central transition frequency of the QDs. Of course the main difference between the population dynamics of a single QD in free space and the population dynamics of a probe QD in a non-cooperative many-QD system is that, in the latter, the probe QD undergoes an energy level shift and a modification of the damping rate due to the presence of the other QDs in the medium. In the sample of our interest which is the typical self-assembled InAs/GaAs QDs and will be extensively introduced in the next chapter, the important parameters in Eqs. (6.1.1) and (6.1.2) are $N = 2.8 \times 10^{14}$ QDs/m², $\omega_0 = 1.105$ eV, $\mu_0 = 100$ Debye and $\sigma = 19$ meV. Based on these values, the inverse of superradiance time in our sample is in the order of 10^{-5} meV which is much smaller than the inhomogeneous line-width and hence the condition of the non-cooperative limit is fulfilled.

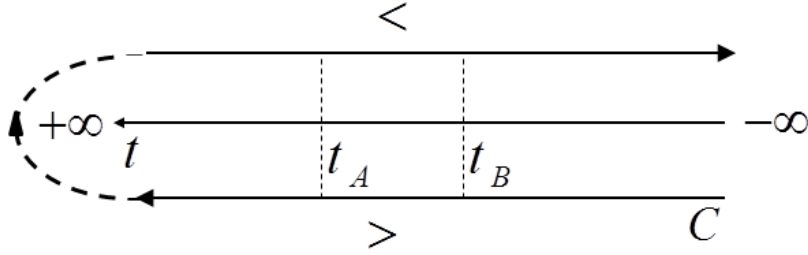


Figure 6.2: Time ordering along the Schwinger-Keldysh time contour.

We now treat the problem of the interaction between different QDs in an ensemble with the quantized radiation field in the dipole and Rotating Wave Approximation (RWA). Since we are interested in the dynamics of a single specific QD, we indicate the dipole moment element of the probe QD by μ_0 and its position by \mathbf{r}_0 , while the dipole moment elements and the position of the other QDs in the medium are represented by μ_0^j and \mathbf{r}_j respectively. The Hamiltonian of the system can be written as

$$H = H_{\text{field}} + \sum_j H_0^j - \mu_0 \cdot [\mathbf{E}(\mathbf{r}_0) + \mathbf{E}_{\text{ext}}(\mathbf{r}_0)] - \sum_j \mu_0^j \cdot [\mathbf{E}_{\text{ext}}(\mathbf{r}_j) + \mathbf{E}(\mathbf{r}_j)], \quad (6.1.3)$$

where H_{field} is the free Hamiltonian of the quantized radiation field and H_0^j is the free Hamiltonian of the j th QD. \mathbf{E} is the corresponding operator of the quantized field in the system and \mathbf{E}_{ext} is any external classical deriving field. In the interaction picture, the time evolution is described by

$$S = T \exp \left(-\frac{i}{\hbar} \int_{-\infty}^{\infty} d\tau V(\tau) \right), \quad (6.1.4)$$

where $V(\tau) = -\mu_0(\tau) \cdot [\mathbf{E}_{\text{ext}}(\mathbf{r}_0, \tau) + \mathbf{E}(\mathbf{r}_0, \tau)]$ is the interaction Hamiltonian of the probe QD and T denotes time ordering. Note that the electromagnetic coupling of QDs is included in the field operator \mathbf{E} since the field acting on the probe QD is emitted or scattered by all the other QDs in the medium. For simplicity, we can represent the time evolution of the correlation functions of the probe QD by the so-called Schwinger-Keldysh time contour C [190] shown in Fig. 6. 2. This contour starts at $t = -\infty$, goes to $t = \infty$ and comes back to $t = -\infty$. Each physical time corresponds to two times on the contour. In this concept, a time ordering operator T_C is introduced that is identical to T on the upper branch (+) and to $1/T$ on the lower branch (-) of the contours and orders all operators with the time argument (-) to the left of those with (+). This means that if $t_A > t_B$ on the lower branch of the Keldysh contour ($t_A > t_B$), it is inverse on the upper branch and $t_A < t_B$. By definition of the Keldysh contour, Eq.(6.1.4) can be written as

$$S_C = T_C \exp \left(-\frac{i}{\hbar} \int_C d\check{\tau} V(\check{\tau}) \right), \quad (6.1.5)$$

where $\check{\tau}$ denotes the time on the contour C and from now on we replace $\check{\tau}$ by τ . Now we need to know the expectation value of the time evolution operator, $\langle S_C \rangle$, where like in previous chapters, $\langle \dots \rangle$ stands for $\text{Tr}\{\rho_0 \dots\}$ with $\rho_0 = \rho(-\infty)$ being the initial density operator at $t = -\infty$. In order to express the expectation value of the exponential operator in Eq.(6.1.5) again as an exponential operator, we make use of a generalization of the cumulant generating function for a classical stochastic variable [191, 192]. We attribute the general variable X to the quantity

$$X \rightarrow \int_C d\tau V(\mathbf{r}_0, \tau) = \int_C d\tau \sum_{\alpha=1}^3 \mu_{\alpha}(\mathbf{r}_0, \tau) [E_{\alpha}^{\text{ext}}(\mathbf{r}_0, \tau) + E_{\alpha}(\mathbf{r}_0, \tau)]. \quad (6.1.6)$$

As shown in appendix (A), $\langle \exp(sX) \rangle$ is actually the momentum-generating function of the variable X and can be written as a function of the cumulants of the distribution,

$$\langle \exp(sX) \rangle_X = \exp\left(\sum_{n=0}^{\infty} \frac{s^n}{n!} \langle\langle X^n \rangle\rangle\right), \quad (6.1.7)$$

where $\langle\langle X^m \rangle\rangle$ are the cumulants and have the following characteristics

$$\begin{aligned} \langle\langle X \rangle\rangle &= \langle X \rangle, \\ \langle\langle X^2 \rangle\rangle &= \langle X^2 \rangle - \langle X \rangle^2, \text{ etc.} \end{aligned} \quad (6.1.8)$$

The series in Eq.(6.1.7) contains an infinite number of terms. To make the problem easier and tractable, we assume that photon statistics in the medium follows a Gaussian distribution in which the cumulants $\langle\langle E^n \rangle\rangle$ vanish for $n > 2$. This is a good approximation for our purpose. Making use of this approximation, the effective time evolution operator which is in fact the expectation value of Eq.(6.1.5), becomes

$$\begin{aligned} S_C^{\text{eff}} = \langle S_C \rangle_{\text{field}} &= T_C \exp \left\{ \frac{i}{\hbar} \int_C d\tau \sum_{\alpha=1}^3 \mu_{\alpha}(\tau) [E_{\alpha}^{\text{ext}}(\mathbf{r}_0, \tau) + \langle E_{\alpha}(\mathbf{r}_0, \tau) \rangle] \right. \\ &\quad \left. - \frac{1}{2\hbar^2} \int_C d\tau_1 \int_C d\tau_2 \sum_{\alpha, \beta=1}^3 \mu_{\alpha}(\tau_1) D_{\alpha\beta}(\mathbf{r}_0, \tau_1; \mathbf{r}_0, \tau_2) \mu_{\beta}(\tau_2) \right\}, \end{aligned} \quad (6.1.9)$$

where

$$D_{\alpha\beta}(1, 2) = \langle\langle T_C E_{\alpha}(\mathbf{r}_1, \tau_1) E_{\beta}(\mathbf{r}_2, \tau_2) \rangle\rangle, \quad (6.1.10)$$

is generally a tensorial Green's function (GF) of the interacting electric field and we have used the abbreviations $1 \equiv \mathbf{r}_1, \tau_1, 2 \equiv \mathbf{r}_2, \tau_2$. In the rest of this chapter, for simplicity, we drop the summation from the equations and hence wherever you see tensorial indexes, it means that a sum should be taken over the tensorial components. In the interaction picture, the slowly varying positive and negative frequency parts of the field and dipole operators are

$$\begin{aligned} \mu(\tau) &= \mu^+(\tau) + \mu^-(\tau) = \tilde{\mu}^+(\tau) e^{i\omega_{\text{pr}}\tau} + \tilde{\mu}^-(\tau) e^{-i\omega_{\text{pr}}\tau}, \\ E(\tau) &= E^+(\tau) + E^-(\tau) = \tilde{E}^+(\tau) e^{i\omega_{\text{pr}}\tau} + \tilde{E}^-(\tau) e^{-i\omega_{\text{pr}}\tau}, \end{aligned} \quad (6.1.11)$$

with ω_{pr} being the transition frequency of the probe QD under study. Now we impose the Rotating Wave Approximation (RWA) in which we neglect the terms with double frequencies like $\mu^+ E^+$ and $\mu^- E^-$. Thus the effective time evolution operator can be written as

$$S_{\text{C}}^{\text{eff}} = T_{\text{C}} \exp \left\{ \frac{i}{\hbar} \int_{\text{C}} d\tau [\mu_{\alpha}^+(\tau) E_{\text{L}\alpha}^-(\mathbf{r}_0, \tau) + \mu_{\alpha}^-(\tau) E_{\text{L}\alpha}^+(\mathbf{r}_0, \tau)] - \frac{1}{2\hbar^2} \int_{\text{C}} d\tau_1 \int_{\text{C}} d\tau_2 \right. \\ \left. \times \sum_{\alpha, \beta=1}^3 \left[\tilde{\mu}_{\alpha}^+(\tau_1) G_{\alpha\beta}(\mathbf{r}_0, \tau_1; \mathbf{r}_0, \tau_2) \tilde{\mu}_{\beta}^-(\tau_2) + \tilde{\mu}_{\alpha}^-(\tau_1) G'_{\alpha\beta}(\mathbf{r}_0, \tau_1; \mathbf{r}_0, \tau_2) \tilde{\mu}_{\beta}^+(\tau_2) \right] \right\}, \quad (6.1.12)$$

where

$$E_{\text{L}\alpha}(\mathbf{r}, \tau) = E_{\alpha}^{\text{ext}}(\mathbf{r}, \tau) + \langle E_{\alpha}(\mathbf{r}, \tau) \rangle, \quad (6.1.13)$$

is the local-field acting on the probe QD, and

$$G_{\alpha\beta}(\mathbf{r}_1, \tau_1; \mathbf{r}_2, \tau_2) = \left\langle \left\langle T_{\text{C}} E_{\alpha}^-(\mathbf{r}_1, \tau_1) E_{\beta}^+(\mathbf{r}_2, \tau_2) \right\rangle \right\rangle e^{-i\omega_{\text{pr}}(\tau_1 - \tau_2)}, \\ G'_{\alpha\beta}(\mathbf{r}_1, \tau_1; \mathbf{r}_2, \tau_2) = \left\langle \left\langle T_{\text{C}} E_{\alpha}^+(\mathbf{r}_1, \tau_1) E_{\beta}^-(\mathbf{r}_2, \tau_2) \right\rangle \right\rangle e^{i\omega_{\text{pr}}(\tau_1 - \tau_2)}. \quad (6.1.14)$$

6.1.2 Green's function on the Schwinger-Keldysh contour

Now we discuss the Green's function introduced in Eq.(6.1.14) with more details. We define the exact and the free-space Green's function on the Keldysh contour as

$$G_{\alpha\beta}(\mathbf{r}_1, t_1; \mathbf{r}_2, t_2) = \left\langle \left\langle T_{\text{C}} E_{\alpha}^-(\mathbf{r}_1, t_1) E_{\beta}^+(\mathbf{r}_2, t_2) \right\rangle \right\rangle, \\ G_{0\alpha\beta}(\mathbf{r}_1, t_1; \mathbf{r}_2, t_2) = \left\langle \left\langle T_{\text{C}} E_{0\alpha}^-(\mathbf{r}_1, t_1) E_{0\beta}^+(\mathbf{r}_2, t_2) \right\rangle \right\rangle, \quad (6.1.15)$$

where E_0 is the electric field in free-space. The time ordering T_{C} implies that for correlated operators, the operator which has an earlier time argument on the Keldysh contour, acts first on the quantum state of the probe QD and then the other one. This means that the field operator acting at an earlier physical time, should be on the right hand side of the field operator acting at a later time. In other words, the operators with time arguments on the upper branch (+) of the Keldysh contour should be on the right hand side of those on the lower side (-). If both operators are on the (+) branch, then the operator with a smaller physical time comes to the right and the other one goes to the left. If both field operators are on the (-), the situation is inverse and the operator with a bigger physical time comes to the right. Based on this description of the time ordering on the Keldysh contour, assuming $t_2 > t_1$ on the physical time line, the contour Green's

function $G(1, 2)$ contains four real-time GFs:

$$\begin{aligned}
G_{\alpha\beta}^{++}(1, 2) &= \left\langle \left\langle E_{\beta}^{+}(\mathbf{r}_2, t_2) E_{\alpha}^{-}(\mathbf{r}_1, t_1) \right\rangle \right\rangle, \\
G_{\alpha\beta}^{-+}(1, 2) &= \left\langle \left\langle E_{\alpha}^{-}(\mathbf{r}_1, t_1) E_{\beta}^{+}(\mathbf{r}_2, t_2) \right\rangle \right\rangle, \\
G_{\alpha\beta}^{+-}(1, 2) &= \left\langle \left\langle E_{\beta}^{+}(\mathbf{r}_2, t_2) E_{\alpha}^{-}(\mathbf{r}_1, t_1) \right\rangle \right\rangle, \\
G_{\alpha\beta}^{--}(1, 2) &= \left\langle \left\langle E_{\alpha}^{-}(\mathbf{r}_1, t_1) E_{\beta}^{+}(\mathbf{r}_2, t_2) \right\rangle \right\rangle.
\end{aligned} \tag{6.1.16}$$

The superscripts \pm specify the contour branches. For example, $-+$ indicates that the first time argument is on the lower and the second time argument on the upper branch of the Keldysh contour and has nothing to do with the negative and positive-frequency components. G^{++} and G^{--} are the time and anti-time ordered propagators. We now define two more Green's function: a retarded G^{ret} and an advanced G^{adv} . They have defined in a way that the retarded Green's function is zero for all negative time differences $t_1 - t_2$ and inversely, the advanced GF is zero for all positive time differences. The retarded Green's function is called retarded because it propagates forward in time and thus the output is delayed from the input. The importance of the retarded Green's function comes from the fact that all measurable quantities are actually retarded correlation functions. The retarded and advanced Green's function are defined through

$$G_{\alpha\beta}^{\text{ret}}(1, 2) = \left\langle \left[E_{\alpha}^{-}(\mathbf{r}_1, t_1), E_{\beta}^{+}(\mathbf{r}_2, t_2) \right] \right\rangle \Theta(t_1 - t_2), \tag{6.1.17}$$

$$G_{\alpha\beta}^{\text{adv}}(1, 2) = \left\langle \left[E_{\alpha}^{-}(\mathbf{r}_1, t_1), E_{\beta}^{+}(\mathbf{r}_2, t_2) \right] \right\rangle \Theta(t_2 - t_1), \tag{6.1.18}$$

where $\Theta(\tau)$ is the Heaviside step function which equals to 1 for $\tau > 0$ and to zero for $\tau < 0$. According to Eqs.(6.1.17) and (6.1.18), if $t_1 > t_2$, the advanced Green's function is zero and if $t_1 < t_2$, then the retarded Green's function is zero. By the definitions of the retarded and advanced Green's function presented in (6.1.17) and (6.1.18), they can also be written in the form of [193],

$$\begin{aligned}
G^{\text{ret}}(1, 2) &= G^{++}(1, 2) - G^{+-}(1, 2) = G^{-+}(1, 2) - G^{--}(1, 2), \\
G^{\text{adv}}(1, 2) &= G^{++}(1, 2) - G^{-+}(1, 2) = G^{+-}(1, 2) - G^{--}(1, 2).
\end{aligned} \tag{6.1.19}$$

Within RWA and in the absence of thermal photons, the free space correspondences of these six forms of the Green's function are

$$\begin{aligned}
G_{0\alpha\beta}^{++}(1, 2) &\approx G_{0\alpha\beta}^{\text{adv}}(1, 2), \\
G_{0\alpha\beta}^{-+}(1, 2) &\approx 0, \\
G_{0\alpha\beta}^{+-}(1, 2) &\approx G_{0\alpha\beta}^{\text{adv}}(1, 2) - G_{0\alpha\beta}^{\text{ret}}(1, 2), \\
G_{0\alpha\beta}^{--}(1, 2) &\approx -G_{0\alpha\beta}^{\text{ret}}(1, 2).
\end{aligned} \tag{6.1.20}$$

We make use of these Green's functions extensively in the rest of this chapter.

6.1.3 Single-QD density matrix equation of motion

The effective time evolution operator that was derived in the previous subsections leads in general to integro-differential equations of motion. In the Markov approximation, we assume that the characteristic decay time of the QD-QD correlations (field cumulants) is short compared to the characteristic time of the QD dynamics. This can happen especially in media with a large inhomogeneous broadening. This means that the QD dynamics doesn't change significantly in the time period between τ_1 and τ_2 and hence these two times can be considered as a single time for the probe QD. We can show this approximation mathematically as δ -correlation of $G_{\alpha\beta}$ and $G'_{\alpha\beta}$ in physical times,

$$\begin{aligned} G_{\alpha\beta}^{AB}(\tau, \tau') &= G_{\alpha\beta}^{AB}(\tau) \delta(\tau - \tau'), \\ G'_{\alpha\beta}{}^{AB}(\tau, \tau') &= G'_{\alpha\beta}{}^{AB}(\tau) \delta(\tau - \tau'), \end{aligned} \quad (6.1.21)$$

With $A, B \in \{+, -\}$, explicitly representing the Keldysh contour branches. Introducing, like in previous chapters, the dimensionless dipole rising and lowering operators respectively as S^+, S^- such that $\mu_{\alpha}^+ = \mu_{0\alpha} S_{\alpha}^-(t)$ and $\mu_{\alpha}^- = \mu_{0\alpha} S_{\alpha}^+(t)$, we arrive at

$$\begin{aligned} S_C^{\text{eff}} = T_C \exp \left\{ \frac{i\mu_{\alpha}}{\hbar} \int_{-\infty}^{\infty} d\tau \left[S_{\alpha}^-(\tau_+) E_{L\alpha}^-(\mathbf{r}_0, \tau) - S_{\alpha}^-(\tau_-) E_{L\alpha}^-(\mathbf{r}_0, \tau) \right. \right. \\ \left. \left. + S_{\alpha}^+(\tau_+) E_{L\alpha}^+(\mathbf{r}_0, \tau) - S_{\alpha}^+(\tau_-) E_{L\alpha}^+(\mathbf{r}_0, \tau) \right] \right. \\ - \frac{1}{2} \int_{-\infty}^{\infty} d\tau \gamma_{\alpha\beta}^c(\omega_{\text{pr}}, \tau) \left[S_{\alpha}^-(\tau_+) S_{\beta}^+(\tau_+) + S_{\alpha}^-(\tau_-) S_{\beta}^+(\tau_-) - 2S_{\alpha}^-(\tau_-) S_{\beta}^+(\tau_+) \right] \\ - \frac{1}{2} \int_{-\infty}^{\infty} d\tau \left[\gamma_{\alpha\beta}^c(\omega_{\text{pr}}, \tau) + \gamma_{\alpha\beta}(\omega_{\text{pr}}, \tau) \right] \\ \times \left[S_{\beta}^+(\tau_+) S_{\alpha}^-(\tau_+) + S_{\beta}^+(\tau_-) S_{\alpha}^-(\tau_-) - 2S_{\beta}^+(\tau_-) S_{\alpha}^-(\tau_+) \right] \\ + \frac{i}{\hbar} \int_{-\infty}^{\infty} d\tau \hbar_{\alpha\beta}^c(\omega_{\text{pr}}, \tau) \\ \times \left[S_{\alpha}^-(\tau_+) S_{\beta}^+(\tau_+) - S_{\alpha}^-(\tau_-) S_{\beta}^+(\tau_-) - S_{\beta}^+(\tau_+) S_{\alpha}^-(\tau_+) + S_{\beta}^+(\tau_-) S_{\alpha}^-(\tau_-) \right] \\ \left. + \frac{i}{\hbar} \int_{-\infty}^{\infty} d\tau \hbar_{\alpha\beta}(\omega_{\text{pr}}, \tau) \left[S_{\beta}^+(\tau_+) S_{\alpha}^-(\tau_+) - S_{\beta}^+(\tau_-) S_{\alpha}^-(\tau_-) \right] \right\}. \end{aligned} \quad (6.1.22)$$

The time arguments τ_+ and τ_- correspond to the upper and lower branch of the Schwinger-Keldysh contour respectively. The first line in Eq.(6.22) describes the interaction of the probe QD with the local field at the position of the probe QD in the RWA regime. The collective rate Γ^c defined as

$$\begin{aligned} \Gamma_{\alpha\beta}^c(\omega_{\text{pr}}, t) &= \frac{\mu_{\alpha}\mu_{\beta}}{\hbar^2} \int_{-\infty}^{\infty} d\tau \left\langle \left\langle E_{\alpha}^-(\mathbf{r}_0, t) E_{\beta}^+(\mathbf{r}_0, t + \tau) \right\rangle \right\rangle e^{i\omega_{\text{pr}}\tau} \\ &= \frac{\mu_{\alpha}\mu_{\beta}}{\hbar^2} \tilde{G}_{\alpha\beta}^{-+}(\mathbf{r}_0, \omega_{\text{pr}}; t), \end{aligned} \quad (6.1.23)$$

is a positive Hermitian matrix, whose eigenvalues are the collective decay and pump rates induced by the incoherent photons inside the medium. The incoherent radiation

inside the medium induces stimulated emission from the excited state to the ground state, if the probe QD is initially excited. As can be seen from Eq.(6.1.23), the collective pump and decay rate is proportional to $\tilde{D}_{\alpha\beta}^{-+}$ which, apart from some dimensional constants, is the spectral energy density of the incoherent radiation at the position and transition frequency of the probe-QD. The Hermitian matrix h^c is the collective light energy shift caused by the incoherent component of the radiation field inside the medium,

$$h_{\alpha\beta}^c(\omega_{pr}, t) = \frac{i}{\hbar} \frac{\mu_\alpha \mu_\beta}{2} \int_0^\infty d\tau \left(\langle\langle E_\alpha^-(\mathbf{r}_0, t) E_\beta^+(\mathbf{r}_0, t - \tau) \rangle\rangle e^{-i\omega_{pr}\tau} - \langle\langle E_\alpha^-(\mathbf{r}_0, t) E_\beta^+(\mathbf{r}_0, t + \tau) \rangle\rangle e^{i\omega_{pr}\tau} \right). \quad (6.1.24)$$

This expression can also be written in the form of

$$h_{\alpha\beta}^c(\omega_{pr}, t) = \frac{\mu_\alpha \mu_\beta}{2\pi\hbar} P \int_{-\infty}^\infty d\omega' \frac{\tilde{D}_{\alpha\beta}^{-+}(\mathbf{r}_0, \omega'; t)}{\omega_{pr} - \omega'} = \frac{\hbar}{2\pi} P \int_{-\infty}^\infty d\omega' \frac{\gamma_{\alpha\beta}^c(\omega', t)}{\omega_{pr} - \omega'}, \quad (6.1.25)$$

where P denotes the principle part of the integral. In systems with a large inhomogeneous broadening, the collective light shift is often negligible since they are often small as compared with the inhomogeneous broadening and is hidden in the broad spectrum of Photoluminescence (PL) measurements. The parameter

$$\begin{aligned} \Gamma_{\alpha\beta}(\omega_{pr}, t) &= \frac{\mu_\alpha \mu_\beta}{\hbar^2} \int_{-\infty}^\infty d\tau \langle\langle [E_\beta^+(\mathbf{r}_0, t + \tau), E_\alpha^-(\mathbf{r}_0, t)] \rangle\rangle e^{i\omega_{pr}\tau} \\ &= 2 \frac{\mu_\alpha \mu_\beta}{\hbar^2} \text{Re} \{ \tilde{G}_{\alpha\beta}^{\text{ret}}(\mathbf{r}_0, \omega_{pr}; t) \}, \end{aligned} \quad (6.1.26)$$

is the spontaneous decay rate of the probe QD in the many-QD medium. Replacing E by the free field, Eq.(6.1.26) gives rise to the well-known free space radiative decay rate [187]

$$\Gamma_0 = \frac{\mu^2 \omega_{pr}^3}{3\pi\hbar\epsilon_0 c^3}. \quad (6.1.27)$$

The corresponding spontaneous contribution to the light energy shift is given by

$$\begin{aligned} h_{\alpha\beta}(\omega_{pr}, t) &= \frac{i}{\hbar} \frac{\mu_\alpha \mu_\beta}{2} \int_0^\infty d\tau \left\{ \langle\langle [E_\alpha^-(\mathbf{r}_0, t), E_\beta^+(\mathbf{r}_0, t - \tau)] \rangle\rangle e^{-i\omega_{pr}\tau} \right. \\ &\quad \left. - \langle\langle [E_\alpha^-(\mathbf{r}_0, t), E_\beta^+(\mathbf{r}_0, t + \tau)] \rangle\rangle e^{i\omega_{pr}\tau} \right\} \\ &= \frac{\mu_\alpha \mu_\beta}{\hbar^2} \text{Im} \{ \tilde{G}_{\alpha\beta}^{\text{ret}}(\mathbf{r}_0, \omega_{pr}; t) \}. \end{aligned} \quad (6.1.28)$$

$h_{\alpha\beta}$ is in fact the Lamb shift of the probe QD excited state modified by the presence of the other QDs in the medium.

The master equation for the single-QD density operator can be obtained from the effec-

tive time-evolution operator presented in Eq.(6.1.22) as

$$\begin{aligned}
\dot{\rho} = & -\frac{i}{\hbar} [H_0, \rho] + i\frac{\mu_\alpha}{\hbar} [(S_\alpha^- E_{L\alpha}^- + S_\alpha^+ E_{L\alpha}^+), \rho] \\
& - i\hbar_{\alpha\beta} [S_\beta^+ S_\alpha^-, \rho] - i\hbar_{\alpha\beta}^c [[S_\beta^+, S_\alpha^-], \rho] \\
& - \frac{\Gamma_{\alpha\beta}}{2} \{S_\beta^+ S_\alpha^- \rho + \rho S_\beta^+ S_\alpha^- - 2S_\alpha^- \rho S_\beta^+\} \\
& - \frac{\Gamma_{\alpha\beta}^c}{2} \{[S_\alpha^-, [S_\beta^+, \rho]] + [S_\beta^+, [S_\alpha^-, \rho]]\},
\end{aligned} \tag{6.1.29}$$

where $H_0 = \hbar\omega_{pr}S^z$ is the free Hamiltonian of the probe QD which S^z is the population difference between the excited and ground states of the probe QD and varies in the range $-\frac{1}{2} < S^z < \frac{1}{2}$. The equation of motion in (6.1.29) is nonlinear and nonlocal, since the light energy shifts and decay rate matrices depend on the surrounding QDs in the medium via the field correlations. Introducing β as geometry factor which relates to the shape of the medium, the general form of the local field is $E_L^+ = E_{ext}^+ + \beta \langle S^- \rangle$. By employing (6.1.29), the equation of motion for different density matrix elements can be derived as

$$\dot{\rho}_{ee} = \Gamma^c - (\Gamma + 2\Gamma^c) \rho_{ee} - i(\Omega^- \rho_{eg} - \Omega^+ \rho_{ge}), \tag{6.1.30}$$

$$\dot{\rho}_{gg} = \Gamma + \Gamma^c - (\Gamma + 2\Gamma^c) \rho_{gg} + i(\Omega^- \rho_{eg} - \Omega^+ \rho_{ge}), \tag{6.1.31}$$

$$\dot{\rho}_{eg} = -i(\omega_{pr} + h + h^c) \rho_{eg} - \left(\frac{\Gamma}{2} + \Gamma^c\right) \rho_{eg} - 2i(\Omega^+ + B \langle S^- \rangle) \rho_{eg}, \tag{6.1.32}$$

where $\Omega^+ = \mu_0 E_{ext}^+ / \hbar$ is the Rabi frequency and $B = \mu_0 \beta / \hbar$. The equation of motion of $\langle S^- \rangle$ can be easily obtained from (6.32), since $\langle S^+ \rangle = \langle S^- \rangle^*$. As already mentioned in chapter 2, the expectation value of any observable Q is obtained by making use of the density matrix operator as $\langle Q \rangle = \text{Tr}\{\rho Q\}$. For example the expectation value of the rising QD dipole operator becomes $\langle S^- \rangle = \rho_{eg}$ with an equation of motion presented in (6.32) and the expectation value of the population difference operator is given by

$$\langle \dot{S}^z \rangle = \frac{\rho_{ee} - \rho_{gg}}{2} = -\frac{\Gamma}{2} - (\Gamma + 2\Gamma^c) \langle S^z \rangle - i(\Omega^- \langle S^- \rangle - \Omega^+ \langle S^+ \rangle). \tag{6.1.33}$$

Generally, the equation of motion for any physical observable related to the probe QD can be obtained from Eq.(6.1.29),

$$\begin{aligned}
\langle \dot{Q} \rangle = & i\omega_{pr} \langle [S^z, Q] \rangle - i\frac{\mu_\alpha}{\hbar} \langle [(S_\alpha^- E_{L\alpha}^- + S_\alpha^+ E_{L\alpha}^+), Q] \rangle \\
& + i\hbar_{\alpha\beta} \langle [S_\beta^+ S_\alpha^-, Q] \rangle + i\hbar_{\alpha\beta}^c \langle [[S_\beta^+, S_\alpha^-], Q] \rangle \\
& - \frac{\Gamma_{\alpha\beta}}{2} \langle S_\beta^+ [S_\alpha^-, Q] - [S_\beta^+, Q] S_\alpha^- \rangle \\
& - \frac{\Gamma_{\alpha\beta}^c}{2} \langle [S_\alpha^-, [S_\beta^+, Q]] + [S_\beta^+, [S_\alpha^-, Q]] \rangle.
\end{aligned} \tag{6.1.34}$$

In the following sections we should calculate the parameters $E_L, \Gamma, h, \Gamma^c, h^c$ as a function of the QD dipole operators and hence derive a close set of nonlinear equations.

6.1.4 The average local-field in a thin layer of QDs

The total field acting upon the probe QD is the superposition of the external field and the mean coherent amplitude of the field scattered by the other QDs in the medium,

$$\mathbf{E}_L(\mathbf{r}, t) = \mathbf{E}^{\text{ext}}(\mathbf{r}, t) + \langle \mathbf{E}(\mathbf{r}, t) \rangle. \quad (6.1.35)$$

At the moment we forget about any external field and calculate the contribution of the surrounding QDs for the local field at the position of the probe QD.

In order to derive the emission from the dipole moments of the QDs in the medium, we need to know the free space retarded Green's function,

$$\mathbf{G}_{0\alpha\beta}^{\text{ret}}(1, 2) = \left\langle \left[\mathbf{E}_{\alpha}^{-}(\mathbf{r}_1, t_1), \mathbf{E}_{\beta}^{+}(\mathbf{r}_2, t_2) \right] \right\rangle \Theta(t_1 - t_2),$$

that is a solution of the homogeneous Maxwell equation with a δ -like source term,

$$\left(\frac{1}{c^2} \frac{\partial^2}{\partial t^2} + \nabla \times \nabla \times \right) \mathbf{G}_0^{\text{ret}}(\mathbf{r}_1, t_1; \mathbf{r}_2, t_2) = -\frac{i\hbar\omega_{\text{pr}}^2}{\epsilon_0 c^2} \delta(\mathbf{r}_1 - \mathbf{r}_2) \delta(t_1 - t_2) \mathbf{1}, \quad (6.1.36)$$

where $\mathbf{G}_0^{\text{ret}}$ is generally a tensor and $\mathbf{1}$ is the unit matrix. According to Ref. [187,194], the solution of retarded Green's function in free space is of the form

$$\mathbf{G}_{0\alpha\beta}^{\text{ret}}(\mathbf{r}, \tau) = \frac{i\hbar}{4\pi\epsilon_0 c} \Theta(\tau) \left[\delta_{\alpha\beta} \frac{\partial^2}{\partial \tau^2} - c^2 \frac{\partial^2}{\partial r_2^{\alpha} \partial r_2^{\beta}} \right] \frac{\delta(\mathbf{r} - c\tau)}{r}, \quad (6.1.37)$$

with $\mathbf{r} = \mathbf{r}_1 - \mathbf{r}_2$, $r = |\mathbf{r}_1 - \mathbf{r}_2|$ and $\tau = t_1 - t_2$. This Green's function has been used in Appendix (B) to derive the electric local field in a thin film of atoms or QDs.

6.1.5 Dyson equation and contour Green's function

In a many-body system of QDs, the Green's function $G(1, 2)$ can be written in terms of a Dyson-integral equation [193], by introducing a formal polarization function $\Pi(1, 2)$,

$$G_{\alpha\beta}(1, 2) = G_{0\alpha\beta}(1, 2) - \iint_{\mathcal{C}} d1' d2' G_{0\alpha\alpha'}(1, 1') \Pi_{\alpha'\beta'}(1', 2') G_{\beta'\beta}(2', 2), \quad (6.1.38)$$

where $\int_{\mathcal{C}} d1$ is the integration over the Schwinger-Keldysh contour as well as spatial integration over the medium. The integration in the Dyson equation (6.1.38) is actually the summation of the perturbation series where the polarization function is determined by the medium response. The polarization function $\Pi(1, 2)$ actually indicates how a photon is absorbed and reemitted by the QDs in the medium. So we have to find a good approximation for the formal polarization function in order to be able to derive the Green's function.

Corresponding to the self-consistent Hartree approximation in many-body theory and in the lowest order in the QD-field coupling, the polarization function is given by the correlation function of dipole operators of interacting QDs,

$$\Pi_{\alpha\beta}(1,2) = \frac{\mu_{\alpha}\mu_{\beta}}{\hbar^2} \sum_j \left\langle \left\langle T_C S_{j\alpha}^+(t_1) S_{j\beta}^+(t_2) \right\rangle \right\rangle \delta(\mathbf{r}_1 - \mathbf{r}_j) \delta(\mathbf{r}_2 - \mathbf{r}_j). \quad (6.1.39)$$

We should now calculate the real-time from the Dyson equation (6.1.38) for the contour GF components. In fact we should convert the time integrations over the Schwinger-Keldysh contour to the integrations over the real-time axis. In order to do this, we have to treat different contour components separately. Taking the initial values presented in Eq.(6.1.20), we can write

$$\begin{aligned} G^{++} &= G_0^{++} - G_0^{++} \Pi^{++} G^{++} + G_0^{++} \Pi^{+-} G^{-+} - G_0^{+-} \Pi^{--} G^{-+} + G_0^{+-} \Pi^{-+} G^{++}, \\ G^{-+} &= -G_0^{--} \Pi^{--} G^{-+} + G_0^{--} \Pi^{-+} G^{++}, \end{aligned} \quad (6.1.40)$$

where for simplifying the formulas, we have used the notation of for example

$$G_0^{--} \Pi^{--} G^{-+} = \iint d1' d2' G_{0\alpha\alpha'}^{--}(1,1') \Pi_{\alpha'\beta'}^{--}(1',2') G_{\beta'\beta}^{-+}(2',2),$$

where the integrations are over the real time from $-\infty$ to ∞ and over the volume of the sample. It is obvious from Fig.(6.2) that when the time is on the upper branch of the Schwinger-Keldysh contour, the direction of the integration over the contour and over the real time axis are along the same direction from $-\infty$ to ∞ and hence the sign of the contour integration is positive. But since the direction of the time path over the lower branch of the contour and that of the real-time are in opposite directions, the sign of the real-time integration is minus which is the reason for minus signs for some terms in Eq.(6.1.40). By employing (6.1.20) and writing all initial values of the free-space Green's functions as a function of the initial values of the free-space retarded and Green's function, we have

$$\begin{aligned} G^{++} &= G_0^{\text{adv}} - G_0^{\text{adv}} [(\Pi^{++} - \Pi^{-+}) G^{++} - (\Pi^{+-} - \Pi^{--}) G^{-+}] \\ &\quad + G_0^{\text{ret}} [\Pi^{-+} G^{++} - \Pi^{--} G^{-+}], \\ G^{-+} &= -G_0^{\text{ret}} (\Pi^{-+} G^{++} - \Pi^{--} G^{-+}). \end{aligned} \quad (6.1.41)$$

Similar to Eq.(6.1.19), we define the retarded and advanced polarization functions as

$$\begin{aligned} \Pi^{\text{ret}}(1,2) &\equiv \Pi^{++}(1,2) - \Pi^{+-}(1,2) = \Pi^{-+}(1,2) - \Pi^{--}(1,2), \\ \Pi^{\text{adv}}(1,2) &\equiv \Pi^{++}(1,2) - \Pi^{-+}(1,2) = \Pi^{+-}(1,2) - \Pi^{--}(1,2). \end{aligned} \quad (6.1.42)$$

Then considering this fact that $G^{\text{adv}} = G^{++} - G^{-+}$, the advanced Green's function is obtained from (6.1.41) and (6.1.42) as

$$G_{\alpha\beta}^{\text{adv}}(1,2) = G_{0\alpha\beta}^{\text{adv}}(1,2) - \iint d1' d2' G_{0\alpha\alpha'}^{\text{adv}}(1,1') \Pi_{\alpha'\beta'}^{\text{adv}}(1',2') G_{\beta'\beta}^{\text{adv}}(2',2). \quad (6.1.43)$$

Since $G_{\alpha\beta}^{\text{ret}}(1,2) = G_{\alpha\beta}^{\text{adv}}(2,1)$, the retarded Green's function becomes

$$G_{\alpha\beta}^{\text{ret}}(1,2) = G_{0\alpha\beta}^{\text{ret}}(1,2) - \iint d1' d2' G_{0\alpha\alpha'}^{\text{ret}}(1,1') \Pi_{\alpha'\beta'}^{\text{ret}}(1',2') G_{\beta'\beta}^{\text{ret}}(2',2), \quad (6.1.44)$$

with

$$\Pi_{\alpha'\beta'}^{\text{ret}}(1,2) = \frac{\mu_{\alpha'}\mu_{\beta'}}{\hbar^2} \sum_j \left\langle \left[S_{j\alpha'}^+(t_1), S_{j\beta'}^-(t_2) \right] \right\rangle \delta(\mathbf{r}_1 - \mathbf{r}_j) \delta(\mathbf{r}_2 - \mathbf{r}_j). \quad (6.145)$$

You can see in (6.144) that G^{ret} is present also in the right hand side of the equation. So, the iteration of this equation gives

$$G^{\text{ret}} = G_0^{\text{ret}} - G_0^{\text{ret}}\Pi^{\text{ret}}G_0^{\text{ret}} + G_0^{\text{ret}}\Pi^{\text{ret}}G_0^{\text{ret}}\Pi^{\text{ret}}G_0^{\text{ret}} - + \dots. \quad (6.146)$$

Returning back to G^{-+} in (6.141) and making use of (6.119), by substituting $\Pi^{-+} = \Pi^{-+} - \Pi^{\text{ret}}$, we obtain

$$G^{-+} = -G_0^{\text{ret}}\Pi^{\text{ret}}G^{-+} - G_0^{\text{ret}}\Pi^{-+}G^{\text{adv}}. \quad (6.147)$$

Iterating over G^{-+} , this equation yields

$$G^{-+} = -\left(G_0^{\text{ret}} - G_0^{\text{ret}}\Pi^{\text{ret}}G_0^{\text{ret}} + G_0^{\text{ret}}\Pi^{\text{ret}}G_0^{\text{ret}}\Pi^{\text{ret}}G_0^{\text{ret}} - + \dots\right)\Pi^{-+}G^{\text{adv}}. \quad (6.148)$$

According to (6.146), the term in the parentheses can be replaced by G^{ret} . Restoring back the full notation, we obtain

$$G_{\alpha\beta}^{-+}(1,2) = -\iint d1'd2' G_{\alpha\alpha'}^{\text{ret}}(1,1')\Pi_{\alpha'\beta'}^{-+}(1',2')G_{\beta'\beta}^{\text{adv}}(2',2), \quad (6.149)$$

with

$$\Pi_{\alpha'\beta'}^{-+}(1,2) = \frac{\mu_{\alpha'}\mu_{\beta'}}{\hbar^2} \sum_j \left\langle \left[S_{j\alpha'}^+(t_1), S_{j\beta'}^-(t_2) \right] \right\rangle \delta(\mathbf{r}_1 - \mathbf{r}_j) \delta(\mathbf{r}_2 - \mathbf{r}_j). \quad (6.150)$$

The quantity Π^{ret} is called the QD response function since the Fourier transform of Π^{ret} gives the susceptibility of the medium. In fact, the iteration of the Dyson equation in (6.146) shows multiple scattering of spontaneous photons by QDs in the medium during the propagation from the source QD to the probe QD. But, Π^{-+} is called the QD source correlation, because its Fourier transform is proportional to the spontaneous emission spectrum of the QDs and Eq.(6.149) says that the incoherent radiation intensity is equal to the sum of the incoherent emission contributions of all QDs propagated in the medium. The equations (6.144), (6.145), (6.149) and (6.150) are the main results of this section and will be used in next section to derive different types of the relaxation rates and energy level shifts in a QD system.

6.2 The relaxation rates and light-level shifts in a single layer of QDs

Based on the theory that was introduced in previous section, we now try to find explicit expressions for the decay rates and level shifts. For this purpose, we start with

the contour polarizations Π^{ret} and Π^{-+} . Since in our sample the QDs are randomly distributed, we make use the continuum approximation and by changing the summation to integration, we can rewrite Eq.(6.1.45) as

$$\Pi_{\alpha\beta}^{\text{ret}}(\mathbf{r}_1, \mathbf{t}_1; \mathbf{r}_2, \mathbf{t}_2) = \int d\mathbf{r} P_{\alpha\beta}^{\text{ret}}(\mathbf{r}, \mathbf{t}_1, \mathbf{t}_2) \delta(\mathbf{r}_1 - \mathbf{r}) \delta(\mathbf{r}_2 - \mathbf{r}), \quad (6.2.1)$$

$$P_{\alpha\beta}^{\text{ret}}(\mathbf{r}, \mathbf{t}_1, \mathbf{t}_2) = \frac{\mu_{\alpha'} \mu_{\beta'}}{\hbar^2} n_0 \Theta(\mathbf{t}_1 - \mathbf{t}_2) \overline{\langle [S_{\alpha}^+(\mathbf{t}_1), S_{\beta}^-(\mathbf{t}_2)] \rangle}, \quad (6.2.2)$$

where n_0 is the QD density and the overline denotes averaging over the spectral inhomogeneous broadening due to the size distribution of QDs. We can similarly obtain from Eq.(6.1.50),

$$\Pi_{\alpha\beta}^{-+}(\mathbf{r}_1, \mathbf{t}_1; \mathbf{r}_2, \mathbf{t}_2) = \int d\mathbf{r} P_{\alpha\beta}^{-+}(\mathbf{r}, \mathbf{t}_1, \mathbf{t}_2) \delta(\mathbf{r}_1 - \mathbf{r}) \delta(\mathbf{r}_2 - \mathbf{r}), \quad (6.2.3)$$

$$P_{\alpha\beta}^{-+}(\mathbf{r}, \mathbf{t}_1, \mathbf{t}_2) = \frac{\mu_{\alpha'} \mu_{\beta'}}{\hbar^2} n_0 \overline{\langle \langle S_{\alpha}^+(\mathbf{t}_1) S_{\beta}^-(\mathbf{t}_2) \rangle \rangle}. \quad (6.2.4)$$

Because the QDs are uniformly distributed in our sample, the polarizations P^{ret} and P^{-+} are independent from the QD position and hence they are not a function of \mathbf{r} and come out of the integrations in (6.2.1) and (6.2.3). Therefore, we have

$$\Pi_{\alpha\beta}^{\text{ret}}(\mathbf{r}_1, \mathbf{t}_1; \mathbf{r}_2, \mathbf{t}_2) = P_{\alpha\beta}^{\text{ret}}(\mathbf{t}_1, \mathbf{t}_2) \delta(\mathbf{r}_1 - \mathbf{r}_2), \quad (6.2.5)$$

$$\Pi_{\alpha\beta}^{-+}(\mathbf{r}_1, \mathbf{t}_1; \mathbf{r}_2, \mathbf{t}_2) = P_{\alpha\beta}^{-+}(\mathbf{t}_1, \mathbf{t}_2) \delta(\mathbf{r}_1 - \mathbf{r}_2). \quad (6.2.6)$$

The retarded Green's function of the many-body system plays an important role in determining the other contour Green's functions. By substituting (6.2.5) in Eq.(6.1.44), we obtain

$$\begin{aligned} G_{\alpha\beta}^{\text{ret}}(\mathbf{r}_1, \mathbf{t}_1; \mathbf{r}_2, \mathbf{t}_2) &= G_{0\alpha\beta}^{\text{ret}}(\mathbf{r}_1, \mathbf{t}_1; \mathbf{r}_2, \mathbf{t}_2) - \int_{-\infty}^{\infty} dt'_1 \int_{-\infty}^{\infty} dt'_2 \\ &\times \int_V d\mathbf{r}'_1 G_{0\alpha\alpha'}^{\text{ret}}(\mathbf{r}_1, \mathbf{t}_1; \mathbf{r}'_1, \mathbf{t}'_1) P_{\alpha'\beta'}^{\text{ret}}(\mathbf{t}'_1, \mathbf{t}'_2) G_{\beta'\beta}^{\text{ret}}(\mathbf{r}'_1, \mathbf{t}_1; \mathbf{r}_2, \mathbf{t}_2). \end{aligned} \quad (6.2.7)$$

To solve this integral equation, we have to make some approximations. The spatial integration in (6.2.7) is over the sample volume. But we extend it to infinity which yields basically to the propagator (Green's function) of an infinitely extended medium. We also treat the problem in the quasistationary limit in which we assume that the $P^{\text{ret}}(\mathbf{t}'_1, \mathbf{t}'_2)$ depends only on the time difference $\tau = \mathbf{t}'_1 - \mathbf{t}'_2$. Consistently with the Markov approximation, we only keep the slowly-varying terms. This means that we consider the field propagation times to be short compared to the characteristic radiative decay time of the QDs. This approximation is applicable to our real sample of interest with a size of about $50\mu\text{m}$. In such a sample, the light propagation time is in the order of 0.01ps , while the radiative decay time is in the order of 1000ps . Taking into account these approximations, we change the integral equation in (6.2.7) into an algebraic equation by a Fourier transformation with respect to $\mathbf{r} \equiv \mathbf{r}_1 - \mathbf{r}_2$ and $\tau \equiv \mathbf{t}_1 - \mathbf{t}_2$. Employing the definition of the Fourier transformation,

$$\tilde{\mathbf{G}}(\mathbf{q}, \omega) = \int_{V_{\infty}} d\mathbf{r} \int_{-\infty}^{\infty} d\tau \mathbf{G}(\mathbf{r}, \tau) e^{-i\omega\tau} e^{i\mathbf{q}\cdot\mathbf{r}}, \quad (6.2.8)$$

the algebraic form of the equation (6.2.7) is

$$\tilde{\mathbf{G}}^{\text{ret}}(\mathbf{q}, \omega; \mathbf{t}) = \frac{\tilde{\mathbf{G}}_0^{\text{ret}}(\mathbf{q}, \omega)}{\mathbf{1} + \tilde{\mathbf{G}}_0^{\text{ret}}(\mathbf{q}, \omega) \cdot \tilde{\mathbf{P}}^{\text{ret}}(\omega; \mathbf{t})}, \quad (6.2.9)$$

where \mathbf{G}^{ret} and \mathbf{P}^{ret} are generally 3×3 matrices and $\mathbf{1}$ is the unity matrix. Ignoring the dipole orientations, the spectrum of \mathbf{P}^{ret} is derived in appendix (C) and has the form

$$\tilde{\mathbf{p}}^{\text{ret}}(\mathbf{t}; \omega) = \frac{1}{3} \frac{\mu^2}{\hbar^2} \mathbf{N} \frac{[\rho_{ee}(\mathbf{t}) - \rho_{gg}(\mathbf{t})]}{i(\omega - \omega_{\text{pr}}) + \frac{\Gamma}{2} + \Gamma^c}. \quad (6.2.10)$$

The factor $2/3$ is due to the orientation averaging. To evaluate the algebraic equation above, we should first approximate the Fourier transform of the free-space retarded Green's function. Referring back to Eq.(6.1.37), the Fourier transform $\mathbf{G}_0^{\text{ret}}(\mathbf{r}, \tau)$ with respect to the correlation time τ is

$$\tilde{\mathbf{G}}_{0\alpha\beta}^{\text{ret}}(\mathbf{r}, \omega) = -\frac{i\hbar\omega^2}{4\pi\epsilon_0 c^2} \left(\delta_{\alpha\beta} - \frac{r_\alpha r_\beta}{r^2} \frac{\partial^2}{\partial r^2} \right) \frac{e^{-i\omega r/c}}{r}. \quad (6.2.11)$$

This can also be written in the tensorial form of [195]

$$\tilde{\mathbf{G}}_0^{\text{ret}}(\mathbf{r}, \omega) = \frac{-i\hbar k^2 e^{-ikr}}{4\pi\epsilon_0 r} \left[\mathbf{P}_1(ikr) \mathbf{1} + \mathbf{P}_2(ikr) \frac{\mathbf{r} \otimes \mathbf{r}}{r^2} \right], \quad (6.2.12)$$

with

$$\mathbf{P}_1(x) = 1 - \frac{1}{x} + \frac{1}{x^2}, \quad \mathbf{P}_2(x) = -1 + \frac{3}{x} - \frac{3}{x^2}. \quad (6.2.13)$$

Finally by taking the Fourier transform with respect to the spatial variable, the free-space retarded Green's function in the reciprocal lattice becomes

$$\begin{aligned} \tilde{\mathbf{G}}_0^{\text{ret}}(\mathbf{q}, \omega) &= \frac{i\hbar}{\epsilon_0} \frac{k^2}{(k^2 + i0) \mathbf{1} - q^2 (\mathbf{1} - \mathbf{q} \otimes \mathbf{q}/q^2)} \\ &= \frac{i\hbar}{\epsilon_0} \left[\frac{k^2}{k^2 - q^2 + i0} \left(\mathbf{1} - \frac{\mathbf{q} \otimes \mathbf{q}}{q^2} \right) + \frac{\mathbf{q} \otimes \mathbf{q}}{q^2} \right], \end{aligned} \quad (6.2.14)$$

where $k = \omega/c$. It has been shown that if we integrate the electric field of a dipole moment with polarization \mathbf{P} over a spherical volume that fully contains the dipole, is equal to $-\mathbf{P}/3\epsilon_0$. But the integration of (6.2.12) over such a volume vanishes. So we manually add an additional term to the free-space retarded Green's function to justify this condition. Therefore we rewrite Eq.(6.2.12) as

$$\tilde{\mathbf{F}}_0^{\text{ret}}(\mathbf{r}, \omega) \rightarrow \tilde{\mathbf{G}}_0^{\text{ret}}(\mathbf{r}, \omega) - \frac{i\hbar}{3\epsilon_0} \delta(\mathbf{r}) \mathbf{1}. \quad (6.2.15)$$

From now on, we continue with this modified version of the free-space Green's function. Note that the added delta function doesn't contribute to the field at positions away from the dipole. Then, the modified free-space retarded Green's function changes to

$$\begin{aligned} \tilde{\mathbf{F}}_0^{\text{ret}}(\mathbf{q}, \omega) &= \tilde{\mathbf{G}}_0^{\text{ret}}(\mathbf{q}, \omega) - \frac{i\hbar}{3\epsilon_0} \mathbf{1} \\ &= -\frac{i\hbar}{\epsilon_0} \left[\frac{\left(\frac{1}{3} q^2 + \frac{2}{3} k^2 \right) \mathbf{1} - \mathbf{q} \otimes \mathbf{q}}{q^2 - k^2 - i0} \right]. \end{aligned} \quad (6.2.16)$$

Introducing the modified version of the exact retarded Green's function in the reciprocal lattice as $\tilde{\mathbf{F}}^{\text{ret}}(\mathbf{q}, \omega) \equiv \tilde{\mathbf{F}}_0^{\text{ret}}(\mathbf{q}, \omega) - \frac{i\hbar}{3\varepsilon_0} \mathbf{1}$, the overall shape of the Dyson equation in (6.2.9) remains unchanged as

$$\tilde{\mathbf{F}}^{\text{ret}}(\mathbf{q}, \omega; t) = \frac{\tilde{\mathbf{F}}_0^{\text{ret}}(\mathbf{q}, \omega)}{\mathbf{1} + \tilde{\mathbf{F}}_0^{\text{ret}}(\mathbf{q}, \omega) \cdot \tilde{\mathbf{P}}^{\text{ret}}(\omega; t)}. \quad (6.2.17)$$

By substituting Eq.(6.2.16) in (6.2.17), the exact retarded Green's function becomes

$$\tilde{\mathbf{F}}^{\text{ret}}(\mathbf{q}, \omega) = -\frac{i\hbar}{\varepsilon_0} \left[\frac{(\frac{1}{3}q^2 + \frac{2}{3}k^2) \mathbf{1} - \mathbf{q} \otimes \mathbf{q}}{(q^2 - k^2 - i0) \mathbf{1} - \frac{i\hbar P^{\text{ret}}}{\varepsilon_0} [(\frac{1}{3}q^2 + \frac{2}{3}k^2) \mathbf{1} - \mathbf{q} \otimes \mathbf{q}]} \right]. \quad (6.2.18)$$

After doing some algebraic analysis over the denominator of Eq.(6.2.18) via deriving the inverse of a matrix (tensor), we can transform Eq.(6.2.18) into the form

$$\tilde{\mathbf{F}}^{\text{ret}}(\mathbf{q}, \omega) = -\frac{i\hbar}{\varepsilon_0} \left[\frac{(\frac{1}{3}q^2 + \frac{2}{3}k^2) \mathbf{1} - \frac{\mathbf{q} \otimes \mathbf{q}}{1 + \frac{2}{3} \frac{i\hbar}{\varepsilon_0} P^{\text{ret}}}}{q^2 - k^2 - \frac{i\hbar P^{\text{ret}}}{\varepsilon_0} (\frac{1}{3}q^2 + \frac{2}{3}k^2) - i0} \right]. \quad (6.2.19)$$

The dynamical polarizability of the QDs is defined [188] as

$$N\alpha(\omega) \equiv \frac{i\hbar}{\varepsilon_0} P^{\text{ret}}(\omega), \quad (6.2.20)$$

where N is the QD density and $\alpha(\omega)$ is the polarizability of a single QD. Employing Eq.(6.2.10) for $P^{\text{ret}}(\omega)$, the QD polarizability is of the form

$$\alpha(t; \omega) = \frac{1}{3} \frac{i\mu^2}{\varepsilon_0 \hbar} \frac{[\rho_{ee}(t) - \rho_{gg}(t)]}{i(\omega - \omega_{\text{pr}}) + \frac{\Gamma}{2} + \Gamma^c} \quad (6.2.21)$$

In electromagnetism of many-body systems, the poles $\pm q_0$ of the retarded exact Green's function (scattering Green's function) give the complex dielectric function of the medium,

$$\varepsilon(\omega) \equiv \frac{q_0^2}{k^2} = 1 + \frac{N\alpha(\omega)}{1 - \frac{1}{3}N\alpha(\omega)}. \quad (6.2.22)$$

This is the famous Lorentz-Lorenz relation between the microscopic QD polarizability $\alpha(\omega)$ and the dielectric function of the medium. This means that our choice of the free-space retarded Green's function and the employment of the Dyson equation have been correct in our approach.

6.2.1 The spontaneous emission rate and the Lamb shift

The spontaneous decay rate, Γ , and the energy Lamb shift, h , of the probe QD are obtained from (6.1.26) and (6.1.28) respectively. It is clear that the spontaneous decay rate is proportional to the real part and the Lamb shift is proportional to the imaginary part

of the spectrum (Fourier transform) of the exact retarded Green's function $D^{\text{ret}}(\omega)$ at the position of the probe QD. So, we should transfer the retarded Green's function in reciprocal space back to the real space. Before doing that, we first simplify the Green's function in the reciprocal lattice and then we analyze it a bit more. Since the dipole moments of the QDs have random orientations in the real space, the vector \mathbf{q} in the reciprocal lattice is also randomly oriented. Making use of the mathematical identity

$$q_\alpha q_\beta \rightarrow \langle q_\alpha q_\beta \rangle = \frac{q^2}{3} \delta_{\alpha\beta}, \quad (6.2.23)$$

averaging over the angular dependencies of Eq.(6.2.19) yields

$$\tilde{F}^{\text{ret}}(\mathbf{q}, \omega) = -\frac{2}{3} \frac{i\hbar}{\epsilon_0} \left[\frac{\frac{1}{3} q^2 \frac{i\hbar}{\epsilon_0} p^{\text{ret}} + k^2 \left(1 + \frac{2}{3} \frac{i\hbar}{\epsilon_0} p^{\text{ret}}\right)}{q^2 - k^2 - \frac{i\hbar p^{\text{ret}}}{\epsilon_0} \left(\frac{1}{3} q^2 + \frac{2}{3} k^2\right) - i0} \right] \frac{1}{\left(1 + \frac{2}{3} \frac{i\hbar}{\epsilon_0} p^{\text{ret}}\right)}. \quad (6.2.24)$$

The inverse Fourier transform of Eq.(6.2.24) has a singularity at the position of the probe QD ($r \rightarrow 0$). This is because we employ the continuum approximation which yields the large- q behavior of the Green's function in the reciprocal lattice. In fact, all QDs located in the vicinity of the probe QD have a great impact on the spontaneous emission and level shift of the probe QD. This requires a full microscopic treatment to take into account all local effects at length scales comparable to the inter-QD distance. In order to avoid such a complicated microscopic approach, we modify the retarded Green's function in the reciprocal lattice by introducing the following regularization,

$$\tilde{F}^{\text{ret}}(\mathbf{q}, \omega^+) \rightarrow \tilde{F}'^{\text{ret}}(\mathbf{q}, \omega^+) = \tilde{F}^{\text{ret}}(\mathbf{q}, \omega^+) \frac{\Lambda^4}{q^4 + \Lambda^4}. \quad (6.2.25)$$

Actually different regularization procedures are possible and (6.2.25) is a convenient one. Note that the regularized retarded Green's function that is introduced in Eq.(6.2.25), tends to the non-regularized Green's function for infinitely large Λ , since

$$\lim_{\Lambda \rightarrow \infty} \frac{\Lambda^4}{q^4 + \Lambda^4} = 1. \quad (6.2.26)$$

We should note that Λ does not have any physical meaning and is just a mathematical parameter for regularization. It has been derived in appendix (D), that in the limit $\Lambda \gg |q_0|$, the inverse Fourier transform of (6.2.25) transforms the retarded Green's function back to real space

$$\begin{aligned} \tilde{F}'^{\text{ret}}(\mathbf{r} = 0, \omega^+) &= \frac{\hbar\omega^3}{6\pi\epsilon_0 c^3} \sqrt{\epsilon(\omega)} \left(\frac{\epsilon(\omega) + 2}{3} \right)^2 \\ &\quad - \frac{i\hbar\omega^3}{6\pi\epsilon_0 c^3} \left[\frac{1}{R} \left(\frac{\epsilon(\omega) + 2}{3} \right)^2 + \frac{1}{R^3} \frac{2}{3} \left(\frac{\epsilon(\omega) + 2}{3\epsilon(\omega)} \right)^2 (\epsilon(\omega) - 1) \right], \end{aligned} \quad (6.2.27)$$

where $R = \sqrt{2}k/\Lambda$. By applying this result to Eq.(6.1.26), the decay rate of the QD-emission finally becomes

$$\Gamma = \Gamma_0 \operatorname{Re} \left[\sqrt{\varepsilon(\omega)} \left(\frac{\varepsilon(\omega) + 2}{3} \right)^2 \right] + \Gamma_0 \operatorname{Im} \left[\frac{1}{R} \left(\frac{\varepsilon(\omega) + 2}{3} \right)^2 + \frac{1}{R^3} \frac{2}{3} \left(\frac{\varepsilon(\omega) + 2}{3\varepsilon(\omega)} \right)^2 (\varepsilon(\omega) - 1) \right], \quad (6.2.28)$$

and the excited state Lamb shift is found to be,

$$h = \frac{\Gamma_0}{2} \operatorname{Im} \left[\sqrt{\varepsilon(\omega)} \left(\frac{\varepsilon(\omega) + 2}{3} \right)^2 \right] - \frac{\Gamma_0}{2} \operatorname{Re} \left[\frac{1}{R} \left(\frac{\varepsilon(\omega) + 2}{3} \right)^2 + \frac{1}{R^3} \frac{2}{3} \left(\frac{\varepsilon(\omega) + 2}{3\varepsilon(\omega)} \right)^2 (\varepsilon(\omega) - 1) \right]. \quad (6.2.29)$$

Equations (6.2.28) and (6.2.29) are the main achievements of this section. The modification of the spontaneous decay rate by local-field corrections in a purely dispersive (lossless) and homogeneous medium has been the interest of a lot of theoretical work. These approaches are based on a cavity around a radiating atom, with cavity characteristics that are essentially the local-field corrections. For example, it has been shown [196, 197] for a probe atom in a purely dispersive atomic system that the spontaneous decay rate in the *Lorentz's virtual cavity* approach is given by

$$\Gamma_{\text{Lor}} = \Gamma_0 \bar{n} \left(\frac{\bar{n}^2 + 2}{3} \right)^2, \quad (6.2.30)$$

where $\bar{n} = \sqrt{\varepsilon}$ is the complex refractive index of the medium. We know that a medium is purely dispersive if the imaginary part of its dielectric function is zero, $\varepsilon''(\omega) = 0$. In that case, the second term in (6.2.28) vanishes and the remaining term is equal to the virtual cavity result, Eq.(6.2.30). We already mentioned that the terms that contain the regularization parameter R , basically originate from the resonant energy transfer between nearest neighbor QDs. The details of these kind of correlations is beyond the scope of this work, but we would like to emphasize that for the case of a purely dispersive medium, the first term in (6.2.29) vanishes and the remaining term of the Lamb shift is a function of the regularization parameter and hence is only a consequence of the correlation between nearest neighbors. A purely dispersive medium is a very rare situation which doesn't happen in practice, because the probe QD is usually in resonance with some other QDs in the medium, implying that there is also absorption in the system and hence the imaginary part of the dielectric function is not zero anymore. This implies that the terms containing the regularization parameters take part in the spontaneous emission and the bulk term (the term that does not contain R) is effective in the Lamb shift.

6.2.2 The collective spontaneous emission rate and collective energy-level shift

According to Eq.(6.1.23), we have to find the spectrum of G^{-+} at the position of the probe QD. Taking the Fourier transform of Eq.(6.1.49) and employing (6.2.6), we can write

$$G_{\alpha\beta}^{-+}(\mathbf{r}_0, \omega) = - \int_V d\mathbf{r} G_{\alpha\alpha'}^{\text{ret}}(\mathbf{r}_0, \mathbf{r}, \omega) P_{\alpha'\beta'}^{-+}(\omega) G_{\beta'\beta}^{\text{adv}}(\mathbf{r}_0, \mathbf{r}, \omega), \quad (6.2.31)$$

where the integration is over the whole sample. By Replacing G^{adv} by $G^{\text{ret}*}$ and averaging over the polarization orientations, Eq.(6.2.31) becomes

$$G^{-+}(\mathbf{r}_0, \omega) = - \int_V d\mathbf{r} |G^{\text{ret}}(\mathbf{r}_0, \mathbf{r}, \omega)|^2 P^{-+}(\omega), \quad (6.2.32)$$

where

$$P^{-+}(\mathbf{r}, t_1, t_2) = \frac{1}{3} \frac{\mu_0}{\hbar^2} N \overline{\langle \langle S^+(t_1) S^-(t_2) \rangle \rangle}. \quad (6.2.33)$$

The factor $2/3$ in (6.2.33) comes from the orientation averaging. By taking the limit of (D.0.3) at $\Lambda \rightarrow \infty$, we obtain the non-regularized retarded Green's function in the real space,

$$\tilde{F}^{\text{ret}}(\mathbf{r}, \omega^+) = - \frac{i\hbar\omega^3}{6\pi\epsilon_0 c^3} \left(\frac{\epsilon(\omega) + 2}{3} \right)^2 \frac{e^{-i\omega\sqrt{\epsilon(\omega)r/c}}}{r}. \quad (6.2.34)$$

We split the complex refractive index into its real, $n(\omega)$, and imaginary $\kappa(\omega)$ values,

$$\bar{n} = \sqrt{\epsilon(\omega)} = n(\omega) + i\kappa(\omega). \quad (6.2.35)$$

Inserting this form of the complex refractive index in the exponential component of the retarded Green's function, it is obvious that $\omega n(\omega)/c$ characterizes the propagation phase shift and $\omega\kappa(\omega)/c$ denotes the inverse absorption/amplification length. By substituting (6.2.34) in (6.2.32) with the definition of (6.2.35), we can write

$$G^{-+}(\mathbf{r}_0, \omega) = \frac{\hbar^2\omega^6}{(6\pi)^2 \epsilon_0^2 c^6} \left| \frac{\epsilon(\omega) + 2}{3} \right|^4 P^{-+}(\omega) \int_V \frac{e^{2\omega\kappa r/c}}{r^2} d\mathbf{r}. \quad (6.2.36)$$

Referring again back to a cylindrical shape for the sample presented in Fig.(B.1), the spatial integration in (6.2.36) in cylindrical coordinates has the form

$$\int_0^R d\rho \int_{-L/2}^{L/2} dz \rho \frac{e^{\frac{2\omega\kappa}{c}\sqrt{z^2+\rho^2}}}{z^2 + \rho^2}, \quad (6.2.37)$$

where R is the radius and L is the thickness or height of the cylinder. The radius is in fact the diameter of the active area of the sample which corresponds to the diameter of the pumping laser spot. In the case of a single layer of QDs, the thickness of the layer is much smaller than the radius ($L \ll R$). Under such a condition, the integration

in (6.2.37) tends to zero. Therefore, the collective spontaneous emission rate and the collective light induced QD energy-level shift are negligible in our medium,

$$\Gamma^c \rightarrow 0, \quad \hbar^c \rightarrow 0. \quad (6.2.38)$$

It has been shown for a 3D system of atomic gases that Γ^c and \hbar^c have nonvanishing values [187]. However, in our quasi 2D sample, these terms disappear.

6.3 Numerical simulation of the spontaneous decay time

Based on the theory that was derived and developed in previous sections, we try in this section to simulate and explain the dynamics of a system which is of our interest from the experimental point of view and shows many features of the emission from QD ensembles. We assume that our medium is initially nonresonantly optically excited with a photon energy above the barrier bandgap and that there is no external field present in the system. We indicated that the collective emission in our 2D sample is negligible and the modification of the spontaneous emission rate originates only from the modification of the local density of optical states due to the presence of the other neighboring QDs around the QD under study. This phenomenon is in fact the Purcell effect in a sample of self-assembled QDs.

Ignoring the collective modifications of the decay rate and the level-shift, we can simply write the dynamic polarizability of the QD in resonance from Eq.(6.2.21) as

$$\alpha(t; \omega) = \frac{4i\pi c^3 \Gamma_0 \langle S^z(t) \rangle}{\omega^3 \Gamma(t)}, \quad (6.3.1)$$

where $\langle S^z(t) \rangle = [\rho_{ee}(t) - \rho_{gg}(t)]/2$ is the population difference. It is obvious from Eq.(6.1.27) that the homogeneous radiative decay rate of the QD, Γ_0^{rad} , should increase as the third power of the QD transition energy by increasing the transition energy which is a size-dependent quantity. But it has been indicated in Ref. [198] that the radiative decay rate decreases with increasing energy. This behavior is due to the decrease of the overlap between the electron and hole wavefunctions as the size of the QD reduces (the QD transition energy increases). Moreover, the homogeneous linewidth of the QD has also a nonradiative component, Γ_0^{nrad} which increases when the transition energy increases. This is probably due to the relative importance of QD surface effects in smaller QDs [198]. Since the increase of the nonradiative component and the decrease of the radiative component of the decay rate by increasing the transition energy relatively cancel each other, we can say with a good approximation that the total homogeneous linewidth of the QDs $\Gamma_0 = \Gamma_0^{\text{rad}} + \Gamma_0^{\text{nrad}}$ is almost the same for all QDs and doesn't change significantly as a function of the QD size.

As we mentioned at the beginning of this chapter, in the sample of our interest, the inhomogeneous broadening σ is large as compared with the radiative emission rate of QDs ($\sigma \gg \Gamma$). This broadening is due to the size distribution of QDs in the sample and has been shown in Fig.(6.3)(a). Any QD in the sample with an arbitrary transition frequency

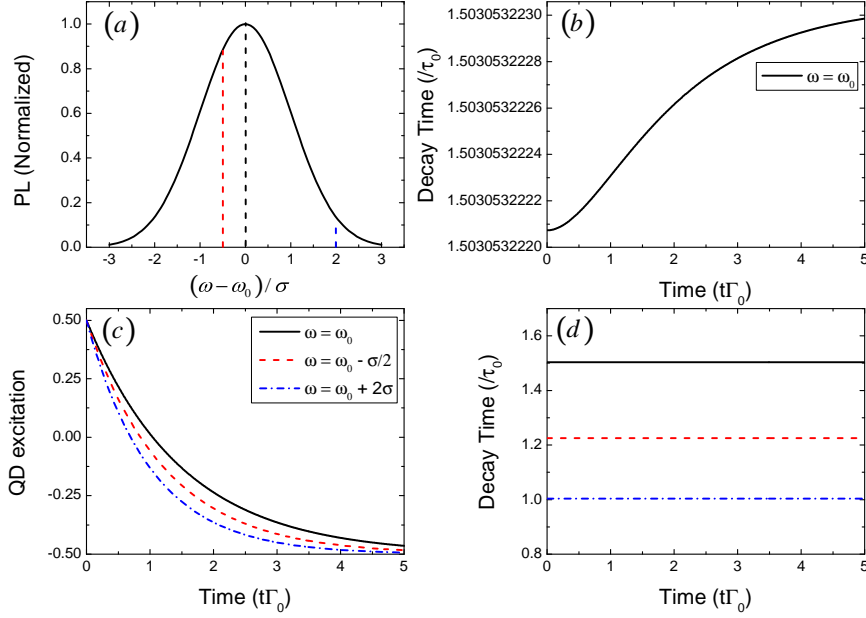


Figure 6.3: (a) The size distribution of QDs which is a Gaussian function with width σ . (b) The evolution of the QD radiative decay time ($\tau = 1/\Gamma$) at the center of the size distribution ($\omega = \omega_0$). (c) The decay of the QD population difference $\langle S^z(t) \rangle$ and (d) the time-variation of their corresponding decay times for QDs with transition frequencies $\omega = \omega_0$ in the centre of the QD size distribution (solid line), $\omega = \omega_0 - \sigma/2$ (dashed line) and $\omega = \omega_0 + 2\sigma$ (dash dotted line). In these simulations, we have assumed that the total density of QDs, N_0 , is 4.5×10^{23} QDs/m³. The initial excitation in these graphs is $\langle S^z(0) \rangle = 1/2$.

ω can interact with those QDs whose transition energies fit the energy interval between $\omega - \Gamma_0/2$ and $\omega + \Gamma_0/2$. Within this interval, we assume that QDs are nearly resonant and they all have transition frequency ω . Assuming that the QD size distribution follows a Gaussian function presented in (6.1.2), the density of QDs which is able to interact with the probe QD with transition energy ω through the dipole-dipole coupling can be obtained as

$$\begin{aligned}
 N(\omega) &= \frac{N_0}{\sqrt{2\pi}\sigma} \int_{\omega - \Gamma_0/2}^{\omega + \Gamma_0/2} e^{-\frac{1}{2} \left(\frac{\omega_{\text{pr}} - \omega_0}{\sigma} \right)^2} d\omega_{\text{pr}} \\
 &= \frac{N_0}{2} \left\{ \text{erf} \left[\frac{\Gamma_0/2 + (\omega - \omega_0)}{\sqrt{2}\sigma} \right] + \text{erf} \left[\frac{\Gamma_0/2 - (\omega - \omega_0)}{\sqrt{2}\sigma} \right] \right\},
 \end{aligned} \tag{6.3.2}$$

where N_0 is the total QD density. By substituting the dynamic polarizability of (6.3.1) in

the bulk component of Eqs.(6.2.28) and (6.2.29) and making use of (6.2.22), we can write

$$\Gamma(\omega, t) = \Gamma_0(\omega) \operatorname{Re} \left[\sqrt{\frac{3 + 2N\alpha(\omega, t)}{3 - N\alpha(\omega, t)}} \left(\frac{3}{3 - N\alpha(\omega, t)} \right)^2 \right], \quad (6.3.3)$$

$$h(\omega, t) = \Gamma_0(\omega) \operatorname{Im} \left[\sqrt{\frac{3 + 2N\alpha(\omega, t)}{3 - N\alpha(\omega, t)}} \left(\frac{3}{3 - N\alpha(\omega, t)} \right)^2 \right], \quad (6.3.4)$$

with N the QD density introduced in (6.3.2). It is obvious that the decay rate and the excited state Lamb shift depend on the population difference. In the absence of any external field, the population difference itself can be obtained from (6.1.33),

$$\langle \dot{S}^z(t) \rangle = -\frac{\Gamma(t)}{2} - \Gamma(t) \langle S^z(t) \rangle. \quad (6.3.5)$$

The combination of (6.3.3) and (6.3.5) indicates clearly that the decay rate is a function of the population difference which is itself a function of the decay rate. Hence a set of nonlinear equations should be solved. There is no exact analytical solution for these nonlinear equations and to obtain exact solutions, we have to treat the problem numerically. The decay of the QD excitation is shown in Fig.(6.3)(c) for three different QD sizes within the QD size distribution. It is shown in Fig. 6.3c,d that the QD radiative lifetime at resonance $\omega = \omega_0$ is 50% larger than the QD radiative decay time in free space. Equivalently, the QD radiative lifetime at resonance is also 50% larger than the QD radiative lifetime far into the tail of the QD size distribution $\omega = \omega_0 + 2\sigma$. The modification of the QD radiative lifetime due to the Purcell effect with a virtual cavity consisting of all other resonant QDs within the sample, is thus slowing down of the emission. It is also obvious from Fig.(6.3)(b,d) that the population difference decays almost single exponentially with a corresponding decay time that doesn't change significantly in time and can be considered to be fixed. This behavior facilitates the simplified analytical analysis in Section (6.4) and also in the next chapter.

We plot the QD radiative decay time within a QD sample, as a function of the QD transition frequency in Fig.(6.4). We first note that the radiative decay time approaches $\tau = 1/\Gamma$ near the edges of the QD size distribution, where the QD density becomes negligible and the Purcell enhancement of the radiative decay time due to the other QDs in the sample thus also becomes negligible. The most important consequence of this figure is that all QDs within the centre of the QD size distribution decay slower within a QD sample than in free-space. We thus observe a kind of radiation trapping due to the presence of other identical QDs within the QD-sample. The other feature that is apparent from Fig.(6.4) is that the width of the radiative decay-time distribution is only half the width of the QD size distribution. This means that the decay-time is approximately proportional to the number of resonant QDs squared, N^2 , rather than to the number of resonant QDs N . This behavior manifests itself in Fig.(6.5) too, where we observe a nearly parabolic increase of the radiative QD decay time as a function of resonant QD density. Another important feature of Fig.(6.4) is that the QD radiative decay time strongly depends on the initial excitation of the QDs. This phenomenon is even more clear in Fig.(6.6) in which we plot the QD radiative decay time as a function of the initial excitation $\langle S^z(0) \rangle$. We observe that the QD radiative decay time is not changed

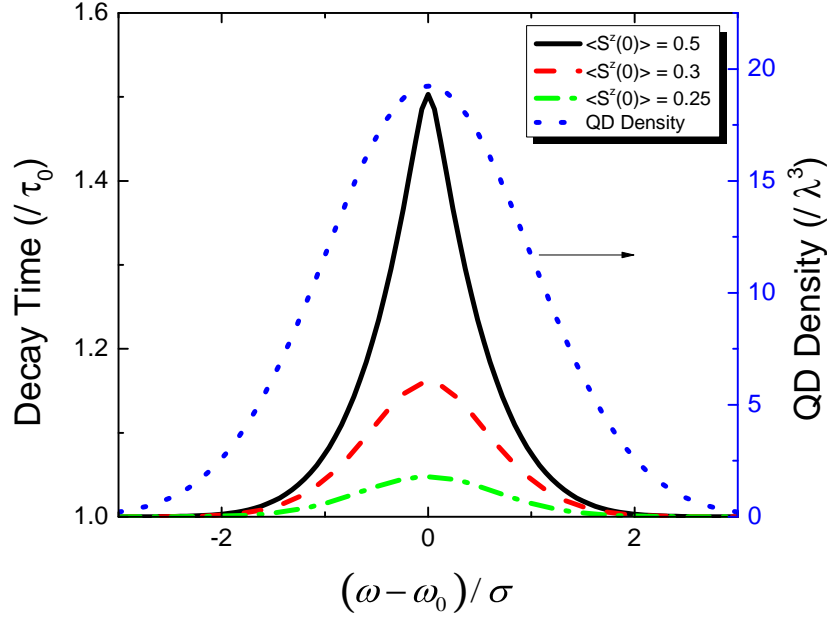


Figure 6.4: (Left axis) The radiative decay time of the QDs in a sample of self-assembled QDs with a size distribution of width σ , for the initial excitations $\langle S^z(0) \rangle = 0.5$ (Solid line), $\langle S^z(0) \rangle = 0.3$ (dashed line) and $\langle S^z(0) \rangle = 0.25$ (dash dotted line). All the parameters are as the same as those of Fig.(6.3). (Right axis) the number of QDs in a volume of a cubic wavelength within the sample. The shape of this curve is identical to the QD size distribution.

from its free-space value by the presence of the other QDs when $\langle S^z(0) \rangle = 0$, i.e. when the other QDs in the sample are (on average) transparent. The Purcell enhancement of the radiative lifetime for QDs near the centre of the QD size distribution is found to be symmetric for $\langle S^z(0) \rangle > 0$ and $\langle S^z(0) \rangle < 0$ and the Purcell enhancement of the radiative lifetime is maximum when all other QDs in the sample are either initially unexcited $\langle S^z(0) \rangle \rightarrow -1/2$ or initially fully excited $\langle S^z(0) \rangle = 1/2$, meaning that all other QDs in the sample either have maximum probability for absorption of a resonant photon or have a maximum probability for stimulated emission of a resonant photon. As mentioned in chapter(1), this behavior is similar to the Dicke's theory for small samples where the spontaneous emission rate in a sample with dimensions smaller than the emission wavelength is maximum when half of quantum emitters are excited.

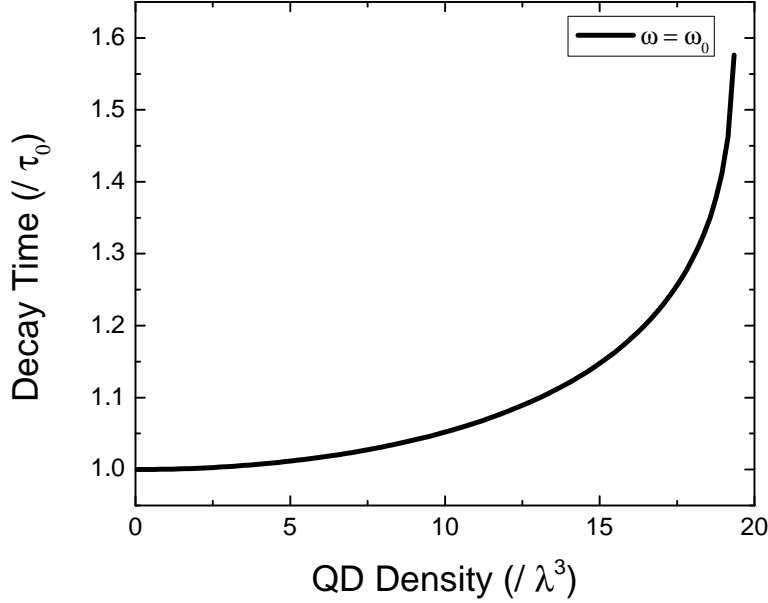


Figure 6.5: The QD radiative decay time as a function of the density of resonant QDs (number of resonant QDs per cubic wavelength).

6.4 Discussion

For a dense medium of identical QDs, Eqs.(6.2.28) and (6.2.29) are only implicit, because the complex dielectric constant depends on the decay rate and the level shift as well as on the short-range correlations between the QDs through the regularization parameter Λ . Therefore the decay rate Γ and the level shift h should be calculated in a self-consistent way. In the previous section, we solved the set of nonlinear equations numerically and found out some interesting features of the dynamical behavior of the QD excitation and its corresponding decay time. In this section, in order to get an analytical feeling of the dynamical behavior of our QD sample, we treat the problem in the limit of a dilute sample with a resonant QD-density of less than one QD per cubic wavelength. For such a dilute QD sample, we can expand the bulk contributions of Γ and h in equations (6.2.28) and (6.2.29) in powers of the resonant QD density N . The bulk contribution are the terms which do not include the local fluctuations (the terms that do not contain the regularization parameter R). Then by separating the QD polarizability, Eq.(6.2.21), into real and imaginary parts $\alpha(\omega) = \alpha'(\omega) + i\alpha''(\omega)$, we write such an expansion as

$$\Gamma = \Gamma_0 \left[1 + \frac{7}{6}\alpha'N + \frac{17}{24}(\alpha'^2 - \alpha''^2)N^2 + O(N^3) \right], \quad (6.4.1)$$

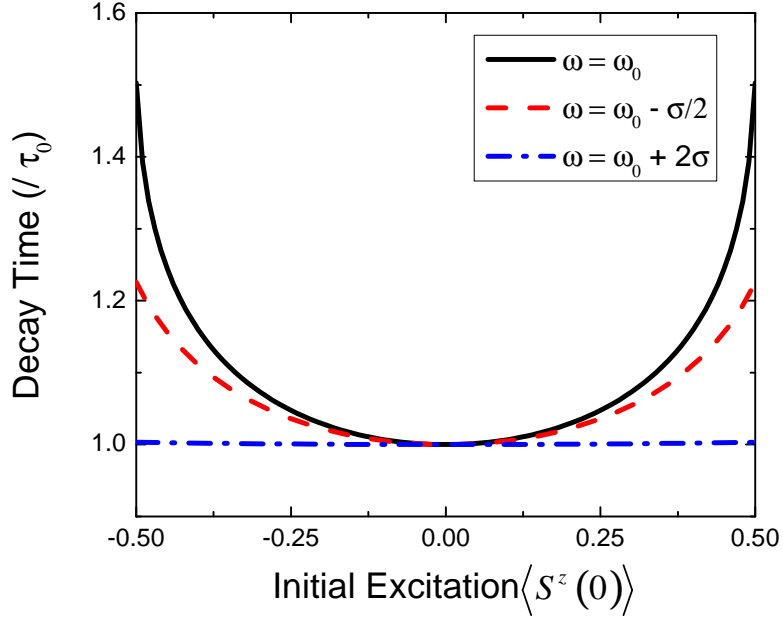


Figure 6.6: The radiative decay time of the QDs versus the initial excitation of the QDs, plotted for QDs with transition frequencies $\omega = \omega_0$ (solid line), $\omega = \omega_0 - \sigma/2$ (dashed line) and $\omega = \omega_0 + 2\sigma$ (dash dotted line).

$$h = \frac{\Gamma_0}{2} \left[\frac{7}{6} \alpha'' N + \frac{17}{12} \alpha' \alpha'' N^2 + O(N^3) \right]. \quad (6.4.2)$$

Referring back to the previous section that the QD radiative decay rate doesn't change significantly in time, we consider Γ as a constant and hence the population difference $\langle S^z(t) \rangle$ which is the only remaining time-dependent term involved in the definition of the decay rate, can be replaced approximately by its initial value $\langle S^z(0) \rangle$. Then the real and imaginary parts of the polarizability can be obtained from (6.2.21) as,

$$\begin{aligned} \alpha'(t; \omega) &= -\frac{2\pi c^3 \Gamma_0}{\omega^3} \frac{\overline{\langle S^z(0) \rangle (\omega - \omega_{pr})}}{(\omega - \omega_{pr})^2 + (\Gamma/2)^2}, \\ \alpha''(t; \omega) &= \frac{2\pi c^3 \Gamma_0}{\omega^3} \frac{\overline{\langle S^z(0) \rangle (\Gamma/2)}}{(\omega - \omega_{pr})^2 + (\Gamma/2)^2}, \end{aligned} \quad (6.4.3)$$

where $\overline{\{\dots\}}$ denotes the averaging over any inhomogeneous broadening. In the case of radiatively broadened two-level QDs (QDs with a finite Γ), it is obvious from Eq.(6.96) that the real part of the polarizability vanishes at resonance and hence Eqs.(6.4.1) and

(6.4.2) can be simplified to

$$\Gamma = \Gamma_0 \left[1 - \frac{17}{24} \alpha''^2 N^2 + O(N^3) \right], \quad (6.4.4)$$

$$\hbar = \frac{\Gamma_0}{2} \left[\frac{7}{6} \alpha'' N + O(N^3) \right]. \quad (6.4.5)$$

Eqs.(6.4.4) and (6.4.5) are the main results of this chapter, again clearly showing slowing down of the emission proportional to N^2 . Although these equations are approximations, they still reveal some important and interesting physical characteristics of our sample. We start with the energy Lamb shift. As has been shown in (6.4.3), the imaginary part of the dynamic polarizability is a function of the initial population difference between the QD ground state and the QD excited state, and varies in the range $-1/2 < \langle S^z \rangle < 1/2$. This means that when the medium is completely inverted or more than half of QDs are excited ($0 < \langle S^z \rangle < 1/2$), the transition frequency is blueshifted ($\hbar > 0$). When most QDs are in their ground-state ($-1/2 < \langle S^z \rangle < 0$), we obtain a red-shift ($\hbar < 0$) and when ($\langle S^z \rangle = 0$), the level-shift vanishes ($\hbar = 0$). This means that the spontaneous emission from an initially inverted system is generally time-dependent (frequency chirping effect) very similar to the chirp in Dicke superradiance [62]. We should emphasize here that this frequency shift is different from the Lorentz-Lorenz (LL) shift, which is due to the dispersion of the refractive index in a purely dispersive medium. At least up to the first order with respect to the QD density, the frequency shift is proportional to the imaginary part of the polarizability which represents the QD absorption [188,199].

Since the main scope of this thesis is on the modification of the QD radiative decay rate, we focus more on Eq.(6.4.4) and explore Γ into more detail. Eq.(6.4.4) explains the general properties of our simulations in the previous section very well. We can rewrite Eq.(6.4.4) in the form

$$\Gamma = \Gamma_0 \left[1 - \frac{17}{24} \left(\frac{N_\lambda \Gamma_0 \langle S^z(0) \rangle}{2\pi^2 \Gamma} \right)^2 + \dots \right], \quad (6.4.6)$$

where $N_\lambda = \lambda^3 N$ is the number of resonant QDs per cubic wavelength. We explain the modifications of the QD radiative decay rate Γ within a QD sample, with respect to the free space radiative decay rate Γ_0 as follows:

- i. The role of the QD density in the radiative decay rate is N_λ^2 . This is in full agreement with the lower density parts of the numerical simulation in Fig.(6.5).
- ii. The influence of the QD transition frequency also manifests itself in the density of resonant QDs. Since the QD size distribution follows a Gaussian function, the density of resonant QDs which can be obtained from (6.3.2) has a Gaussian shape as well. Since the modification of the radiative QD decay time is proportional to the square power of the resonant QD density, the width of the decay-time distribution is half of the width of the QD distribution. This behavior is quite clear in the numerical simulation of Fig.(6.4).

- iii. Regarding the effect of the initial excitation on the QD radiative decay rate, it is again obvious in Fig.(6.6) that the decay rate is proportional to the initial excitation squared. We can see clearly that when half of the QDs are excited, the electromagnetic interaction between the QDs vanishes and the QDs decay with their free-space decay rate ($\Gamma = \Gamma_0$). But when all the QDs are excited or only one QD is excited, then the radiative coupling of QDs becomes maximum and the decay rate reaches its slowest value.

The dependence of the decay time and the emission energy shift (Lamb shift) on the QD density and the level of excitation, is similar to subradiant emission due to a cooperative process. However, in our randomly-distributed sample, cooperative effects are absent. The phenomenon that we observe is closest to what is called radiation trapping or imprisonment of resonance radiation, is a phenomenon in physics where radiation is trapped in the system through a mechanism in which a photon is emitted by one atom or QD and is absorbed by another one before the photon can escape from the system. In the formalism of this chapter, this emission and reabsorption process manifests itself in the modification of the local electric field in the system of both dispersive and absorbing QDs. The local-field correction in a fully dispersive 3D medium has been extensively treated. But when absorbing atoms or QDs are also present in the system, then all local-field corrections become a function of the excitation level as well. This is the main difference between a fully dispersive medium and our system which is both dispersive and absorptive. Up to our knowledge, this phenomenon has not been theoretically or experimentally treated for QD systems. In the next chapter, we will introduce a technique which allows to track the effect of radiation trapping in a sample of self-assembled InAs/GaAs QDs.

6.5 Summary

In this chapter, we theoretically investigated the spontaneous emission rate in a two-dimensional sample of self-assembled QDs, in which QDs follow a Gaussian size distribution and are randomly distributed in the sample. Due to the large inhomogeneous broadening in such samples, the dephasing time is usually shorter than the characteristic superradiance time required to build up a coherent emission. That's why it is unlikely that we can observe cooperative effects in this type of samples. However it is possible to observe and measure collective effects. In randomly distributed QD samples, the local field acting upon each QD is strongly modified by altering some parameters like the QD density and the initial excitation. We found that the emission is slower in dense QD samples. In the case of dilute QD samples, the increase of the radiative decay time is proportional to the QD density squared. We also found that the collective radiative decay time is proportional to the square power of the initial excitation $\langle S^z(0) \rangle$, where $\langle S^z(0) \rangle = 0$ if half of the QDs are excited. The collective emission thus vanishes when exactly half of the QDs are excited. However, when the QD system is either weakly excited (only one QD is initially excited) or highly excited (all QDs excited,

except one), the electromagnetic coupling between the QDs in the ensemble and thus also the emission decay time is maximum. This phenomenon is called radiation trapping and is a consequence of the local-field modification in a system that is composed of both dispersive (excited) and absorptive (not excited) QDs.

Chapter 7

Collective reflection: Time Resolved Differential Reflectivity Experiments

In many-body systems, such as an ensemble of quantum dots, the local electric field that acts on each component (QD) of the ensemble is different from the macroscopic Maxwell field in the system. This field modification originates from the mutual electromagnetic dipole-dipole coupling between the QDs and can strongly modify the decay rate of the collective excitation and also induces an energy shift of the collective emission (Lamb shift). The importance of the local field on the super-radiance phenomenon was described by Friedberg *et al.* [200]. By calculating the reflection and transmission of ultrashort light pulses through a thin resonant medium and taking into account the local-field effects, Benedict *et al.* [201] showed that cooperative processes can give rise to bistable transmission on the time scale of the superradiant emission which can be much shorter than the relaxation time. The local-field correction does not give rise only to cooperative effects, but it can also govern collective effects especially in systems with large inhomogeneous broadening in which cooperative processes are partially or completely suppressed. The inhomogeneous broadening is usually large in self-assembled QDs due to the broad size distribution of the QDs. Basically in samples with sizes much larger than the emission wavelength, it is difficult to observe cooperative phenomena like superradiance or subradiance. Now the question is whether collective effects like radiation trapping are also absent in these QD ensembles or not. We answered this question in the previous chapter from a theoretical point of view where we investigated the collective excitation dynamics of an ensemble of two-level objects (QDs) as well as the collective energy resonance shifts due to the modification of the local-field acting upon each QD in the ensemble. We indicated that the collective decay rate of a QD ensemble is a function of the total number of interacting QDs. For example, in the limit of a low areal density of resonant QDs (less than one QD per cubic wavelength), the decay

rate is proportional to the squared power of the QD density. We also showed that the initial excitation of the QD ensemble plays an important role in the modification of the of the spontaneous emission decay rate. At a certain degree of excitation where half of QDs in the ensemble are populated on average, the collective decay time is minimum. For lower and higher excitation, the QD-population decay time is always larger as compared to the case where only one QD is excited or only one QD is unexcited, at which the decay time reaches its maximum value. This phenomenon is well-known as radiation trapping and has been already investigated for atomic systems. Up to our knowledge, there has not been any experimental evidence to show this effect for QD ensembles.

Now the other question is how it is possible to observe collective effects in QD ensembles. We will indicate in this chapter that it is possible to track the modification of the QD excitation decay time by employing a technique called Time Resolved Differential Reflectivity (TRDR). TRDR is a pump-probe experiment to measure the charge carrier dynamics inside the QDs. This means that the pump-induced modification of the sample reflection is studied as a function of the pump-probe delay time. The TRDR technique has been employed in many experiments especially on quantum wells to study physical mechanisms, like e.g. the ultrafast and recombination dynamics of resonantly excited quantum-well excitons [202], the coherent polarization dynamics in GaAs multiple quantum wells [203, 204], the coherent nonlinear optical response of single QDs through ultrafast near-field spectroscopy [205], the suppression of exciton-polariton light absorption in multiple quantum well Bragg structures [206], and the effect of point defects on the TRDR time profile of quantum wells [207].

This technique has some major differences with the other spectroscopic experiments. For example, in Time Resolved Photoluminescence (TRPL), which is a quite popular spectroscopic technique. However in TRPL, the luminescence efficiency is a critical factor which is sensitive to the sample temperature as well as to the number of non-radiative recombination centers within the sample. The Photoluminescence Excitation (PLE) technique has this restriction as well. Although all of our TRDR experiments have been done at low temperatures (4K), optical absorption based experiments like time resolved differential transmission [208, 209] or TRDR [210], overcome the problem of low luminescence efficiency at high temperature. An added advantage of TRDR as compared with differential transmission is that we don't have to remove the substrate which makes the sample more protected against mechanical tension and temperature cycling during the measurement.

In section (7.1) of this chapter, we formulate the TRDR experiment from the mathematical point of view and we show that in these experiments, it is possible to measure the lifetime of the QD excitation. In section (7.2), we will introduce self-assembled InAs\GaAs QDs as our sample and subsequently a brief description of charge carrier dynamics in such samples in section (7.3). In section (7.4), we explain how our TRDR setup works. Then in sections (7.5) and (7.6), we analyze our pump-power dependent and probe-frequency dependent TRDR measurements with the help of the theory we developed in chapter (6). We will provide strong evidence that we observe radiative coupling between the different quantum dots, resulting in modified radiative lifetimes due to radiation trapping. At the end, we shortly discuss the results in literature of

Time Resolved Photoluminescence (TRPL) experiments on similar QD samples and try to compare them with our TRDR-based results.

7.1 Differential reflection from a planar quantum dot sample

In classical optics, the reflection of light from a single boundary is described by the Fresnel formulae [66]. But this treatment works well only in the linear and stationary regime when all dynamical processes in the medium have been damped out. When many QDs inside a layer are initially excited, the medium is not linear anymore and this approach fails to describe transient nonlinear processes. For closely enough spaced QDs, the dipole-dipole interaction between the QDs will modify the QD-field dynamics and hence influence the collective reflection. In the case of weak nonlinear regime where the total QD population within the sample is very close to the ground state, the local field effects (caused by dipole-dipole interactions) yield a constant shift of the resonance frequency. In this case, the problem can be simplified to a semi-linear problem where the frequency dynamics can be neglected. The weak nonlinear regime has been extensively investigated in the past [211]. In a pump-probe experiment, the sample becomes populated by the pump and hence turns into a nonlinear material. In this section, we formulate a description for the reflectivity of a probe pulse from a QD sample. As has been schematically depicted in Fig.(7.1), in a differential reflectivity experiment, we assume that the pump pulse is nonresonant with respect to the QDs and has a photon energy above the GaAs barrier bandgap, surrounding the InAs\GaAs QD-layer. The charge carriers will thus be generated in the barrier layer and will subsequently diffuse towards the QDs. In this way, the QDs will be incoherently excited. Then, after a delay time τ , a probe pulse arrives with a central frequency ω_L ,

$$\mathbf{E}_{\text{pr}}(t, \tau) = \frac{1}{2} \mathbf{E}_0(t, \tau) (e^{i\omega_L t} + e^{-i\omega_L t}), \quad (7.1.1)$$

which is in resonance with a part of the inhomogeneously broadened InAs\GaAs QD spectrum. After being reflected from the sample, the probe pulse is detected by a slow photodetector. We assume that in our sample, a single QD layer is positioned at a distance d below the front surface. The time-profile of the probe laser pulse can best be approximated by a Gaussian shape with a pulse width T ,

$$\mathbf{E}_0(t) = \mathbf{E}_0 e^{-\frac{1}{2} \left(\frac{t-\tau}{T} \right)^2}. \quad (7.1.2)$$

We should emphasize that the notion τ in this chapter stands for the delay time between the excitation and the probe laser pulse and should not be confused with τ in the previous chapter which was denoting the correlation time between the dipole operators of a QD. If a probe laser pulse is focused on a QD sample, the incident field will be partially reflected from the front surface, $\mathbf{E}_s(t)$, while the field further propagates into the sample and will also be partially reflected from the QD-layer, $\mathbf{E}_{\text{QD}}(t)$. The total electric field reflected from the sample, is the superposition of these two fields. The higher order

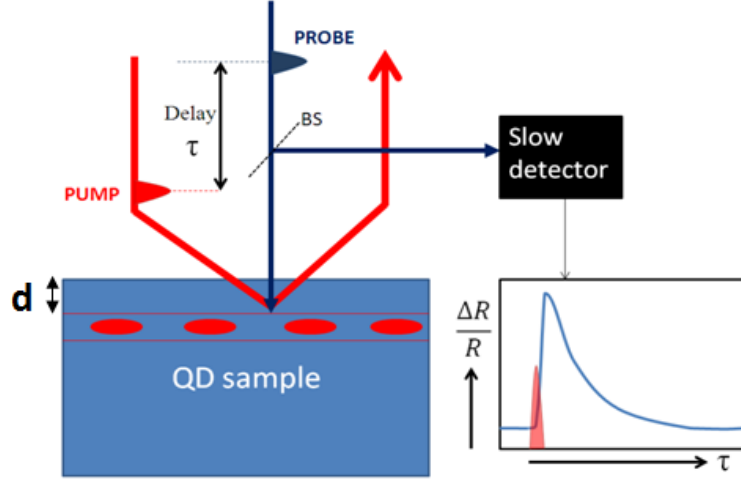


Figure 7.1: Schematic picture of the Time Resolved Differential Reflectivity (TRDR) experiment, showing a pump beam which excites the QD. After a time delay τ , the reflectivity is monitored by the probe beam. A slow detector measures the transient reflectivity R/R (strongly simplified picture).

reflections are neglected. Since we assume that the incident field is focused on the QD layer, we neglect the reflection from the back side of the sample, which is out of focus in the experiment. Similar to what has been mentioned about the total electric field, the total magnetic field is also a superposition of the magnetic field reflected from the front surface, H_s , and the magnetic field reflected from the QD layer, H_{QD} . In the case of the perpendicular incidence, we indicate the fields only with their scalar values. Obviously, the electric and magnetic fields are perpendicular to each other. Since the Gaussian part of the probe field is the slowly-varying part of the field as compared with the fast-oscillating part, we assume that the probe pulse shape doesn't change significantly by the reflection from the front surface of the sample. Following the Fresnel formulas [103], the components of the probe laser fields reflected from the front surface are

$$\begin{aligned} E_s &= r_s E_0 e^{-\frac{1}{2}\left(\frac{t-\tau}{\tau}\right)^2} (e^{i\omega_L t} + e^{-i\omega_L t}), \\ H_s &= \varepsilon_0 c r_s E_0 e^{-\frac{1}{2}\left(\frac{t-\tau}{\tau}\right)^2} (e^{i\omega_L t} + e^{-i\omega_L t}), \end{aligned} \quad (7.1.3)$$

where ε_0 is the free space permittivity, c is the speed of light in free space and r_s is the reflection coefficient of the host material,

$$r_s = \frac{n-1}{n+1}, \quad (7.1.4)$$

where n is the refractive index of the host material. The probe laser field emitted from the QD-layer is

$$\begin{aligned} E_{\text{QD}}(t) &= E_{\text{QD}}^{(+)}(t) + E_{\text{QD}}^{(-)}(t), \\ H_{\text{QD}}(t) &= H_{\text{QD}}^{(+)}(t) + H_{\text{QD}}^{(-)}(t). \end{aligned} \quad (7.1.5)$$

where $E_{\text{QD}}^{(+)}(t)$ and $E_{\text{QD}}^{(-)}(t)$ are the positive and negative frequency components. We choose the coordinate system in a way that for each QD, z is along $\mathbf{r} - \mathbf{r}_i$, with \mathbf{r} the position of the observation point and \mathbf{r}_i , the position of the i th QD. Then θ is the angle between z and the QD dipole moment $\boldsymbol{\mu}$ and \mathbf{e}_{x_i} is the unit vector in the direction of $(\mathbf{r} - \mathbf{r}_i) \times [(\mathbf{r} - \mathbf{r}_i) \times \boldsymbol{\mu}]$. As already derived in chapter(2), the emitted fields from each QD are

$$\begin{aligned} E_{\text{QD}}^{(+)}(\mathbf{r}, t) &= \frac{\mu_0}{4\pi\epsilon_0 c^2 r} \sum_{i=1}^N \mathbf{e}_{x_i} \omega_i^2 \sin \theta_i e^{-ik_i \mathbf{e}_r \cdot \mathbf{r}_i} S_i^-(t - rn/c), \\ H_{\text{QD}}^{(+)}(\mathbf{r}, t) &= \frac{\mu_0}{4\pi c r} \sum_{j=1}^N \mathbf{e}_{y_j} \omega_j^2 \sin \theta_j e^{-ik_j \mathbf{e}_r \cdot \mathbf{r}_j} S_j^-(t - rn/c), \end{aligned} \quad (7.1.6)$$

where S^- is the QD dipole lowering operator. Oppositely, S^+ is the QD dipole rising operator. In the far-field regime $r \gg r_i$, the problem becomes easier and we can make use of the approximation $\mathbf{r} - \mathbf{r}_i \approx \mathbf{r}$. Consequently, z is along \mathbf{r} and \mathbf{e}_{x_i} is along the opposite direction of the QD dipole moment. The interaction energy between the emitting QD and the electromagnetic field is supposed to be smaller than the QD transition energy; otherwise we cannot attribute a well defined transition frequency to the QD. This is the Born approximation, which implies that the retardation in the time dependence of the QD dipole operators can be simplified to [212]

$$S_j^-\left(t - \frac{r}{c}\right) = S_j^-(t) \Theta\left(t - \frac{rn}{c}\right) e^{ik_j r}, \quad S_j^z\left(t - \frac{r}{c}\right) = S_j^z(t) \Theta\left(t - \frac{rn}{c}\right), \quad (7.1.7)$$

where $\Theta(t)$ is the unit step function. For emission in the direction perpendicular to the QD sample, $\theta = \pi/2$ and $\mathbf{e}_r \cdot \mathbf{r}_i = 0$. The electromagnetic fields emitted from the QD layer at the front surface at a distance d from the QD layer, are of the form

$$\begin{aligned} E_{\text{QD}}^{(+)}(d, t) &= \frac{\mu_0}{4\pi\epsilon_0 c^2 d} \sum_{i=1}^N \omega_i^2 S_i^-(t) e^{\frac{i\omega_i n d}{c}} \Theta(t - nd/c), \\ H_{\text{QD}}^{(+)}(d, t) &= \frac{\mu_0}{4\pi c d} \sum_{j=1}^N \omega_j^2 S_j^-(t) e^{\frac{i\omega_j n d}{c}} \Theta(t - nd/c). \end{aligned} \quad (7.1.8)$$

In Eq.(7.1.8), μ_0 is the QD dipole moment and ω_j is the energy band gap of the j th QD. The negative-frequency part of the electric and magnetic fields can be obtained by $E_{\text{QD}}^{(-)} = \left(E_{\text{QD}}^{(+)}\right)^*$ and $H_{\text{QD}}^{(-)} = \left(H_{\text{QD}}^{(+)}\right)^*$ respectively. As is indicated in Eq.(7.1.8), the fields emitted from the QDs at the front surface have a phase shift of $\Delta\phi = n\omega_i d/c$ with respect the emission of the QD layer.

The quantity which is measurable by the detectors is actually the corresponding Poynting vector of the total reflected electromagnetic wave. The Poynting vector is the directional energy flux density (the rate of energy transfer per unit area per time). In the interaction picture, the Poynting vector can be written as

$$\begin{aligned}
\mathbf{R}(\mathbf{d}, t) &= (\mathbf{E}_s(\mathbf{d}, t) + \mathbf{E}_{\text{QD}}(\mathbf{d}, t)) \times (\mathbf{H}_s(\mathbf{d}, t) + \mathbf{H}_{\text{QD}}(\mathbf{d}, t)) \\
&= \frac{1}{2} \varepsilon_0 c |r_s|^2 E_0^2 e^{-\left(\frac{t-\tau}{T}\right)^2} \\
&\quad + \frac{E_0 \mu_0}{8\pi c d} e^{-\frac{1}{2}\left(\frac{t-\tau}{T}\right)^2} (e^{i\omega_L t} + e^{-i\omega_L t}) \sum_{j=1}^N \omega_j^2 \left[r_s e^{\frac{i\omega_j n d}{c}} \langle S_j^+(t) \rangle + \text{H.c.} \right] \\
&\quad + \frac{\mu_0^2}{8\varepsilon_0 \pi^2 c^3 d^2} \sum_{i,j=1}^N \omega_i^2 \omega_j^2 e^{i(\omega_i - \omega_j) \frac{n d}{c}} \langle S_i^+(t) S_j^-(t) \rangle,
\end{aligned} \tag{7.1.9}$$

In deriving Eq.(7.1.9), we have ignored terms with frequencies $\omega_i + \omega_j$ or $\omega_{i,j} + \omega_L$, since in the Rotating Wave Approximation (RWA), in classical stochastics, these terms does not appear in the signal due to time averaging. In addition, the correlation operators have been put in normal order. The first term in Eq.(7.1.9) is the reflection of the incident wave from the front surface. The second term corresponds to the correlation of the surface reflection and the field emitted from the QD layer and the last term is the emission emitted from the QD layer. The last term is much smaller than the first two terms and will be neglected [205].

In order to derive the expectation value of the QD dipole operator, we refer back to the previous chapter. Assuming that the absorption of light in the medium is negligible, we can write from (6.1.32),

$$\langle \dot{S}_j^-(t) \rangle = - \left(i\omega_j + \frac{\Gamma}{2} \right) \langle S_j^-(t) \rangle - 2i \left(\Omega^+ + B \langle S_j^- \rangle \right) \langle S_j^z(t) \rangle, \tag{7.1.10}$$

with

$$\Omega^+ = \Omega_0 e^{-\frac{1}{2}\left(\frac{t-\tau}{T}\right)^2} e^{-i\omega_L t} e^{\frac{i\omega_L n d}{c}}, \tag{7.1.11}$$

where $\Omega_0 = (1 - r_s) E_0 \mu_0 / \hbar$ is the Rabi frequency and $\exp(i\omega_j n d / c)$ is due to the phase shift which the probe laser undertakes after transmission through the capping layer to reach the layer of QDs. In Eq.(7.1.10), $\langle S_j^z \rangle$ is the population difference, $\Gamma = 2\gamma + \gamma^c$ is the QD decay rate and B is a shape factor due to the local-field correction. Moreover, because of large inhomogeneous broadening in the medium, we have put the energy level shifts included in ω_j . The solution of the differential equation in (7.1.10) is

$$\begin{aligned}
\langle S_j^-(t) \rangle &= -2i\Omega_0 \int_{-\infty}^t e^{-(i\omega_j + \frac{\Gamma}{2})(t-t')} e^{2iB \int_t^{t'} \langle S_j^z(t'') \rangle dt''} \\
&\quad \times e^{-\frac{1}{2}\left(\frac{t'-\tau}{T}\right)^2} e^{\frac{i\omega_L n d}{c}} \langle S_j^z(t') \rangle dt'.
\end{aligned} \tag{7.1.12}$$

Since the decay rate of the QD is in the order of nanoseconds, the population difference $\langle S^z \rangle$ and the exponential term that decays with Γ remain almost unchanged during the

Gaussian pulse (1.6 ps) and can be taken out of the integrand. The QD polarization becomes

$$\begin{aligned} \langle S_j^-(t) \rangle = & -2i\Omega_0 \sqrt{\frac{\pi}{2}} \langle S_j^z(\tau) \rangle T e^{-\frac{\Gamma}{2}(t-\tau)} e^{\frac{i\omega_L n d}{c}} e^{-i\omega_j t} e^{2iB \int_t^\tau \langle S_j^z(t') \rangle dt'} \\ & \times e^{(\omega_j - \omega_L)\tau} e^{-\frac{1}{2}(\omega_j - \omega_L)^2 T^2} \times \operatorname{erfc} \left[\frac{i(\omega_j - \omega_L) T}{\sqrt{2}} - \frac{t - \tau}{\sqrt{2}T} \right], \end{aligned} \quad (7.1.13)$$

where $\operatorname{erfc}(x)$ is the error function. The immediate message of Eq.(7-13) is observed from the Gaussian function $\exp[-(\omega_j - \omega_L)^2 T^2/2]$ which implies that only those QDs which are in resonance with the probe laser, i.e. whose transition frequencies are detuned from the probe laser central frequency not more than the probe laser spectral width T^{-1} (we assume a transform limited probe laser pulse). Up to now, we assumed that all QDs are identical. But in reality, they have different transition frequencies following a size distribution with a relatively large width. This size distribution results in an inhomogeneously broadened lineshape, which can be expressed by a Gaussian function centered on a central transition frequency ω_0 ,

$$g(\omega, \omega_0) = \frac{1}{\sigma\sqrt{2\pi}} e^{-\frac{1}{2}\left(\frac{\omega - \omega_0}{\sigma}\right)^2}, \quad (7.1.14)$$

where σ is the inhomogeneous broadening. For the sake of a simplified analytical solution, we assume that all the QDs whose transition energies fit the narrow spectral width of the probe laser pulse with the central frequency ω_L are identical and hence have transition frequency ω_L . Therefore, by using (7.1.14), the number of QDs which are resonant with the probe laser pulse is proportional to

$$N_{\text{pr}} \propto \frac{N}{\sigma\sqrt{2\pi}} e^{-\frac{1}{2}\left(\frac{\omega_{\text{pr}} - \omega_0}{\sigma}\right)^2}, \quad (7.1.15)$$

where N is the total number of QDs in the active region of the medium. In the resonant case ($\omega_j = \omega_L$), the QD polarization (7.1.13) becomes

$$\begin{aligned} \langle S_j^-(t) \rangle = & -2i\Omega_0 \sqrt{\frac{\pi}{2}} \langle S_j^z(\tau) \rangle T e^{-\frac{\Gamma}{2}(t-\tau)} e^{\frac{i\omega_L n d}{c}} e^{-i\omega_L t} \\ & \times e^{2iB \int_t^\tau \langle S_j^z(t') \rangle dt'} \operatorname{erfc} \left(-\frac{t - \tau}{\sqrt{2}T} \right). \end{aligned} \quad (7.1.16)$$

By substituting Eq.(7.1.16) in the second term of (7.1.9), the reflected signal in the real-time domain reads

$$\begin{aligned} R(t) = & \frac{\varepsilon_0 c |r_s|^2}{2} E_0^2 e^{-(\frac{t-\tau}{T})^2} + \frac{r_s(1-r_s)\hbar\Omega_0^2\omega_L^2}{\sqrt{2\pi}4cd} T N_{\text{pr}} \langle S_j^z(\tau) \rangle e^{-\frac{\Gamma}{2}(t-\tau)} e^{-\frac{1}{2}\left(\frac{t-\tau}{T}\right)^2} \\ & \times \operatorname{erfc} \left(-\frac{t - \tau}{\sqrt{2}T} \right) \left\{ i e^{\frac{2i\omega_L n d}{c}} e^{2iB \int_t^\tau \langle S_j^z(t') \rangle dt'} + \text{H.c.} \right\}. \end{aligned} \quad (7.1.17)$$

The slow photodetectors are not fast enough to record the reflectivity in real time, but they measure the transient reflectivity signal at a pump-probe delay time τ . The reflectivity at a time delay τ can be calculated by an integration of the reflectivity over the

real time domain,

$$\begin{aligned} R(\tau) = \int_{-\infty}^{\infty} R(t, \tau) dt = \frac{\varepsilon_0 c |r_s|^2 E_0^2}{2T\sqrt{\pi}} + \left\{ \frac{ir_s(1-r_s)\hbar\Omega_0^2\omega_L^2}{4\pi cd} \sqrt{\frac{\pi}{2}} T N_{pr} \langle S_j^z(\tau) \rangle e^{\frac{2i\omega_j nd}{c}} \right. \\ \left. \times \int_{-\infty}^{\infty} e^{-\frac{\Gamma}{2}(t-\tau)} e^{2iB \int_t^\tau \langle S_j^z(t') \rangle dt'} e^{-\frac{1}{2}\left(\frac{t-\tau}{T}\right)^2} \operatorname{erfc}\left(-\frac{t-\tau}{\sqrt{2}T}\right) dt + \text{H.c.} \right\}. \quad (7.1.18) \end{aligned}$$

Here we again have some slow-varying and some fast terms in the integrand. By changing $t \rightarrow \tau$ for slowly-varying terms and taking them out of the integral and performing the integration over only fast terms centered at $t = \tau$, we obtain

$$R(\tau) \simeq \frac{\varepsilon_0 c |r_s|^2 E_0^2}{2T\sqrt{\pi}} + \frac{r_s(1-r_s)\hbar\Omega_0^2\omega_L^2 T^2}{2cd} N_{pr} \langle S_j^z(\tau) \rangle \sin\left(\frac{2\omega_L nd}{c}\right). \quad (7.1.19)$$

In deriving Eq.(7.1.19), we made use of

$$\int_{-\infty}^{\infty} e^{-\frac{1}{2}\left(\frac{t-\tau}{T}\right)^2} \operatorname{erfc}\left(-\frac{t-\tau}{\sqrt{2}T}\right) dt = \sqrt{2\pi}T. \quad (7.1.20)$$

It is clear from (7.1.19) that the Reflectivity is proportional to the population difference. Provided the probe laser is in resonance with the QDs, the equation of motion for the population difference is already derived in (6.1.33),

$$\langle \dot{S}^z \rangle = -\frac{\gamma}{2} - (\gamma + 2\gamma^c) \langle S^z \rangle - i(\Omega^- \langle S^- \rangle - \Omega^+ \langle S^+ \rangle). \quad (7.1.21)$$

By substituting (7.1.16) in (7.1.21), the solution is

$$\begin{aligned} \langle S^z(t) \rangle = -\pi\Omega_0^2 T^2 \cos\left(\frac{\omega_L nd}{c}\right) e^{-\Gamma(t-\tau)} \left[1 + \operatorname{erf}\left(\frac{t-\tau}{\sqrt{2}T}\right) \right]^2 \\ - \frac{\gamma}{2\Gamma} + \left(\langle S^z(0) \rangle + \frac{\gamma}{2\Gamma} \right) e^{-\Gamma t}, \end{aligned} \quad (7.1.22)$$

where $\Gamma = \gamma + 2\gamma^c$ is the total decay rate of the population difference. In obtaining this solution, we have again taken the slowly-varying terms out of the time-integrations. We indicated in the previous chapter that in our quasi two dimensional sample, γ^c is negligible as compared with γ . The first term in Eq.(7.1.22) is a modification of the population difference induced by the probe laser pulse and is obviously effective only after the arrival of the probe laser. The second and third terms are simply the decay of an initially excited QD in the absence of any external (probe laser) field. By putting $t \rightarrow \tau$ in Eq.(7.1.22) and substituting in (7.1.19), the reflectivity becomes

$$\begin{aligned} R(\tau) = \frac{\varepsilon_0 c |r_s|^2 E_0^2}{2T\sqrt{\pi}} - \frac{r_s \hbar \Omega_0^2 \omega_L^2 T^2}{2cd} N_{pr} \sin\left(\frac{2\omega_L nd}{c}\right) \\ \times \left[-\pi\Omega_0^2 T^2 \cos\left(\frac{\omega_L nd}{c}\right) - \frac{\gamma}{2\Gamma} + \left(\langle S^z(0) \rangle + \frac{\gamma}{2\Gamma} \right) e^{-\Gamma\tau} \right]. \quad (7.1.23) \end{aligned}$$

We are interested in the differential reflectivity signal $\Delta R(t, \tau) = R(t, \tau) - R_0(t, \tau)$, in which the reflected Poynting vector due to pump laser excited QDs is subtracted from

the reflected Poynting vector for unexcited QDs. The reflectivity when the sample is not initially pumped, R_0 , can be immediately obtained by putting $\langle S^z(\tau) \rangle = -1/2$ in (7.1.23). Since the first term is common for both initial conditions, it cancels out. This subtraction thus only manifests itself in the second term of Eq.(7.1.23). The detected signal in a Time Resolved Differential Reflectivity experiment is the difference of the reflectivities when the sample is initially excited and when the QDs are in their ground state. Then we can write

$$\Delta R(\tau) = R(\tau) - R_0(\tau) \simeq -\frac{r_s \hbar \Omega_0^2 \omega_L^2 T^2}{2cd} N_{pr} \sin\left(\frac{2\omega_L nd}{c}\right) W(\tau), \quad (7.1.24)$$

$$W(\tau) = W(0) e^{-\Gamma\tau}, \quad (7.1.25)$$

with the initial population $W(0) = \langle S^z(0) \rangle + 1/2$. The variation of W is like

$$-\frac{1}{2} < \langle S_j^z(\tau) \rangle < \frac{1}{2} \rightarrow 0 < W(\tau) < 1. \quad (7.1.26)$$

Eqs.(7.1.24) and (7.1.25) are the main results of this section. Some important features are clear in the differential reflectivity signal. First of all, the total reflected beam from the sample is a superposition of the field emitted from the QD layer and the field reflected directly from the front surface of the sample. Depending on the distance between these two surfaces, this superposition can be either constructive or destructive. This effect manifests itself mathematically in the phase shift factor $\sin(2\omega_L nd/c)$ presented in Eq.(7.1.24). Another important issue about the transient reflectivity is that the TRDR signal at any delay time, is proportional to the population at that time. This population decays with a rate that has been derived and extensively explained in the previous chapter.

7.2 Sample details

The time resolved differential reflectivity experiment is implemented on a five-layered self-assembled InAs/GaAs QD sample grown by molecular beam epitaxy on (100) GaAs, by employing the Stranski-Krastanow (SK) growth mode. First, a 295 nm GaAs buffer layer was deposited at 580°C. Then the temperature was lowered to 490°C for the growth of five layers of QDs. Each layer constitutes of a 30 nm layer of GaAs followed by 2.1 MLs of InAs which forms the QD layer. The separation of the QD layers is large enough to guarantee that there is not any electronic coupling between them. Finally, the sample is capped with a 137nm GaAs layer at a temperature of 580°C. Atomic Force Microscopy (AFM) images (Fig.(7.2)) of the uncapped sample, show that the QDs are distributed on planes with an areal density of $2.8 \times 10^{10} \text{cm}^{-2}$, implying that the average QD-QD distance is approximately 60nm. The photoluminescence spectrum of this sample at 5K and the excitation energy of 1.59eV is presented in Fig.(7.3). At a high excitation power of 5kW/cm², we can fit the PL spectrum with a sum of two Gaussian functions. The first peak is the QD ground state (GS) at a transition energy of 1.105

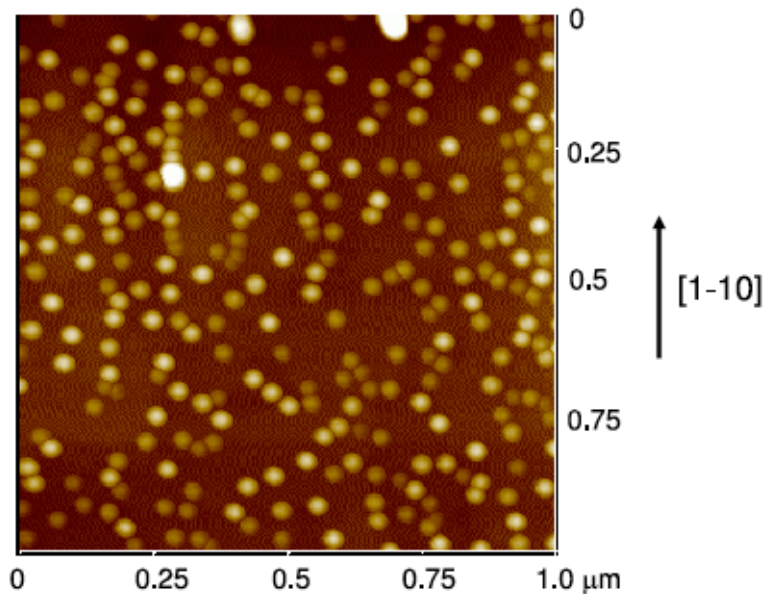


Figure 7.2: Atomic Force Microscopy (AFM) image of uncovered InAs/GaAs QDs. The sample area in this figure is $1 \times 1 \mu\text{m}$ and the black-to-white height contrast is 15nm, Ref [213].

eV while the second peak is the QD excited state (ES) which is centered at 1.15 eV. The spectral widths of the ground and the excited states are 19 and 40 meV respectively. In our TRDR experiments, as long as the excitation power remains below 1000 kW/cm^2 , only the QD ground states will be populated and we can ignore the first excited state. However, we also performed an experiment as a function of the excitation density up to 1.75 kW/cm^2 , where the excited state might be partially populated.

7.3 Charge carrier dynamics in InAs/GaAs quantum dots

By employing the TRDR technique, we are able to track the charge carrier dynamics in a QD. The pump laser pulse generates charge carriers in the GaAs barrier by exciting the sample with photon energy above the GaAs bandgap. The photogenerated carriers will first diffuse towards the QDs and subsequently be captured into the QD confinement states, possibly by using the wetting layer as an intermediate state for carrier capture. The captured charge carriers subsequently relax further to the QD ground state, unless the ground state becomes fully occupied, at which point the excited QD levels will also become initially populated. In the case of InAs/GaAs QDs, this cascade-like relax-

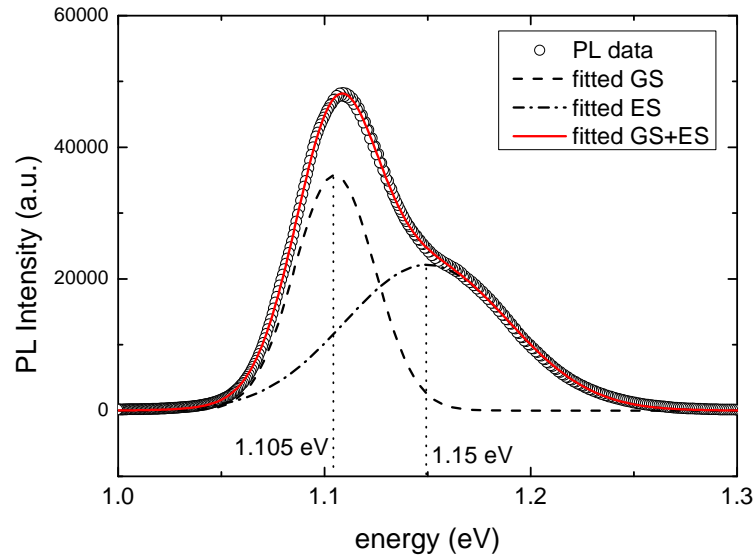


Figure 7.3: The PL spectrum of self-assembled InAs\GaAs QDs at 5K and the excitation energy of 1.59 eV, fitted with two Gaussian distributions. The peak of the Ground state (GS) transition energy is at 1.105 eV with a spectral width of 19 meV and the peak of the Excited State (ES) is at 1.15 eV with a spectral width of 40 meV.

ation of charge carriers from the higher excited states to the lower states mediated by carrier-carrier scattering (Auger effect) [214,215] or multiphonon emission [215,216] has been already reported, based on integrated Photoluminescence (PL) and the Time Resolved Photoluminescence (TRPL) experiments. In some other works, the simultaneous fast filling of the QD states with a short capture time is concluded which can mainly originate from the diffusion of charge carriers in the GaAs barrier [217], multiphonon relaxation of the excited hole states [218] or an efficient Auger relaxation [219]. The simultaneous capture of photogenerated carriers from the GaAs barrier to the QD levels has been also verified in Ref. [220,221] through a set of pump-power dependent TRPL measurements, under a relatively high pump power ($860\text{W}/\text{cm}^2$). They claim that such a fast capture or correspondingly relaxation time at least for relatively high pump power densities, occurs through a finite continuum of density of states, as already observed by Toda *et al* [222]. It could be also related to the existence of intrinsic crossed transitions of hybrid dimensionality (0D-2D) between the bound QD states and the delocalized states [223]. However, it has been shown for InP QDs that the carriers relax to lower QD energy levels by undergoing stepwise (cascade) relaxations from the higher energy levels [224]. The review of the literature indicates that there is not yet a comprehensive theory to explain the relaxation mechanisms of charge carriers from the barrier and wetting layer towards the QD lower energy levels. It seems that the relaxation mechanism is greatly sensitive to the type of QD, the sample structure and the growth condition. In

a certain sample, one or several relaxation channels may occur at the same time.

Recombination of electron-hole pairs, or excitons, occurs through radiative recombination at low temperature. The radiative recombination rate strongly depends on the photonic reservoir in the environment surrounding the QDs. The photonic density of states in a photonic reservoir depends on the geometry of the medium that contains the QDs as well as on the spatial and spectral distribution of the QDs. The modification of the radiative recombination rate is the main focus of this thesis and has been theoretically investigated for different QD systems in the previous chapters. In this chapter, we present experimental evidence for the modification of the radiative decay times (inverse of radiative recombination rate) for an ensemble of self-assembled InAs/GaAs QDs. In these samples, the QDs have different sizes and are randomly distributed in the sample. The QD size distribution follows a Gaussian function for both the ground and excited states as depicted in Fig.(7.3). In next sections we will investigate the radiative decay times in more detail.

7.4 Time Resolved Differential Reflectivity experimental setup

In TRDR technique, the pump beam generates charge carriers in the GaAs barrier, which subsequently populate the lowest available QD states. The occupation of the QD states by charge carriers induce an absorption bleaching on their corresponding optical transitions. As depicted schematically in Fig.(7.4), a 76.6 MHz mode-locked Titanium-Sapphire (Ti:Sa) laser generates pump pulses which are horizontally polarized and have a hyperbolic-secant-squared shape with a pulsewidth of 1.6 ps and a corresponding spectral width of 1 meV. The pump beam hits the sample under an angle of 45° with respect to the QD plane and is focused to an area of approximately $55\mu\text{m}$. The sample is kept in a cryostat which provides a temperature of 5K. The photo-generated population in the QD, modifies the complex dielectric constant of the QD medium which in turn modulates the optical absorption and reflection of the QD.

The pump induced population dynamics in the QD sample can be monitored by a probe pulse which is tuned into resonance with the QDs. The probe pulse is the output of the Optical Parametric Oscillator (OPO) [226,227] which is synchronously pumped by the same Ti:Sa laser and tunable between 1030 and 1300 nm. The spectral width of the probe laser is identical to the spectral width of the pump laser and is approximately 1 meV. The probe laser is thus resonant with a subset of QDs with an average spacing of 460 nm between the resonant QDs at the center of the QD size distribution. Since the OPO is synchronously pumped by the Ti:Sa laser, the pump and probe pulses have a fixed time delay and can be employed for two-color pump-probe differential reflectivity measurements. The delay time between the pump and the probe pulses is changed by an optical delay line which can be moved by a stepper motor. The length of our optical delay line allows for a 2.5 ns maximum time delay. The probe beam is focused perpendicularly on the sample by means of a graded index lens and has a spot size of approximately $25\mu\text{m}$.

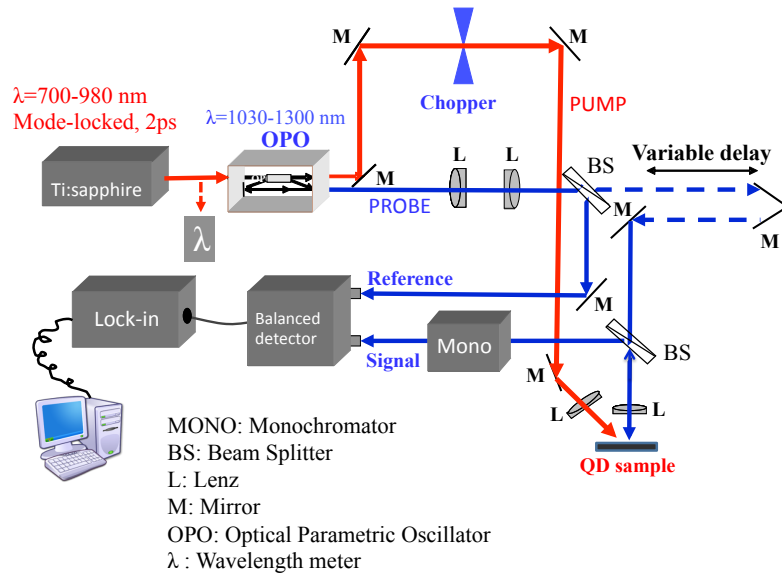


Figure 7.4: Experimental setup of the Time Resolved Differential Reflectivity spectroscopy (Reprinted from ref. [225])

The reflection of the probe beam from the sample is collected with the same lens and is detected by a balanced photodetector. A balanced photodetector is used to significantly suppress the probe laser intensity noise. We put a monochromator (MONO in the picture) right before the detector to filter out residual pump laser light as well as emitted PL from the sample. The signal due to the probe laser reflection is synchronously amplified with a lock-in amplifier and is finally sent to the computer. By mechanically chopping the pump beam and by measuring the reflected probe intensity with a lock-in amplifier, the pump induced changes of the QD population are monitored. We measure the differential reflectivity $\frac{\Delta R}{R_0} = \frac{R - R_0}{R_0}$ as a function of the pump-probe delay time where R is the probe reflectivity when the sample is pumped and R_0 is the reflectivity when the sample is not excited. Reflectivity transients are recorded at time intervals of 2 ps for the rising edge and at a time interval of 60 ps at the trailing edge in order to speed up the TRDR measurements. An example of such a TRDR measurement is shown in Fig.(7.5).

7.5 Pump-power dependent measurement

The decay of the TRDR signal for three different pump powers is shown in Fig.(7.6). It is clear from this figure that the TRDR decay time strongly depends on the initial

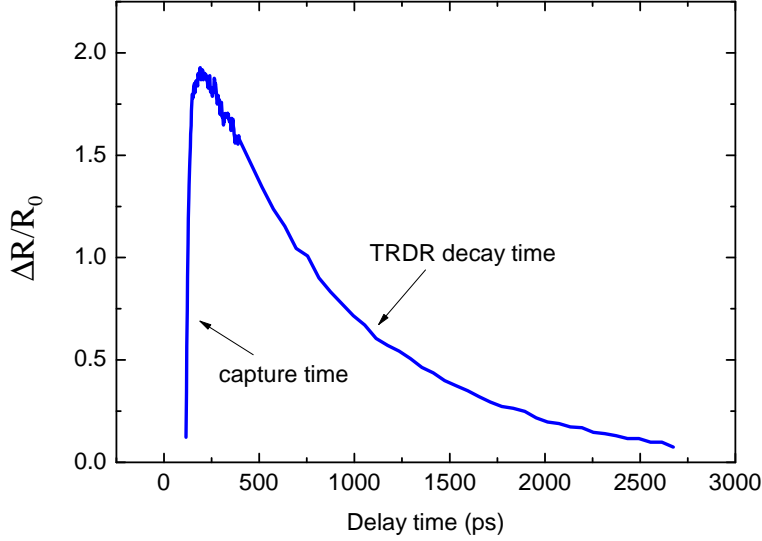


Figure 7.5: The measured differential reflectivity signal as a function of the pump-probe delay time.

excitation of the sample which in turn is a function of the pump power. Here, we try to explain this behavior qualitatively. In the first section of this chapter, we showed that, in TRDR experiments we actually measure the dynamics of the QD population. On the other hand, in the previous chapter, we derived the spontaneous decay rate of a dilute sample of resonant self-assembled QDs as

$$\Gamma = \Gamma_0 \left[1 - \frac{17}{24} \left(\frac{N_\lambda \Gamma_0 \langle S^z(0) \rangle}{2\pi^2 \Gamma} \right)^2 + \dots \right], \quad (7.5.1)$$

where N_λ is the number of resonant QDs within a cubic wavelength, Γ_0 is the homogeneous linewidth of the single QD and $\langle S^z(0) \rangle$ is the averaged initial excitation of the sample and varies between $-1/2$ and $1/2$. The higher orders of the expansion in (7.5.1) are negligible, as compared to the first two terms.

The initial excitation of the sample obviously depends on the pump power. At higher pump power, the number of photogenerated charge carriers in the barrier increases and the number of charge carriers which diffuses towards the QDs and is captured into the QDs, also increases. But, the relation between the number of photogenerated charge carriers and the occupation of the QD ground state is not linear. It is actually only linear for low pump powers, but tends to a finite value for a sufficiently large pump powers. This is a kind of saturation effect and is caused due to the finite number of QDs in the sample which host the generated electron-hole pairs (excitons). Considering QDs as simple two-level objects, the ratio of the number of excited QDs, N_{exc} , and the total

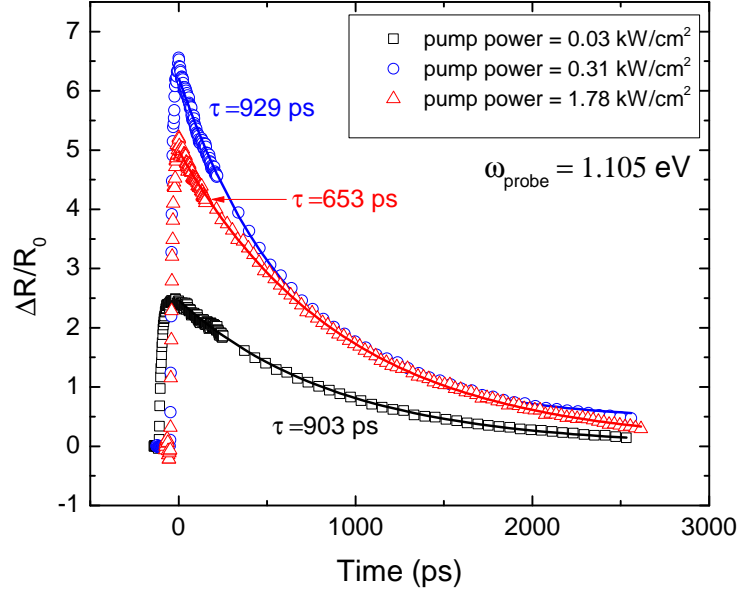


Figure 7.6: Experimental TRDR decay traces, measured at three different pump powers. The solid lines are the corresponding fitted single exponential functions. The probe power in this experiment is 800mW/cm².

number of QDs, N_{sat} , follows an exponential equation [202],

$$\frac{N_{\text{exc}}}{N_{\text{sat}}} = 1 - e^{-k_{\text{abs}} I_{\text{pump}}}, \quad (7.5.2)$$

where k_{abs} is an absorption cross section (area), and I_{pump} is the total number of photons per unit area per pulse. The parameter k_{abs} is more a fitting parameter and can be directly deduced from experimental pump-power dependent measurements and specifically from the point at which the excitation decay time becomes minimum. Making use of the Eq.(7.5.2) and the definition $\langle S^z(0) \rangle = (N_{\text{exc}}/N_{\text{sat}}) - 1/2$, Eq.(7.5.1) can be written in the form,

$$\frac{\Gamma}{\Gamma_0} \simeq 1 - \frac{17}{24} \left(\frac{N_{\lambda} \Gamma_0}{2\pi^2 \Gamma} \right)^2 \left(\frac{1}{2} - e^{-k_{\text{abs}} I_{\text{pump}}} \right)^2. \quad (7.5.3)$$

The normalized decay time of the spontaneous emission ($\tau/\tau_0 = \Gamma_0/\Gamma$) from an infinitely large and uniform sample of self-assembled QDs as a function of the pump power density has been simulated by means of Eq.(7.5.3) and is shown in the bottom graph of Fig.(7.7). For this simulation, we have assumed the density of QDs to be $N = 2.2 \times 10^{11}$ QD/cm² and the absorption cross section was fitted to be $k_{\text{abs}} = 1.74 \times 10^{-6}$ cm². This parameter has been deduced from the position of the minimum of the experimental data in the upper graph of Fig.(7.7). This simulation is performed

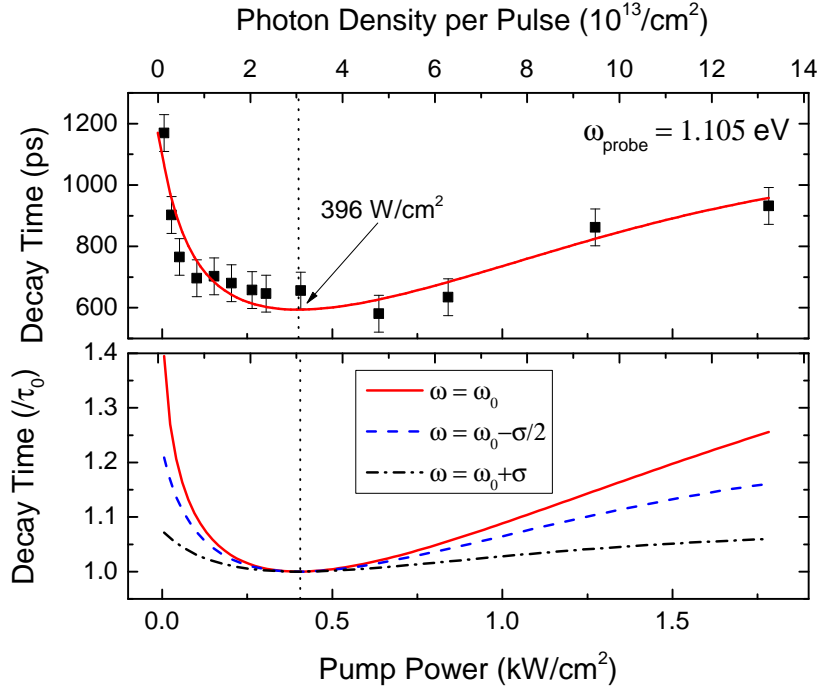


Figure 7.7: (Top) The experimental TRDR decay time as a function of the pump power. The solid line is for making the data more traceable and is not a fitting. The minimum of the decay time occurs around the pump power of $396 \text{ W}/\text{cm}^2$. The probe power is $800 \text{ mW}/\text{cm}^2$. The absorption cross section obtained that gives rise to this value of pump power is $k_{\text{abs}} = 1.74 \times 10^{-6} \text{ cm}^2$. (Bottom) Theoretical simulation of the decay time of the QD excitation, based on the theory of the collective spontaneous emission of self-assembled QDs introduced in chapter 6. In this simulation, the absorption cross section that is obtained from the experimental data has been used.

for three groups of resonant QDs. One group belongs to the QDs which are probed at the center of the size distribution ($\omega = \omega_0$) of the QD size distribution which has a Gaussian lineshape with broadening σ . One group belongs to a set of QDs probed on the left tail ($\omega = \omega_0 - \sigma/2$) and another one to a set of QDs probed on the right tail ($\omega = \omega_0 + \sigma$) of the QD size distribution. This simulation graph predicts two interesting consequences. First, we observe that for QDs which are closer to the centre of the QDs size distribution, the variation of the spontaneous decay time is stronger. This means that, for any fixed pump power, the decay time is larger for QDs near the centre of the QD size distribution, which have a higher density within the sample. This effect will be discussed in more detail in the next section. Another important prediction of this simulation is that the emission decay time has a minimum for a certain pump power at which half of the QDs are excited. For all other pump powers, either at lower or at higher power, the decay time is larger. This is a counter-intuitive quantum effect for the spontaneous emission decay time. One might think that the electromagnetic coupling

between the QDs is stronger when all QDs are initially excited and inversely, the electromagnetic coupling between the QDs is very weak in the limit of very low pump powers, since for sufficiently low pump power, only one QD is excited, and one might think that this singly excited QD should decay with emission rate of a single isolated QD. But, as is clear from Fig.(7.7), this is not the case and the decay tends to its slowest rates at both very low and very high pump powers. In fact, the system evolves in the same way when the sample is either excited very strongly or very weakly. Contradictory to the classical view, in the case when only one single QD is excited, the electromagnetic interaction between the QDs is strong and the QD system decays with the slowest possible collective decay rate and undergoes the maximum radiation trapping effect. We should emphasize here that in such a system, we don't know which single QD is excited. This is a crucial condition which can in turn give rise to a strong modification of the decay time in the limit of low pump power. Of course, this phenomenon occurs also at very high excitations. In fact, the decay time of the QD system is the same for the cases where either one QD is initially excited and all other QDs are empty or all QDs except one are excited. That's why the effect of radiative coupling vanishes when half of the QDs are excited and the spontaneous decay time is symmetric around this point. This means that the radiation trapping effect is absent at this point and the QD decays with its natural decay rate in a homogeneous medium. We have experimentally verified this phenomenon as is shown in the upper graph of Fig.(7.7). This experiment is done for QDs which are probed in the centre of the QD size distribution and the probe power density is $800\text{mW}/\text{cm}^2$.

Of course, we don't observe a complete symmetrical distribution of decay times in Fig.(7.7), which originates from the fact that there is not a linear relation between the pump power and the number of excited QDs. This relation is actually an exponential function which is introduced in (7.5.2). For the sake of a more precise interpretation of our experimental pump-power dependent decay times, we split our data into two regimes. One for low pump powers, in which less than half of QDs are initially excited and another one for higher pump powers. We do this splitting because in reality, a QD is not a simple two-level system, and the excited state transition should also be taken into account. Moreover, the QD ground-state itself is degenerate and can potentially host two electron-hole pairs, forming a biexciton. However, our theoretical simulations are based on the interaction of two-level objects. At low pump powers, we can claim that the contribution of the biexciton and the QD excited state is weak. In a good approximation, we are dealing with singly occupied ground-state excitons within the QDs. In this regime, our theoretical simulations and experimental data are in a good qualitative agreement. Up to our knowledge, we observe the decrease of the radiative decay time with increasing pump power for the first time in QD samples. For low pump powers, the electromagnetic coupling of QDs is stronger for lower excitation and hence the *radiation trapping* phenomenon becomes more feasible at lower excitations.

The situation becomes more complicated in the regime in which the pump power is high enough to excite more than half of the QDs. Since, by further increasing of the pump power, the contribution of the biexciton and the excited state excitation becomes more and more important. When the excited state is populated, after each decay of a ground state exciton, the ground state is refilled by relaxation of charge carriers from

the excited state. This combination of the refilling and decaying processes increases the overall experimentally observed TRDR and TRPL decay time. When there is state filling of the ground-state at high pump powers, we should basically observe a plateau-like variation of the ground-state decay at early times of the decay. This is because of the refilling of the ground-state by relaxation of carriers from the excited-state. But we don't observe such an effect even at very high pump powers. Although we don't observe any slow decay of the ground-state at initial times of the decay and the variation of our experimental decay times apparently matches our theoretical simulations quite well, we cannot claim that the increase of the TRDR decay time with pump power in the high pump-power regime is only due to the radiative coupling of QDs. We conclude that the measured increase of the TRDR decay time at low excitation is due to the radiation trapping effect while the increase of the TRDR decay time at high excitation is due a (presently unknown) mixture of the radiation trapping effect and the refilling of the ground state from the excited state.

In Fig.(7.7), there is obviously a good qualitative agreement between our experimental results and the simulations based on the theory introduced in the previous chapter.

7.6 Probe-frequency dependent measurement

In the previous section, we explained the influence of the initial excitation on the decay time of the differential reflectivity or correspondingly on the lifetime of QD excitation. We already mentioned that the density of resonant QDs plays a very important role on the modification of the lifetime of the QD excitation. In this section, we focus on this phenomenon in more detail. As you can see in Fig.(7.8), we have measured the decay of the TRDR as a function of the pump-probe delay time at a series of probe energies. The probe power in this experiment is $800\text{mW}/\text{cm}^2$. The graph on the left belongs to a relatively low pump power ($100\text{W}/\text{cm}^2$), where only the QD ground state contributes to the reflectivity. This is confirmed also by Fig.(7.9)(a) in which the spectrum of the TRDR amplitudes, fully matches the QD ground-state distribution. This also provides experimental evidence for Eq.(7.1.24) since it shows that the TRDR amplitude is proportional to the number of QDs that are in resonance with the probe pulse. For low pump power, the TRDR decay curve in Fig.(7.8)(a) can be fitted by a single-exponential function. It can also be seen that the decay time of such a single-exponential decay strongly depends on the frequency (energy) of the probe pulse with respect to the centre of the QD size distribution. In Fig.(7.8)(b), we have repeated this series of measurements at a 10 times larger pump power ($1\text{kW}/\text{cm}^2$). In this case, an additional channel takes part in the reflectivity due to the population of the first excited state of the QD. The TRDR amplitudes for this series of measurements is plotted as a function of the probe energy in Fig.(7.9)(b). You can see that the largest amplitude is near the centre of the QD excited state. This reveals that, in the case of really high pump powers, the population of the excited-state exciton has a strong contribution to the reflectivity from the sample. As is clear from Fig.(7.8)(b), the TRDR signal initially decays very fast with a decay time of less than 100 ps and then decays much more slowly with a decay time in the order of nano seconds. Consequently, we have fitted the TRDR decay curves with a double-exponential

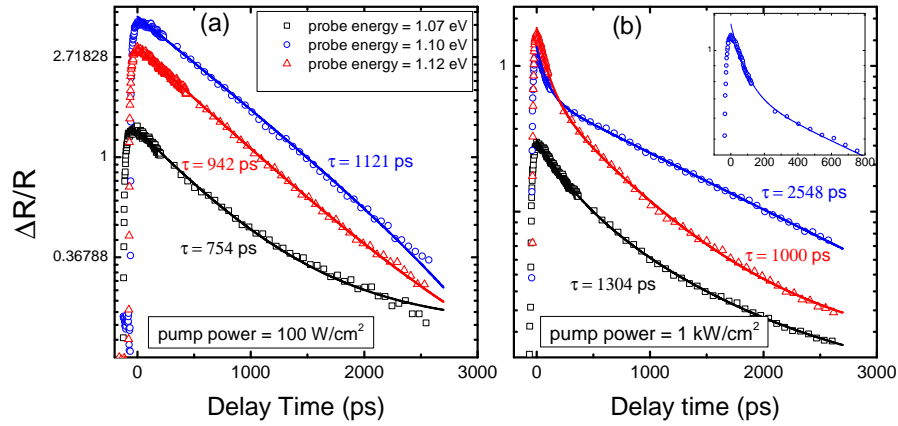


Figure 7.8: The TRDR signal as a function of the pump-probe delay time for (a) pump power of $100\text{W}/\text{cm}^2$ and (b) $1\text{kW}/\text{cm}^2$, at a probe energy of 1.07 eV (square), 1.10 eV (circle) and 1.12 eV (triangle). The TRDR decays in the low pump power case (a) are fitted by a single exponential function, while the TRDR decays in the high power case (b) are fitted by a double exponential function. The inset on the right hand side graph is a zoom over the early-time decay of the TRDR to clarify the fast overshoot of the decay. The solid lines are the fitted functions to the decay part of the TRDR. The probe power in this experiment is $800\text{mW}/\text{cm}^2$.

function. The corresponding amplitudes of the fast and slow channels of the decay are separately shown in Fig.(7.10) as a function of the probe energy. We observe that the highest amplitude of the faster channel is close to the centre of the QD excited-state distribution. This means that this channel originates from the QD excited state population. For the slower channel, we observe a peak near the centre of the QD ground state distribution, as well as an increase towards the centre of the QD excited-state distribution, for probe energies above 1.13 eV . This behavior is understandable since in this range of energies, we mainly probe the excited-state excitation. But, for energies less than 1.13 eV , we are in the spectral range of the ground-state transition and we can claim that we only measure the ground-state lifetime below 1.13 eV . In this thesis, we don't study the relaxation mechanisms inside or recombination rates of the excited-state excitons and we focus only on the decay of the ground-state excitons (slower channel).

The TRDR decay time of the QD ground-state excitation is plotted in Fig.(7.11)(a) as a function of the probe energy for both low and high pump-powers. In both cases, we clearly observe that the TRDR decay time is larger for QDs close to the centre of the QD ground-state distribution. This is a strong evidence for the electromagnetic interaction between the QDs. Since, the QD-QD coupling is proportional to the QD density that is resonant with the probe laser, we expect stronger electromagnetic QD-QD coupling, and thus a longer TRDR decay time, near the peak of the PL spectrum as compared to the tail of the PL spectrum. An important consequence of this experiment is that a stronger QD-

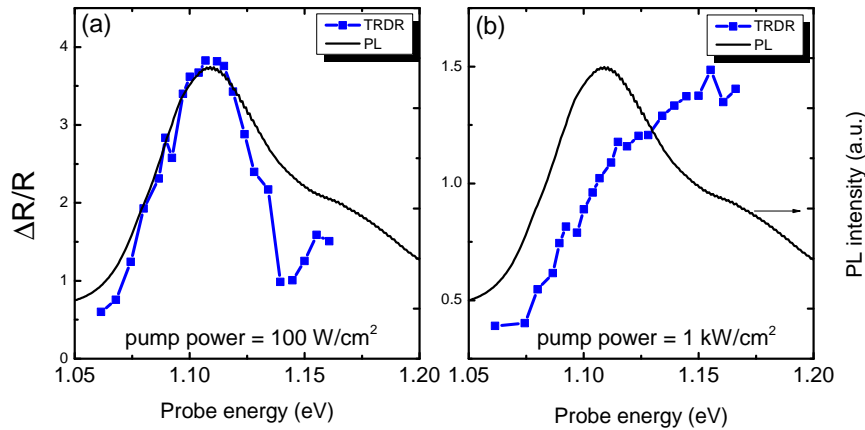


Figure 7.9: The amplitude of the TRDR decay for a pump power of (a) $100\text{W}/\text{cm}^2$, and (b) $1\text{kW}/\text{cm}^2$. The amplitude of the reflectivity matches the QD ground state distribution for the lower-power case and the QD excited state distribution for the high-power case. The probe power in the TRDR experiment is $800\text{mW}/\text{cm}^2$.

QD electromagnetic coupling gives rise to an enhanced ground-state TRDR lifetime. In fact, in a dense system of many-QDs, like in our sample of self-assembled InAs/GaAs QDs, the ground-state exciton decays slower in denser samples due to the enhanced radiative coupling between the QDs, since the light is trapped in the QD system for a longer time. In literature, this phenomenon is well known as *radiation trapping* which is a collective effect due to the dipole-dipole coupling between the QDs. This phenomenon was theoretically predicted in the previous chapter as a collective quantum effect and is again plotted in Fig.(7.11)(b) to provide a better comparison with the experimental data. We observe a good qualitative agreement between our experiments and our theoretical simulations. Similar to our discussion in the previous section about the pump-power dependent measurements, here we also have to consider the possibility of the contribution of the state-filling effect in the enhancement of the TRDR decay time at high pump powers. Although we don't observe any plateau-like variation of the ground-state decay at early times and the spectral shape of the TRDR decay time distribution is in a good qualitative agreement with our theoretical prediction, we cannot ignore the influence of the state-filling at high pump powers. We should emphasize here that if there is any state-filling from the excited-state, this effect should be basically uniform for all QDs within the QD size distribution. State filling hence is not able to explain the observed Gaussian-shape spectral distribution of the ground-state decay times. However, state filling probably increases all decay times with the same factor. That's why we conclude that the Gaussian shape of the decay time distribution mainly originates from the radiative interaction between the QDs.

It can be easily observed from Fig.(7.11), that the width of the decay time distribution

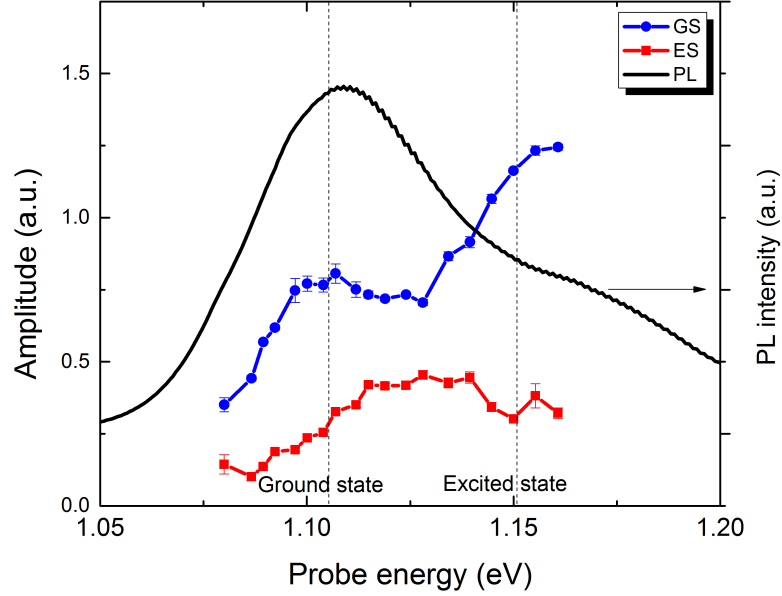


Figure 7.10: The amplitude of the fast decaying (squares) and the slowly decaying (circles) part of the TRDR decay transients for high pump powers ($1\text{kW}/\text{cm}^2$). The probe power in the TRDR experiment is $800\text{mW}/\text{cm}^2$.

is much narrower than the width of the QD size distribution, which is equal to the width of the ground-state PL spectrum. After fitting the decay time distribution with a Gaussian function, we find that the width of the decay-time distributions is 13.6 meV and 11.3 meV for low and high pump power respectively, while the width of the QD size distribution is 19 meV , as obtained from Fig.(7.3). Indicating the width of the PL-spectrum by σ , the width of the decay-time distribution is 0.72σ for low pump power and 0.59σ for high pump-power. In the theoretical simulation, the width of the decay time distribution is 0.71σ which is very close to the corresponding experimental values. The reason for this narrowing can be easily deduced from Eq.(7.5.3). The radiative decay time of an ensemble of QDs is proportional to the square of the resonant QD density. As is shown in Fig.(7.3), the QD size distribution can be described by a Gaussian function,

$$N_\lambda \propto e^{-\frac{1}{2}\left(\frac{\omega-\omega_0}{\sigma}\right)^2}, \quad (7.6.1)$$

with $\omega = 2\pi c/\lambda$, and the decay time distribution ($\tau = 1/\Gamma$) becomes, using Eq.(7.5.3),

$$\frac{\tau}{\tau_0} \propto N_\lambda^2 \propto \left(e^{-\frac{1}{2}\left(\frac{\omega-\omega_0}{\sigma}\right)^2}\right)^2 = e^{-\frac{1}{2}\left(\frac{\omega-\omega_0}{0.71\sigma}\right)^2}. \quad (7.6.2)$$

We again observe a good qualitative agreement between our experimental TRDR decay time versus the probe energy and the theoretical simulation of the excitation lifetime

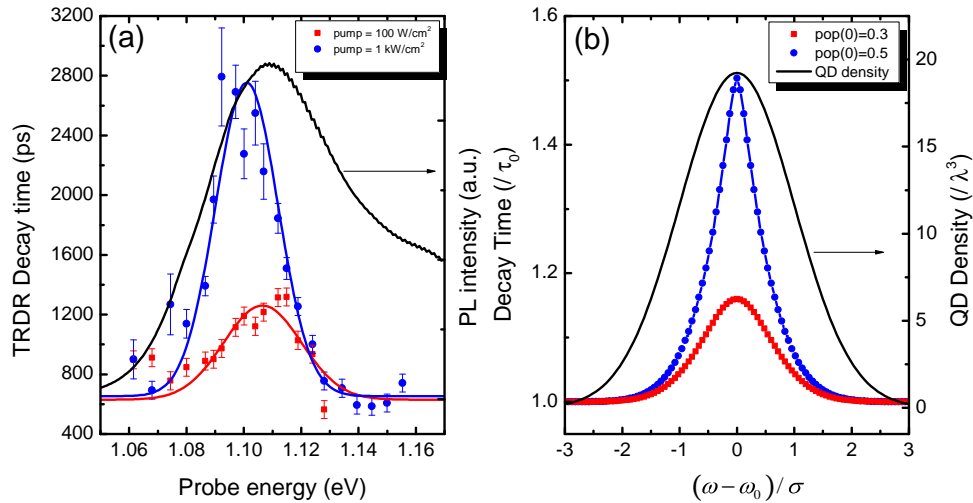


Figure 7.11: (a) On the left axis, the experimental TRDR decay time for low pump power, 100W/cm² (squares), and for high pump power, 1kW/cm² (circles). On the right axis, the PL intensity measured at 4K and the excitation energy of 1.59eV. The probe power is 800mW/cm². (b) On the left axis, theoretical simulation of the spontaneous QD decay time as a function of the QD transition frequency. On the right axis, a graph of the QD size distribution which is in fact the fitting of the ground-state part of the PL spectrum with a Gaussian function as shown in Fig.(7.3).

of an ensemble of QDs. In Fig.(7.11), we also observe the influence of the initial pump power excitation on the TRDR decay time. The TRDR decay time for strongly pumped 1kW/cm² QDs is much larger than for weakly pumped 100W/cm² QDs. This effect has already been extensively discussed in the previous section for a larger variety of pump powers.

We observed very good qualitative agreement between theory and experiment, but not yet full quantitative agreement. This might be due to the approximations that we had to make. For example, we have theoretically assumed that our sample is infinitely large, but our experimental sample is limited by the limited size of the pump spot on the sample. Another assumption in our theoretical approach is that all QDs are uniformly distributed in the sample, which is of course not completely true. Our simulations can qualitatively interpret our experiments, which means that the physics behind our simulations also governs our experiments. We believe that, in our TRDR experiments, we are able to measure the effect of electromagnetic coupling between the QDs on the lifetime of the ground-state excitons in QDs. This radiative coupling is mediated by the long-range dipole-dipole interaction between QDs. The important message of this chapter is that in self-assembled QD samples, in which cooperative effects are absent due to the large inhomogeneous broadening, it is still possible to observe a collective quantum ef-

fect like radiation trapping. The crucial condition of the corresponding quantum state is that we don't know which QDs are initially excited. We indicated both theoretically and experimentally that in denser samples, the radiative coupling between the QDs is more effective and the lifetime of the QD sample is longer than the decay time of an isolated QD. We also showed that when half of the QDs are excited, the radiative coupling effect vanishes. When only one single QD within the QD-ensemble is excited or all QDs are excited except one single QD, the influence of the radiative coupling is maximum and the QD system shows its longest exciton lifetime.

7.7 Time Resolved Photoluminescence (TRPL) experiments

Regarding the pump-power dependent effects, we already referred to some works on the relaxation mechanism of photogenerated charge carriers in QD samples by means of the integrated PL and TRPL techniques [214–221]. In almost all of these investigations, the state filling effect has been observed for the QD ground-state at high excitation powers. The plateau-like variation of the QD excitation at the early times of the decay is a sign of the state filling. In this situation, the decay of the ground-state occurs simultaneously by relaxation of charge carriers from higher energy levels that in turn enhances the overall decay time of the QD ground-state by increase of the excitation density. However, we don't observe any trace of the state filling of the ground state in our pump-probe experiment even at high pump powers. This supports our position to attribute the observed pump-power dependent effects of our experiments mostly to the collective radiative processes especially that they are in a good qualitative agreement with our theoretical predictions. But we still prefer to keep this probability as well that the enhancement of the decay time of the ground-state excitation might be partially due to the state filling effect particularly at high pump powers. However, we should emphasize that up to our knowledge, the decrease of the decay time by increase of the pump power in the low pump-power regime has been reported only in one TRPL-based article [228] as shown in the inset of Fig.(7.12)(a). In that work, they interpret this behavior in this way that at low pump powers, the coupling of QDs is very weak and the QDs decay with their natural decay time. By increasing the pump power, the correlation between QDs grows up and hence the TRPL decay time decreases due to the superradiant phenomena. But further increase of the excitation power leads to the saturation of the QD ground-state, resulting in a progressive increase of the decay time. According to the introduction and early discussions of chapters (6) and (7), the cooperative effects like superradiance is not likely in two-level samples with large inhomogeneous broadening. That's why we think this justification is not so accurate and a full excitation-power dependent analysis based on local-field corrections such as our approach in the current and previous chapters of this thesis is required.

There have also been some TRPL-based works in the past decade on the transient decay time as a function of the detection energy which actually represents the QD transition energy in the ensemble. Comparing these papers to each other, we don't see a unique pattern for the variation of the decay time as a function of the energy. For example,

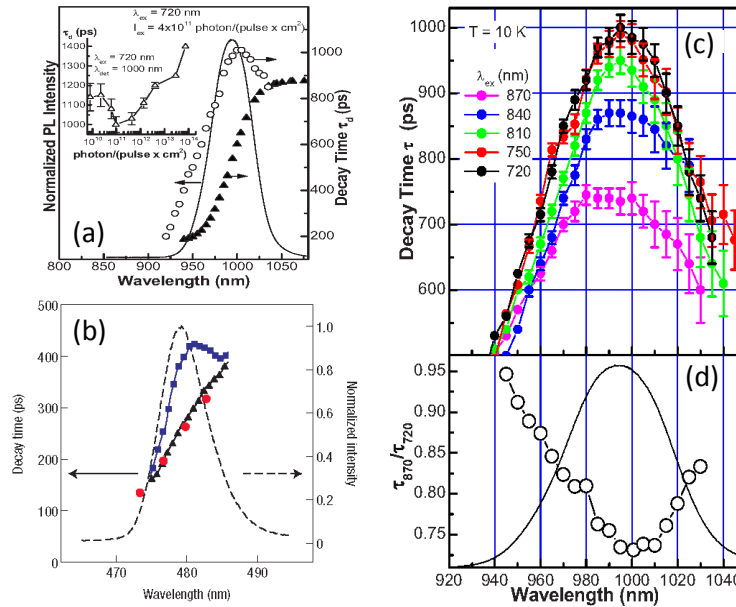


Figure 7.12: (a) TRPL decay time at different detection wavelengths. The inset is the TRPL decay time as a function of the pump power. Graph from Ref. [228] (b) TRPL decay time at different detection wavelengths for non-resonant and quasi-resonant excitation. Graph from Ref. [56]. (c) TRPL decay time as a function of the detection wavelength for a range of excitation wavelength from non-resonant (720 nm) to quasi-resonant (870 nm) excitations. (d) ratio of the corresponding decay times of the quasi-resonant and non-resonant excitations at different wavelengths. Graphs in (c) and (d) from Ref. [228].

in Refs. [229] and [198], they don't observe any QD-density dependent effect. In fact, they observe that the decay time decreases with the increase of the transition energy almost linearly. However, in some other works, a QD-density dependent PL decay times similar to what we observe in our TRDR-based experiment is reported. For instance, Scheibner *et al.* [56] indicate a peak for the lifetime (decay time) of CdSe (ZnSe) under non-resonant excitation with energy above the barrier (Fig.(7.12)(b)). Of course the focus of this paper is on the QD lifetimes under quasi-resonant excitation and they use the non-resonant lifetimes as a reference to show the superradiance phenomena and the minimum of the lifetime at the maximum of the PL spectrum. Although such a QD-density dependent decay time is to some extent observed in this paper as radiation trapping even for non-resonant excitation, but they don't present a reasonable reason for this phenomena. A similar effect is reported in Ref. [228] for In $_{0.4}$ Ga $_{0.6}$ As QDs and is shown in Fig.(7.12)(c). they clearly observe a QD-density dependent variation of the QD lifetime very similar to our results for various excitation energies in a range from the quasi-resonant to above the barrier. In all cases, a peak of the decay time is observed

at the maximum of the PL spectrum. As you can see in Fig.(7.12)(d), the ratio of the quasi-resonant and the non-resonant decay times has a minimum at the peak of the PL spectrum. Following the same logic of Ref. [56], this phenomena is attributed to the superradiance effect. But also in this paper, they don't present any clear reason for the density-dependent decay time under non-resonant excitation.

In the theoretical development of the radiation trapping, we assumed that the active region of the sample is infinitely large. This means that the pump-laser spot size should be much larger than the emission wavelength otherwise, we probably don't observe any collective radiative effect. Moreover, the excitation power density is also important and plays a significant role in determining the values of the decay times. In the papers that we see some similarities with our results [56, 228], the size of the active area and the excitation power density are not clear, but in Ref. [229] and [198] that we don't see any evidence for the QD radiative coupling, the excitation power density is very low and almost 10 times weaker than our lowest pump-power density. Concentrating on the lower pump-power spectrum of the decay time in Fig.(7.11), you can imagine that if we reduce the pump-power density by a factor of 10, then the variation of the lifetimes with energy may become probably less than the accuracy of the measured lifetimes and the Gaussian-like dependence of the decay time on the energy is no longer observable. At the end, we conclude that the observation of the collective decay time in QD ensembles is very sensitive to the sample size and the excitation conditions. There are similarities between our TRDR-based results and some TRPL-based papers while there are many other TRPL-based papers in literature in which there is not any trace of interaction between the QDs. Although we guess that the differences are due to the sample structures and the excitation levels, but we prefer to keep this discussion open because we have not theoretically or experimentally studied the case of TRPL.

7.8 Summary

In this chapter, we first proved that the Time Resolved Differential Reflectivity (TRDR) signal is directly proportional to the averaged population difference in a QD system. Hence the variation of the TRDR signal with the pump-probe delay time corresponds to the QD excitation dynamics in real-time.

We presented experiments on the TRDR decay time as a function of the pump-power density and the probe energy. We experimentally observed an enhancement of the TRDR decay time for QDs close to the center of the size distribution. This enhancement of the TRDR decay time provides experimental evidence for an electromagnetic coupling between the QDs. The electromagnetic coupling manifests itself as a quantum correction to the local-field in a medium which is both dispersive and absorptive, depending on the optical excitation level. We show that the radiative interaction between the QDs vanishes when half of the QDs are excited and half are empty. In this situation, the QD system decays with the natural decay time of a single isolated QD. However for other excitation levels, the radiative coupling between the QDs gives rise to a slowing

down of the radiative decay time. For example, when only one QD in the ensemble is excited or all QDs except one are excited, the local-field correction in the system yields the maximum modification of the excitation decay time. This effect is due to the emission of light by one QD and the subsequent absorption of the photon by another QD in the ensemble. This process is inherently an incoherent process and is called radiation trapping. In this chapter, we thus presented experimental evidence for the theoretical approach, introduced in chapter (6).

Appendix A

Moments and Cumulants of a probability distribution

Any distribution of a variable can be characterized by a number of features (mean, variance, ...) and the moments of the probability distribution of a random variable are related to these probability parameters. The first moment is referred to as the distribution's mean or expectation value. The expectation value or the average of any function y of the variable X is defined by

$$\langle y(X) \rangle = \int_{-\infty}^{\infty} y(X) f(X) dX, \quad (\text{A.0.1})$$

where $f(X)$ is the probability density function of the variable X . In the 1-dimensional case, the moments of a random variable X are defined as

$$m_1 = \langle X \rangle, \quad m_2 = \langle X^2 \rangle, \quad \dots, \quad m_n = \langle X^n \rangle. \quad (\text{A.0.2})$$

For example, for a Gaussian distribution function $f(X) = \frac{1}{\sigma_X \sqrt{2\pi}} e^{-\frac{(X-X_0)^2}{2\sigma_X^2}}$ where X_0 is the mean and σ_X is the distribution width, the moments of the distribution are

$$\begin{aligned} m_1 = \langle X \rangle &= \int_{-\infty}^{\infty} X f(X) dX = X_0, \\ m_2 = \langle X^2 \rangle &= \int_{-\infty}^{\infty} X^2 f(X) dX = \sigma_X^2 + X_0^2, \\ m_3 = \langle X^3 \rangle &= \int_{-\infty}^{\infty} X^3 f(X) dX = 3\sigma_X^2 X_0 + X_0^3, \\ &\vdots \end{aligned} \quad (\text{A.0.3})$$

In probability theory, the moment-generating function of a random variable X is defined as $\langle e^{sX} \rangle$ with s a real number. The reason for defining this function is that, it can be used

to find all the moments of the distribution. The series expansion of e^{sX} is

$$e^{sX} = 1 + sX + \frac{s^2 X^2}{2!} + \frac{s^3 X^3}{3!} + \dots \quad (\text{A.0.4})$$

Making use of the definition of the moments, we take the expectation value of Eq.(A.0.4), we can write

$$\langle e^{sX} \rangle = 1 + sm_1 + \frac{s^2 m_2}{2!} + \frac{s^3 m_3}{3!} + \dots, \quad (\text{A.0.5})$$

where m_n is the n th moment around zero. In probability theory and statistics, the cumulants of a probability are a set of quantities that provide an alternative to the moments of the distribution. The moments determine the cumulants in a sense that any two probability distributions with identical moments, have identical cumulants as well and vice versa. The cumulants $\langle\langle X^n \rangle\rangle$ of a random variable X , are defined via the cumulant-generating function $g(s)$ which is the logarithm of the moment-generating function as

$$g(s) = \log(\langle e^{sX} \rangle) = \sum_{n=1}^{\infty} \frac{s^n}{n!} \langle\langle X^n \rangle\rangle. \quad (\text{A.0.6})$$

The cumulant-generating function exists if and only if the tails of the probability distribution are dominated by an exponential decay, like a normal or Gaussian probability distribution. The relation between the cumulants and the moments of a distribution function can be easily derived from Eq.(A.0.6),

$$1 + \sum_{n=1}^{\infty} \frac{s^n}{n!} \langle X^n \rangle = \exp\left(\sum_{n=1}^{\infty} \frac{s^n}{n!} \langle\langle X^n \rangle\rangle\right), \quad (\text{A.0.7})$$

Giving rise to the relations

$$\begin{aligned} \langle\langle X \rangle\rangle &= \langle X \rangle, \\ \langle\langle X^2 \rangle\rangle &= \langle X^2 \rangle - \langle X \rangle^2, \\ \langle\langle X^3 \rangle\rangle &= \langle X^3 \rangle - 3\langle X^2 \rangle \langle X \rangle + 2\langle X \rangle^3, \\ &\vdots \end{aligned} \quad (\text{A.0.8})$$

Considering a Gaussian distribution, by replacing Eq.(A.0.3) in Eq.(A.0.8), the cumulants are

$$\begin{aligned} \langle\langle X \rangle\rangle &= X_0, \\ \langle\langle X^2 \rangle\rangle &= \sigma_X^2, \end{aligned} \quad (\text{A.0.9})$$

Where σ_X^2 is the variance of the distribution. The higher-order cumulants become zero.

Appendix B

The local field in a thin layer

Considering the i th QD positioned at \mathbf{r}_i as the probe QD, the electric field radiated by the j th QD at \mathbf{r}_j with electric dipole $\mu_j = \mu_0 e^{-i\omega_j \tau} \mathbf{e}_{\mu_j}$ at the position of the probe QD can be obtained through

$$\begin{aligned} E^j(\mathbf{r}_{ij}, \omega_j) &= -\frac{i}{\hbar} \int_{-\infty}^{\infty} d\tau \mu_j(\omega_j, \tau) \cdot \mathbf{G}_0^{\text{ret}}(\mathbf{r}_{ij}, \tau) \\ &= -\frac{i}{\hbar} \int_{-\infty}^{\infty} d\tau \mu e^{-i\omega_j \tau} \mathbf{e}_{\mu_j} \cdot \mathbf{G}_0^{\text{ret}}(\mathbf{r}_{ij}, \tau). \end{aligned} \quad (\text{B.0.1})$$

Since in the context of the QD-field coupling, the projection of j th QD dipole field on the dipole moment of the probe QD (i th QD) is physically important. Then, E_{ji} , the projection of the field in Eq.(B.0.1) along the probe QD become

$$E^{ij}(\mathbf{r}_{ij}, \omega_j) = -\frac{i\mu}{\hbar} \int_{-\infty}^{\infty} d\tau e^{-i\omega_j \tau} \mathbf{e}_{\mu_j} \cdot \mathbf{G}_0^{\text{ret}}(\mathbf{r}_{ij}, \tau) \cdot \mathbf{e}_{\mu_i}. \quad (\text{B.0.2})$$

By inserting (6.1.37) in (B.0.2), we obtain

$$E_{\alpha\beta}^{ij}(\mathbf{r}_{ij}, \omega_j) = \frac{-\mu}{4\pi\epsilon_0} \left[\delta_{\alpha\beta} \frac{\omega_j^2}{c^2} + \frac{r_\alpha r_\beta}{r^2} \frac{\partial^2}{\partial r^2} \right] \frac{e^{-i\omega_j r/c}}{r}. \quad (\text{B.0.3})$$

According to the definition of the field component presented in Eq.(B.0.3), we can attribute r_α/r and r_β/r to the dipole moment orientations of the emitting and probe QD respectively. We can write Eq.(B.0.3) also in the form of

$$E_{\alpha\beta}^{ij}(\mathbf{r}_{ij}, \omega_j) = \frac{-\mu k_j^2}{4\pi\epsilon_0} \frac{e^{-i\omega_j r/c}}{r} \left[P_1(ik_j r) + P_2(ik_j r) \frac{r_\alpha r_\beta}{r^2} \right], \quad (\text{B.0.4})$$

where $k_j = \omega_j/c$ and

$$P_1(x) = 1 - \frac{1}{x} + \frac{1}{x^2}, \quad P_2(x) = -1 + \frac{3}{x} - \frac{3}{x^2}. \quad (\text{B.0.5})$$

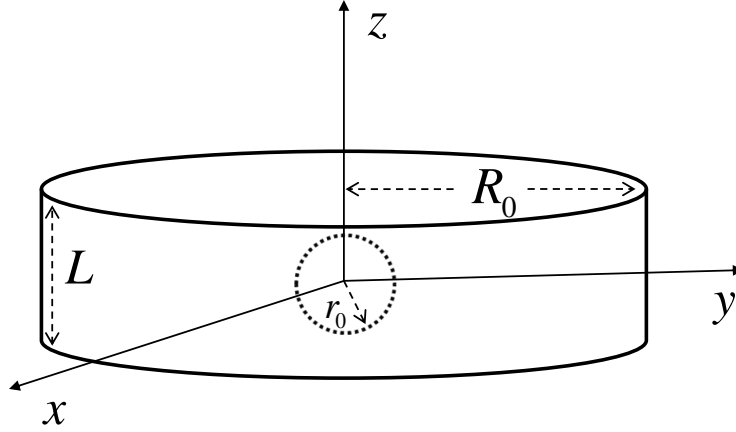


Figure B.1: The shape of the QD sample. The real sample has a disk-like shape which can be approximated by a cylinder with an infinitesimal thickness.

Note that apart from some multiplier constants, Eq.(B.0.4) is equal to the dipole-dipole coupling which has been frequently used in previous chapters. We assume that the QD dipole polarizations are randomly oriented. Then, by averaging over the polarization direction,

$$\frac{r_\alpha r_\beta}{r^2} \rightarrow \left\langle \frac{r_\alpha r_\beta}{r^2} \right\rangle = \frac{1}{3} \delta_{\alpha\beta}, \quad (\text{B.0.6})$$

the retarded Green's function simplifies to

$$E^{ij}(\mathbf{r}_{ij}, \omega_j) = \frac{-\mu k_j^2}{6\pi\epsilon_0} \frac{e^{-ik_j r_{ij}}}{r_{ij}}. \quad (\text{B.0.7})$$

The total field acting upon the probe QD is the sum of the emission from all other QDs. We assume that our medium has a disk-like shape which is actually a cylinder with radius R_0 and an infinitely small thickness L along the z axis as depicted in Fig.(B.1). We choose the origin of coordinates at the center of the disk and we assume that the probe QD is positioned on the origin. We cut out a small virtual sphere of radius r_0 around the probe QD and categorize the QDs into two groups: the QDs inside this sphere and QDs outside the sphere. It has been shown that the contribution of the QDs inside this sphere cancel out the effect of each other and hence the sum of the fields emitted from the QDs inside the virtual sphere is zero at the position of the probe QD [103]. The contribution of the QDs outside the sphere can be calculated in the continuous approximation,

$$E_L = N_v \int_{V-V_0} E^{ij}(\mathbf{r}_{ij}) dV_j, \quad (\text{B.0.8})$$

where N_v is the QD density and V_0 is the volume embedded by the virtual sphere of radius r_0 . Proceeding in the cylindrical coordinates, the position of each QD in the medium is determined by the parameters (ρ, φ, z) in which the distance of any QD from the probe QD is $r = \sqrt{\rho^2 + z^2}$. The integration of Eq.(B.0.8) becomes

$$E_L = \frac{-\mu k_j^2}{6\pi\epsilon_0} \int_0^{2\pi} d\varphi \frac{e^{-ik_j r_{ij}}}{r_{ij}} \left[\left(\int_{-L/2}^{-r_0} dz + \int_{r_0}^{L/2} dz \right) \int_0^{R_0} \rho d\rho + \int_{-r_0}^{r_0} dz \int_{\sqrt{r_0^2 - z^2}}^{R_0} \rho d\rho \right]. \quad (\text{B.0.9})$$

After performing the integrations, we obtain

$$E_L = -\frac{2N_v\mu}{3\epsilon_0} e^{-\frac{ik_j L}{2}} + \frac{2N_v\mu}{3\epsilon_0} e^{-ir_0 k_j} + \frac{2i\mu N_v r_0 k_j}{3\epsilon_0} e^{-ir_0 k_j} - \frac{i\mu N_v k_j}{3\epsilon_0} \int_{-L/2}^{L/2} \rho \frac{e^{ik_j \sqrt{\rho^2 + z^2}}}{\sqrt{\rho^2 + z^2}} d\rho. \quad (\text{B.0.10})$$

The local electric field we obtained up to this point is exact. We can now make some approximations. In the limit $r_0 \rightarrow 0$,

$$E_L = \frac{2N_v\mu}{3\epsilon_0} - \frac{2N_v\mu}{3\epsilon_0} e^{-\frac{ik_j L}{2}} - \frac{i\mu N_v k_j}{3\epsilon_0} \int_{-L/2}^{L/2} \rho \frac{e^{ik_j \sqrt{\rho^2 + z^2}}}{\sqrt{\rho^2 + z^2}} d\rho. \quad (\text{B.0.11})$$

You can see that the local field remains finite in the limit $r_0 \rightarrow 0$, while $E^{ij}(\mathbf{r}_{ij})$ has a singularity at $r_{ij} \rightarrow 0$. If we go one step further and take the limit of Eq.(B.0.11) for $L \rightarrow 0$, $R_0 \rightarrow \infty$, the integral vanishes and we simply obtain

$$E_L = \frac{2P}{3\epsilon_0}, \quad (\text{B.0.12})$$

which is identical to the famous classical Lorentz-Lorenz local-field correction. Here $P = N_v \langle \mu \rangle$ is the polarization of the medium. In the limit of a thin film with an infinitely small thickness, the polarization P tends to the surface polarization and n is practically the surface QD density.

Appendix C

Derivation of P^{ret} and P^{+-}

According to Eq.(6.2.2), the parameter P^{ret} is given by

$$P^{\text{ret}}(t; \tau) = \frac{2}{3} \frac{\mu^2}{\hbar^2} N \Theta(\tau) \overline{\langle S^+(t) S^-(t+\tau) - S^-(t+\tau) S^+(t) \rangle}. \quad (\text{C.0.1})$$

The factor $2/3$ results from the orientation averaging over α, β . Therefore, the first step to obtain the Fourier transform of the susceptibility is to find the correlation terms of the kind $\langle S^+(t) S^-(t+\tau) \rangle$. The eigenstates of the probe QD are $|g\rangle$ and $|e\rangle$ which refer to the ground and excited states respectively. In this basis, the matrices of the dipole rising and lowering operators will be

$$S^- = \begin{pmatrix} 0 & 1 \\ 0 & 0 \end{pmatrix}, \quad S^+ = \begin{pmatrix} 0 & 0 \\ 1 & 0 \end{pmatrix}, \quad S^z = \frac{1}{2} \begin{pmatrix} -1 & 0 \\ 0 & 1 \end{pmatrix}. \quad (\text{C.0.2})$$

Then, the expectation value of these operators can be written through $\langle S^\pm \rangle = \text{Tr}(\rho S^\pm)$ as

$$\langle S^- \rangle = \rho_{eg}, \quad \langle S^+ \rangle = \rho_{ge}, \quad \langle S^z \rangle = \frac{1}{2} (\rho_{ee} - \rho_{gg}). \quad (\text{C.0.3})$$

Indicating $\langle S^- \rangle$ by its corresponding density matrix element ρ_{eg} , and in the absence of any external field, we can write from (6.1.32),

$$\dot{\rho}_{eg} = - \left(i\omega_{\text{pr}} + \frac{\Gamma}{2} + \Gamma^c \right) \rho_{eg}. \quad (\text{C.0.4})$$

In Eq.(C.0.4), we have ignored the contribution of $\hbar + \hbar^c$ in the frequency modification of the probe QD since the transition frequency of the probe QD is obtained from $\omega_{\text{pr}} = \omega_0 + \Delta_{\text{pr}}$ in which Δ_{pr} is an inhomogeneous broadening due to the size distribution of QDs and is much larger than the Lamb and collective frequency shifts. Choosing $t = t$ as the initial time, the value of ρ_{eg} at $t = t + \tau$ will be

$$\rho_{eg}(t + \tau) = \rho_{eg}(t) e^{-(i\omega_{\text{pr}} + \frac{\Gamma}{2} + \Gamma^c)\tau}. \quad (\text{C.0.5})$$

Replacing the matrix element on the left hand side of the equation by the expectation value of the lowering dipole operator, we can rewrite Eq.(C.0.5) in the form

$$\langle S^-(t+\tau) \rangle = \langle e | \rho | g \rangle e^{-(i\omega_{pr} + \frac{\Gamma}{2} + \Gamma^c)\tau}. \quad (\text{C.0.6})$$

In order to obtain the correlation function $\langle S^+(t) S^-(t+\tau) \rangle$, we resort the Lax-Onzager theorem [121] in which we replace ρ in Eq.(C.0.6) by ρS^+ that yields

$$\langle S^+(t) S^-(t+\tau) \rangle = \rho_{ee}(t) e^{-(i\omega_{pr} + \frac{\Gamma}{2} + \Gamma^c)\tau}. \quad (\text{C.0.7})$$

Similarly, by substituting $S^+ \rho$ instead of ρ , we obtain

$$\langle S^-(t+\tau) S^+(t) \rangle = \rho_{gg}(t) e^{-(i\omega_{pr} + \frac{\Gamma}{2} + \Gamma^c)\tau}. \quad (\text{C.0.8})$$

The combination of (C.0.1), (C.0.7) and (C.0.8) gives

$$P^{\text{ret}}(t; \tau) = \frac{2}{3} \frac{\mu^2}{\hbar^2} N \Theta(\tau) \overline{[\rho_{ee}(t) - \rho_{gg}(t)] e^{-(i\omega_{pr} + \frac{\Gamma}{2} + \Gamma^c)\tau}}. \quad (\text{C.0.9})$$

The Fourier transform of (C.0.9) becomes

$$\tilde{P}^{\text{ret}}(t; \omega) = \frac{2}{3} \frac{\mu^2}{\hbar^2} N \frac{\overline{[\rho_{ee}(t) - \rho_{gg}(t)]}}{i(\omega - \omega_{pr}) + \frac{\Gamma}{2} + \Gamma^c}. \quad (\text{C.0.10})$$

We continue with derivation of P^{+-} . From Eq.(6.2.4), we have

$$\begin{aligned} P^{+-}(t; \tau) &= \frac{2}{3} \frac{\mu^2}{\hbar^2} N \overline{(\langle S^+(t) S^-(t+\tau) \rangle - \langle S^+(t) \rangle \langle S^-(t+\tau) \rangle)} \\ &= \frac{\mu^2}{\hbar^2} N \overline{\langle S^+(t) S^-(t+\tau) \rangle}. \end{aligned} \quad (\text{C.0.11})$$

The factor $2/3$ is again due to the orientation averaging. In contradiction to the case of P^{ret} , the correlation time τ in Eq.(C.0.11) can have both negative and positive values. Then the Fourier transformation of P^{+-} becomes

$$\begin{aligned} \tilde{P}^{+-}(t; \omega) &= \frac{2}{3} \frac{\mu^2}{\hbar^2} N \int_{-\infty}^{\infty} d\tau e^{-i\omega\tau} \overline{\langle S^+(t) S^-(t+\tau) \rangle} \\ &= \frac{2}{3} \frac{\mu^2}{\hbar^2} N \left\{ \int_{-\infty}^0 d\tau e^{-i\omega\tau} \overline{\langle S^+(t) S^-(t+\tau) \rangle} + \int_0^{\infty} d\tau e^{-i\omega\tau} \overline{\langle S^+(t) S^-(t+\tau) \rangle} \right\}. \end{aligned} \quad (\text{C.0.12})$$

The first integration is over the negative values of τ and can be equally replaced by its positive correspondence $\int_0^{\omega} d\tau e^{-i\omega\tau} \overline{\langle S^+(t+\tau) S^-(t) \rangle}$. Hence, Eq.(C.0.12) will be simplified to

$$\tilde{P}^{+-}(t; \omega) = \frac{2}{3} \frac{\mu^2}{\hbar^2} N \int_{-\infty}^{\infty} d\tau e^{-i\omega\tau} \overline{(\langle S^+(t) S^-(t+\tau) \rangle + \langle S^+(t+\tau) S^-(t) \rangle)}. \quad (\text{C.0.13})$$

Similar to the procedure that we followed to obtain $\tilde{P}^{\text{ret}}(t; \omega)$, we arrive at

$$\tilde{P}^{+-}(t; \omega) = \frac{4\mu^2}{3\hbar^2} N \frac{\overline{\rho_{ee}(t)}}{(\omega - \omega_{pr})^2 + (\frac{\Gamma}{2} + \Gamma^c)^2}. \quad (\text{C.0.14})$$

Appendix D

Inverse Fourier transformation of the retarded Green's function

By replacing the dynamic polarizability by the dielectric constant of (6.2.22) in Eq.(6.2.24), we obtain

$$\tilde{f}'^{\text{ret}}(\mathbf{q}, \omega) = -\frac{2}{3} \frac{i\hbar}{\epsilon_0} \left[\frac{\left(\frac{\epsilon(\omega)-1}{3\epsilon(\omega)}\right) \mathbf{q}^2 + k^2}{\left(\frac{3}{\epsilon(\omega)+2}\right) \mathbf{q}^2 - k^2 \left(\frac{3\epsilon(\omega)}{\epsilon(\omega)+2}\right) - i0} \right]. \quad (\text{D.0.1})$$

The Fourier transformation of Eq.(D.0.1) is defined through

$$\tilde{\mathbf{F}}(\mathbf{r}, \omega) = (2\pi)^{-3} \int d\mathbf{q} \tilde{\mathbf{F}}(\mathbf{q}, \omega^+) e^{-i\mathbf{q}\cdot\mathbf{r}}, \quad (\text{D.0.2})$$

which in the limit $\Lambda \gg k\sqrt{\epsilon(\omega)}$ becomes

$$\begin{aligned} \tilde{f}'^{\text{ret}}(\mathbf{r}, \omega^+) = \frac{i\hbar k^3}{6\pi\epsilon_0 r} & \left\{ -\left(\frac{\epsilon(\omega)+2}{3}\right)^2 e^{-ik\sqrt{\epsilon(\omega)}r} \right. \\ & \left. + \left(\frac{\epsilon(\omega)+2}{3}\right)^2 \cos\left(\frac{\Lambda r}{\sqrt{2}}\right) e^{-\frac{\Lambda r}{\sqrt{2}}} - \frac{\Lambda^2}{3k^2} \frac{[\epsilon(\omega)+2]}{3\epsilon(\omega)} [\epsilon(\omega)-1] \sin\left(\frac{\Lambda r}{\sqrt{2}}\right) e^{-\frac{\Lambda r}{\sqrt{2}}} \right\}. \end{aligned} \quad (\text{D.0.3})$$

with $r = |\mathbf{r} - \mathbf{r}_0|$. The retarded Green's function at the position of the probe QD is then obtained from (D.0.3), by putting $\mathbf{r} = \mathbf{r}_0$,

$$\begin{aligned} \lim_{r \rightarrow 0} \tilde{f}'^{\text{ret}}(\mathbf{r}, \omega^+) = \frac{\hbar\omega^3}{6\pi\epsilon_0 c^3} \sqrt{\epsilon(\omega)} \left(\frac{\epsilon(\omega)+2}{3}\right)^2 \\ - \frac{i\hbar\omega^3}{6\pi\epsilon_0 c^3} \left[\frac{1}{R} \left(\frac{\epsilon(\omega)+2}{3}\right)^2 + \frac{1}{R^3} \frac{2}{3} \left(\frac{\epsilon(\omega)+2}{3\epsilon(\omega)}\right)^2 (\epsilon(\omega)-1) \right], \end{aligned} \quad (\text{D.0.4})$$

with $R = \sqrt{2}k/\Lambda$.

Bibliography

- [1] Q. Gong, P. Offermans, R. Notzel, P. M. Koenraad, and J. H. Wolter, "Capping process of InAs/GaAs quantum dots studied by cross-sectional scanning tunneling microscopy," *Applied Physics Letters*, vol. 85, no. 23, pp. 5697–5699, 2004.
- [2] A. Barenco, D. Deutsch, A. Ekert, and R. Jozsa, "Conditional quantum dynamics and logic gates," *Physical Review Letters*, vol. 74, no. 20, pp. 4083–4086, 1995.
- [3] G. Schedelbeck, W. Wegscheider, M. Bichler, and G. Abstreiter, "Coupled quantum dots fabricated by cleaved edge overgrowth: From artificial atoms to molecules," *Science*, vol. 278, no. 5344, pp. 1792–1795, 1997.
- [4] H. J. Krenner, M. Sabathil, E. C. Clark, A. Kress, D. Schuh, M. Bichler, G. Abstreiter, and J. J. Finley, "Direct observation of controlled coupling in an individual quantum dot molecule," *Physical Review Letters*, vol. 94, no. 5, p. 057402, 2005.
- [5] X. D. Xu, B. Sun, P. R. Berman, D. G. Steel, A. S. Bracker, D. Gammon, and L. J. Sham, "Coherent optical spectroscopy of a strongly driven quantum dot," *Science*, vol. 317, no. 5840, pp. 929–932, 2007.
- [6] G. W. Bryant, G. Solomon, and B. Inc., *Optics of quantum dots and wires*. Artech House semiconductor materials and devices library, Boston: Artech House,, 2005.
- [7] L. Esaki and R. Tsu *IBM Res. Note*, pp. RC–2418, 1969.
- [8] L. Esaki and R. Tsu *IBM J. Res. Develop.*, vol. 14, p. 61, 1970.
- [9] I. N. Stranski and L. Krastanow *Sitzungsber. Akad. Wiss. Wien Math. Naturwiss. KL. Abt. IIB Chemie*, vol. 146, p. 797, 1937.
- [10] M. S. Skolnick and D. J. Mowbray, "Self-assembled semiconductor quantum dots: Fundamental physics and device applications," *Annual Review of Materials Research*, vol. 34, pp. 181–218, 2004.
- [11] M. Sugawara, *Self-assembled InGaAs/GaAs quantum dots*. Semiconductors and semimetals, San Diego, CA: Academic Press, 1999.
- [12] M. A. Walling, J. A. Novak, and J. R. E. Shepard, "Quantum dots for live cell and in vivo imaging," *International Journal of Molecular Sciences*, vol. 10, no. 2, pp. 441–491, 2009.

- [13] K. Hoshino, A. Gopal, M. S. Glaz, D. A. Vanden Bout, and X. J. Zhang, "Nanoscale fluorescence imaging with quantum dot near-field electroluminescence," *Applied Physics Letters*, vol. 101, no. 4, p. 043118, 2012.
- [14] J. Vaillancourt and X.-J. Lu *Optics and Photonics Letters*, vol. 4, p. 1, 2011.
- [15] G. Konstantatos and E. H. Sargent, "Solution-processed quantum dot photodetectors," *Proceedings of the Ieee*, vol. 97, no. 10, pp. 1666–1683, 2009.
- [16] R. I. Karasik, K. P. Marzlin, B. C. Sanders, and K. B. Whaley, "Multiparticle decoherence-free subspaces in extended systems," *Physical Review A*, vol. 76, no. 1, p. 012331, 2007.
- [17] H. Hammer, "Collective states in highly symmetric atomic configurations and single-photon traps," *Optics and Spectroscopy*, vol. 99, no. 2, pp. 320–337, 2005.
- [18] J. P. Clemens, L. Horvath, B. C. Sanders, and H. J. Carmichael, "Collective spontaneous emission from a line of atoms," *Physical Review A*, vol. 68, no. 2, p. 023809, 2003.
- [19] M. D. Eisaman, A. Andre, F. Massou, M. Fleischhauer, A. S. Zibrov, and M. D. Lukin, "Electromagnetically induced transparency with tunable single-photon pulses," *Nature*, vol. 438, no. 7069, pp. 837–841, 2005.
- [20] A. Kuzmich, W. P. Bowen, A. D. Boozer, A. Boca, C. W. Chou, L. M. Duan, and H. J. Kimble, "Generation of nonclassical photon pairs for scalable quantum communication with atomic ensembles," *Nature*, vol. 423, no. 6941, pp. 731–734, 2003.
- [21] A. T. Black, J. K. Thompson, and V. Vuletic, "On-demand superradiant conversion of atomic spin gratings into single photons with high efficiency," *Physical Review Letters*, vol. 95, no. 13, p. 133601, 2005.
- [22] L. Novotny and B. Hecht, *Principles of nano-optics*. Cambridge ; New York: Cambridge University Press, 2006.
- [23] E. M. Purcell, "Spontaneous emission probabilities at radio frequencies," *Physical Review*, vol. 69, no. 11-1, pp. 681–681, 1946.
- [24] F. Demartini, G. Innocenti, G. R. Jacobovitz, and P. Mataloni, "Anomalous spontaneous emission time in a microscopic optical cavity," *Physical Review Letters*, vol. 59, no. 26, pp. 2955–2958, 1987.
- [25] M. V. Artemyev, U. Woggon, R. Wannemacher, H. Jaschinski, and W. Langbein, "Light trapped in a photonic dot: Microspheres act as a cavity for quantum dot emission," *Nano Letters*, vol. 1, no. 6, pp. 309–314, 2001.
- [26] W. Jhe, A. Anderson, E. A. Hinds, D. Meschede, L. Moi, and S. Haroche, "Suppression of spontaneous decay at optical frequencies - test of vacuum-field anisotropy in confined space," *Physical Review Letters*, vol. 58, no. 7, pp. 666–669, 1987.

- [27] M. Bayer, T. L. Reinecke, F. Weidner, A. Larionov, A. McDonald, and A. Forchel, "Inhibition and enhancement of the spontaneous emission of quantum dots in structured microresonators," *Physical Review Letters*, vol. 86, no. 14, pp. 3168–3171, 2001.
- [28] M. Bayer, P. Hawrylak, K. Hinzer, S. Fafard, M. Korkusinski, Z. R. Wasilewski, O. Stern, and A. Forchel, "Coupling and entangling of quantum states in quantum dot molecules," *Science*, vol. 291, no. 5503, pp. 451–453, 2001.
- [29] P. R. Berman, *Cavity quantum electrodynamics. Advances in atomic, molecular, and optical physics Supplements*, Boston: Academic Press, 1994.
- [30] K. H. Drexhage, "Influence of a dielectric interface on fluorescence decay time," *J. Luminescence*, vol. 1-2, p. 693, 2000.
- [31] W. L. Barnes, "Fluorescence near interfaces: the role of photonic mode density," *Journal of Modern Optics*, vol. 45, no. 4, pp. 661–699, 1998.
- [32] V. P. Bykov, *Radiation of atoms in a resonant environment. Series in optics and photonics*, Singapore ; River Edge, NJ: World Scientific, 1993.
- [33] V. N. Bogomolov, S. V. Gaponenko, I. N. Germanenko, A. M. Kapitonov, E. P. Petrov, N. V. Gaponenko, A. V. Prokofiev, A. N. Ponyavina, N. I. Silvanovich, and S. M. Samoilovich, "Photonic band gap phenomenon and optical properties of artificial opals," *Physical Review E*, vol. 55, no. 6, pp. 7619–7625, 1997.
- [34] A. F. Koenderink, M. Kafesaki, C. M. Soukoulis, and V. Sandoghdar, "Spontaneous emission in the near field of two-dimensional photonic crystals," *Optics Letters*, vol. 30, no. 23, pp. 3210–3212, 2005.
- [35] A. V. Akimov, A. Mukherjee, C. L. Yu, D. E. Chang, A. S. Zibrov, P. R. Hemmer, H. Park, and M. D. Lukin, "Generation of single optical plasmons in metallic nanowires coupled to quantum dots," *Nature*, vol. 450, no. 7168, pp. 402–406, 2007.
- [36] H. P. Urbach and G. L. J. A. Rikken, "Spontaneous emission from a dielectric slab," *Physical Review A*, vol. 57, no. 5, pp. 3913–3930, 1998.
- [37] D. Topygin and L. Brand, "Fluorescence decay of dph in lipid-membranes - influence of the external refractive-index," *Biophysical Chemistry*, vol. 48, no. 2, pp. 205–220, 1993.
- [38] P. M. A. Dirac, "Emission and absorption of radiation," *Proc. R. Soc. A*, vol. 114, p. 243, 1927.
- [39] V. Weisskopf and E. Wigner *Z. Phys.*, vol. 65, p. 18, 1930.
- [40] V. Weisskopf and E. Wigner *Z. Phys.*, vol. 63, p. 54, 1930.
- [41] T. Förster *Ann. Phys. (Leipzig)*, vol. 2, p. 55, 1948.
- [42] A. O. Govorov, "Spin and energy transfer in nanocrystals without tunneling," *Physical Review B*, vol. 68, no. 7, p. 075315, 2003.

- [43] C. R. Kagan, C. B. Murray, and M. G. Bawendi, "Long-range resonance transfer of electronic excitations in close-packed cdse quantum-dot solids," *Physical Review B*, vol. 54, no. 12, pp. 8633–8643, 1996.
- [44] G. Parascandolo and V. Savona, "Long-range radiative interaction between semiconductor quantum dots," *Physical Review B*, vol. 71, no. 4, p. 045335, 2005.
- [45] J. J. Hopfield, "Theory of the contribution of excitons to the complex dielectric constant of crystals," *Physical Review*, vol. 112, no. 5, pp. 1555–1567, 1958.
- [46] L. C. Andreani, F. Tassone, and F. Bassani, "Radiative lifetime of free-excitons in quantum-wells," *Solid State Communications*, vol. 77, no. 9, pp. 641–645, 1991.
- [47] U. Bockelmann, "Exciton relaxation and radiative recombination in semiconductor quantum dots," *Physical Review B*, vol. 48, no. 23, pp. 17637–17640, 1993.
- [48] D. S. Citrin, "Radiative lifetimes of excitons in quantum-wells - localization and phase-coherence effects," *Physical Review B*, vol. 47, no. 7, pp. 3832–3841, 1993.
- [49] B. Gil and A. V. Kavokin, "Giant exciton-light coupling in zno quantum dots," *Applied Physics Letters*, vol. 81, no. 4, pp. 748–750, 2002.
- [50] R. H. Dicke, "Coherence in spontaneous radiation processes," *Physical Review*, vol. 93, no. 1, pp. 99–110, 1954.
- [51] R. H. Dicke, *The Coherence Brightened Laser*. Quantum Electronics, New York: Columbia University Press, 1964.
- [52] N. E. Rehler and J. H. Eberly, "Superradiance," *Physical Review A*, vol. 3, no. 5, p. 1735, 1971.
- [53] N. Skribanowitz, I. P. Herman, J. C. Macgillivray, and M. S. Feld, "Observation of dicke superradiance in optically pumped Hf gas," *Physical Review Letters*, vol. 30, no. 8, pp. 309–312, 1973.
- [54] J. C. Macgillivray and M. S. Feld, "Theory of superradiance in an extended, optically thick medium," *Physical Review A*, vol. 14, no. 3, pp. 1169–1189, 1976.
- [55] D. N. Klyshko, M. Chekhova, and S. Kulik, *Physical foundations of quantum electronics*. Singapore ; Hackensack, N.J.: World Scientific, 2011.
- [56] M. Scheibner, T. Schmidt, L. Worschech, A. Forchel, G. Bacher, T. Passow, and D. Hommel, "Superradiance of quantum dots," *Nature Physics*, vol. 3, no. 2, pp. 106–110, 2007.
- [57] R. G. DeVoe and R. G. Brewer, "Observation of superradiant and subradiant spontaneous emission of two trapped ions," *Physical Review Letters*, vol. 76, no. 12, pp. 2049–2052, 1996.
- [58] D. Pavolini, A. Crubellier, P. Pillet, L. Cabaret, and S. Liberman, "Experimental-evidence for subradiance," *Physical Review Letters*, vol. 54, no. 17, pp. 1917–1920, 1985.

- [59] T. Bienaimé, N. Piovella, and R. Kaiser, "Controlled dicke subradiance from a large cloud of two-level systems," *Physical Review Letters*, vol. 108, no. 12, p. 123602, 2012.
- [60] R. Bonifacio and L. A. Lugiato, "Cooperative radiation processes in 2-level systems - superfluorescence," *Physical Review A*, vol. 11, no. 5, pp. 1507–1521, 1975.
- [61] S. Prasad and R. J. Glauber, "Initiation of superfluorescence in a large sphere," *Physical Review A*, vol. 31, no. 3, pp. 1583–1597, 1985.
- [62] M. Gross and S. Haroche, "Super-radiance - an essay on the theory of collective spontaneous emission," *Physics Reports-Review Section of Physics Letters*, vol. 93, no. 5, pp. 301–396, 1982.
- [63] M. G. Benedict, *Super-radiance : multiatomic coherent emission*. Optics and optoelectronics series, Bristol, UK ; Philadelphia: Institute of Physics, 1996.
- [64] H. A. Lorentz *Wiedem. Ann.*, vol. 9, p. 641, 1880.
- [65] L. Lorenz *Wiedem. Ann.*, vol. 11, p. 70, 1881.
- [66] M. Born and E. Wolf, *Principles of optics; electromagnetic theory of propagation, interference, and diffraction of light*. Oxford, New York,: Pergamon Press, 5th ed., 1975.
- [67] C. M. Bowden and J. P. Dowling, "Near-dipole-dipole effects in dense media: Generalized maxwell-bloch equations," *Physical Review A*, vol. 47, no. 2, pp. 1247–1251, 1993.
- [68] N. Bloembergen, *Nonlinear optics; a lecture note and reprint volume*. Frontiers in physics, New York,: W. A. Benjamin, 1965.
- [69] J. J. Maki, M. S. Malcuit, J. E. Sipe, and R. W. Boyd, "Linear and nonlinear optical measurements of the Lorentz local field," *Physical Review Letters*, vol. 67, no. 8, pp. 972–975, 1991.
- [70] V. A. Sautenkov, H. vanKampen, E. R. Eliel, and J. P. Woerdman, "Dipole-dipole broadened line shape in a partially excited dense atomic gas," *Physical Review Letters*, vol. 77, no. 16, pp. 3327–3330, 1996.
- [71] J. Ruostekoski and J. Javanainen, "Quantum field theory of cooperative atom response: Low light intensity," *Physical Review A*, vol. 55, no. 1, pp. 513–526, 1997.
- [72] J. Ruostekoski and J. Javanainen, "Lorentz-Lorenz shift in a Bose-Einstein condensate," *Physical Review A*, vol. 56, no. 3, pp. 2056–2059, 1997.
- [73] C. M. Bowden and C. C. Sung, "1st-order and 2nd-order phase-transitions in the dicke model - relation to optical bistability," *Physical Review A*, vol. 19, no. 6, pp. 2392–2401, 1979.
- [74] F. A. Hopf, C. M. Bowden, and W. H. Louisell, "Mirrorless optical bistability with the use of the local-field correction," *Physical Review A*, vol. 29, no. 5, pp. 2591–2596, 1984.

- [75] H. E. Schmidt, H. Haug, and S. W. Koch, "Theoretical explanation of the absorptive optical bistability in semiconductors due to band-gap shrinkage," *Applied Physics Letters*, vol. 44, no. 8, pp. 787–789, 1984.
- [76] M. P. Hehlen, H. U. Gudel, Q. Shu, J. Rai, S. Rai, and S. C. Rand, "Cooperative bistability in dense, excited atomic systems," *Physical Review Letters*, vol. 73, no. 8, pp. 1103–1106, 1994.
- [77] A. S. Manka, J. P. Dowling, C. M. Bowden, and M. Fleischhauer, "Piezophotonic switching due to local-field effects in a coherently prepared medium of 3-level atoms," *Physical Review Letters*, vol. 73, no. 13, pp. 1789–1792, 1994.
- [78] A. V. Andreev, V. I. Emel'ianov, and I. A. Il'inskii, *Cooperative effects in optics : superradiance and phase transitions*. Malvern physics series, Bristol ; Philadelphia: Institute of Physics Pub., 1993.
- [79] T. Holstein, "Imprisonment of resonance radiation in gases .2.," *Physical Review*, vol. 83, no. 6, pp. 1159–1168, 1951.
- [80] D. Kouznetsov, J. F. Bisson, K. Takaichi, and K. Ueda, "High-power single-mode solid-state laser with a short, wide unstable cavity," *Journal of the Optical Society of America B-Optical Physics*, vol. 22, no. 8, pp. 1605–1619, 2005.
- [81] A. C. G. Mitchell and M. W. Zemansky, *Resonance radiation and excited atoms*. Cambridge Eng.: University Press, 1961.
- [82] A. F. Molisch and B. P. Oehry, *Radiation trapping in atomic vapours*. New York: Clarendon Press, 1998.
- [83] N. N. Bezuglov, A. N. Klucharev, A. F. Molisch, M. Allegrini, F. Fuso, and T. Stacewicz, "Nonlinear radiation trapping in an atomic vapor excited by a strong laser pulse," *Physical Review E*, vol. 55, no. 3, pp. 3333–3350, 1997.
- [84] A. E. Siegman, *Amplified spontaneous emission in lasers*. University Series Books, 1986.
- [85] M. S. Feld and J. C. Macgillivray, "Superradiance," *Curr. Phys.*, vol. 21, p. 7, 1980.
- [86] C. K. N. Patel and R. E. Slusher, "Photon echoes in gases," *Physical Review Letters*, vol. 20, no. 20, p. 1087, 1968.
- [87] S. L. McCall and E. L. Hahn, "Self-induced transparency," *Physical Review*, vol. 183, no. 2, p. 457, 1969.
- [88] Y. Lai and H. A. Haus, "Quantum-theory of solitons in optical fibers .1. time-dependent hartree approximation," *Physical Review A*, vol. 40, no. 2, pp. 844–853, 1989.
- [89] Y. Lai and H. A. Haus, "Quantum-theory of solitons in optical fibers .2. exact solution," *Physical Review A*, vol. 40, no. 2, pp. 854–866, 1989.
- [90] O. Kocharovskaya, "Amplification and lasing without inversion," *Physics Reports-Review Section of Physics Letters*, vol. 219, no. 3-6, pp. 175–190, 1992.

- [91] L. V. Hau, S. E. Harris, Z. Dutton, and C. H. Behroozi, "Light speed reduction to 17 metres per second in an ultracold atomic gas," *Nature*, vol. 397, no. 6720, pp. 594–598, 1999.
- [92] V. Balic, D. A. Braje, P. Kolchin, G. Y. Yin, and S. E. Harris, "Generation of paired photons with controllable waveforms," *Physical Review Letters*, vol. 94, no. 18, p. 183601, 2005.
- [93] M. O. Scully and A. A. Svidzinsky, "The super of superradiance," *Science*, vol. 325, no. 5947, pp. 1510–1511, 2009.
- [94] M. O. Scully, "Correlated spontaneous emission on the Volga," *Laser Physics*, vol. 17, no. 5, pp. 635–646, 2007.
- [95] M. O. Scully, E. S. Fry, C. H. R. Ooi, and K. Wodkiewicz, "Directed spontaneous emission from an extended ensemble of n atoms: Timing is everything," *Physical Review Letters*, vol. 96, no. 1, p. 010501, 2006.
- [96] I. E. Mazets and G. Kurizki, "Multiatom cooperative emission following single-photon absorption: Dicke-state dynamics," *Journal of Physics B-Atomic Molecular and Optical Physics*, vol. 40, no. 6, pp. F105–F112, 2007.
- [97] J. H. Eberly, "Emission of one photon in an electric dipole transition of one among n atoms," *Journal of Physics B-Atomic Molecular and Optical Physics*, vol. 39, no. 15, pp. S599–S604, 2006.
- [98] S. Das, G. S. Agarwal, and M. O. Scully, "Quantum interferences in cooperative dicke emission from spatial variation of the laser phase," *Physical Review Letters*, vol. 101, no. 15, p. 153601, 2008.
- [99] A. Svidzinsky and J. T. Chang, "Cooperative spontaneous emission as a many-body eigenvalue problem," *Physical Review A*, vol. 77, no. 4, p. 043833, 2008.
- [100] R. Friedberg and J. T. Manassah, "Effects of including the counterrotating term and virtual photons on the eigenfunctions and eigenvalues of a scalar photon collective emission theory," *Physics Letters A*, vol. 372, no. 14, pp. 2514–2521, 2008.
- [101] A. A. Svidzinsky and M. O. Scully, "Evolution of collective n atom states in single photon superradiance: Effect of virtual lamb shift processes," *Optics Communications*, vol. 282, no. 14, pp. 2894–2897, 2009.
- [102] M. O. Scully, "Collective Lamb Shift in Single Photon Dicke Superradiance," *Physical Review Letters*, vol. 102, no. 14, p. 143601, 2009.
- [103] J. D. Jackson, *Classical electrodynamics*. New York: Wiley, 3rd ed., 1999.
- [104] R. H. Pantell and H. E. Puthoff, *Fundamentals of quantum electronics*. New York: Wiley, 1969.
- [105] N. Zettili, *Quantum mechanics : concepts and applications*. Chichester, U.K.: Wiley, 2nd ed., 2009.

- [106] R. H. Lehmberg, "Radiation from an N-Atom System . I. General Formalism," *Physical Review A*, vol. 2, no. 3, p. 883, 1970.
- [107] R. H. Lehmberg, "Radiation from an N-Atom System . II. Spontaneous Emission from a Pair of Atoms," *Physical Review A*, vol. 2, no. 3, p. 889, 1970.
- [108] W. H. Louisell, *Quantum statistical properties of radiation*. New York,: Wiley, 1973.
- [109] G. S. Agarwal, *Quantum Statistical Theories of Spontaneous Emission and their Relation to other Approaches*. Springer Tracts in Modern Physics, Berlin: Springer, 1974.
- [110] Z. Ficek and R. Tanas, "Entangled states and collective nonclassical effects in two-atom systems," *Physics Reports-Review Section of Physics Letters*, vol. 372, no. 5, pp. 369–443, 2002.
- [111] L. Mandel and E. Wolf, *Optical coherence and quantum optics*. Cambridge England ; New York, NY, USA: Cambridge University Press, 1995.
- [112] L. C. Andreani, *Confined Electrons and Photons*. Plenum Press, 1994.
- [113] F. Tassone, F. Bassani, and L. C. Andreani, "Resonant and surface-polaritons in quantum-wells," *Nuovo Cimento Della Societa Italiana Di Fisica D-Condensed Matter Atomic Molecular and Chemical Physics Fluids Plasmas Biophysics*, vol. 12, no. 12, pp. 1673–1687, 1990.
- [114] S. Jorda, "Quantum-theory of the interaction of quantum-well excitons with electromagnetic wave-guide modes," *Physical Review B*, vol. 50, no. 4, pp. 2283–2292, 1994.
- [115] Z. Ficek, R. Tanas, and S. Kielich, "Quantum beats and superradiant effects in the spontaneous emission from 2 nonidentical atoms," *Physica A*, vol. 146, no. 3, pp. 452–482, 1987.
- [116] P. W. Milonni and P. L. Knight, "Retardation in resonant interaction of 2 identical atoms," *Physical Review A*, vol. 10, no. 4, pp. 1096–1108, 1974.
- [117] P. W. Milonni and P. L. Knight, "Retarded interaction of 2 nonidentical atoms," *Physical Review A*, vol. 11, no. 3, pp. 1090–1092, 1975.
- [118] M. J. Stephen, "First-order dispersion forces," *Journal of Chemical Physics*, vol. 40, no. 3, p. 669, 1964.
- [119] D. A. Hutchinson and H. F. Hamerka, "Interaction effects on lifetimes of atomic excitations," *Journal of Chemical Physics*, vol. 41, no. 7, p. 2006, 1964.
- [120] D. G. Welsch, H. T. Dung, and L. Knöll, *Dipole-dipole coupling in the presence of dispersing and absorbing bodies*, vol. 51 of *PROGRESS OF PHYSICS*. 2003.
- [121] M. O. Scully and M. S. Zubairy, *Quantum optics*. Cambridge ; New York: Cambridge University Press, 1997.
- [122] S. V. Gaponenko, *Introduction to nanophotonics*. Cambridge u.a.: Cambridge Univ. Press, 1. publ. ed., 2010.

- [123] G. Nienhuis and C. T. J. Alkemade, "Atomic radiative transition-probabilities in a continuous medium," *Physica B & C*, vol. 81, no. 1, pp. 181–188, 1976.
- [124] A. Kavokin, J. J. Baumberg, G. Malpuech, and F. P. Laussy, *Microcavities*. Oxford: Oxford Univ. Press, 2007.
- [125] E. Yablonovitch, "Inhibited spontaneous emission in solid-state physics and electronics," *Physical Review Letters*, vol. 58, no. 20, pp. 2059–2062, 1987.
- [126] C. Piermarocchi, P. Chen, L. J. Sham, and D. G. Steel, "Optical rky interaction between charged semiconductor quantum dots," *Physical Review Letters*, vol. 89, no. 16, p. 167402, 2002.
- [127] P. Borri, W. Langbein, U. Woggon, M. Schwab, M. Bayer, S. Fafard, Z. Wasilewski, and P. Hawrylak, "Exciton dephasing in quantum dot molecules," *Physical Review Letters*, vol. 91, no. 26, p. 267401, 2003.
- [128] G. Y. Slepyan, Y. D. Yerchak, S. A. Maksimenko, and A. Hoffmann, "Wave propagation of Rabi oscillations in one-dimensional quantum dot chain," *Physics Letters A*, vol. 373, no. 15, pp. 1374–1378, 2009.
- [129] G. Y. Slepyan, Y. D. Yerchak, A. Hoffmann, and F. G. Bass, "Strong electron-photon coupling in a one-dimensional quantum dot chain: Rabi waves and rabi wave packets," *Physical Review B*, vol. 81, no. 8, p. 085115, 2010.
- [130] T. Förster, *Modern Quantum Chemistry*. New York: Academic, 1965.
- [131] A. A. Svidzinsky, J. T. Chang, and M. O. Scully, "Dynamical evolution of correlated spontaneous emission of a single photon from a uniformly excited cloud of n atoms," *Physical Review Letters*, vol. 100, no. 16, p. 160504, 2008.
- [132] T. Yu and J. H. Eberly, "Finite-time disentanglement via spontaneous emission," *Physical Review Letters*, vol. 93, no. 14, p. 140404, 2004.
- [133] S. Hughes, "Modified spontaneous emission and qubit entanglement from dipole-coupled quantum dots in a photonic crystal nanocavity," *Physical Review Letters*, vol. 94, no. 22, p. 227402, 2005.
- [134] Z. Ficek, R. Tanas, and S. Kielich, "Cooperative effects in the spontaneous emission from 2 nonidentical atoms," *Optica Acta*, vol. 33, no. 9, pp. 1149–1160, 1986.
- [135] E. Rephaeli, S. E. Kocabas, and S. H. Fan, "Few-photon transport in a waveguide coupled to a pair of colocated two-level atoms," *Physical Review A*, vol. 84, no. 6, p. 063832, 2011.
- [136] G. Y. Chen, N. Lambert, C. H. Chou, Y. N. Chen, and F. Nori, "Surface plasmons in a metal nanowire coupled to colloidal quantum dots: Scattering properties and quantum entanglement," *Physical Review B*, vol. 84, no. 4, p. 045310, 2011.
- [137] C. E. Susa and J. H. Reina, "Correlations in optically controlled quantum emitters," *Physical Review A*, vol. 85, no. 2, p. 022111, 2012.

- [138] N. Engheta, "Circuits with light at nanoscales: Optical nanocircuits inspired by metamaterials," *Science*, vol. 317, no. 5845, pp. 1698–1702, 2007.
- [139] P. Bharadwaj, B. Deutsch, and L. Novotny, "Optical antennas," *Adv. Opt. Photon.*, vol. 1, p. 438, 2009.
- [140] R. Esteban, T. V. Teperik, and J. J. Greffet, "Optical patch antennas for single photon emission using surface plasmon resonances," *Physical Review Letters*, vol. 104, no. 2, p. 026802, 2010.
- [141] P. Biagioni, J. S. Huang, and B. Hecht, "Nanoantennas for visible and infrared radiation," *Reports on Progress in Physics*, vol. 75, no. 2, p. 024402, 2012.
- [142] G. Y. Slepyan, Y. D. Yerchak, S. A. Maksimenko, A. Hoffmann, and F. G. Bass, "Mixed states in rabi waves and quantum nanoantennas," *Physical Review B*, vol. 85, no. 24, p. 245134, 2012.
- [143] A. Pierret, M. Hocevar, S. L. Diedenhofen, R. E. Algra, E. Vlieg, E. C. Timmering, M. A. Verschuuren, G. W. G. Immink, M. A. Verheijen, and E. P. A. M. Bakkers, "Generic nano-imprint process for fabrication of nanowire arrays," *Nanotechnology*, vol. 21, no. 6, p. 065305, 2010.
- [144] M. T. Borgstrom, G. Immink, B. Ketelaars, R. Algra, and E. P. A. M. Bakkers, "Syn-energetic nanowire growth," *Nature Nanotechnology*, vol. 2, no. 9, pp. 541–544, 2007.
- [145] N. Akopian, G. Patriarche, L. Liu, J. C. Harmand, and V. Zwiller, "Crystal phase quantum dots," *Nano Letters*, vol. 10, no. 4, pp. 1198–1201, 2010.
- [146] M. P. van Kouwen, M. H. M. van Weert, M. E. Reimer, N. Akopian, U. Perinetti, R. E. Algra, E. P. A. M. Bakkers, L. P. Kouwenhoven, and V. Zwiller, "Single quantum dot nanowire photodetectors," *Applied Physics Letters*, vol. 97, no. 11, p. 113108, 2010.
- [147] M. H. M. van Weert, N. Akopian, U. Perinetti, M. P. van Kouwen, R. E. Algra, M. A. Verheijen, E. P. A. M. Bakkers, L. P. Kouwenhoven, and V. Zwiller, "Selective excitation and detection of spin states in a single nanowire quantum dot," *Nano Letters*, vol. 9, no. 5, pp. 1989–1993, 2009.
- [148] L. Allen and J. H. Eberly, *Optical resonance and two-level atoms*. Interscience monographs and texts in physics and astronomy, v 28, New York,: Wiley, 1975.
- [149] D. S. Citrin, "Long intrinsic radiative lifetimes of excitons in quantum wires," *Physical Review Letters*, vol. 69, no. 23, pp. 3393–3396, 1992.
- [150] E. W. Bogaart and J. E. M. Haverkort, "Anomalous exciton lifetime by electromagnetic coupling of self-assembled inas/gaas quantum dots," *Journal of Applied Physics*, vol. 107, no. 6, p. 064313, 2010.
- [151] C. A. Balanis, *Antenna theory : analysis and design*. New York: Wiley, 2nd ed., 1997.
- [152] Y. Ota, S. Iwamoto, N. Kumagai, and Y. Arakawa, "Spontaneous two-photon emission from a single quantum dot," *Physical Review Letters*, vol. 107, no. 23, p. 233602, 2011.

- [153] A. S. Ilyinsky, G. J. Slepyan, and A. J. Slepyan, *Propagation, scattering and dissipation of electromagnetic waves*. IEE electromagnetic waves series, London: Peregrinus, 1993.
- [154] J. I. Cirac and P. Zoller, "A scalable quantum computer with ions in an array of microtraps," *Nature*, vol. 404, no. 6778, pp. 579–581, 2000.
- [155] J. I. Cirac and P. Zoller, "Quantum computations with cold trapped ions," *Physical Review Letters*, vol. 74, no. 20, pp. 4091–4094, 1995.
- [156] D. Leibfried, E. Knill, S. Seidelin, J. Britton, R. B. Blakestad, J. Chiaverini, D. B. Hume, W. M. Itano, J. D. Jost, C. Langer, R. Ozeri, R. Reichle, and D. J. Wineland, "Creation of a six-atom 'schrödinger cat' state," *Nature*, vol. 438, no. 7068, pp. 639–642, 2005.
- [157] P. Kok, H. Lee, and J. P. Dowling, "Creation of large-photon-number path entanglement conditioned on photodetection," *Physical Review A*, vol. 65, no. 5, p. 052104, 2002.
- [158] D. Leibfried, M. D. Barrett, T. Schaetz, J. Britton, J. Chiaverini, W. M. Itano, J. D. Jost, C. Langer, and D. J. Wineland, "Toward heisenberg-limited spectroscopy with multiparticle entangled states," *Science*, vol. 304, no. 5676, pp. 1476–1478, 2004.
- [159] V. Giovannetti, S. Lloyd, and L. Maccone, "Quantum-enhanced measurements: Beating the standard quantum limit," *Science*, vol. 306, no. 5700, pp. 1330–1336, 2004.
- [160] V. Giovannetti, S. Lloyd, and L. Maccone, "Quantum metrology," *Physical Review Letters*, vol. 96, no. 1, p. 010401, 2006.
- [161] R. Tanas and Z. Ficek, "Entangling two atoms via spontaneous emission," *Journal of Optics B-Quantum and Semiclassical Optics*, vol. 6, no. 3, pp. S90–S97, 2004.
- [162] Z. Ficek and S. Swain, "Quantum interference in optical fields and atomic radiation," *Journal of Modern Optics*, vol. 49, no. 1-2, pp. 3–42, 2002.
- [163] J. von Zanthier, T. Bastin, and G. S. Agarwal, "Measurement-induced spatial modulation of spontaneous decay and photon arrival times," *Physical Review A*, vol. 74, no. 6, p. 061802(R), 2006.
- [164] E. Rozbicki and P. Machnikowski, "Quantum kinetic theory of phonon-assisted excitation transfer in quantum dot molecules," *Physical Review Letters*, vol. 100, no. 2, p. 027401, 2008.
- [165] Z. Y. Tang, N. A. Kotov, and M. Giersig, "Spontaneous organization of single CdTe nanoparticles into luminescent nanowires," *Science*, vol. 297, no. 5579, pp. 237–240, 2002.
- [166] S. K. Hong, S. Nam, and K. H. Yeon, "Excitonic quantum interference in a quantum dot chain with rings," *Nanotechnology*, vol. 19, no. 15, p. 155402, 2008.

- [167] Z. Y. Tang, Z. L. Zhang, Y. Wang, S. C. Glotzer, and N. A. Kotov, "Self-assembly of CdTe nanocrystals into free-floating sheets," *Science*, vol. 314, no. 5797, pp. 274–278, 2006.
- [168] A. N. Al-Ahmadi and S. E. Ulloa, "Extended coherent exciton states in quantum dot arrays," *Applied Physics Letters*, vol. 88, no. 4, p. 043110, 2006.
- [169] A. Sukhanova, Y. Volkov, A. L. Rogach, A. V. Baranov, A. S. Sussha, D. Klinov, V. Oleinikov, J. H. M. Cohen, and I. Nabiev, "Lab-in-a-drop: controlled self-assembly of cdse/zns quantum dots and quantum rods into polycrystalline nanostructures with desired optical properties," *Nanotechnology*, vol. 18, no. 18, p. 185602, 2007.
- [170] A. Sitek and P. Machnikowski, "Interplay of coupling and superradiant emission in the optical response of a double quantum dot," *Physical Review B*, vol. 80, no. 11, p. 115319, 2009.
- [171] S. Mokhlespour, J. E. M. Haverkort, G. Slepian, S. Maksimenko, and A. Hoffmann, "Collective spontaneous emission in coupled quantum dots: Physical mechanism of quantum nanoantenna," *Physical Review B*, vol. 86, no. 24, p. 245322, 2012.
- [172] A. Laucht, J. M. Villas-Boas, S. Stobbe, N. Hauke, F. Hofbauer, G. Bohm, P. Lodahl, M. C. Amann, M. Kaniber, and J. J. Finley, "Mutual coupling of two semiconductor quantum dots via an optical nanocavity," *Physical Review B*, vol. 82, no. 7, p. 075305, 2010.
- [173] E. Gallardo, L. J. Martinez, A. K. Nowak, D. Sarkar, H. P. van der Meulen, J. M. Calleja, C. Tejedor, I. Prieto, D. Granados, A. G. Taboada, J. M. Garcia, and P. A. Postigo, "Optical coupling of two distant inas/gaas quantum dots by a photonic-crystal microcavity," *Physical Review B*, vol. 81, no. 19, p. 193301, 2010.
- [174] S. Reitzenstein, A. Löffler, A. Kubanek, C. Hofmann, M. Kamp, J. P. Reithmaier, A. Forchel, V. D. Kulakovskii, L. V. Keldysh, I. V. Ponomarev, and T. L. Reinecke, "Coherent photonic coupling of semiconductor quantum dots (vol 31, pg 1738, 2006)," *Optics Letters*, vol. 31, no. 23, pp. 3507–3507, 2006.
- [175] N. W. Ashcroft and N. D. Mermin, *Solid state physics*. New York,: Holt, 1976.
- [176] J. v. Bladel, *Electromagnetic fields*. IEEE Press series on electromagnetic wave theory, Hoboken, N.J. Chichester: Wiley-Interscience ; John Wiley, distributor, 2nd ed., 2007.
- [177] R. E. Jorgenson and R. Mittra, "Efficient calculation of the free-space periodic green-function," *Ieee Transactions on Antennas and Propagation*, vol. 38, no. 5, pp. 633–642, 1990.
- [178] R. M. Shubair and Y. L. Chow, "Efficient Computation of the Periodic Green-Function in Layered Dielectric Media," *IEEE Transactions on Microwave Theory and Techniques*, vol. 41, no. 3, pp. 498–502, 1993.

- [179] S. Oroskar, D. R. Jackson, and D. R. Wilton, "Efficient computation of the 2D periodic Green's function using the Ewald method," *Journal of Computational Physics*, vol. 219, no. 2, pp. 899–911, 2006.
- [180] V. Twersky, "On the scattering of waves by an infinite grating," *IRE Trans. on Antennas and Propagation*, vol. 4, pp. 330–345, 1956.
- [181] C. M. Linton, "The Green's function for the two-dimensional Helmholtz equation in periodic domains," *Journal of Engineering Mathematics*, vol. 33, no. 4, pp. 377–402, 1998.
- [182] G. Valerio, P. Baccarelli, P. Burghignoli, and A. Galli, "Comparative analysis of acceleration techniques for 2-D and 3-D Green's functions in periodic structures along one and two directions," *Ieee Transactions on Antennas and Propagation*, vol. 55, no. 6, pp. 1630–1643, 2007.
- [183] S. M. Dutra, *Cavity quantum electrodynamics : the strange theory of light in a box*. Wiley series in lasers and applications, New York: J. Wiley, 2005.
- [184] V. Buzek, "Dynamics of an excited 2-level atom in the presence of n-1 unexcited atoms in the free space," *Physical Review A*, vol. 39, no. 4, pp. 2232–2235, 1989.
- [185] M. O. Scully, "Enhancement of the index of refraction via quantum coherence," *Physical Review Letters*, vol. 67, no. 14, pp. 1855–1858, 1991.
- [186] J. P. Dowling and C. M. Bowden, "Near dipole-dipole effects in lasing without inversion - an enhancement of gain and absorptionless index of refraction," *Physical Review Letters*, vol. 70, no. 10, pp. 1421–1424, 1993.
- [187] M. Fleischhauer and S. F. Yelin, "Radiative atom-atom interactions in optically dense media: Quantum corrections to the Lorentz-Lorenz formula," *Physical Review A*, vol. 59, no. 3, pp. 2427–2441, 1999.
- [188] M. Fleischhauer, "Spontaneous emission and level shifts in absorbing disordered dielectrics and dense atomic gases: A green's-function approach," *Physical Review A*, vol. 60, no. 3, pp. 2534–2539, 1999.
- [189] S. Yelin and M. Fleischhauer, "Modification of local field effects in two level systems due to quantum corrections," *OPTICS EXPRESS*, vol. 1, p. 160, 1997.
- [190] L. V. Keldysh and Z. Eksp *JETP Lett.*, vol. 20, p. 2018, 1965.
- [191] C. W. Gardiner, *Handbook of stochastic methods for physics, chemistry, and the natural sciences*. Springer series in synergetics, Berlin ; New York: Springer-Verlag, 2nd ed., 1985.
- [192] M. Fleischhauer, "Relation between the N-Atom Laser and the One-Atom Laser," *Physical Review A*, vol. 50, no. 3, pp. 2773–2776, 1994.
- [193] A. L. Fetter and J. D. Walecka, *Quantum theory of many-particle systems*. International series in pure and applied physics, New York,: McGraw-Hill, 1971.

- [194] E. A. Power, *Introductory quantum electrodynamics*. Mathematical physics series, New York,: American Elsevier Pub. Co., 1965.
- [195] P. de Vries, D. V. van Coevorden, and A. Lagendijk, "Point scatterers for classical waves," *Reviews of Modern Physics*, vol. 70, no. 2, pp. 447–466, 1998.
- [196] J. Knoester and S. Mukamel, "Intermolecular forces, spontaneous emission, and superradiance in a dielectric medium - polariton-mediated interactions," *Physical Review A*, vol. 40, no. 12, pp. 7065–7080, 1989.
- [197] P. W. Milonni, "Field quantization and radiative processes in dispersive dielectric media," *Journal of Modern Optics*, vol. 42, no. 10, pp. 1991–2004, 1995.
- [198] J. Johansen, S. Stobbe, I. S. Nikolaev, T. Lund-Hansen, P. T. Kristensen, J. M. Hvam, W. L. Vos, and P. Lodahl, "Size dependence of the wavefunction of self-assembled InAs quantum dots from time-resolved optical measurements," *Physical Review B*, vol. 77, no. 7, p. 073303, 2008.
- [199] J. Guo, A. Gallagher, and J. Cooper, "Lorentz-lorenz shift in an inhomogeneously broadened medium," *Optics Communications*, vol. 131, no. 4-6, pp. 219–222, 1996.
- [200] R. Friedberg, S. R. Hartmann, and J. T. Manassah, "Frequency shifts in emission and absorption by resonant systems of two-level atoms," *Phys. Rep. C*, vol. 7, p. 101, 1973.
- [201] M. G. Benedict, V. A. Malyshev, E. D. Trifonov, and A. I. Zaitsev, "Reflection and transmission of ultrashort light-pulses through a thin resonant medium - local-field effects," *Physical Review A*, vol. 43, no. 7, pp. 3845–3853, 1991.
- [202] F. Fernandez-Alonso, M. Righini, A. Franco, and S. Selci, "Time-resolved differential reflectivity as a probe of on-resonance exciton dynamics in quantum wells," *Physical Review B*, vol. 67, no. 16, p. 165328, 2003.
- [203] B. Pal and A. S. Vengurlekar, "Coherent effects in spectrally resolved pump-probe differential reflectivity measurements at exciton resonance in GaAs quantum wells," *Physical Review B*, vol. 68, no. 12, p. 125308, 2003.
- [204] B. Pal and A. S. Vengurlekar, "Time-resolved excitonic coherent polarization dynamics in GaAs multiple quantum wells," *Physical Review B*, vol. 68, no. 20, p. 205331, 2003.
- [205] T. Guenther, C. Lienau, T. Elsaesser, M. Glanemann, V. M. Axt, T. Kuhn, S. Eshlaghi, and A. D. Wieck, "Coherent nonlinear optical response of single quantum dots studied by ultrafast near-field spectroscopy," *Physical Review Letters*, vol. 89, no. 5, p. 057401, 2002.
- [206] G. R. Hayes, J. L. Staehli, U. Oesterle, B. Deveaud, R. T. Phillips, and C. Ciuti, "Suppression of exciton-polariton light absorption in multiple quantum well Bragg structures," *Physical Review Letters*, vol. 83, no. 14, pp. 2837–2840, 1999.
- [207] S. Kim, E. Oh, J. U. Lee, D. S. Kim, S. Lee, and J. K. Furdyna, "Effect of point defect and Mn concentration in time-resolved differential reflection in GaN," *Applied Physics Letters*, vol. 88, no. 26, p. 262101, 2006.

- [208] D. Birkedal, J. Bloch, J. Shah, L. N. Pfeiffer, and K. West, "Femtosecond dynamics and absorbance of self-organized InAs quantum dots emitting near 1.3 μm at room temperature," *Applied Physics Letters*, vol. 77, no. 14, pp. 2201–2203, 2000.
- [209] T. S. Sosnowski, T. B. Norris, H. Jiang, J. Singh, K. Kamath, and P. Bhattacharya, "Rapid carrier relaxation in $\text{In}_{0.4}\text{Ga}_{0.6}\text{As}/\text{GaAs}$ quantum dots characterized by differential transmission spectroscopy," *Physical Review B*, vol. 57, no. 16, pp. R9423–R9426, 1998.
- [210] A. Othonos, "Probing ultrafast carrier and phonon dynamics in semiconductors," *Journal of Applied Physics*, vol. 83, no. 4, pp. 1789–1830, 1998.
- [211] J. C. Eilbeck, "Reflection of short pulses in linear optics," *Journal of Physics Part a General*, vol. 5, no. 9, p. 1355, 1972.
- [212] V. I. Yukalov and E. P. Yukalova, "Dynamics of quantum dot superradiance," *Physical Review B*, vol. 81, no. 7, p. 075308, 2010.
- [213] E. W. Bogaart, *Transient differential reflection spectroscopy on quantum dot nanostructures*. Thesis, 2006.
- [214] F. Adler, M. Geiger, A. Bauknecht, F. Scholz, H. Schweizer, M. H. Pilkuhn, B. Ohnesorge, and A. Forchel, "Optical transitions and carrier relaxation in self assembled InAs/GaAs quantum dots," *Journal of Applied Physics*, vol. 80, no. 7, pp. 4019–4026, 1996.
- [215] B. Ohnesorge, M. Albrecht, J. Oshinowo, A. Forchel, and Y. Arakawa, "Rapid carrier relaxation in self-assembled $\text{In}_x\text{Ga}_{1-x}\text{As}/\text{GaAs}$ quantum dots," *Physical Review B*, vol. 54, no. 16, pp. 11532–11538, 1996.
- [216] R. Heitz, M. Veit, N. N. Ledentsov, A. Hoffmann, D. Bimberg, V. M. Ustinov, P. S. Kopev, and Z. I. Alferov, "Energy relaxation by multiphonon processes in InAs/GaAs quantum dots," *Physical Review B*, vol. 56, no. 16, pp. 10435–10445, 1997.
- [217] S. Raymond, S. Fafard, P. J. Poole, A. Wojs, P. Hawrylak, S. Charbonneau, D. Leonard, R. Leon, P. M. Petroff, and J. L. Merz, "State filling and time-resolved photoluminescence of excited states in $\text{In}_x\text{Ga}_{1-x}\text{As}/\text{GaAs}$ self-assembled quantum dots," *Physical Review B*, vol. 54, no. 16, pp. 11548–11554, 1996.
- [218] R. Heitz, A. Kalburge, Q. Xie, M. Grundmann, P. Chen, A. Hoffmann, A. Madhukar, and D. Bimberg, "Excited states and energy relaxation in stacked InAs/GaAs quantum dots," *Physical Review B*, vol. 57, no. 15, pp. 9050–9060, 1998.
- [219] A. Fiore, P. Borri, W. Langbein, J. M. Hvam, U. Oesterle, R. Houdre, R. P. Stanley, and M. Ilegems, "Time-resolved optical characterization of InAs/InGaAs quantum dots emitting at 1.3 μm ," *Applied Physics Letters*, vol. 76, no. 23, pp. 3430–3432, 2000.
- [220] G. Raino, G. Visimberga, A. Salhi, M. De Vittorio, A. Passaseo, R. Cingolani, and M. De Giorgi, "Simultaneous filling of InAs quantum dot states from the GaAs barrier under nonresonant excitation," *Applied Physics Letters*, vol. 90, no. 11, p. 111907, 2007.

- [221] K. Neudert, F. Trojánek, K. Kuldová, J. Oswald, A. Hospodková, and P. Malý, "Ultrafast photoluminescence spectroscopy of InAs/GaAs quantum dots," *Phys. Status. Solidi C*, vol. 6, pp. 853–856, 2009.
- [222] Y. Toda, O. Moriwaki, M. Nishioka, and Y. Arakawa, "Efficient carrier relaxation mechanism in InGaAs GaAs self-assembled quantum dots based on the existence of continuum states," *Physical Review Letters*, vol. 82, no. 20, pp. 4114–4117, 1999.
- [223] A. Vasanelli, R. Ferreira, and G. Bastard, "Continuous absorption background and decoherence in quantum dots," *Physical Review Letters*, vol. 89, no. 21, p. 216804, 2002.
- [224] V. Zwiller, M. E. Pistol, D. Hessman, R. Cederstrom, W. Seifert, and L. Samuelson, "Time-resolved studies of single semiconductor quantum dots," *Physical Review B*, vol. 59, no. 7, pp. 5021–5025, 1999.
- [225] D. Sreenivasan, *Capture, relaxation and recombination in quantum dots*. Thesis, 2008.
- [226] A. Nebel, C. Fallnich, R. Beigang, and R. Wallenstein, "Noncritically phase-matched continuous-wave mode-locked singly resonant optical parametric oscillator synchronously pumped by a ti-sapphire laser," *Journal of the Optical Society of America B-Optical Physics*, vol. 10, no. 11, pp. 2195–2200, 1993.
- [227] H. M. van Driel, "Synchronously pumped optical parametric oscillators," *Appl. Phys. B*, vol. 60, p. 411, 1995.
- [228] Y. I. Mazur, V. G. Dorogan, E. J. Marega, G. G. Tarasov, D. F. Cesar, V. Lopez-Richard, G. E. Marques, and G. J. Salamo, "Mechanisms of interdot coupling in (In,Ga)As/GaAs quantum dot arrays," *Applied Physics Letters*, vol. 94, no. 12, p. 123112, 2009.
- [229] A. Fiore, U. Oesterle, R. P. Stanley, R. Houdre, F. Lelarge, M. Ilegems, P. Borri, W. Langbein, D. Birkedal, J. M. Hvam, M. Cantoni, and F. Bobard, "Structural and electrooptical characteristics of quantum dots emitting at 1.3 μm on gallium arsenide," *Ieee Journal of Quantum Electronics*, vol. 37, no. 8, pp. 1050–1058, 2001.

Summary

Electromagnetic Coupling of Quantum Dots

In our work, we have theoretically and experimentally investigated the electromagnetic coupling in different quantum dot (QD) systems. The optical interaction between the QDs is in fact a dipole-dipole interaction, which is mediated by both real and virtual photons. The real photons are responsible for the spontaneous and incoherent energy transfer and the exchange of virtual photons governs the coherent coupling between the QDs.

In this thesis, we started with the simplest case of a two-QD system. The analysis carried out allows us to propose that the collective spontaneous emission of a QD ensemble provides an opportunity for the design of quantum nano-antennas whose radiative properties are dictated by the initial state of the system. Just by changing the QD-QD distance, we are able to increase (superradiance) or decrease (subradiance) the PL intensity as well as the spontaneous emission rate in a particular emission direction compared to the uncoupled system. A change of the QD-QD separation will also modify the amplitude and width of the emission spectrum. From the experimental point of view, the spontaneous emission spectrum (PL), and the emission dynamics can be easily measured by locating the detectors at different angular positions around the radiating QD system. The directionality of the emission is one of the key characteristic of a quantum antenna in which nano-scale quantum correlations give rise to far-field consequences.

We then extended this concept to a more complicated system of a 2D periodic rectangular lattice of QDs. In such structures, the lattice constant and the phase shift imposed by the initial excitation play important roles. If two rectangular lattices are intermixed, the separation of QDs in each unit cell is another variable that comes into play. By engineering appropriate values for the lattice periodicity, the QD-QD separation and the phase shift, we can achieve almost any desired value for the single-lattice and collective QD emission rates. Similar to the simple case of the two-QD system, the collective emission rate of a two-lattice system can also be either superradiant (faster) and subradiant (slower) as compared with the emission rate of the single lattice.

Proceeding one step further towards even more complicated structures, we studied self-assembled QDs in which the QDs are randomly distributed in a plane and follow a Gaussian size distribution. Due to the large inhomogeneous broadening in such samples, the dephasing time is usually shorter than the characteristic superradiance time required to build up a coherent emission. That's why it is unlikely that we can observe cooperative effects in these type of samples. However it is possible to observe and measure collective effects. In randomly distributed QD samples, the local field acting upon each QD is strongly modified by altering some parameters like the QD density and the initial excitation. We found that the emission is slower in dense QD samples. In the case of dilute QD samples, the increase of the radiative decay time is proportional to the QD density squared. We also found that the collective radiative decay time is proportional to the square power of the initial population difference. The collective emission thus vanishes when exactly half of the QDs are excited. However, when the QD system is either weakly excited (only one QD is initially excited) or highly excited (all QDs excited, except one), the electromagnetic coupling between the QDs in the ensemble and thus also the emission decay time is maximum. This phenomenon is called radiation trapping and is a consequence of the local-field modification in a system that is composed of both dispersive (excited) and absorptive (not excited) QDs. This phenomenon and its consequences are verified experimentally in our work for a sample of self-assembled InAs/GaAs QDs. By employing the Time Resolved Differential Reflectivity (TRDR) technique, we measured the decay time of the QD excitation. We showed that the emission rate of those QDs which are closer to the center of the size distribution and thus are of higher density, is slower than that of the QDs in the tails of the QD size distribution. Moreover, we indicated that for a certain pump-power that statistically half of the QDs are excited, the emission decay time is minimum. This point corresponds to the zero population difference at which the collective effects are absent. However, for the higher and lower pump-powers, the emission rate is faster. We clearly observed that for very low and very high pump powers, the decay time tends to a maximum value, which is an indication for more effective collective effects in these pump-power regimes.

Acknowledgement

In order to develop a theory for analyzing and interpreting our anomalous experimental data, I had to take some initial steps first. I started from the simplest system and finally arrived at the most complicated structure similar to our real sample with a lot of degrees of disorder. Taking over all of these steps was very time-consuming. It is even more difficult when you have to do this in an experimental group with a different style of expectations with more or less sharp deadlines. However when you are thinking how to develop a theory, nobody knows when you arrive at the final stage. That is why my special thank goes to my daily supervisor, Dr. J.E.M. Haverkort, first for trusting me and giving me the opportunity to work in PSN and then for his understanding of my especial situation and being patient enough with me. Jos, you always had time for me and tried to keep me in line. Thank you for everything.

I thank my promoters, Prof.dr. A. Fiore, Prof.dr. M.E. Flatté and the other members of the committee, Prof.dr. A.F. Koenderink, Prof.dr. S. Maksimenko, Prof.dr.ir. O.J. Luiten and Prof.dr. D. Lenstra. Thank you for reading my thesis. your comments were very helpful to improve the quality of my thesis. I would like to thank also Prof.dr. Gregory Slepian for many things that I learned from him in the field of theoretical quantum electrodynamics.

I would like to thank all the staff members of PSN. Prof.dr. P.M. Koenraad for his perfectly leading the group and encouraging supports, and Prof.dr. A. Fiore as my first promotor for his helpful comments on my work. I also thank Prof.dr. E.P.A.M. Bakkers, Prof.dr. J. Gómez Rivas, Dr. R.W. van der Hijden and Dr. A. Silov for their scientific and social supports and discussions.

I am grateful to all technicians of PSN, Frank van Otten, Jos van Ruijven, Rene van Veldhoven, Peter Nouwens, Rian Hamhuis, Martine van Vlokhoven and Tom Eijkemans for their helps and technical supports without whom nothing goes smoothly in the clean room and optical labs.

I am thankful to all secretaries of PSN in recent years. M. van Doorne, A. Langenhuizen, T.J.H. Botman-van Amelsvoort and S. Krooswijk-Manche. I would like to express my deep appreciation to Margriet not only for the administrative matters but also for her personality and her efforts like a mother to make PSN a friendly and enjoyable place for

everybody.

I had many friends and colleagues in PSN who are still in the group or have already left. First of all I thank my office mates, Thuy, Yingchao, Elmoez, Hina, Timothy and Dick, for all unforgettable moments we shared in the office and in the lab. I am also thankful to Adam, Antony, Cem, David, Dondu, Ekber, Erwin, Ikarus, Ilaria, Jens, Joost, Junji, Mehmet, Murat, Nicolas, Niek, Nut, Rosalinda, Saeedeh, Sartoon, Simone, Tian, Tilman and Zilli and all other PSNers though their names are not mentioned here. I really enjoyed our scientific and social discussions we had together specially in our former coffee room and with some of you in the PSN football team. I am indebted to Nicolae, Erwin and Kevin from M2N group for training and assisting me in working with the sputtering machine and fabricating amazing gold nanorings and also Grzegorz from AMOLF for the amazing Fourier microscopy. I also thank the students, Steef, Franck, Franchesca and Willem who showed interest in my project.

I would like to acknowledge COBRA research institute and Eindhoven University of Technology for their financial supports and providing me the instruments I required to perform my measurements.

Outside the work environment, the family and friends make your life. When you are abroad, your nice friends play the role of your family as well. I am grateful to the great community of Iranian students in Eindhoven. Ali & Niloofar, Saeed & Saeedeh, Pouyan & Ellaheh, Hamid & Azar, Hossein & Samaneh, Amin & Parisa, Hooman & Negar, Mahmoud & Fahimeh, Ali & Erfaneh, Pouya & Solmaz, Mohammad & Flora, Saber & Sama, Ali & Mojgan, Hamed & Negar, Kamyar & Pegah, Raheleh, Reza, Amin, Parsa, Mehdi, Fatemeh, Sara, Sahel and many other dear friends. I appreciate all memorable and wonderful moments and gatherings we had together and thank you for letting me feel home. I would like to express my especial appreciation to Ali and Niloofar who have been always so kind to me by considering me as a member of their own family especially in the last two years. I thank also my best friends in Mainz, Ali & Nadia, Saeed & Fahimeh and Abolfazl & Sima for all the nice things you made for us.

Words are not enough to thank my parents. Maman, Baba, I owe you my entire life. I appreciate your sincere and infinite supports and prays. Your encouragements have always inspired me to be strong and move on. I also express my deep gratitude to my sisters, Sedigheh and Tahereh and my father, mother, brothers and sister-in-law, for their love and supports and making my life meaningful.

At the end but with extreme importance, I would like to express my especial and deep gratitude to my lovely wife, Leila. You were always there for me in all happy and sad moments. Achieving this success was not possible without your sincere supports. you helped me in maintaining the positive spirit. Thank you for tolerating the difficulties of living with me. I love you so much.

Curriculum vitae

Salman Mokhlespour is born on 16 February 1982 in Isfahan, Iran. After finishing his high school and pre-university education in Isfahan, he entered Isfahan University of Technology in 2000. He received a bachelor degree in solid-state physics from department of physics in 2004. He then entered Shiraz University in 2004 and received his master degree in solid-state and atomic physics from physics department in 2007. His master project was on *Energy Transfer by Electromagnetic Pulses* and was carried out under supervision of Prof. M. Barati. He moved to the Netherlands in November 2007 where he was appointed as a PhD candidate in the group of Photonics and Semiconductor Nanophysics (PSN) at the department of Applied Physics, Eindhoven University of Technology. The research done during his PhD on *Electromagnetic Coupling of Quantum Dots* is presented in this dissertation and is carried out under supervision of prof.dr. A. Fiore, prof.dr. M.E. Flatté and dr. J.E.M. Haverkort.

